Geological Survey of Finland 2019

Adakitic plutonic rocks in the Finnish Precambrian: Evolution and areal, chemical, physical and age variations

Tapio Ruotoistenmäki

Academic Dissertation

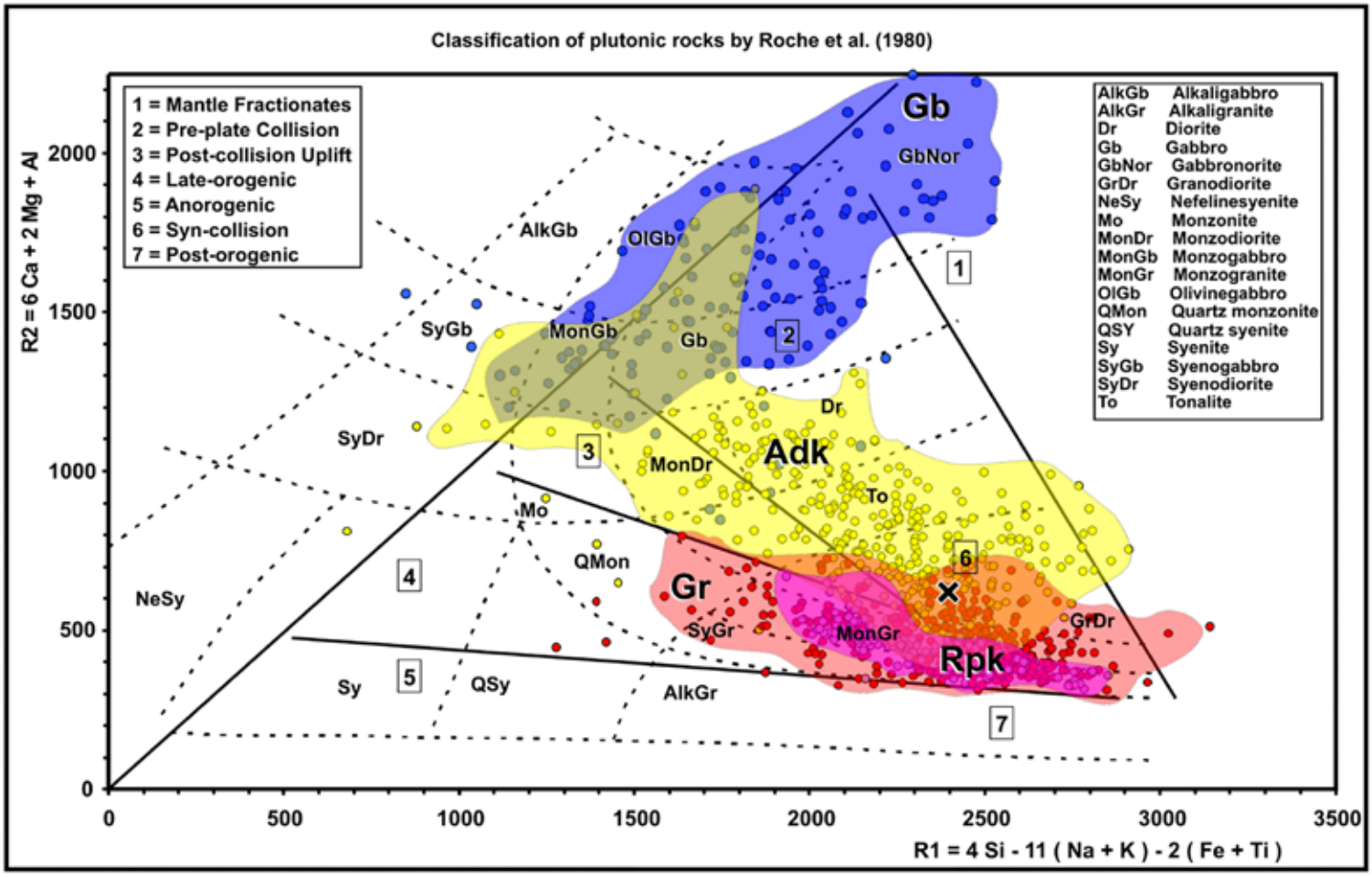

GTK
gtk.fi

Adakitic plutonic rocks in the Finnish Precambrian: Evolution and areal, chemical, physical and age variations

by

Tapio Ruotoistenmäki
Hannuksenkuja 4A5
FI-02270 Espoo, Finland

ancora imparo

ACADEMIC DISSERTATION

To be presented, with the permission of the Faculty of Science of the University of Helsinki, for public criticism in the University of Helsinki, main building, Auditorium XII, Fabianinkatu 33, on February 20th, 2019, at 12 o'clock noon

Unless otherwise indicated, the figures have been prepared by the author of the publication.

Geological Survey of Finland
Espoo 2019

Supervisors: Professor O. Tapani Rämö
Department of Geosciences and Geography
University of Helsinki, Finland

Docent Pentti Hölttä
Geological Survey of Finland
Espoo, Finland

Reviewers: Professor Paterno R. Castillo
Scripps Institution of Oceanography
University of San Diego, California, USA

Docent Esa Heilimo
Geological Survey of Finland
Kuopio, Finland

Opponent: Docent Markku Väisänen
Department of Geography and Geology
University of Turku, Finland

Front cover: Rock type and tectonic classification of Finnish adakitic (Adk), granitic (Gr + Rapakivi, Rpk) and gabbroic (Gb) plutonic rock samples from Proterozoic sub-areas.
The cross (x) indicates the geometric mean of all Finnish plutonic rock samples (AFP).

Ruotoistenmäki, T. 2019. Adakitic plutonic rocks in the Finnish Precambrian: Evolution and areal, chemical, physical and age variations. *Geological Survey of Finland*, Espoo. 146 pages, 97 figures and 15 tables.

ABSTRACT

Adakitic plutonic rocks, or 'adakitoids', representing melts fractionated below plagioclase stability depths in the lower crust to upper mantle, cover a substantial fraction of the Finnish bedrock. Only some supracrustal sub-areas lack adakitic plutonic rock outcrops. In this study, I provide a summary of adakitoids in the Finnish Precambrian: their areal, chemical and physical variations and their evolution. The samples are considered on a regional to local area scale in five separate sections. It is shown that adakitoids constitute a distinct chemically defined rock group, which overlaps groups defined by 'traditional' mineralogical and chemical methods.

A very effective high-resolution tool for studying adakitoid chemistry is found to be the incompatible–compatible diagram ('Pearce–Peate spectrum') combined with normalization by geometric means of all Finnish plutonic rocks samples (AFP) from the Rock Geochemical Database of Finland (RGDB) maintained by the Geological Survey of Finland (GTK). The characteristics of adakitoids are considered by comparing their chemical spectra with those of granite and gabbro samples from the same database. The most distinct features of adakitoids are their relatively high Sr, Eu and ratios of LREE/HREE (light/heavy rare earth elements) and compatible elements/HREE. Moreover, their AFP-normalized spectra have relative maxima at Ba, K, Na_2O, Ti, Li, CaO, V, Mn, Fe, Co and Mg.

The adakitic plutonic rocks vary from granodiorites to tonalites and gabbros. The Proterozoic adakitoids are denser than Archaean adakitoids, reflecting their more mafic (sanukitoid) composition. However, their magnetic properties are alike. In Proterozoic sub-areas, the main characteristics of adakitoids and the average of all-plutonic rocks clearly differ, with the exception of two 'oceanic' sub-areas, whose spectral peaks coincide with those of the adakitoids, although with somewhat different trends. However, in Archaean sub-areas, the averages of all-plutonic rocks and adakitoids significantly correlate, which refers to similar evolutionary conditions and processes for both adakitoids and crust as a whole.

In this study, the Proterozoic adakitoids are generally connected with 'modern type' plate tectonic processes, while Archaean crust and adakitoids (TTGs) are primarily connected with collision, stacking and over-/underthrusting of inferred pre-existing microplates. However, in the Archaean Ilomantsi sub-area in eastern Finland, evolution related to 'modern', plate tectonic subduction is preferred. The chemical and mineralogical differences between adakitoids, sanukitoids and TTGs are obscure and overlapping. Therefore, straightforward association of these rock types with certain tectonothermal processes using tectonomagmatic geochemical discriminant diagrams must be carried out with care.

The relative contents of pyroxenes, garnet and amphiboles in the restite of adakitic melts are evaluated by using the content ratios of trace elements, whose partition coefficients for presumed basaltic source rocks

differ substantially. The dominant restite minerals are interpreted to be clinopyroxene and orthopyroxene for both Proterozoic and Archaean adakitoids, while garnet and amphiboles also characterize the restites of Archaean adakitoids. The rapakivi granites correlate strongly negatively with adakitoids, thus giving indications of the characteristics of the complementary restitic material of the adakitoids. However, due to their complex uplift history, the rapakivis cannot be directly considered as adakitoid restites.

Proterozoic adakitic magma series are considered in a local-scale study on a collision zone in central Finland. In this zone, even the most mafic adakitoids are characterized by a distinctly fractionated spectrum with relatively high contents of incompatibles and low values for compatibles when compared to non-adakitic, tholeitic magma series. Examples of low-SiO_2, Proterozoic post-collisional adakitoids cross-cutting Archaean crust close to the Archaean–Proterozoic border are also examined. Their homogeneous zircons and relatively high ε_{Nd} values refer to local-scale underthrusting/subduction-related genesis and minor crustal contamination.

The isotopic ages from Archaean adakitoid zircons considered here range from ca. 2620 to 3000 Ma, the magmatic ages bracketing more tightly between ca. 2690–2740 Ma. The high contents of older inherited and younger, overprinted zircons reflect their complex and multistage history.

The adakitoids can all be classified as representing plagioclase instability depth melts. They form a continuity from 'true', subduction-related adakites to TTGs and sanukitoids, their chemical and mineralogical differences being obscure. As such, they provide a very valuable and informative window into magmatic processes existing at upper mantle/lower crustal depths. Their potential for economic mineralizations, especially REE, Au and Cu, remains to be considered. Moreover, the characteristics of crust between their present location and source depth can be studied by analysing their xenoliths and chemical contamination on their way up to the present surface. Thus, their profound and comprehensive study will provide valuable information on the evolution of our Precambrian crust.

Keywords: Finland, Archaean, Proterozoic, adakite, adakitic, adakitoid, TTG, sanukitoid, plutonic rock, geochemistry, geophysics, petrophysics, absolute age, evolution

Tapio Ruotoistenmäki
Hannuksenkuja 4A5
FI-02270 Espoo, Finland

p. 040487464

E-mail: truotois@gmail.com

ISBN 978-952-217-399-7 (paperback)
ISBN 978-952-217-400-0 (pdf)

Layout: Elvi Turtiainen Oy
Printing house: Grano Oy

CONTENTS

INTRODUCTION

When studying the Tertiary lavas on Adak Island in the Aleutian arc, Kay (1978) concluded that these lavas represent products of slab melting. Similar magmatic rocks, called adakites, have since been identified and studied by several authors. For example, Drummond & Defant (1990) and Defant & Drummond (1990) interpreted adakites as products of partial melting of a young (<20–30 Ma), gently dipping subducted slab. Defant & Drummond (1990) and Thorkelson & Breitsprecher (2005) summarized adakites as high-silica (SiO_2 >56%), high-alumina (Al_2O_3 > 15%), plagioclase- and amphibole-bearing lavas with Na_2O > 3.5%, high Sr (>400 ppm), low Y (<18 ppm), high Sr/Y (>40), low Yb (<1.9) and high La/Yb (>20).

Martin et al. (2005) considered the characteristics of adakites, Archaean TTGs (tonalite–trondhjemite–granodiorites) and sanukitoids, all of which they linked to slab melting and interaction with peridotitic mantle. Either slab melts have been contaminated with mantle components (late Archaean TTGs and high-silica adakites) or mantle melts have been metasomatized by slab melts (sanukitoids and low-silica adakitoids).

In his review paper on adakites, Moyen (2009) summarized that rocks with a high Sr/Y and La/Yb signature can be achieved by various processes: 1) by melting of a high Sr/Y and La/Yb (enriched) source, 2) by deep melting, with abundant residual garnet, 3) by fractional crystallization or AFC, or 4) by interactions of felsic melts with the mantle, causing selective enrichment in LREE (light rare earth elements) and Sr over HREE (heavy rare earth elements). He concluded that the classical model of 'slab melting' provides the best explanation for the genesis of high-silica adakites, while the low-silica adakites are products of garnet-present melting of an adakite-metasomatized mantle. Moreover, he noted that the 'continental', high-potassium adakites correspond to a diversity of petrogenetic processes, and most of them are different from both low- and high-silica adakites. He concluded that Archaean adakites show a bimodal composition range, with some very high Sr/Y examples reflecting deep melting (>2.0 GPa) of a basaltic source, while lower Sr/Y rocks are formed by shallower (1.0 GPa) melting of similar sources. The Archaean TTGs are relatively heterogeneous, which refers to a diversity of sources and processes in their genesis.

The main geochemical features of adakites summarized by Castillo (2006) are presented in Table 1. He pointed out that there are numerous examples of adakitic rocks that are not directly related to slab melting in subduction processes. Moreover, the volume of adakite produced by slab melting is probably less than that of adakitic rocks produced by other possible processes. He also noted that slab melting is not the most effective mechanism to produce large volumes of Archaean TTGs. For example, in the Fiskenæsset region, southern West Greenland, Hua Huang et al. (2013) interpreted ca. 2.95–2.79 Ga metamorphosed TTGs to be generated by partial melting of hydrous basalts (amphibolites) at the base of a thickened magmatic arc, leaving a rutile-bearing eclogite residue.

Table 1. Main geochemical features of adakites (Castillo 2006).

Characteristics	Possible features related to subducted slab melting
High SiO_2 (≥56 wt%)	High-P melting of eclogite/garnet amphibolite
High Al_2O_3 (≥15 wt%)	At ca. 70 wt% SiO_2; high P partial melting of eclogite or amphibolite
Low MgO (<3 wt%)	Low Ni and Cr; if primary melt, not derived from a mantle peridotite
High Sr (>300 ppm)	Melting of plagioclase or absence of plagioclase in the residue
No Eu anomaly	Either minor plagioclase residue or source basalt depleted in Eu
Low Y (<15 ppm)	Indicative of garnet (to a lesser extent, of hornblende or clinopyroxene) as a residual phase
High Sr/Y (>20)	Higher than that produced by normal crystal fractionation; indicative of garnet and amphibole as a residual phase
Low Yb (<1.9 ppm)	Meaning low HREE; indicative of garnet as a residual phase
High La/Yb (>20)	LREE enriched relative to HREE; indicative of garnet as a residual phase
Low HFSEs (Nb, Ta)	As in most arc lavas; Ti phase or hornblende in the source
Low $^{87}Sr/^{86}Sr_i$ (<0.704)	low $^{206}Pb/^{204}Pb$, K/La, Rb/La, Ba/La and high initial $^{143}Nd/^{144}Nd$; normal-MORB signature

Early Cretaceous Sr-rich silicic magmatism in the Kitakami area of the Honshu Arc in NE Japan has been studied by Tsuchiya & Kanisawa (1994). In the area, the high-Sr rocks (Sr > ca. 500 ppm, SiO_2 > 60 wt%, Sr/Y > ca. 40) are characterized by high Na_2O, Al_2O_3, Ga, P, Ba and Sr, while K_2O, Mn, total FeO, MgO, Rb, Pb and Y are lower than in low-Sr samples (Sr/Y < ca. 40). Moreover, the Kitakami high-Sr rocks are characterized by positive magnetic anomalies. They concluded that if basaltic rocks are partially melted at low pressures (0.8 to 1.6 GPa; i.e. depths of between ca. 30–60 km), partial melts have relatively low Sr/Y ratios because plagioclase in the restite phase retains Sr but not Y. However, if melting occurs at higher pressures, above ca. 1.5–1.6 GPa, leaving eclogite or hornblende eclogite restite, the resulting magmas can have high Sr/Y because Y is strongly partitioned in garnet but Sr is not. Thus, they proposed that the Kitakami low-Sr melts are derived from lower pressures and crustal depths, while the high-Sr magmas are derived from partial melting of subducting oceanic slab and sediments at depths of ca. 70–80 kilometres, possibly mixed with magma derived from overlying mantle wedge.

The economic potential of adakites was evaluated by Mungall (2002), who noted that adakitic magmas can be highly oxidized and potentially fertile for Au and Cu. He commented that the very existence of large Au and Cu deposits may indicate slab melting or the release of supercritical fluids in the source regions of the parent magma. For example, potassium and SiO_2 rich, altered adakites control the largest porphyry Cu deposit in Qulong, China (Hu et al. 2015).

However, Richards & Kerrich (2007) concluded that there appears to be no obvious role for adakitic magmas or slab melts in the genesis of either alkalic-type Au deposits or Au-rich porphyry Cu deposits. Moreover, they criticize the incomplete number of samples and analysis of lavas reported by Kay (1978) and Defant & Drummond (1990). Richards & Kerrich (2007) emphasized the variable roles of melts and fluids from subducting slab, sedimentary wedge, mantle wedge and lower crust in producing adakitic magma. Garrison & Davidson (2003) also emphasized that basaltic magmas derived from mantle wedge could produce adakitic characteristics. In addition, discerning between slab and lower crustal melting using simple geochemical criteria (such as the Sr/Y ratio) is not unambiguous.

Svecofennian calc-alkaline and adakite-like 1.90–1.86 Ga magmatism in SW Finland has been reported by Väisänen et al. (2006). They connected the compositional differences with variations in the depth and site of melting along a subduction zone. The older, calc-alkaline magmatism is related to melting of the mantle wedge, while younger adakite-like magmatism requires deeper melting of subducting slab contaminated by mantle wedge. Mattila (2004) studied six dome-shaped synorogenic plutons in south-eastern Finland and north-western Russia. The strongly fractionated REE geochemistry and associated Ta–Nb depletion of the synorogenic rocks of the study areas indicate that the sources for these units have been formed in volcanic arc environments. Based on Sm–Nd isotopic data, two different arc settings were established: a juvenile island arc, with positive ε_{Nd} (1.88 Ga) values, and an active margin, with mainly negative ε_{Nd} (1.88 Ga) values. Mattila (2004) concluded that the LREE-enriched and HREE-depleted trace element geochemistries of the investigated synorogenic granitoids, together with high Sr-concentrations, indicate that these granitoids are 'adakites', formed by partial melting of subducting hydrous garnet-amphibolite. This is further supported by the relatively high Mg numbers and Ni and Cr concentrations, which indicate interaction between ascending adakitic magmas and the overlying mantle wedge.

Svetov et al. (2004) investigated ca. 3.0 Ga adakitic rocks found in the basalt–andesite–dacite–rhyolite (BADR) island-arc association of the Upper Archaean Vedlozero–Segozero greenstone belt in the Fennoscandian shield. They straightforwardly concluded that these rocks indicate convergent (interplate) ocean–continent transition zones and subduction-related tectonics in these ancient systems.

When considering granitoid magmatism related to Neoarchaean plate tectonics in Karelian and Kola cratons, Halla et al. (2009) divided granitoids into three groups: groups 1–2 comprising high and low HREE (heavy rare earth elements) TTGs related to low- and high-angle (-pressure) subduction and group 3 consisting of high Ba–Sr sanukitoids related to melting of an enriched mantle source, probably as a result of a slab breakoff following a continental collision or attempted subduction of a thick oceanic plateau or TTG protocontinent.

Heilimo et al. (2010) also divided Archaean TTGs into low-HREE and high-HREE groups. The composition of the low-HREE TTG group (high SiO_2 and low Mg) indicates that their parental melts have been produced from eclogite in the garnet stability field under high-pressure conditions. The other group of high-HREE TTGs (lower SiO_2 and elevated Mg) was possibly derived from a garnet-free low-pressure source with a possible mantle contribution. Moreover, there is no comprehensive geochemical classification separating the sanukitoid series from the TTG series.

Scaillet & Prouteau (2001 and references therein) emphasized that Archaean TTGs have been less contaminated by mantle interaction than typical Cenozoic adakites. They proposed relatively high T, low P, and possibly higher H_2O melts from gently dipping slabs as a source for Archaean TTG-type magmatism having adakitic characteristics. Smithies (2000) noted that the relatively low magnesium content of Archaean TTGs might be due to gently dipping underthrusting of oceanic plateaus, thus avoiding a significant ínfluence from the underlying peridotitic mantle. Condie (2005) also agreed that adakites are probably slab melts. However, he concluded that TTGs may be produced by partial melting of hydrous mafic rocks in the lower crust in arc systems or in the Archaean, perhaps in the root zones of oceanic plateaus. He connected depletion in heavy REE and low Nb/Ta ratios in high-Al TTGs with garnet and low-Mg amphibole in the restite, whereas moderate to high Sr values allow little, if any, plagioclase in the restite. Thus, the melting has occurred in the hornblende eclogite stability field at a depth between ca. 40–80 km and temperatures between 700 and 800 ºC.

Kröner et al. (2011) studied ancient, ca. 3.65 to 3.53 Ga tonalitic gneisses of the gneiss complex in Swaziland and a 3.53 Ga felsic metavolcanic sample of the Theespruit formation, the oldest unit of the Barberton greenstone belt, South Africa. They challenged the popular view that early Archaean TTGs and greenstones are principally of juvenile origin and formed in primitive arc or oceanic environments. Instead, they suggested extensive recycling of even the earliest-formed granitoid crust and mixing with juvenile material to produce successive generations of TTGs and associated felsic volcanic rocks. Moyen

(2011) also commented that crustal recycling was already a rather prominent process in the Archaean.

When considering the geochemical and petrophysical characteristics of Archaean plutonic rocks of adakitic affinity in Finland, Ruotoistenmäki (2012) noted that adakitic plutonic rocks appear to represent a continuous compositional series, from TTGs with variable Na_2O/K_2O and low Ba+Sr to sanukitoids with low Na_2O/K_2O and increasing Ba+Sr. He contrasted the relatively wide distribution and large volume of Archaean adakitic (TTG) rocks compared to those that are unequivocally interpreted as resulting from Archaean subduction processes, and concluded that processes such as crustal thickening by tectonic stacking and/or underplating by anomalously hot upper mantle could plausibly generate plagioclase-rich Archaean adakitic melts, leaving restites rich in compatible elements and HREE. It must also be emphasized that Finnish bedrock commonly shows metamorphic pressures from ca. 3 to 6 kbar (the maximum locally reaching 11–12 kbar); i.e. erosion and/or tectonic uplift up to ca. 10 (– …38) kilometres (e.g. Hölttä & Paavola 2000, Korsman et al. 1999 and references therein), thus resulting in significant uplift of primary sources of adakitoids and erosion of their inferred supracrustal counterparts.

From the considerations above, it becomes clear that the genetic link of adakites and adakitic rocks, including TTGs and sanukitoids, to slab melting is ambiguous. Castillo (2006) noted that the adakite studies have generated confusion because the definition of adakite combines compositional criteria with genetic interpretation. Moyen (2011) emphasized the loose definition of the term TTG in the literature. Therefore, in this study, the terms ‘adakitic’ or ‘adakitoid’ are used to refer to plutonic rocks having adakitic characteristics and apparently lower crust/upper mantle fractionation depths.

The classification of rock types is commonly based on their texture and mineralogy defined visually (e.g. Streckeisen 1976). However, more extensive and tedious classification by chemical analysis must be used to confirm rock-type characteristics in more detail and accuracy (Cox et al. 1979, Frost et al. 2001, de La Roche et al. 1980). Thus, it is evident that the number of known outcrops of this special adakitic rock group has so far been very sparse in Finland, and the definition of adakitic rocks must be made by chemical analysis of samples taken from outcrops. In this study, instead of visually sampling in the field, I selected plutonic rock samples from the very large Rock Geochemical Database of Finland (RGDB; Rasilainen et al. 2007) fulfilling the chemical definition of adakitic rocks above (Defant & Drummond 1990, Thorkelson & Breitsprecher 2005). This approach manifolds the number of the known adakitic plutonic rocks in Finland, making it possible to reliably analyse their characteristics using statistical methods.

This report provides a primary summary of adakitic plutonic rocks in Finnish Precambrian, their areal, chemical, isotopic (age) and physical variations and their evolution. The samples are considered on a regional to local sample scale in 5 separate sections. It is shown that adakitoids constitute a distinct new chemically defined rock group overlapping those groups defined by ‘traditional’ mineralogical and chemical methods.

In the first section, I consider the regional features of all Finnish adakitic rock samples from the Rock Geochemical Database of Finland and compare them with granitic and gabbroic samples from the same database. The samples cover both Archaean and Proterozoic domains in Finland with variable sampling density. The felsic granitic and mafic gabbroic rocks are chosen for comparison to emphasize and detect features that are only characteristic of adakitoids. In addition, in this section, Finnish adakitoids are also compared with selected examples of adakites, TTGs and sanukitoids adopted from the literature. Moreover, the mineralogy of their fractionation restites is considered.

In the second section, I consider in more detail plutonic RGDB rock samples from four Archaean and four Proterozoic sub-areas in southern and central Finland and demonstrate the differences between ‘non-adakitic’ and adakitic plutonic rocks (including TTGs and sanukitoids). Moreover, the correlations between the chemistry of the sub-areas (i.e. of adakitoids and ‘non-adakitic’ crustal averages) are examined.

In the third section, I consider in detail the chemical and isotopic characteristics of eight adakitic samples selected from the four Archaean sub-areas studied in the previous section. Their characteristics are also compared with

Proterozoic adakitoids from southern Finland, with chemistry adopted from the literature.

In the fourth section, I consider the characteristics of a high-Al, high-Sr, high magnetite and LREE-enriched mafic rock series on a Proterozoic collision zone in southern Finland having adakitic characteristics when normalized to a common value of SiO_2 = 60% using a 'regression curve normalization' method introduced here. The most mafic samples of these rocks possibly approach the primary source rock characteristics of the adakitoids. This rock group is compared with a more felsic, but (still) less fractionated tonalitic plutonic rock series sampled on the same profile.

In the fifth section, I introduce high-Al, high-Sr, post-collisional adakitic intrusives located in Archaean crust close to a Proterozoic-Archaean collision zone in central Finland. This section is based on updated lithogeochemical and isotopic studies by Ruotoistenmäki et al. (2001).

In the last section, a summary of previous sections is provided.

This report mainly concentrates on data from southern to central Finland, south of ca. 67°N. Northern sub-areas in Lapland are only briefly considered.

1 ADAKITIC PLUTONIC ROCKS IN FINLAND; GENERAL CHARACTERISTICS

This section considers the regional features of Finnish adakitoids and compares them with granites and gabbros. In this section, a sample is 'loosely' classified as an adakitoid if it fulfills at least 6 of 8 criteria defined above by Defant & Drummond (1990; '75% adakitoids'). Thus, for example, some degree of alteration and contamination of the sampled rocks is allowed. The samples cover both Archaean and Proterozoic domains in Finland with variable sampling density. Plutonic rocks were selected for the study because it is assumed that they correspond more closely to (present) upper crustal compositions compared to supracrustal igneous rocks that may have been more susceptible to alteration processes. When considering the tectonic settings of Andean rocks, Wilson (1989) noted a close spatial association between calc-alkalic volcanic and plutonic rocks. She concluded that the plutonic roots represent high-level (<10 km) magma chambers. These ideas can be applied also in this work, since in the deeply eroded Finnish bedrock we often only see the plutonic root zones of the former volcanic rocks. The granitic and gabbroic plutonic rocks were chosen for comparison to emphasize and detect features that are only characteristic of adakitoids. As a special granite group, the characteristics of anorogenic Finnish rapakivi samples, carrying signatures from the lower and upper crust (Rämö & Haapala 2005), are also considered. Moreover, I compare Finnish adakitoids with selected examples of adakites, TTGs and sanukitoids adopted from the literature. The restite mineralogy of fractionation of adakitic rocks is also considered.

1.1 Samples and standards used in this study

The data used in this study are from the Rock Geochemical Database of Finland (RGDB) by Rasilainen et al. (2007). The data and descriptions are freely available on the web pages of the Geological Survey of Finland (GTK): http://hakku.gtk.fi/en/locations/search / Rock geochemical data of Finland.

The sampling strategy has been based on a stratified procedure described in Rasilainen et al. (2007), where the number of samples per area depends on the lithological variation seen on geological maps. The sample spacing of lithogeochemical primary data used in this study varies between ca. 0–10 km, the majority (ca. 80%) of samples being closer than 6 km (Ruotoistenmäki 2016). The analytical methods have been explained in detail in Sandström (1996) and Rasilainen et al. (2007).

The elements, standards, units and analytical methods used in this study are presented in

Table 2. Elements, standards, measurement units and analytical methods used in this study. Values of C1 chondrite are from Anders & Grevesse (1989) and Kerrich & Wyman (1996). AFP gmean = geometric mean of all Finnish plutonic rock samples. AFP nbdat = number of samples used for calculation the AFP gmean. The samples were analysed in the chemical laboratory of the Geological Survey of Finland (Rasilainen et al. 2007). Note that for some elements analysed by various methods, the C1 value is the same but AFP varies.

Element	Method	Unit	AFP gmean	AFP nbdat	C1 Chondrite	Element	Method	Unit	AFP gmean	AFP nbdat	C1 Chondrite
Al	ICPAES	[ppm]	9622.43	3051	8679.70	Nd	ICPMS	[ppm]	23.37	3052	0.45
Al_2O_3	XRF	[%]	14.75	3059	1.64	Ni	ICPAES	[ppm]	11.10	2627	11000.00
Ba	ICPAES	[ppm]	89.70	2983	2.34	P	ICPAES	[ppm]	407.52	3053	1221.98
Ba	XRF	[ppm]	577.90	3044	2.34	P_2O_5	XRF	[%]	0.14	2825	0.28
Ca	ICPAES	[ppm]	3165.02	3058	9219.63	Pb	XRF	[ppm]	30.08	2982	2.47
CaO	XRF	[%]	2.56	3059	1.29	Pr	ICPMS	[ppm]	6.86	2965	0.09
Ce	ICPMS	[ppm]	54.30	3054	0.60	Rb	XRF	[ppm]	90.16	2970	2.30
Co	ICPAES	[ppm]	6.60	2921	502.00	Rb	ICPMS	[ppm]	79.45	3030	2.30
Co	ICPMS	[ppm]	9.64	2634	502.00	Sc	ICPMS	[ppm]	10.14	2542	5.82
Cr	ICPAES	[ppm]	19.22	2404	2660.00	Sc	ICPAES	[ppm]	2.88	2951	5.82
Dy	ICPMS	[ppm]	2.89	2891	0.24	SiO_2	XRF	[%]	65.28	3059	22.80
Er	ICPMS	[ppm]	1.54	2841	0.16	Sm	ICPMS	[ppm]	4.44	3003	0.15
Eu	ICPMS	[ppm]	0.88	3021	0.06	Sr	XRF	[ppm]	283.44	3051	7.80
Fe	ICPAES	[ppm]	20946.00	3056	190443.40	Sr	ICPAES	[ppm]	12.32	3033	7.80
FeO	XRF	[%]	3.10	3059	24.50	Ta	ICPMS	[ppm]	0.51	2931	0.01
Ga	XRF	[ppm]	25.16	3037	10.00	Tb	ICPMS	[ppm]	0.55	2986	0.04
Gd	ICPMS	[ppm]	3.94	3003	0.20	Th	ICPMS	[ppm]	6.39	3013	0.03
Hf	ICPMS	[ppm]	3.86	3047	0.10	Th	ICPAES	[ppm]	15.51	2272	0.03
Ho	ICPMS	[ppm]	0.54	2912	0.06	Ti	ICPAES	[ppm]	1228.55	3058	437.64
K	ICPAES	[ppm]	4686.19	3055	556.21	Ti	ICPMS	[ppm]	2179.01	3055	437.64
K_2O	XRF	[%]	2.55	3053	0.07	TiO_2	XRF	[%]	0.38	3054	0.07
La	ICPMS	[ppm]	28.01	3043	0.24	Tm	ICPMS	[ppm]	0.20	2958	0.02
La	ICPAES	[ppm]	24.66	2957	0.24	U	ICPMS	[ppm]	1.52	2981	0.01
Li	ICPAES	[ppm]	19.41	2872	1.50	V	XRF	[ppm]	54.63	2940	56.50
Lu	ICPMS	[ppm]	0.19	2968	0.02	V	ICPMS	[ppm]	36.60	2915	56.50
Mg	ICPAES	[ppm]	4745.62	3058	98910.04	V	ICPAES	[ppm]	25.02	2972	56.50
MgO	XRF	[%]	1.13	2946	16.40	Y	XRF	[ppm]	16.57	2909	1.56
Mn	ICPAES	[ppm]	258.64	3031	1990.36	Y	ICPMS	[ppm]	14.72	3056	1.56
MnO	XRF	[%]	0.06	2990	0.26	Y	ICPAES	[ppm]	6.73	3047	1.56
Na	ICPAES	[ppm]	772.78	3049	5000.07	Yb	ICPMS	[ppm]	1.36	2910	0.16
Na_2O	XRF	[%]	3.56	3036	0.67	Zr	ICPMS	[ppm]	141.36	3051	3.94
Nb	ICPMS	[ppm]	7.29	3045	0.25	Zr	XRF	[ppm]	157.87	3041	3.94

Analytical methods:

XRF: X-ray fluorescence spectrometry using pressed powder pellets.

ICPAES: Inductively coupled plasma atomic emission spectrometry after aqua regia digestion.

ICPMS: Inductively coupled plasma mass spectrometry after hydrofluoric acid-perchloric acid dissolution and lithium metaborate/ sodium perborate fusion.

For detailed descriptions of the analytical methods, see Sandström (1996) and Rasilainen et al. (2007).

Table 2. The element concentrations are normalized by C1 chondrite (Anders & Grevesse 1989, Kerrich & Wyman 1996) and the geometric mean of all Finnish plutonic rocks (AFP), including 1275 samples from Archaean plus 1784 from Proterozoic domains, i.e. 3059 samples from the RGDB.

From Table 2, it can be seen that the contents of some elements (e.g. vanadium) can vary significantly, depending on the method of analysis used. This may be due to the location of the element in various minerals, for example in silicates, sulphides or oxides (e.g. Sandström 1996). In the following, it will be seen that the trends, variations and peak locations of elements of both Archaean and Proterozoic sub-area samples in corresponding rock groups have many similarities, despite the large age differences. Such age-independent systematic characteristics support the reliability of the used methods. In this study, the main emphasis is on considering the general trends and amplitude variations of various rock groups. Thus, many interesting details will be less considered, but still presented as indications for further studies.

In this study, the geometric means (gmean) of concentrations have generally been used, because it was observed that for almost all elements within the Finnish plutonic sample set, the distribution of concentrations is positively skewed, i.e. with a long 'tail' at the maximum end of the distribution curve (Ruotoistenmäki 2016). In such cases, the arithmetic mean (amean) would be biased towards high values. For example, for TiO_2 in Figure 1, amean is 0.54% and gmean 0.38%. This fact has often been neglected in the literature when reporting statistics from analysis for large numbers of samples. If the distribution curve approaches normal (e.g. Al_2O_3 in Fig. 1; amean 15.0%, gmean 14.7%) or is negatively skewed (tail on the minimum side, such as that of SiO_2; amean 65.9%, gmean 65.3%), both the arithmetic and geometric averages approach each other. When there are multiple peaks (e.g. K_2O; amean 3.2, gmean 2.5; and SiO_2), the geometric average is also a less reliable estimate

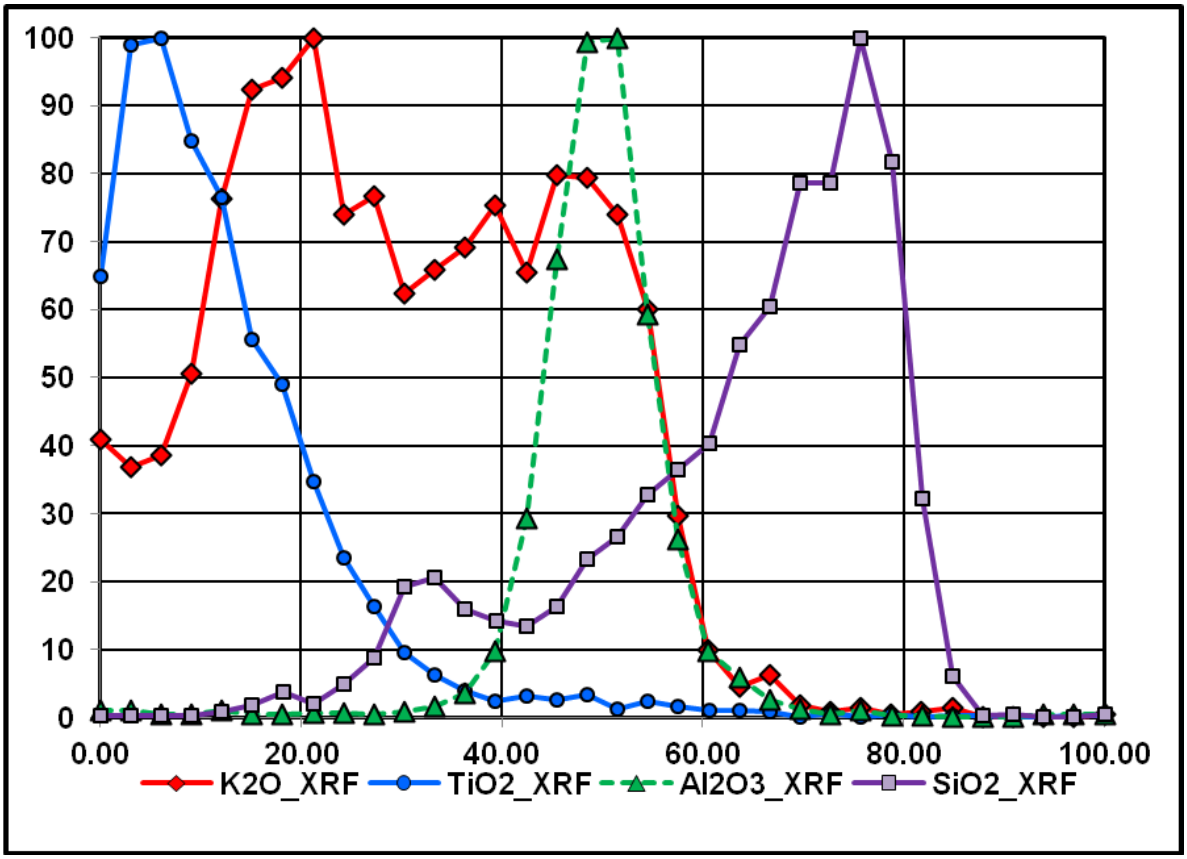

Fig. 1. Examples of the distribution of K_2O (multiple peaks), TiO_2 (skewed to maxima), Al_2O_3 (almost 'normal' distribution) and SiO_2 (multiple peaks, skewed to minima). For comparison, the corresponding frequencies (y-axis) and element prc contents (x-axis) have been scaled to vary between 0–100.

and, for instance, visually selected peak (modal) values should be used.

In Figure 2, two data groups (A.Adak and P.Adak) have been normalized by AFP and C1 chondrite. In the diagrams, concentrations normalized by AFP vary around unity, whereas chondrite-normalized concentrations vary from ca. 0.001 to close to 1000. Therefore, the chondrite-normalized spectra on a logarithmic scale appear very similar, and almost identical, while on a linear scale for the AFP-normalized spectra, the differences in trends, amplitudes and signs of peaks are distinct. For example, the high Sr peaks and sharp step from HREE to compatibles Lu → Ca are difficult to detect in the C1-normalized spectrum. Moreover, the differences in trends LREE → HREE are very difficult to distinguish in the C1-normalized spectrum. These diagrams clearly demonstrate that, when considering and comparing crustal rocks of Finland, the best standard is AFP because of its high resolution compared to C1. The data of the diagrams in Figure 2 will be considered in more detail later in the text.

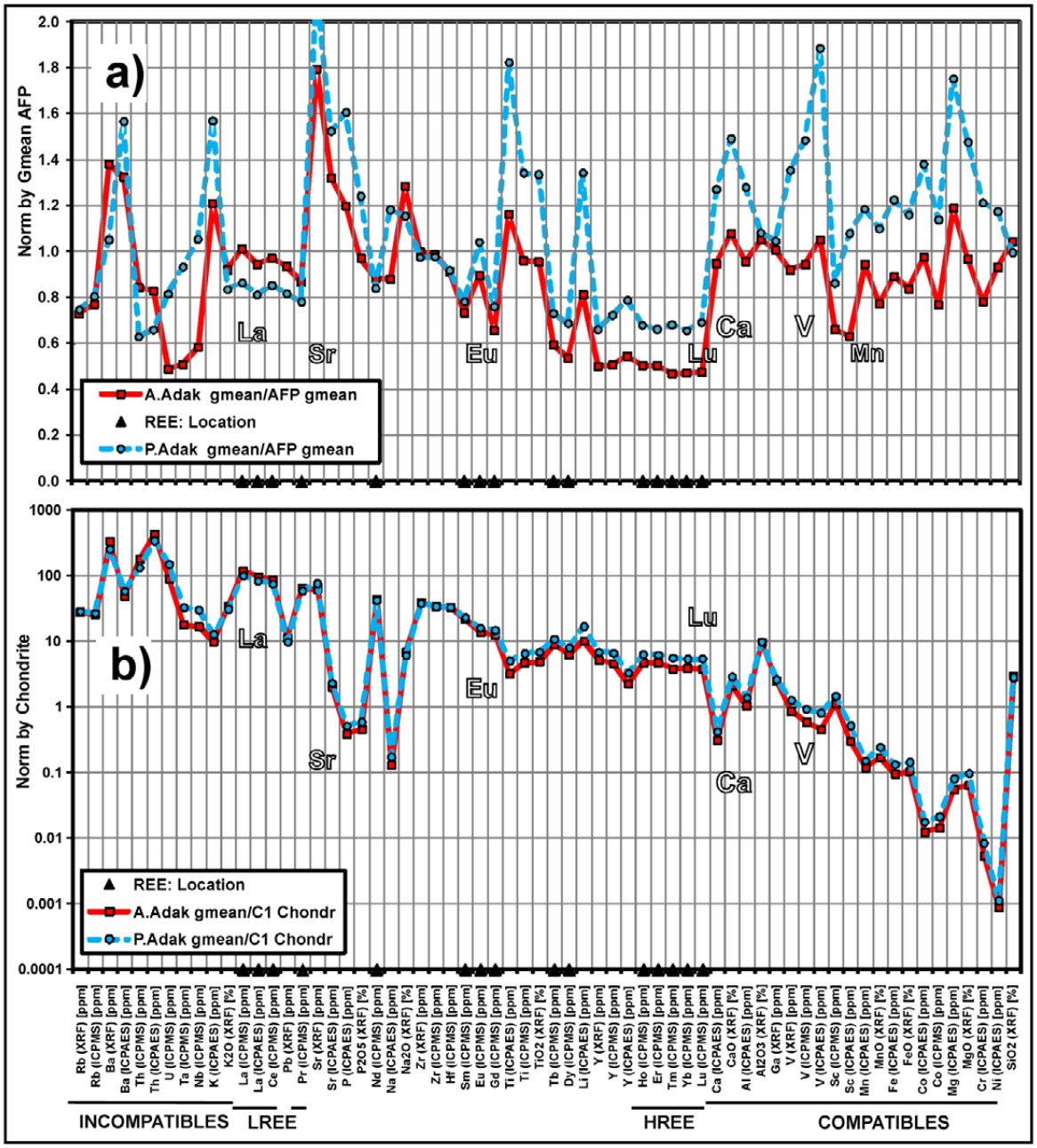

Fig. 2. Example of the normalization of Archaean and Proterozoic adakitic sample groups (A.Adak and P.Adak) by (a) the geometric means of all Finnish plutonic rock samples (AFP), and (b) C1 chondrite. Note the much better resolution of peaks and trends (slopes) on linear scale AFP-normalized diagrams compared to logarithmic scale C1-normalized diagrams. The location of REE has been marked by black triangles on the x-axis.

In the diagrams in Figure 2, the rock groups are chemically compared by using the incompatible → compatible sequence ('PP spectrum') defined by Pearce & Parkinson (1993) and Pearce & Peate (1995), who studied the various components of subduction-related arc magmas. In this study, the AFP-normalized PP spectrum is generally used for the comparison of various rock groups because of their high resolution, as demonstrated above. It must be emphasized that normalization by AFP does not refer to any genetic link between AFP and normalized data. The linear scale of AFP normalization simply 'magnify visible' the relative differences and characteristics of the various data analysed here.

Location of samples

Figure 3 presents a simplified map of the bedrock of Finland, modified af ter Korsman et al. (1997). The subdivision of sub-areas has been partly adopted from Nironen et al. (2002), Lehtinen et al. (2005) and Vaasjoki et al. (2005). However, some of their sub-area borders are poorly defined and, therefore, I have used GTK regional scale geophysical maps and data to define and combine the borders of some regional- and local-scale sub-areas. The term 'sub-area' is used in this study instead of terms such as 'terrain', 'block', 'belt', 'domain' and 'complex', which have been used variably and often non-systematically for defining geologically solid units in Finland. The sub-area division is the same that I used in the Lithogeochemical Atlas of Finland (Ruotoistenmäki 2016), where the statistics on the chemistry of each sub-area and rock types are described.

In the following, the terms 'Archaean' and 'Proterozoic' are associated with rocks sampled in the Archaean or Proterozoic sub-areas in Figure 3. It must be noted that in some cases on the Archaean side, the zircon age of the rock sample may be Proterozoic, although the primary material can contain a significant component of recirculated/remelted Archaean crust (e.g. Huhma 1986). Moreover, the Archaean–Proterozoic border is dependent on the current erosion level in collision areas characterized by over- and underthrusting tectonics, as demonstrated in the seismic cross-section in Figure 67.

Figure 4 depicts the distribution of all 3059 plutonic rock samples in the database (RGDB), and Figure 5 to Figure 6 illustrate the distributions of the granitic and gabbroic samples used in this study. The names of rock types are based on those given in the rock geochemistry database by Rasilainen et al. (2007). It must be emphasized that in some cases, the rock types are based on field observations. Therefore, the maps and diagrams must be considered as a statistical entity where some individual details can be erratic.

The symbols emphasized with red dots on the maps refer to adakitic samples. In the following, the adakitic granite and gabbro samples are omitted from the corresponding diagrams of all gabbros and granites and included in the diagrams of adakitoids whose areal distribution is given in Figure 4. In this section, a sample is (if not otherwise mentioned) classified 'loosely' as an 'adakitoid' if it fulfills at least 6 of 8 criteria defined above by Defant & Drummond (1990) and Thorkelson & Breitsprecher (2005), i.e. '75% adakitoids', thus including samples possibly modified by contamination, alteration and metamorphic processes.

From the maps, it can be seen that, when excluding some Archaean supracrustal sub-areas (green and grey in Fig. 3), the coverage of plutonic rocks in Finland is relatively large and relatively homogeneous in most sub-areas. The gabbros are sparser compared to granitic rocks and they are clustered in groups that are more distinct. The areal distribution and quantity of plutonic rocks having adakitic characteristics is surprisingly large in Figure 4. In Archaean areas, the number of adakitoids (6/8 criteria fulfilled = '75% adakitoids') is 540/1275 samples (42%) and that of 8/8 adakitoids ('100% adakitoids') is 178/1275 samples (14%). Correspondingly, in Proterozoic areas, the number of '75% adakitoids' is 323/1784 samples (18%) and that of '100% adakitoids' is 106/1784 samples (6%). Thus, the relative number of adakitic samples (/ TTGs / sanukites) in Archaean areas is more than twice that in Proterozoic areas. Käpyaho et al. (2006) noted that the Finnish part of the western Karelian Province mostly (~80%) consists of migmatized and unmigmatized, ~2.90–2.745 Ga TTG gneisses. However, as given above,

the adakitic samples cover 'only' 14–42% of all plutonic samples collected from Archaean subareas, which is not consistent with their very high percentage of coverage value, or their TTGs do not fulfil the definition of adakitoids given above.

During this work, I also tested the distribution of sanukitoids in the database. Sanukitoids have been interpreted as derivatives from melting of enriched mantle wedge above the subducting slab, thus having a genesis that is close to that proposed for adakitoids. Halla (2005) defined sanukitoids as primitive rocks, with SiO_2 55–60%, Mg numbers > 0.6, Ni > 100 ppm, Cr > 200 ppm, K_2O > 1%, Sr and Ba > 500 ppm and Rb/Sr < 0.1. Moreover, sanukitoids are strongly LREE enriched with minor negative Eu anomalies. Surprisingly, while adakitoids are so common, less than ten samples out of 3059 plutonic rock samples had sanukitoid characteristics as defined above (only one fulfilling all sanukitoid criteria). However, more 'sanukitic adakitoids' were obtained, when using slightly broader sanukitoid criteria adopted from Heilimo et al. (2010): SiO_2 = 55–70%, Na_2O/K_2O = 0.5–3, MgO = 1.5–9%, Mg number = 45–65, K_2O = 1.5–5.0%, Ba+Sr > 1400 ppm and $(Gd/Er)_N$ = 2–6; see Figure 31 and Figure 32.

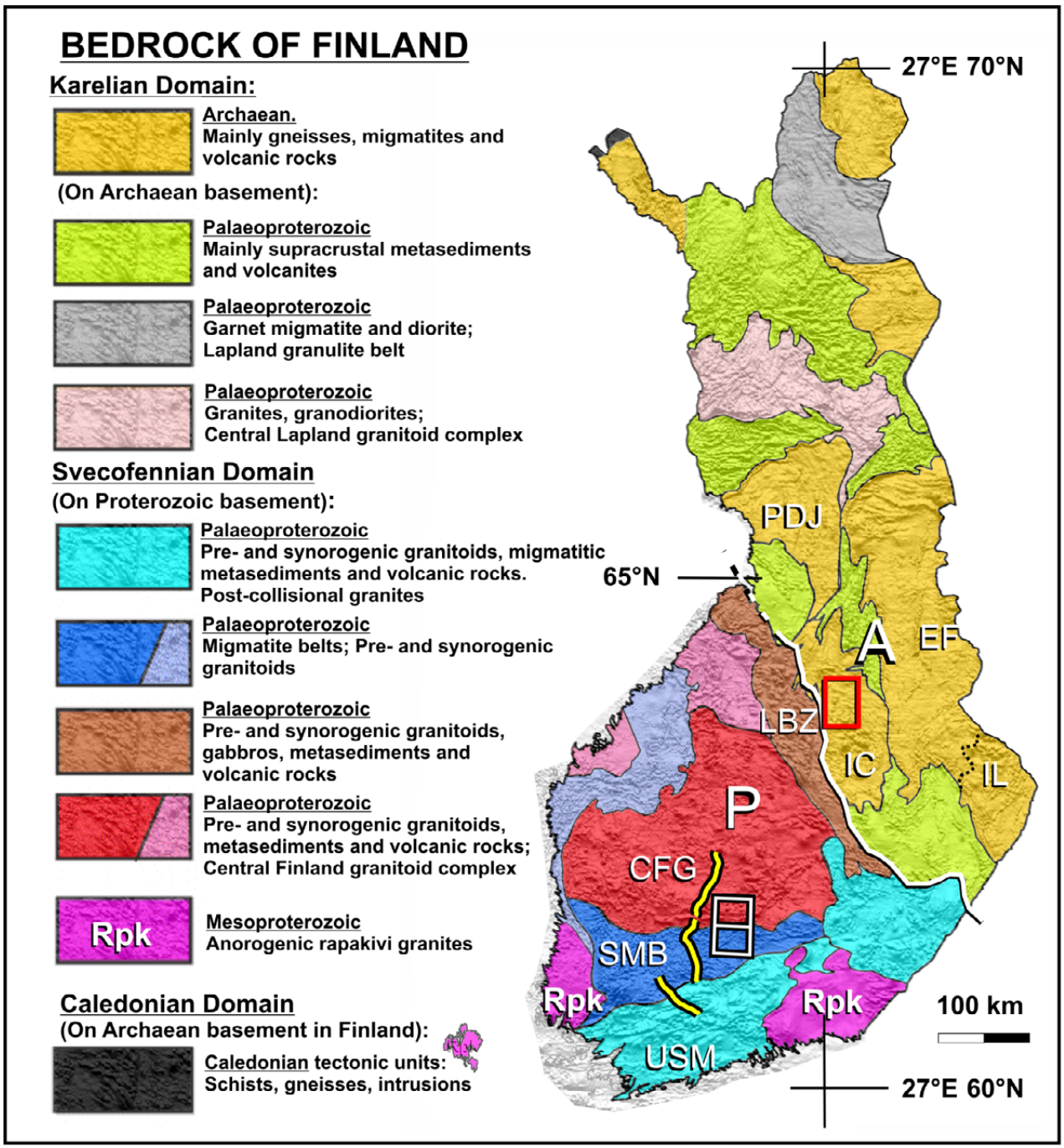

Fig. 3. Bedrock of Finland modified after Korsman et al. (1997). The major trends have been emphasized by combining the map with the hillshaded magnetic high-altitude map of GTK, Finland (for details, see e.g. Korhonen 2005 and Hautaniemi et al. 2005). The white line gives the approximate border of Archaean (A) and Proterozoic (P) sub-areas in Finland. The sub-areas are the same as used in the Lithogeochemical Atlas of Finland (Ruotoistenmäki 2016): LBZ = Ladoga–Bothnian bay zone. Rpk = rapakivi sub-areas in southern Finland. USM = Uusimaa sub-area, SMB = southern Finland migmatite sub-area, CFG = central Finland granitoid sub-area, EF = eastern Finland sub-area, IL = Ilomantsi sub-area (southernmost part of EF bordered by the dotted line), IC = Iisalmi sub-area, PDJ = Pudasjärvi sub-area. The white-black squares border the local-scale study area of Padasjoki-Kaipola considered in section 4. The thick yellow-black lines show the location of the FIRE seismic reflection profile considered in the same section. The red square borders the Iisalmi-Lapinlahti area considered in section 5.

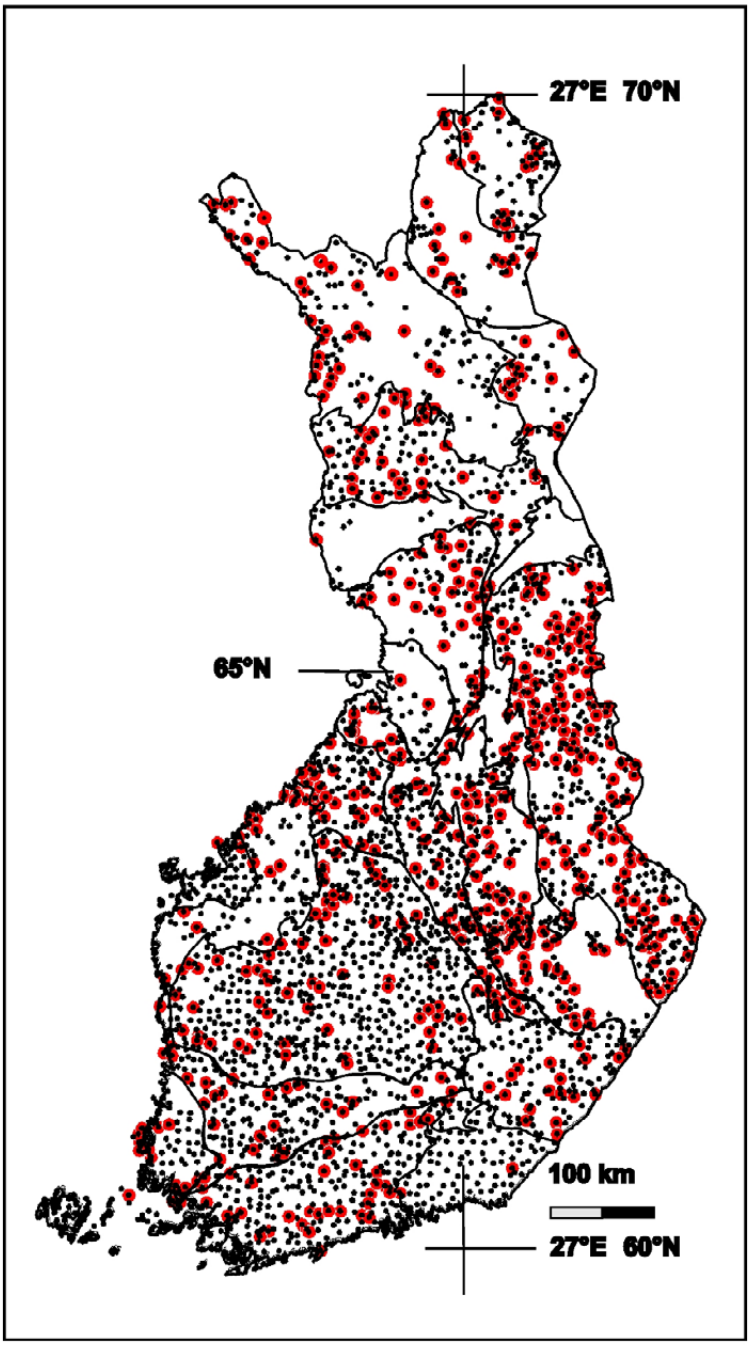

Fig. 4. Location of all the plutonic rock samples in the database (RGDB). Red dots refer to adakitic samples. The lithological borderlines are from Figure 3. On the map, a sample is classified 'loosely' as 'adakitic' if it fulfills at least 6 of 8 criteria defined above by Defant & Drummond (1990) and Thorkelson & Breitsprecher (2005), i.e. '75% adakitoid'.

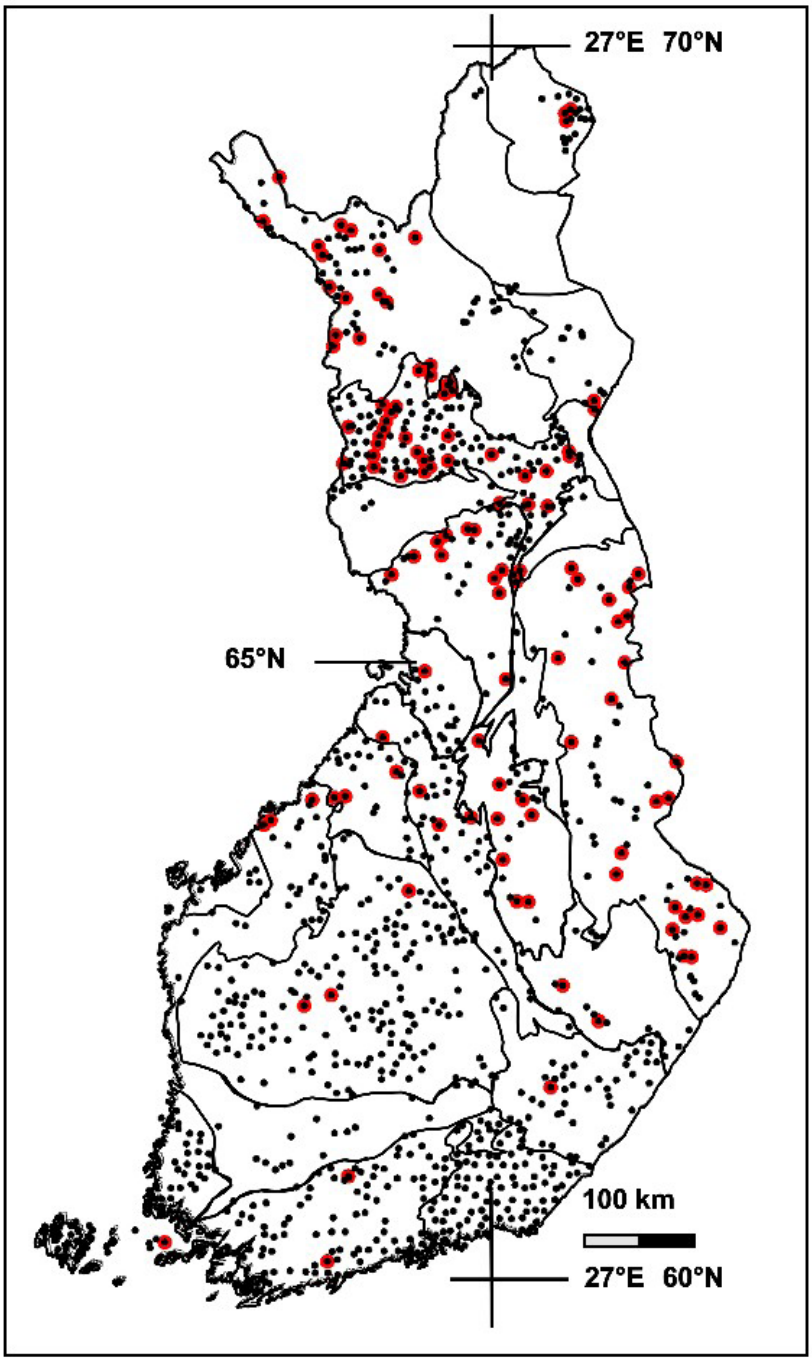

Fig. 5. Location of the granitic samples studied in this work. Red dots refer to adakitic 'granites'. The lithological borderlines are from Figure 3.

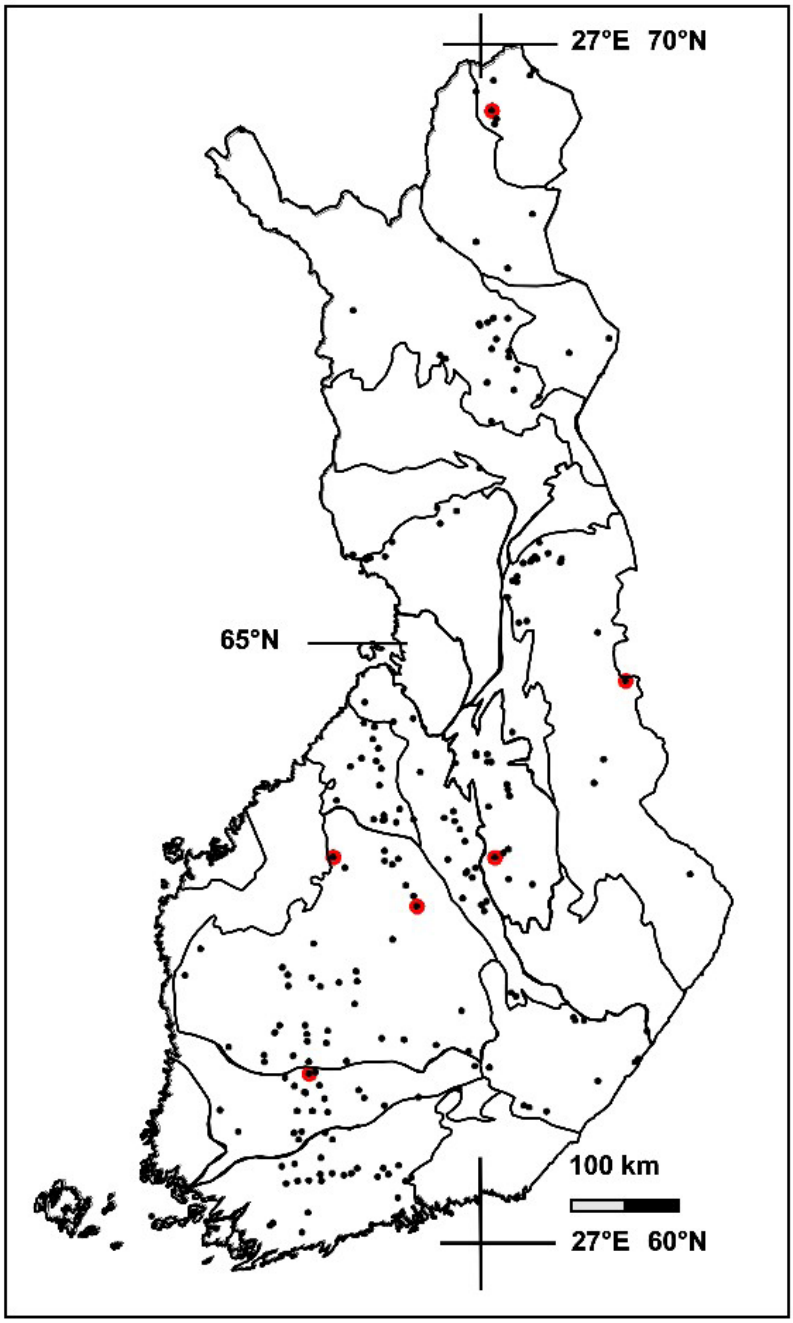

Fig. 6. Location of the gabbroic samples studied in this work. Red dots refer to adakitic ‘gabbros’. The lithological borderlines are from Figure 3.

1.2 Petrophysical characteristics of the samples

Figure 7 presents a statistical summary of the densities (D) [kg/m^3] and magnetic susceptibilities (K) [SI*10^6] of all plutonic rock samples (AFP) and separately Archaean and Proterozoic plutonic area samples (AFP-Arch and AFP-Prot). The statistical parameters in the figure are trendsetting because the distributions are not normal. For example, the given arithmetic averages are not reliable estimations for expectation values and the modal (most common), peak values from the distribution curves are more plausible. The major characteristics of these rocks are the significantly higher density of Proterozoic plutonic rocks (average ca. 2653, mode 2685 kg/m^3) compared to Archaean plutonic rocks (average ca. 2574, mode 2629 kg/m^3). This refers to higher amounts of mafic minerals in Proterozoic plutonic rocks. This is also supported by the higher susceptibilities of paramagnetic values of Proterozoic samples (ca. 220*10^{-6} SI) compared to Archaean (ca. 150*10^{-6} SI). The high ferrimagnetic peak of Archaean samples (around ca. 15 000*10^{-6} SI) refers to a higher relative content of magnetite in these samples and thus the evolutionary environment favouring oxide precipitation (magnetite) before iron-containing mafic silicates (e.g. Puranen 1989). In summary, Proterozoic sub-area samples are more mafic but magnetite poor, while Archaean samples are more felsic but magnetite rich.

Figure 8 depicts the cumulative frequencies of densities and susceptibilities of granitic, gabbroic and adakitic samples. From the diagrams, it can be seen that Proterozoic granites (446 samples) are clearly denser (gmean ca. 2640 kg/m^3) than Archaean granites (336 samples, gmean ca. 2620 kg/m^3), but mainly paramagnetic (susceptibility below ca. 1000*10^{-6} SI, mode ca. 160*10^{-6} SI), while the majority of Archaean granites are strongly ferrimagnetic (susceptibility above ca. 1000*10^{-6} SI, modes at ca. 90*10^{-6} and 16 000*10^{-6} SI). As in all plutonic rocks above, iron is also mainly in silicates in Proterozoic granites, while Archaean samples contain less iron in silicates but more magnetite. The rapakivi granite samples are the densest granites (gmean ca. 2654 kg/m^3, 147 samples) and contain both para- and ferrimagnetic components (main peaks at ca. 160*10^{-6} and 1600*10^{-6}SI).

The Archaean gabbros (74 samples) are generally denser (bimodal gmean ca. 2970 kg/m^3) than Proterozoic gabbros (gmean ca. 2950 kg/m^3, 137 samples). Their magnetic distributions are practically identical, mainly ferrimagnetic (gmeans of both ca. 2000*10^{-6}; modes at ca. 1000*10^{-6} SI and 630*10^{-6} SI, respectively).

Proterozoic adakitoids are ca. 30 kg/m^3 denser (gmean ca. 2720 kg/m^3, 323 samples) than Archaean adakitoids (gmean ca. 2690 kg/m^3, 540 samples). Their magnetic distributions are almost identical, having both paramagnetic and ferrimagnetic components (modes at ca. 250*10^{-6}, 180*10^6 and 20 000*10^{-6}, 9000*10^{-6} SI). The higher density and slightly higher paramagnetic values of Proterozoic adakitoids refer to their more mafic average composition.

From Figure 8, it can be summarized that the densities of samples from Proterozoic and Archaean sub-areas clearly differ for gabbros, granites and adakitic rocks. The high-density group of Archaean gabbros is interesting, because Archaean granites and adakitoids are clearly less dense. The susceptibilities of gabbros and adakitoids are almost identical, but those of granites (granitoids) differ significantly, referring to variable amounts of magnetite, pyrrhotite and mafic minerals. In particular, the high magnetite content of Archaean granites is significant.

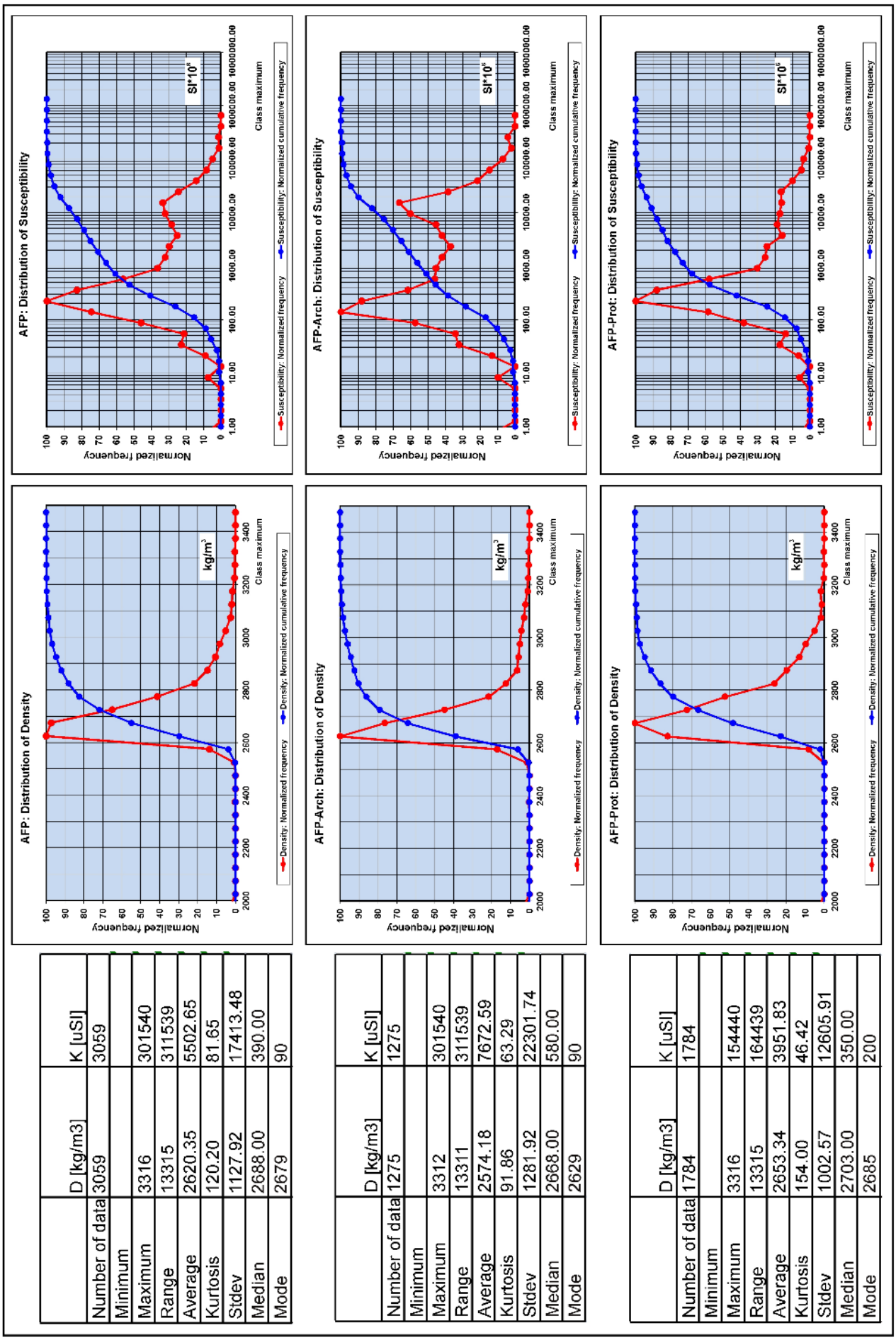

	D [kg/m3]	K [uSI]
Number of data	3059	3059
Minimum		
Maximum	3316	301540
Range	13315	311539
Average	2620.35	5502.65
Kurtosis	120.20	81.65
Stdev	1127.92	17413.48
Median	2688.00	390.00
Mode	2679	90

	D [kg/m3]	K [uSI]
Number of data	1275	1275
Minimum		
Maximum	3312	301540
Range	13311	311539
Average	2574.18	7672.59
Kurtosis	91.86	63.29
Stdev	1281.92	22301.74
Median	2668.00	580.00
Mode	2629	90

	D [kg/m3]	K [uSI]
Number of data	1784	1784
Minimum		
Maximum	3316	154440
Range	13315	164439
Average	2653.34	3951.83
Kurtosis	154.00	46.42
Stdev	1002.57	12605.91
Median	2703.00	350.00
Mode	2685	200

Fig. 7. Petrophysical characteristics of all plutonic samples (AFP), Archaean plutonic samples (AFP–Arch) and Proterozoic plutonic samples (AFP–Prot).

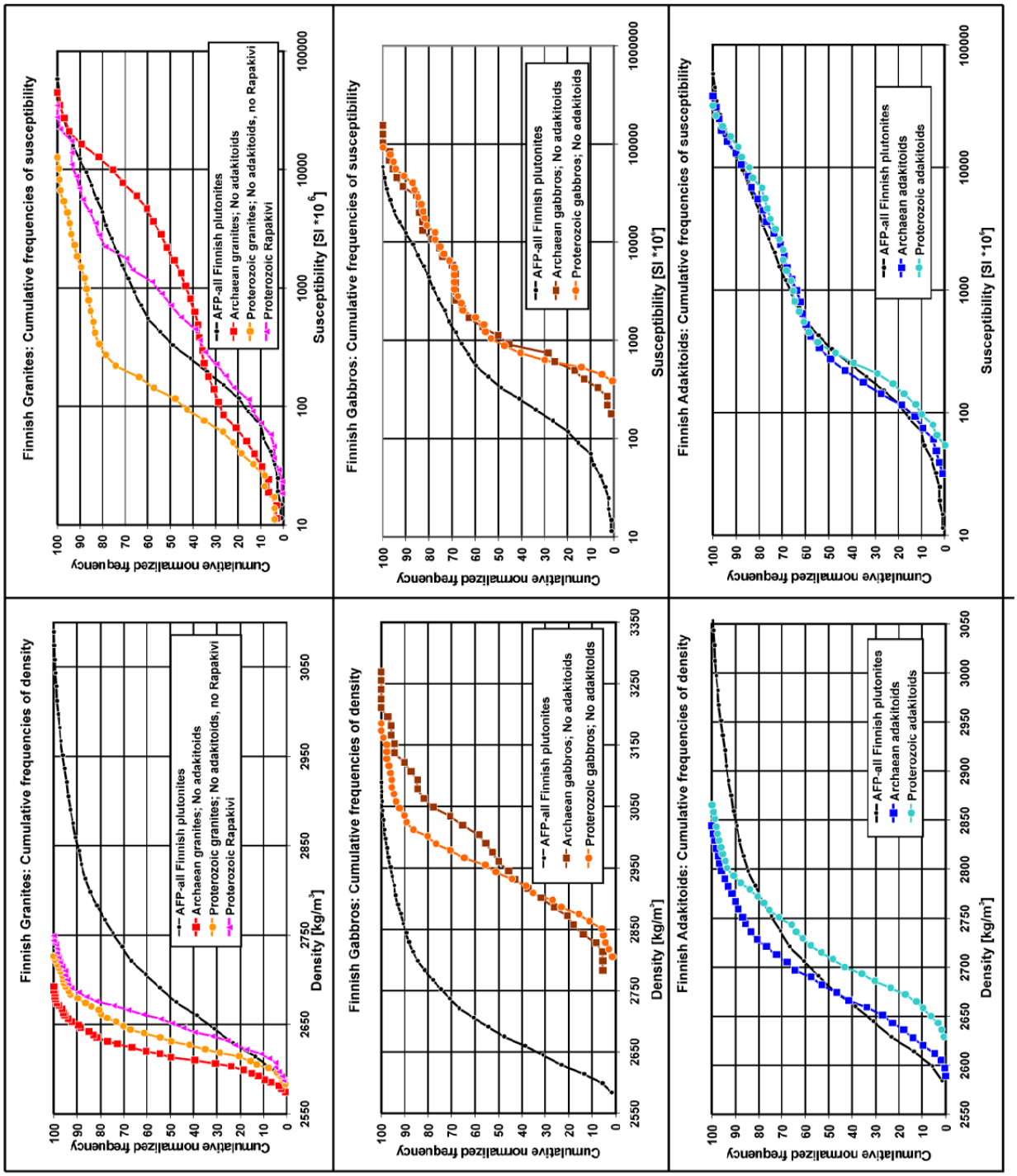

Fig. 8. Cumulative frequencies of densities and susceptibilities of the samples.

1.3 Chemical characteristics of the samples

In this report, various geochemical and petrophysical diagrams are considered to distinguish and emphasize the main characteristics of the samples, thus also testing their resolution ability. It must be emphasized that conclusions based solely on geochemical tectonomagmatic discrimination diagrams must be made with care. For example, Wang and Glower (1992) have demonstrated that even relatively young (Jurassic) continental rift basalts very often plot erratically in MORB and arc basalt fields in tectonomagmatic geochemical discriminant diagrams. Condie (2005) also noted that care is needed when using geochemical data on mobile elements in studying rock genesis, sources and evolution. In this section, the following diagrams are utilized:

R1-R2 diagrams

The R1-R2 diagrams by de La Roche et al. (1980), Batchelor & Bowden (1985) and Rollinson (1993) in Figure 9 and Figure 10 can be used for rapid, preliminary lithological and tectonomagmatic classification based on the geochemistry of major elements. The wide scatter of granitic and gabbroic samples in the diagrams demonstrates the statistical character of this study. Some sample names given by field geologists clearly differ from those in the diagram, perhaps representing strongly fractionated or altered samples from large gabbroic or granitic outcrops. Thus, in general, 'granites' represent more felsic and 'gabbros' more mafic plutonic rock entities in the following diagrams (names given without quotation marks).

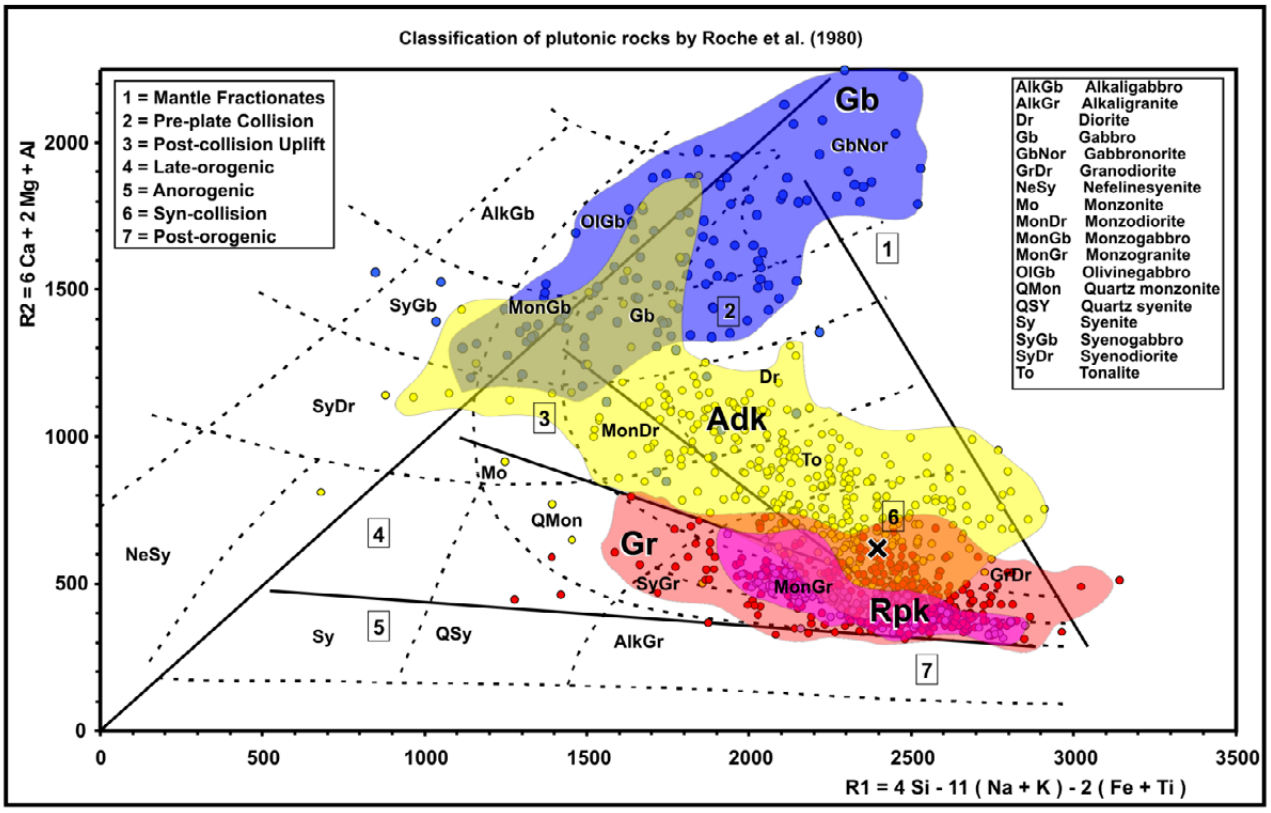

Fig. 9. Classification of samples from Proterozoic areas in the R1-R2 diagram (De La Roche et al. 1980). The tectonomagmatic fields have been adopted from Batchelor & Bowden (1985) and rock-type boundaries have been modified according to Rollinson (1993). Gb: 'Gabbroic' samples (blue), Adk: Adakitoids (yellow), Gr: 'Granitic' samples (red), Rpk: rapakivi granites (purple). The names of rock types are based on those given in the rock geochemistry database by Rasilainen et al. (2007). The enveloping curves of rock groups have been manually drawn by rejecting the most distinct outliers. The cross (x) in the 'syn-collision' field refers to the granodioritic, geometric mean of all Finnish plutonic rock samples (AFP; Table 2).

In the diagrams in Figure 9 and Figure 10, the Proterozoic and Archaean granites are classified as syn-collisional to late-orogenic monzo- and syenogranites, some samples being quartz monzonites and granodiorites. The scattering of Archaean samples is narrower and granodioritic samples are sparser. The Proterozoic rapakivi samples, representing samples evolved in processes in both lower and upper crust (Rämö & Haapala 2005) plot very tightly in syenogranitic, monzogranitic, granodioritic, 'late-orogenic, syn-collisional' fields.

The Proterozoic gabbros in Figure 9 are mainly located in gabbro–monzogabbro–gabbronorite fields. Tectonomagmatically, they are in pre-plate collision, or mantle fractionate fields. The Archaean gabbros in Figure 10 are less varied, mainly concentrating on olivine gabbro–gabbronorite fields, and are of the pre-plate collision or mantle fractionate type.

The Proterozoic adakitoids range in the diagram in Figure 9 from pre- to syn- and post-collisonal fields, the majority being syn-collisional tonalites. Their rock types vary from granodiorites to tonalites, diorites and gabbros. The Archaean adakitoids in Figure 10 are more widely scattered, having a more significant granodioritic–monzogranitic–syenogranitic sample group with syn- and late orogenic characteristics.

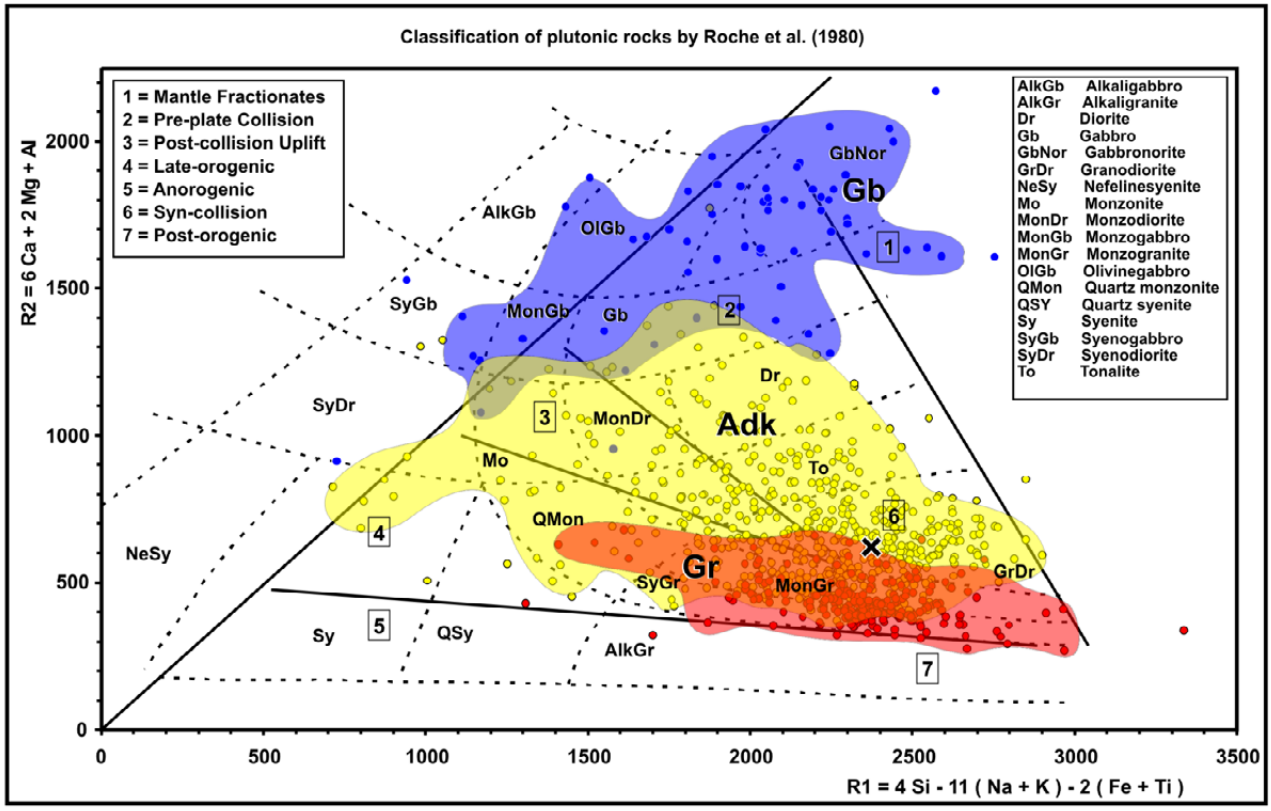

Fig. 10. Classification of samples from Archaean areas in the R1-R2 diagram (De La Roche et al. 1980). For an explanation of the fields and rock names in the diagram, see the caption of Figure 9.

Na_2O+K_2O vs SiO_2 diagram

A simpler, but more illustrative classification method in Figure 11 depicts the Na_2O+K_2O vs SiO_2 diagram by Cox et al. (1979), modified for plutonic rocks by Wilson (1989). In the diagrams, the Proterozoic adakitoid samples are mainly in sub-alkaline diorite, quartz-diorite and granite fields. In addition, the Archaean samples are located in the diorite–granite fields. Moreover, there is a more alkaline sample group compared to Proterozoic adakitoids. The gabbroic samples of both groups are mainly in gabbro fields, some being dioritic. The Proterozoic gabbros have a significant alkaline group compared to Archaean samples, which are mainly sub-alkaline. The Archaean granite samples mainly plot in the granite field, while some Proterozoic 'granites' are in the quartz-diorite field. Both granite groups are more alkaline compared to the gabbros and adakitoids above. The Proterozoic rapakivi samples are tightly located in a narrow granite–alkali-granite field.

FeO/(FeO+MgO) vs SiO_2 diagram

The FeO/(FeO+MgO) vs SiO_2 diagram by Frost et al. (2001) extrapolated to ultramafic SiO_2 contents is given in Figure 12. They used this diagram to distinguish ferroan, 'anorogenic' (A-type) granites (granitoids) from magnesian plutonic rocks. In the diagrams, the majority of Archaean and Proterozoic adakitoid samples are magnesian. The distributions of both Archaean and Proterozoic gabbros are identical, the majority of samples being low-Fe-type magnesian with fewer samples on the ferroan side. The majority of granite samples, especially the rapakivi samples, are ferroan A-type.

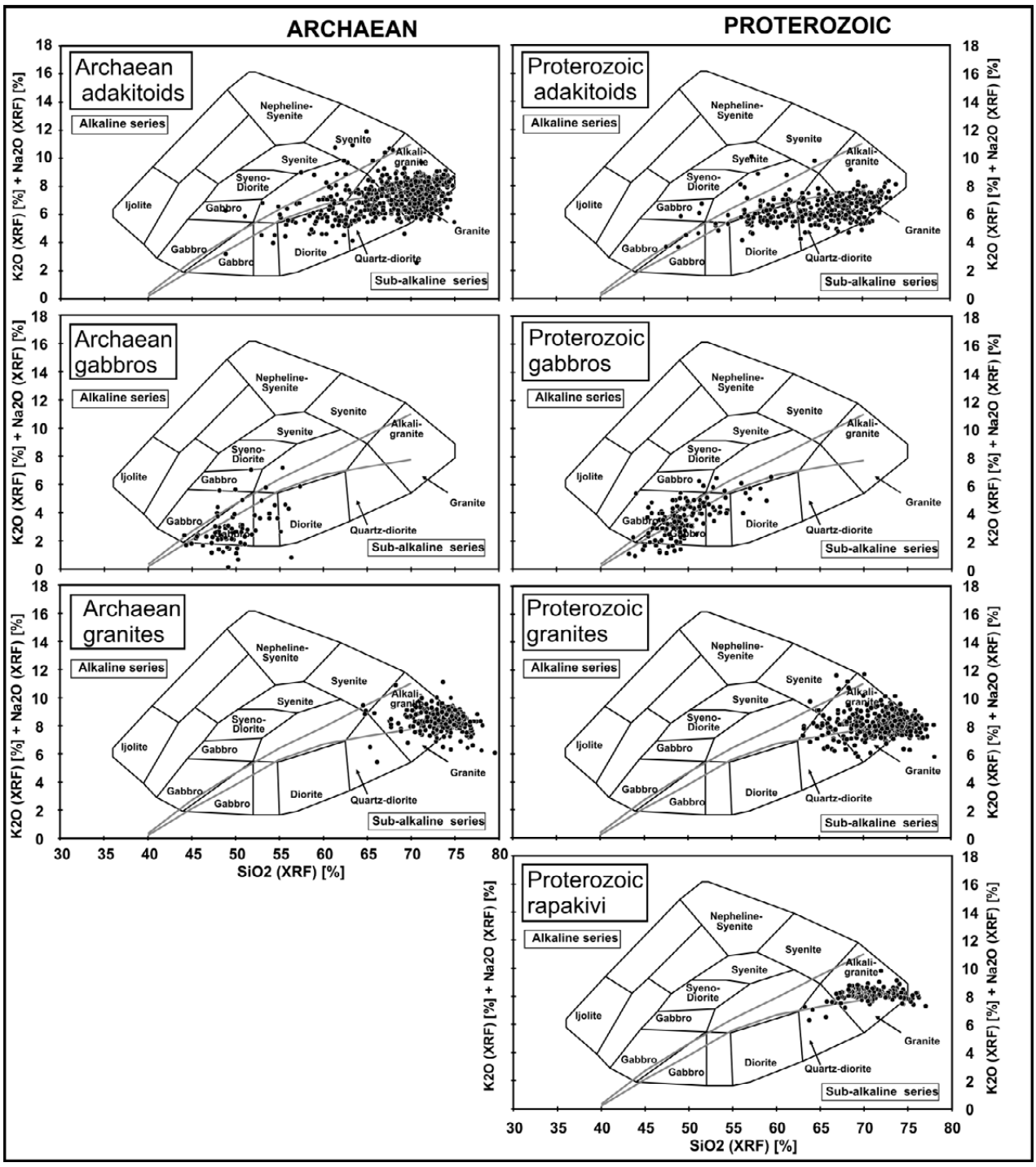

Fig. 11. Classification of samples in the Na_2O+K_2O vs SiO_2 diagram by Cox et al. (1979) modified for plutonic rocks by Wilson (1989). The enveloping border lines, representing the alkaline/sub-alkaline boundary zone, have been adopted from Rickwood (1989).

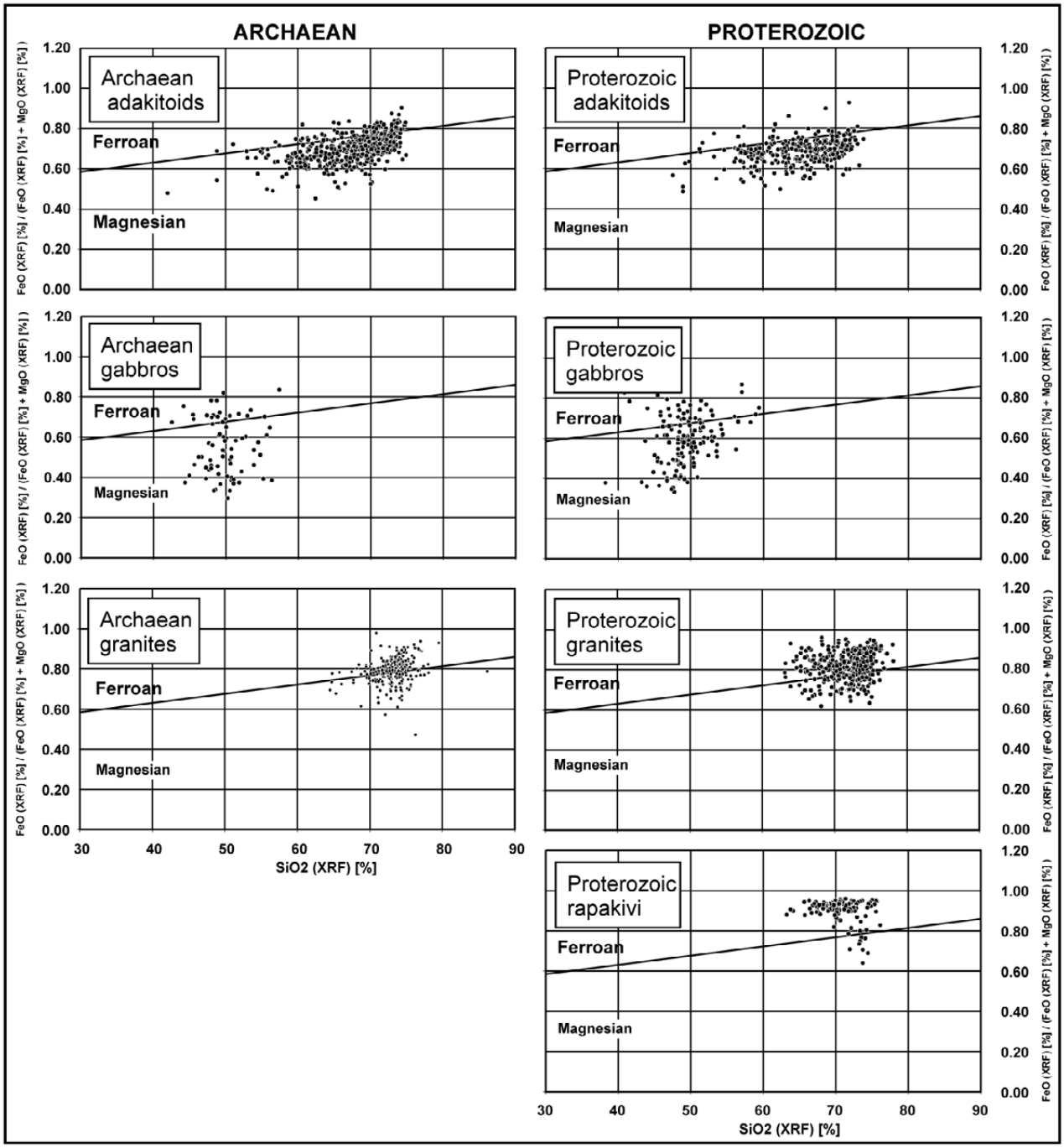

Fig. 12. Classification of samples in the FeO/(FeO+MgO) vs SiO_2 diagram by Frost et al. (2001).

A/CNK vs SiO_2 diagram

The A/CNK (=Mol Al_2O_3 / (Na_2O+K_2O+CaO)) vs SiO_2 diagram by Chappell & White (1974) is given in Figure 13. They used this diagram to distinguish 'sedimentary' (S-type) granitoids from 'true' igneous (I-type) plutonic rocks. Chappell & White (1974) defined S-types as resulting from the partial melting of metasedimentary source rocks during anatexis or ultrametamorphism. I-types are derived from source rocks of igneous composition that have not gone through the surface weathering process, or from the crystal fractionation of magmas. Herzberg (1995) noted that that granites *sensu stricto* have not been formed by the fractional crystallization of basalt or andesite, but rather by partial melting of pre-existing crustal rocks such as metapelites, which means that they should normally be of the S-type.

In the diagrams, the Archaean and Proterozoic adakitoid and gabbroic samples are distinctly of the I-type. The lack of S-type adakitoids is significant, referring to the absence of sedimentary wedge material (if they are subduction related), or the signature of sedimentary material may have been lost during the remelting and fractionation processes. The Archaean granites are mainly I-type, while a significant number of Proterozoic granite samples are also of the S-type, thus reflecting circulation and anatexis of sedimentary material, possibly related to plate tectonic processes.

The rapakivi samples are more tightly of the I-type, with the exception of a small but distinct group of some high SiO_2 (>70%) samples being S-type. These samples possibly refer to a crustal contamination component during their multi-stage fractionation and ascent processes.

K_2O+Na_2O-CaO vs SiO_2 diagram

The K_2O+Na_2O-CaO vs SiO_2 diagram by Frost et al. (2001) extrapolated to ultramafic SiO_2 contents is given in Figure 14. Using this diagram, they classified plutonic rocks into alkalic, alkali-calcic, calc-alkalic and calcic sub-types based on their composition. In the diagrams, the Proterozoic adakitoids are concentrated in calcic and calc-alkalic fields, while Archaean adakitoids are more widely distributed between alkalic and calcic fields. Wilson (1989) stated that at the present time, magmas of the calc-alkaline series are restricted in their occurrence to subduction-related tectonic settings. Consequently, she noted that the recognition of calc-alkaline characteristics in the geochemistry of ancient volcanic sequencies may be an important petrogenetic indicator. The distributions of Proterozoic gabbros are more calc-alkalic compared to Archaean gabbros, which are more calcic. The distributions of Archaean and Proterozoic granites are similar, both belonging to calc-alkalic and alkali-calcic classes. However, there is a significant low-SiO2 group (SiO2 < 70%) in Proterozoic granites. The rapakivi samples are mainly alkali-calcic, with a few high-SiO_2 samples being calc-alkalic.

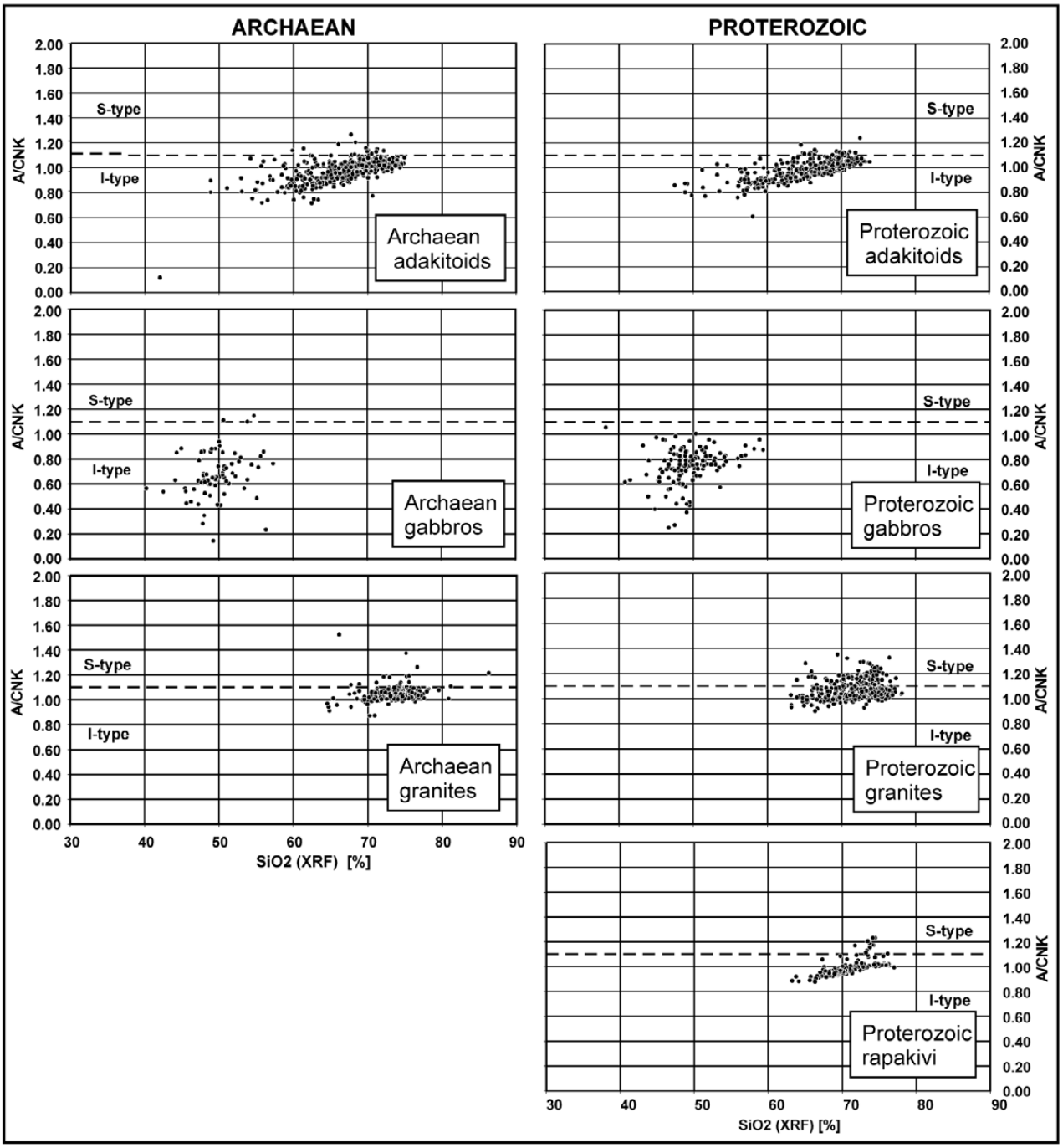

Fig. 13. Classification of samples in the A/CNK vs SiO_2 diagram by Chappell & White (1974).

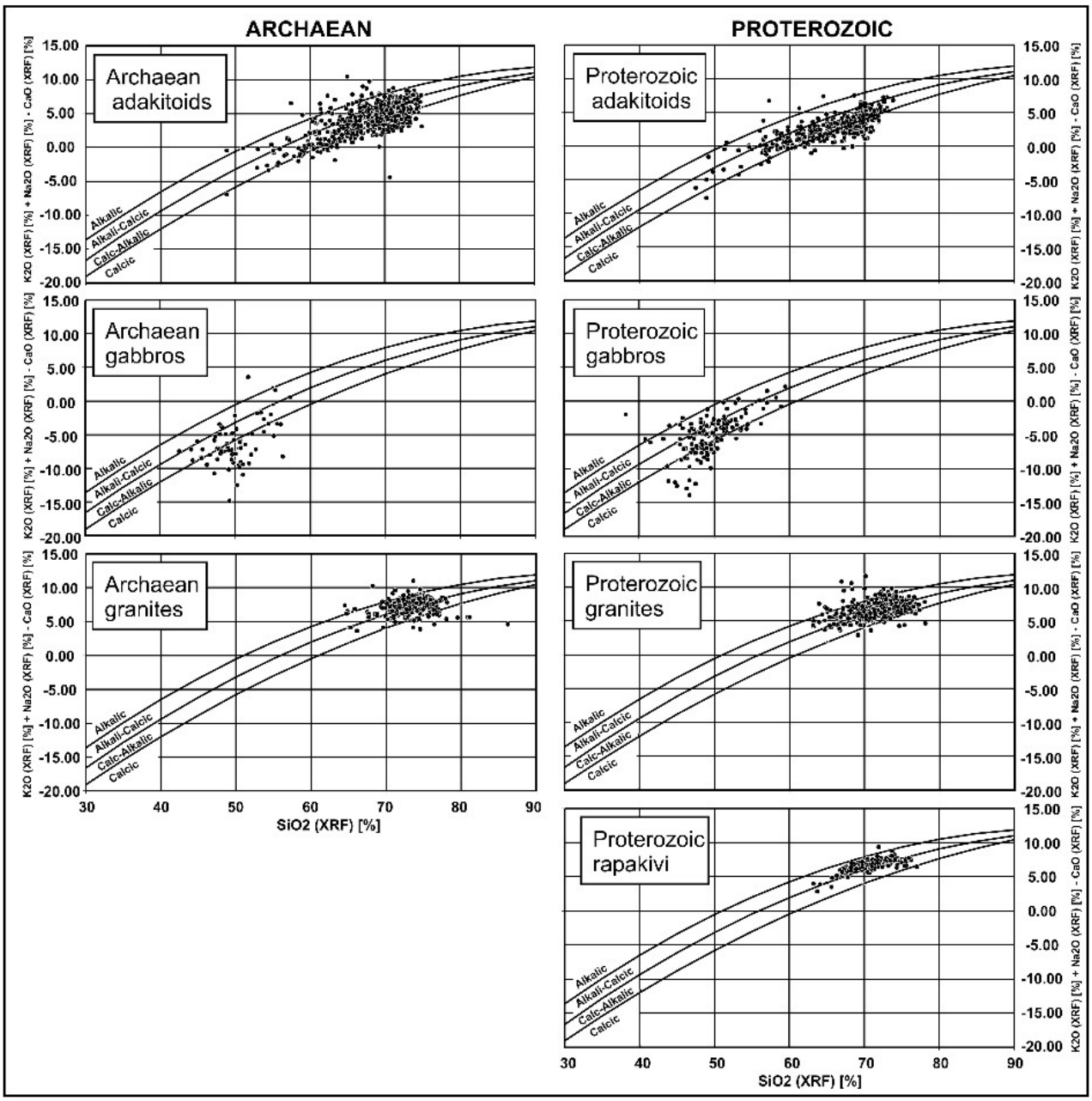

Fig. 14. Classification of samples in the K_2O+Na_2O-CaO vs SiO_2 diagram by Frost et al. (2001).

Nb/Ta vs Zr/Sm diagram

The Nb/Ta vs Zr/Sm diagram shown in Figure 15 can be used for studying the fractionation processes of plutonic rocks, such as the tectonomagmatic evolution of early continental crust (Foley et al. 2002). The diagram presents the Nb/Ta vs Zr/Sm ratios of oceanic island basalts (OIB), mid-ocean ridge basalts (MORB), island-arc basalts (IAB) and continental rocks (TTG, adakites and continental crust). In the diagram, the adakite group is characterized by decreasing Nb/Ta and increasing Zr/Sm ratios.

Foley et al. (2002) concluded that the coupled low Nb/Ta and high Zr/Sm of the early continental crust is due to partial melting of low-magnesium amphibolite and not partial melting of eclogite. On the contrary, Rapp et al. (2003) inferred that partial melting of hydrous basalt in eclogite facies produces granitoid liquids with major and trace element compositions equivalent to Archaean TTG, including the low Nb/Ta and high Zr/Sm ratios of 'average' Archaean TTG. Moreover, they proposed that TTG magmatism may have taken place beneath granite-greenstone complexes developing along Archaean intraoceanic island arcs by imbricate thrust stacking and tectonic accretion. According to Xiong (2006), model melts with TTG trace element characteristics are in equilibrium with rutile-bearing anhydrous and hydrous (amphibole bearing) eclogitic residues, but not rutile-free, amphibole-dominated residues. Rutile appears to be a necessary residual phase to account for the characteristic negative Nb–Ta anomaly in the TTG.

The data groups used in this study are strongly overlapping in this diagram, and I only use geometric averages of the sample groups to examine their general differences and characteristics.

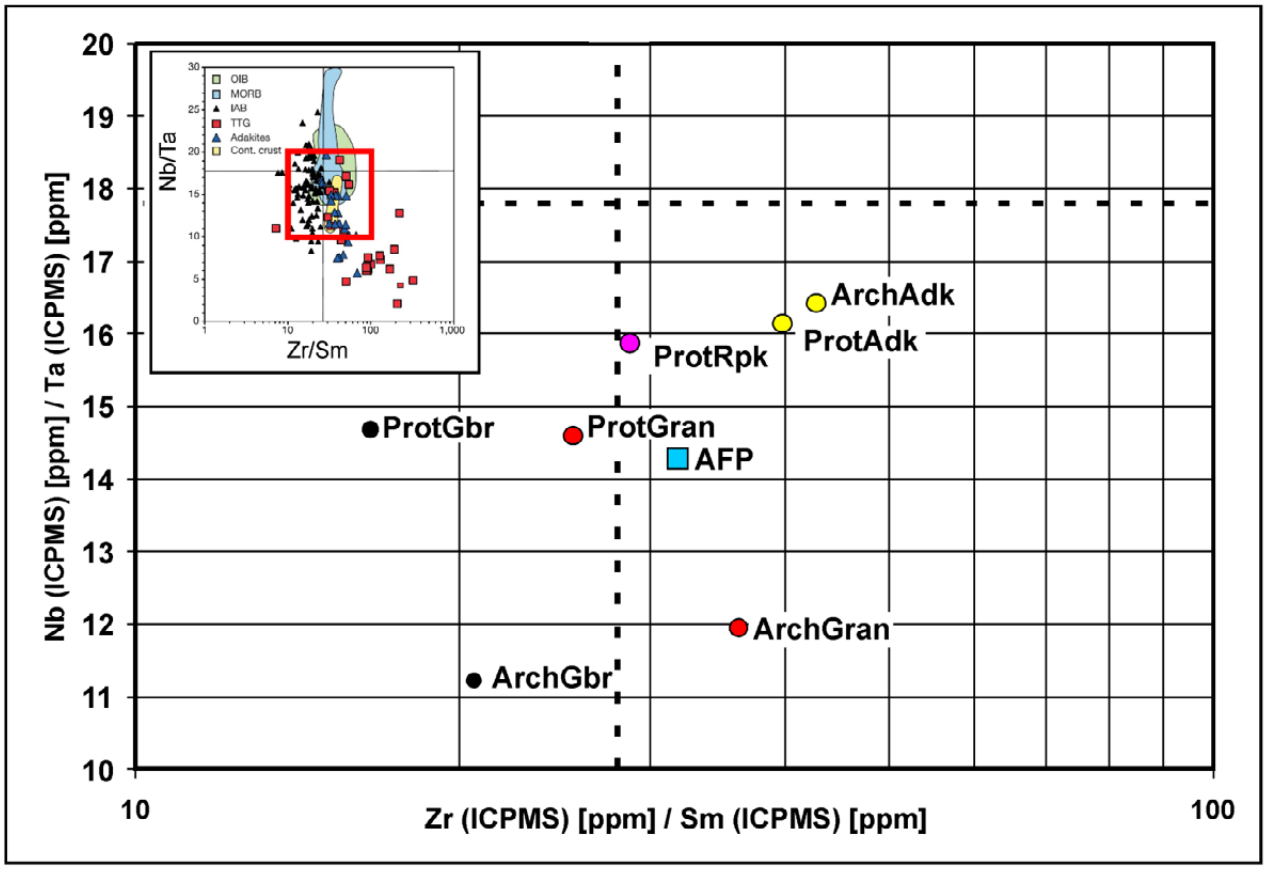

Fig. 15. Classification of the rock groups using the geometric means of the sample elements in the Nb/Ta vs Zr/Sm diagram by Foley et al. (2002) (inset upper left). The location of the borders of the diagram has been marked with a red square in the inset. The intersection of the dashed lines represents the trace element signature of primitive mantle. AFP = all Finnish plutonic rock samples considered in this study. ArchAdk = Archaean adakitoids, ArchGbr = Archaean gabbros, ArchGran = Archaean granites, ProtAdk = Proterozoic adakitoids, ProtGbr = Proterozoic gabbros, ProtGran = Proterozoic granites, ProtRpk = Proterozoic rapakivi granites.

In the diagram in Figure 15, the averages of Archaean and Proterozoic adakitic samples are in both the high Nb/Ta and high Zr/Sm adakite group. They are also very close to each other compared to granites and gabbros, which could indicate similarities in the adakitoid source conditions, independent of age differences. The high Zr/Sm ratio is connected with clinopyroxene in the restite based on experimental studies by Rapp et al. (2003). Their highest Nb/Ta ratios do not directly support either of the models described above.

The Proterozoic and Archaean gabbros and granites have symmetric trend differences in the diagram. The Archaean gabbros and granites have clearly lower Nb/Ta and higher Zr/Sm than their Proterozoic counterparts. When considering the order of elements in the PP diagram, in Figure 2, for example, it can be noted that Ta is 'more incompatible' than Nb and Zr 'more incompatible' than Sm. Thus, trends in Figure 15 indicate that Archaean granites and gabbros are more enriched in incompatibles (lower Nb/Ta and higher Zr/Sm) than the corresponding Proterozoic rocks. These differences may indicate higher pressure and/or temperature environments in the evolution of Archaean plutonic rocks. Moreover, granites are more enriched than gabbros (higher Zr/Sm), as can be expected.

The averages of Proterozoic granites and rapakivi granites are relatively close to each other in the diagram. The average of all Finnish plutonic rocks (AFP) is roughly in the middle of the continental crust field, as can be expected (which emphasizes the usability of AFP for the normalization standard). However, it is also in the middle of the adakite group by Foley et al. (2002), which clearly shows that this diagram alone cannot be used for the discrimination of adakitoid samples.

1.4 Comparison of chemical 'spectra' of the samples

REE spectra

Figure 16 and Figure 17 present C1 chondrite- and AFP-normalized REE patterns for the adakitic, granitic and gabbroic samples considered in this study. In the diagrams, the chondrite-normalized REE spectra of adakitic samples are steepest, i.e. the LREE/HREE (or La/Yb) ratio is clearly highest, referring to a high degree of fractionation. Their Eu anomalies are similar to gabbros: flat in chondrite-normalized and positive in AFP-normalized spectra, referring to a higher plagioclase content (e.g. Wilson 1989) and thus fractionation depths greater than plagioclase stability depths of ca. 30–60–... km (see e.g. Table 1 and Fig. 97). In the C1-normalized diagram in Figure 16, the slope of Archaean adakitoids is steepest, being very close to that of Karelian sanukitoids described by Heilimo et al. (2010); see also Figure 18, demonstrating the significantly higher La/Yb ratios in Archaean sub-areas of eastern and northern Finland.

The slope of gabbros is gentler in chondrite-normalized spectra and positive in AFP spectra, referring to their mafic mantle source. Their Eu values are flat in chondrite-normalized and positive in AFP-normalized spectra, referring to lower crust/upper mantle source depths.

The slopes of granites are dipping in chondrite-normalized and flat in AFP-normalized diagrams. In AFP-normalized diagrams, they are characterized by relative Eu minima, referring to mid-crustal fractionation depths, where plagioclase is stable. In both diagrams, the rapakivi granite samples are characterized by an exceptionally high REE content. In the AFP-normalized diagram, their slope is positive, with increasing HREE values, similar to gabbroic samples. In chondrite-normalized diagrams, this feature is more weakly shown by a slightly gentler slope of rapakivi and gabbro samples. The rapakivi granites also have Eu minima in both diagrams, which refer to plagioclase in restite and thus upper/mid-crustal fractionation depths, where plagioclase is stable (e.g. Rollinson 1993, Martin & Moyen 2002), or the restitic source of rapakivi magma is primarily depleted of plagioclase.

Thus, in AFP-normalized spectra, adakitoids have features of granitic and gabbroic rocks: a steep slope resembling granites, but high Eu values resembling gabbros. Rapakivis have the opposite features: low Eu values resembling granites, but HREE>LREE like gabbros.

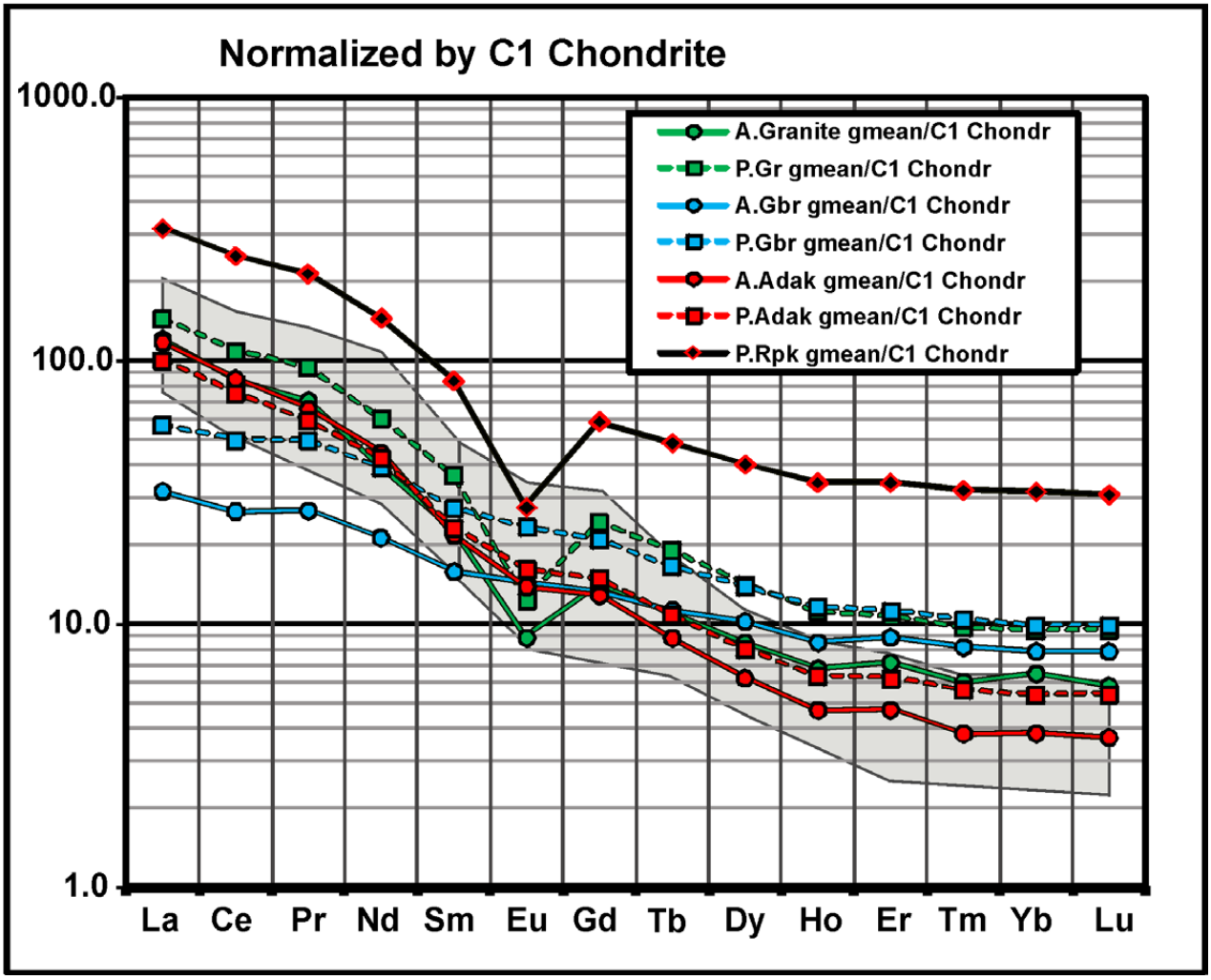

Fig. 16. Chondrite-normalized REE patterns for the granitic, gabbroic and adakitic samples considered in this study. The shaded grey area indicates the distribution of Neoarchaean late to post-tectonic sanukitoid intrusions sampled in the Karelian Province, Finland, by Heilimo et al. (2010). The analytical methods / units are ICPMS / ppm (Table 2).

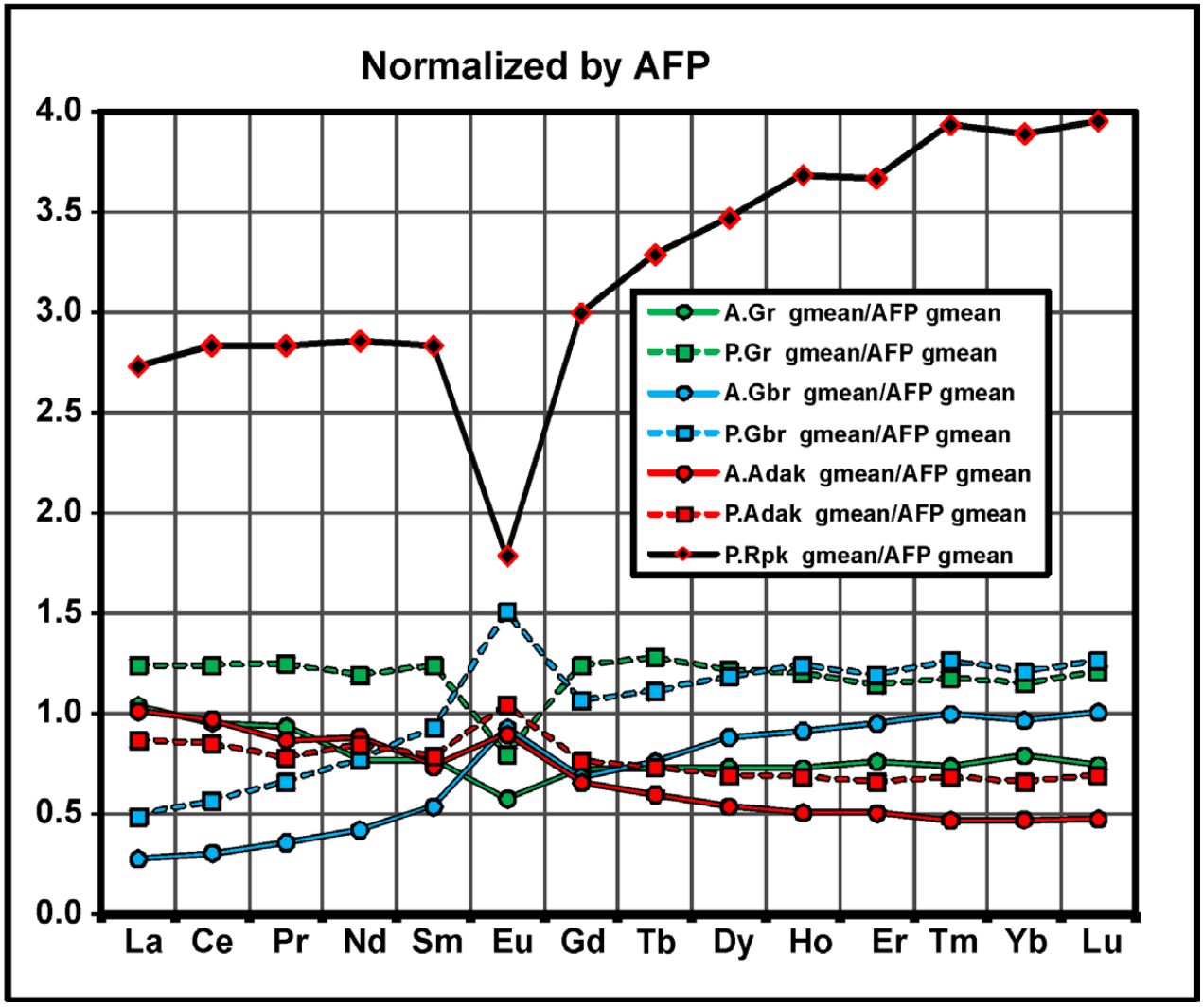

Fig. 17. AFP-normalized REE patterns for the granitic, gabbroic and adakitic samples considered in this study. The analytical methods / units are ICPMS / ppm (Table 2).

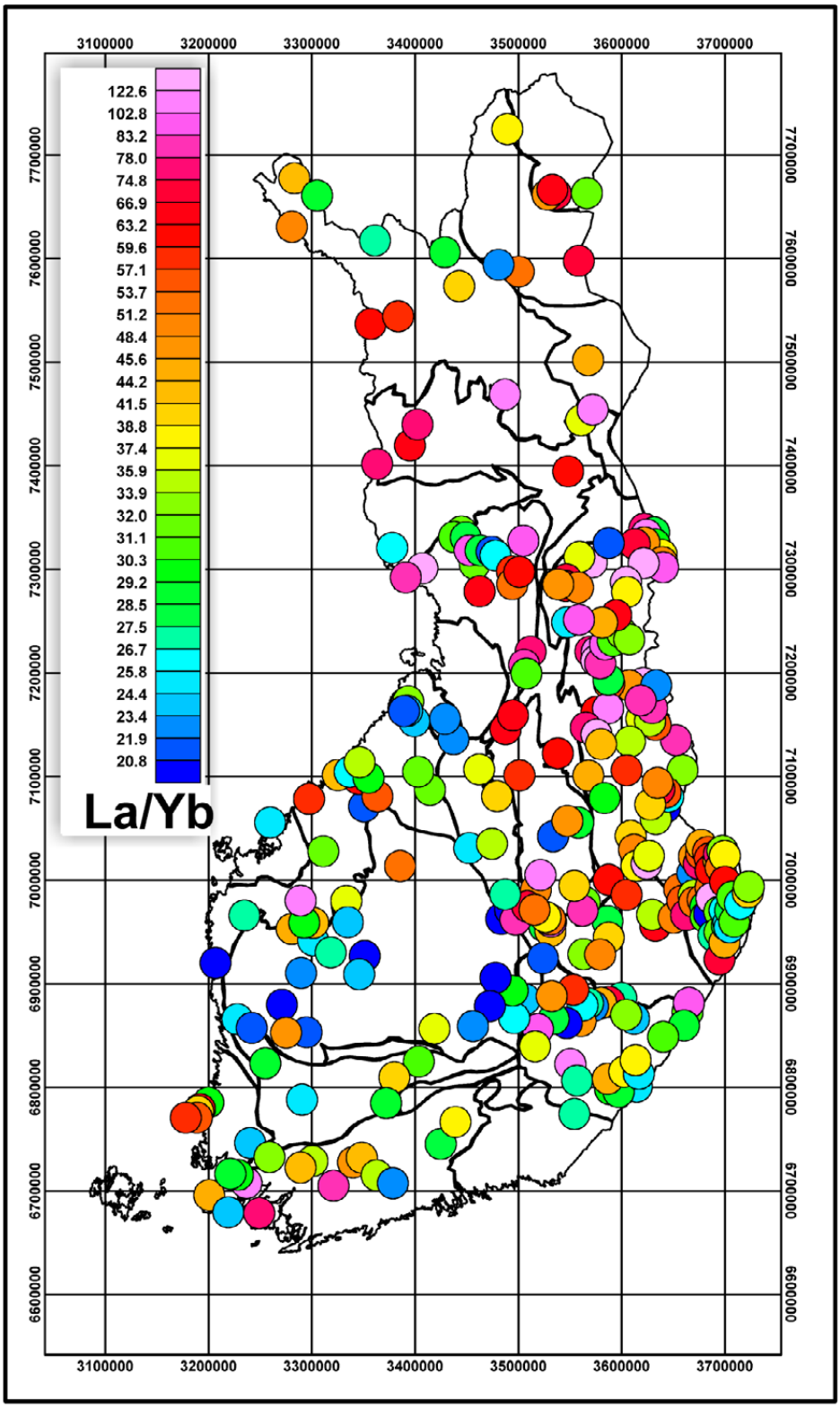

Fig. 18. La/Yb ratios of Finnish adakitoids referring to the degree of REE fractionation. Note the significantly higher ratios in Archaean sub-areas of eastern and northern Finland. The analytical methods / units are ICPMS / ppm (Table 2).

Corner point coordinates in WGS-85:
Lower left KKJ: 6600000 3100000 / WGS-84: N 59.32° E 020.00°
Upper right KKJ:7700000 3700000 / WGS-84: N 69.30° E 032.07°

Pearce–Peate (PP) spectra

In Figure 19 to Figure 21, rock groups are chemically compared using the incompatible → compatible sequence defined by Pearce & Peate (1995; 'PP spectra'). In the diagrams, the geometric means of the elements are normalized by the geometric means of all Finnish plutonic rock samples (AFP) and by C1 chondrite (Anders & Grevesse 1989, Kerrich & Wyman 1996). For the values of AFP and C1, see Table 2. In this report, linear-scale AFP-normalized data are preferred because they more clearly emphasize the differences between the rock groups, as is demonstrated in the diagrams in Figure 2 and diagrams below. The variations in the data are demonstrated in the diagrams by vertical red lines between the first and third quartiles of cumulative distributions of normalized values. It must be noted that the amplitude scale in the diagrams is very variable, especially because of the constant sum effect due to varying values of SiO_2; see e.g. Wilson (1989) and Rollinson (1993). Thus, in the following, the main emphasis is not on absolute values, but on the relative amplitudes and trends of chemical variations.

The red lines in the diagrams demonstrate that the variations of the elements in rock groups are relatively large. However, when considering the Proterozoic and Archaean AFP-normalized lines of the same rock types, it can be seen that they generally have similar trends and peak locations, even though their evolution histories are in most cases separated by an age gap of several hundred Ma, and up to greater than one Ga. Thus, it can be concluded that the variations in the lines reflect the true general characteristics of rock groups.

Adakitoids: AFP-normalized spectra

The PP spectra of Proterozoic and Archaean adakitic rock groups are presented in Figure 19. A significant feature of both AFP-normalized spectra is the relative enrichment of light REE (LREE) compared to heavy REE (HREE). The group ratios of AFP-normalized data ($LREE_{ave}$/$HREE_{ave}$) (↓ see box below) are ca. 2.0 and 1.3 for Archaean and Proterozoic adakitoids; i.e. the REE spectrum of Archaean adakitoids is clearly steeper. There are also relative Eu and Sr maxima in the diagrams, which, in combination with low values of HREE, suggest deeper (greater than ca. 30–60–… km) fractionation depths in the lower crust/upper mantle, below the plagioclase stability field (i.e. increased plagioclase in the melt phase), and with ± garnet ± clinopyroxene ± orthopyroxene ± hornblende in the restite (e.g. Martin & Moyen 2002, Rollinson 1993 and references therein). It is interesting to note that although the LREE/HREE is steeper for Archaean adakitoids, the relative amplitudes of Eu and Sr maxima are clearly higher for Proterozoic adakitoids (see also Fig. 96). These characteristics could refer to a more plagioclase-rich source for Proterozoic adakitoids; they are less fractionated (gentler REE), but still more plagioclase in melt. As noted above in section 1.2., the higher density and slightly higher paramagnetic values of Proterozoic adakitoids refer to their more mafic average composition.

A very significant and characteristic feature of the AFP-normalized PP spectra of adakitoids is also the rapid increase in compatible elements compared to HREE (= $Compatibles_{ave}$/$HREE_{ave}$; see box below↓). In the diagrams in Figure 19, these ratios are ca. 1.9 for both Archaean and Proterozoic adakitoids. In connection with the apparently great fractionation depth concluded above, this trend can be connected to a primarily mafic (basaltic) source and/or contamination by melts from upper mantle/mantle wedge at the lower crust–upper mantle boundary.

It must be emphasized that this HREE → compatibles (Lu → Ca) step cannot be detected in C1- or MORB-normalized spectra, as demonstrated in Figure 2.

$LREE_{ave}$/$HREE_{ave}$ =
Average [La_{ICPMS}, La_{ICPAES}, Ce_{ICPMS}] / Average[Ho_{ICPMS}, Er_{ICPMS}, Tm_{ICPMS}, Yb_{ICPMS}, Lu_{ICPMS}]

$Compatibles_{ave}$/$HREE_{ave}$ =
Average [Ca_{ICPAES}, CaO_{XRF}, Al_{ICPAES}, $Al_2O_{3\ XRF}$, Ga_{XRF}, V_{XRF}, V_{ICPMS}, V_{ICPAES}, Sc_{ICPMS}, Sc_{ICPAES}, Mn_{ICPAES}, MnO_{XRF}, Fe_{ICPAES}, FeO_{XRF}, Co_{ICPAES}, Co_{ICPMS}, Mg_{ICPAES}, MgO_{XRF}, Cr_{ICPAES}, Ni_{ICPAES},] / Average[Ho_{ICPMS}, Er_{ICPMS}, Tm_{ICPMS}, Yb_{ICPMS}, Lu_{ICPMS}]

It must also be noted that low Rb, Th and U refer to a low degree of crustal contamination of adakitoids during their ascent into their present location (e.g. Wilson 1989). Moreover, the minima of these mobile elements in both Archaean and Proterozoic adakitoids indicate that they have been mobilized before the main fractionation of adakitic melts. When considering the geochemistry of granulites in Lewisian amphibolite-facies gneisses from north-west Scotland, Weaver & Tarney (1981) concluded that the depletion of K, Rb, Th and U (in granulites), but not other incompatible trace elements, cannot be explained by magmatic processes but as a result of granulite-facies metamorphism, with these elements being removed by an active fluid phase. Martin et al. (2005 and references therein) attributed the extreme Rb depletion observed in adakites from Mexico to the presence of metasomatic amphibole in a peridotitic source. Thus, (at least) two-stage fractionation of adakitoids can be proposed: 1) removal of the fluid phase and 2) magmatic fractionation.

It is also interesting to note the relatively high AFP-normalized K_{ICPAES} peaks compared to lower K_2O_{XRF} only being characteristic of adakitoids, while the opposite is observed for granites in the diagrams in Figure 21 (and both low for gabbros in Fig. 20). The high K_{ICPAES} values could be attributed to the high content of biotite (soluble in agua regia) relative to potassium feldspar (less-/non-soluble; for details, see Tarvainen et al. 1996).

In contrast to potassium, in Archaean adakitoids, Na_{ICPAES} is distinctly lower than Na_2O_{XRF}. In adakitoids, high Na_2O can be attributed to increased Na plagioclase (albite). The minima of Na_{ICPAES} and scandium in the Archaean adakitoid spectrum can be interpreted to refer to amphiboles (Na and Sc) and garnet (Sc) in restite of Archaean adakites (Rollinson 1993, p. 108: Mineral/melt partition coefficients for basaltic liquids).

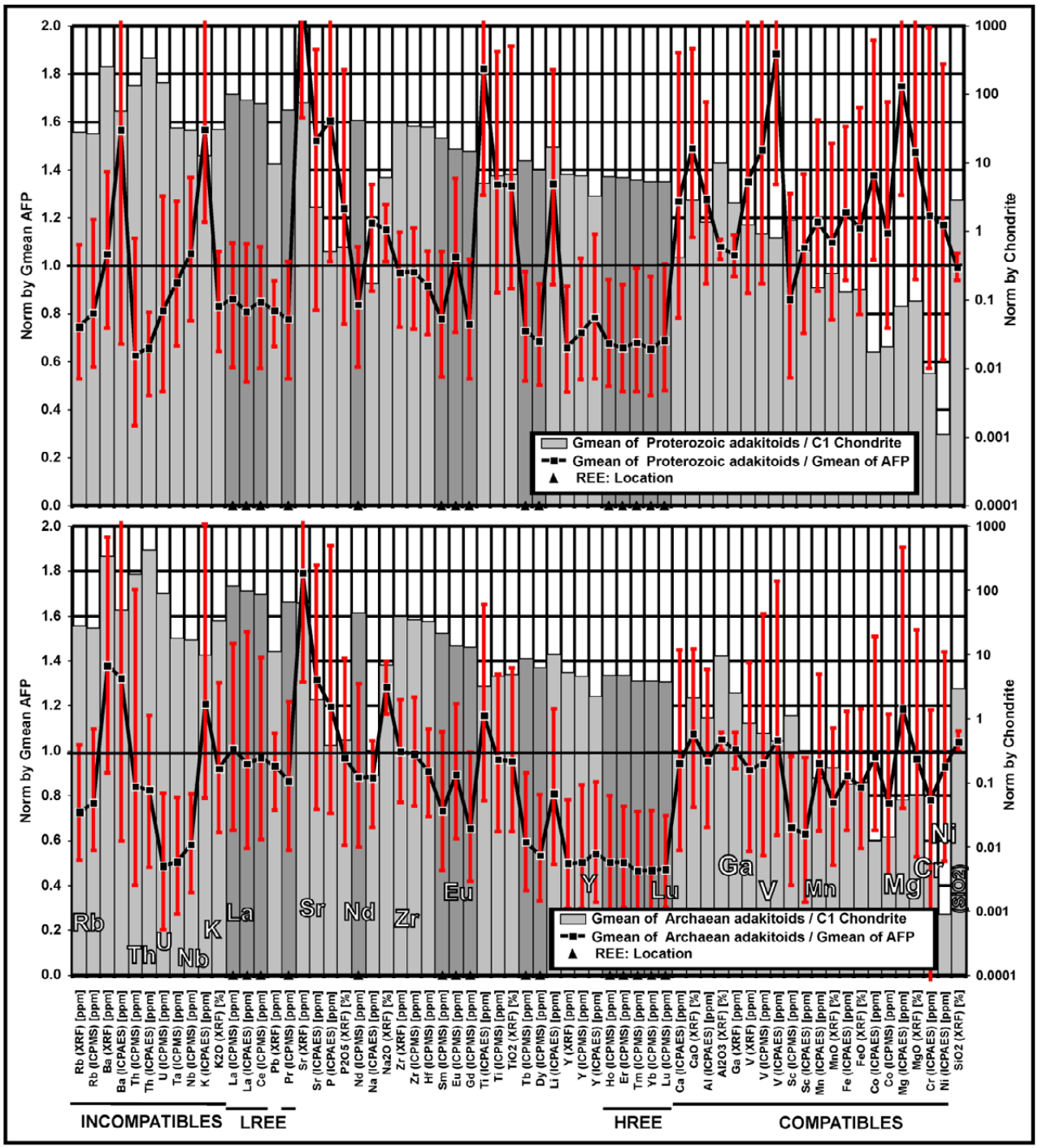

Fig. 19. Characteristics of Proterozoic and Archaean adakitoids arranged in the incompatible → compatible order according to Pearce and Peate (1995). The black line connects values normalized by AFP (geometric averages of all Finnish plutonic rock samples; Table 2). The vertical red lines denote the first and third quartiles of cumulative distributions of AFP-normalized values. The grey bars indicate the values of geometric means normalized by C1 chondrite. The locations of REE are emphasized by triangles on the x-axis and by darker grey bars. In the diagram, the locations of some elements considered more closely in the text are also emphasized. The black lines below the x-axis indicate the locations of some element groups considered in this report. It must be emphasized that SiO_2 does not belong to 'compatibles' but is separately shown here only for comparison.

Gabbros: AFP-normalized spectra

In the PP diagrams of gabbros in Figure 20, the AFP-normalized trends are opposite to those of adakitoids, increasing from incompatibles to compatibles, as can be expected for mafic rocks. In particular, the slopes of REE of the gabbroic samples are opposite to that of adakitoids: The $LREE_{ave}/HREE_{ave}$ ratios of AFP-normalized data are ca. 0.3 and 0.4 for Archaean and Proterozoic gabbros, respectively.

The $compatibles_{ave}/HREE_{ave}$ ratio is even larger than that of adakitoids, being ca. 2.8 and 2.2 for Archaean and Proterozoic gabbros, respectively, reflecting the high portion of mafic minerals (mantle component) in these rocks. Opaque minerals (sulphides and oxides) may also affect the high level of incompatible elements in gabbros. Moreover, like adakitoids, gabbros also have relative Eu and Sr maxima referring to lower crust/upper mantle genesis, below the plagioclase stability depth. The increased AFP-normalized Na_{ICPAES} relative to Na_2O_{XRF} in gabbros can be associated with high contents of amphiboles relative to Na plagioclase (albite).

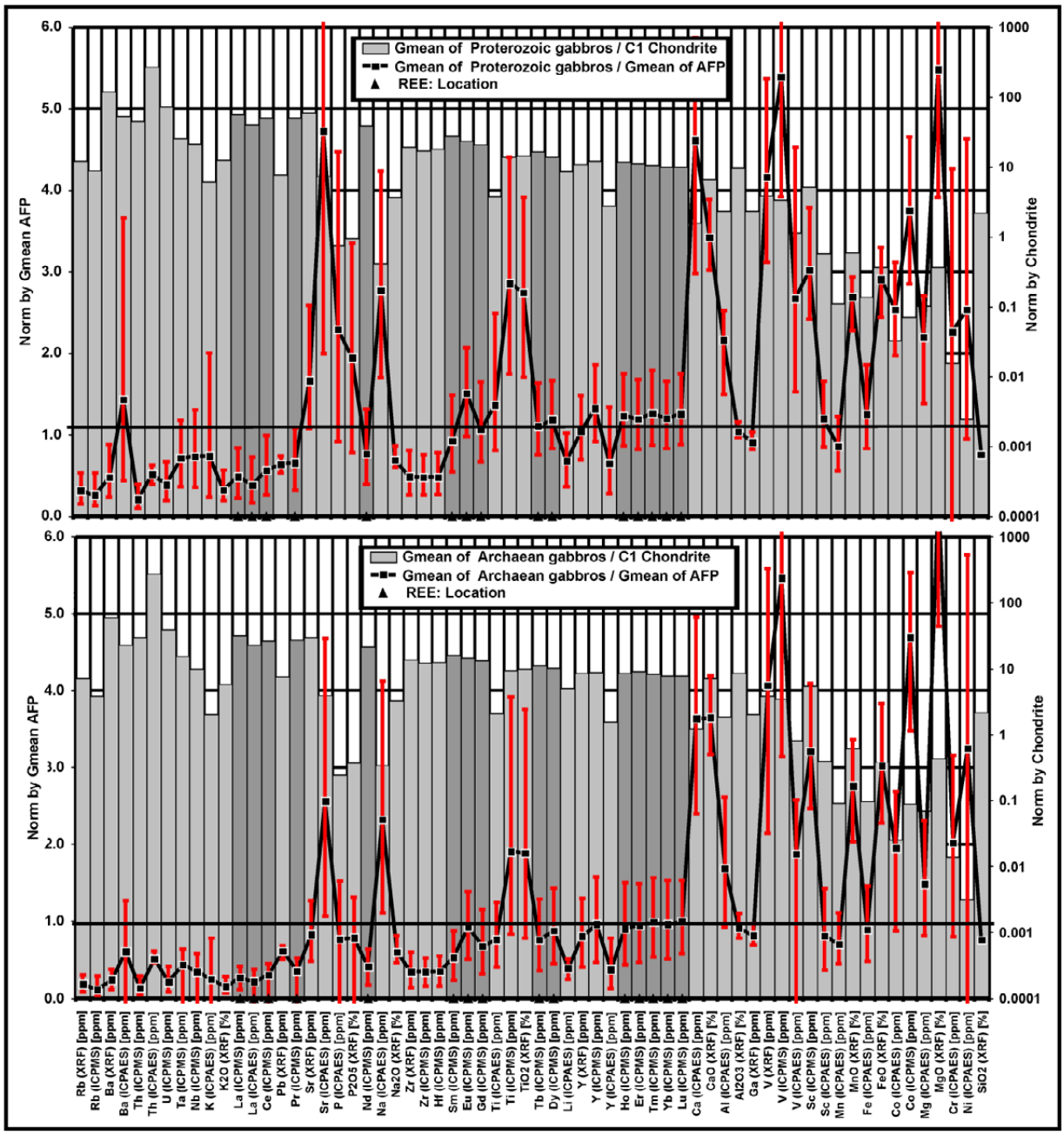

Fig. 20. Pearce–Peate diagrams of Proterozoic and Archaean gabbros. Note that the vertical scale is larger than that of adakitoids in Figure 19 and granites in Figure 21.

Granites: AFP-normalized spectra

The PP diagrams of granitic samples are presented in Figure 21 and Figure 22. In the AFP-normalized diagrams, 'normal' granites follow a descending trend from incompatibles to compatibles. The $LREE_{ave}/HREE_{ave}$ ratios of Archaean and Proterozoic granites are much lower than those of the adakitoids, being ca. 1.4 and 1.1, respectively. However, the ratio of rapakivi granites in Figure 22 is exceptional, being ca. 0.7, i.e. clearly increasing from LREE to HREE. In all granite diagrams, the relative proportion of compatibles is low, $compatibles_{ave}/HREE_{ave}$ ratios being ca. 0.6, 0.5 and 0.2 for Archaean, and Proterozoic granites and rapakivi granites, respectively.

All granites have relative Eu minima and low Sr, referring to stable plagioclase in the restite and thus shallower, mid- to upper crustal fractionation depths compared to those of adakitoids and gabbros. In addition, the peaks in Rb, Th and U of the granites (opposite to adakitoids) refer to upper crustal source material and fluid enriched magma.

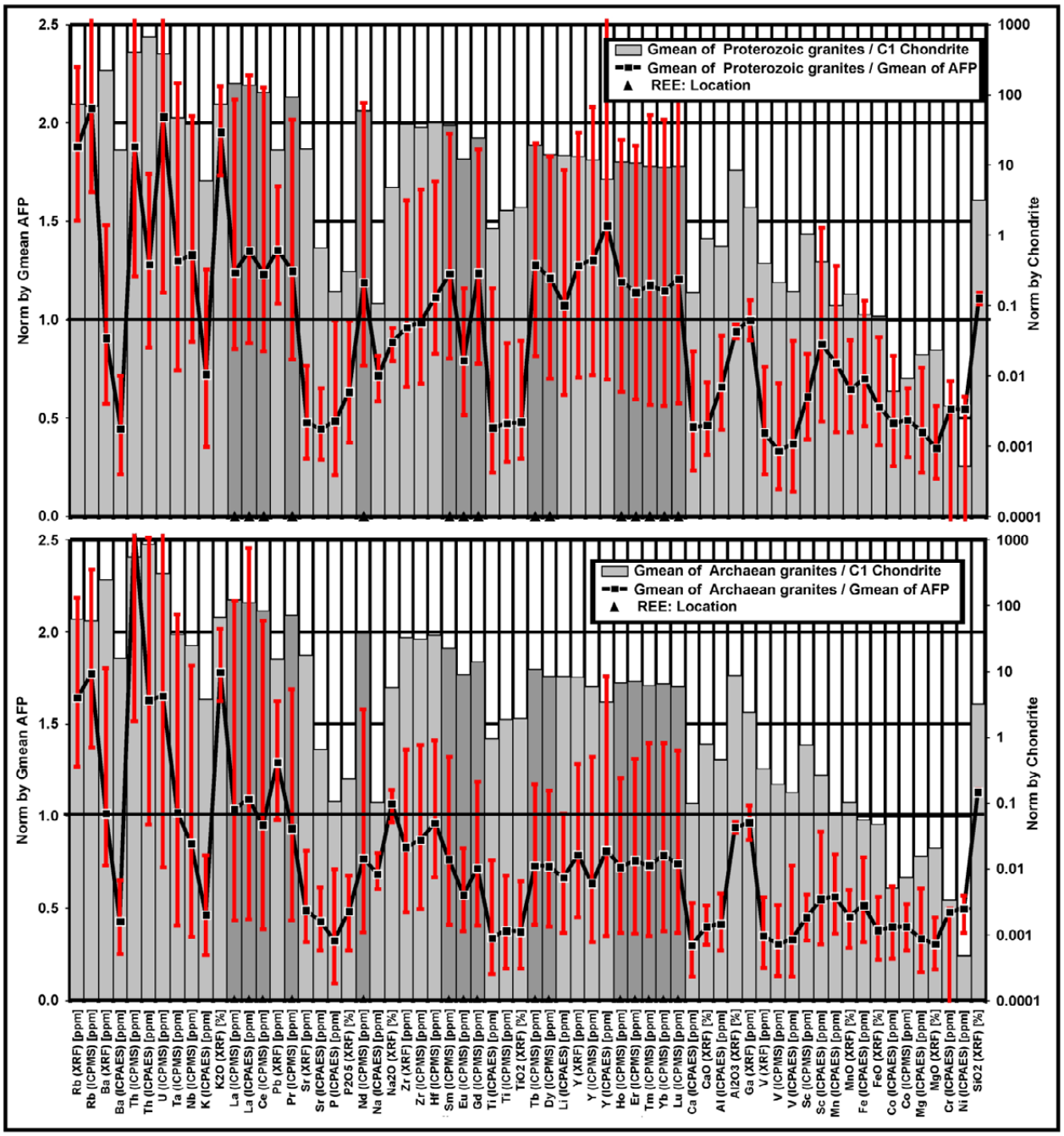

Fig. 21. Pearce–Peate diagrams of Proterozoic and Archaean granites.

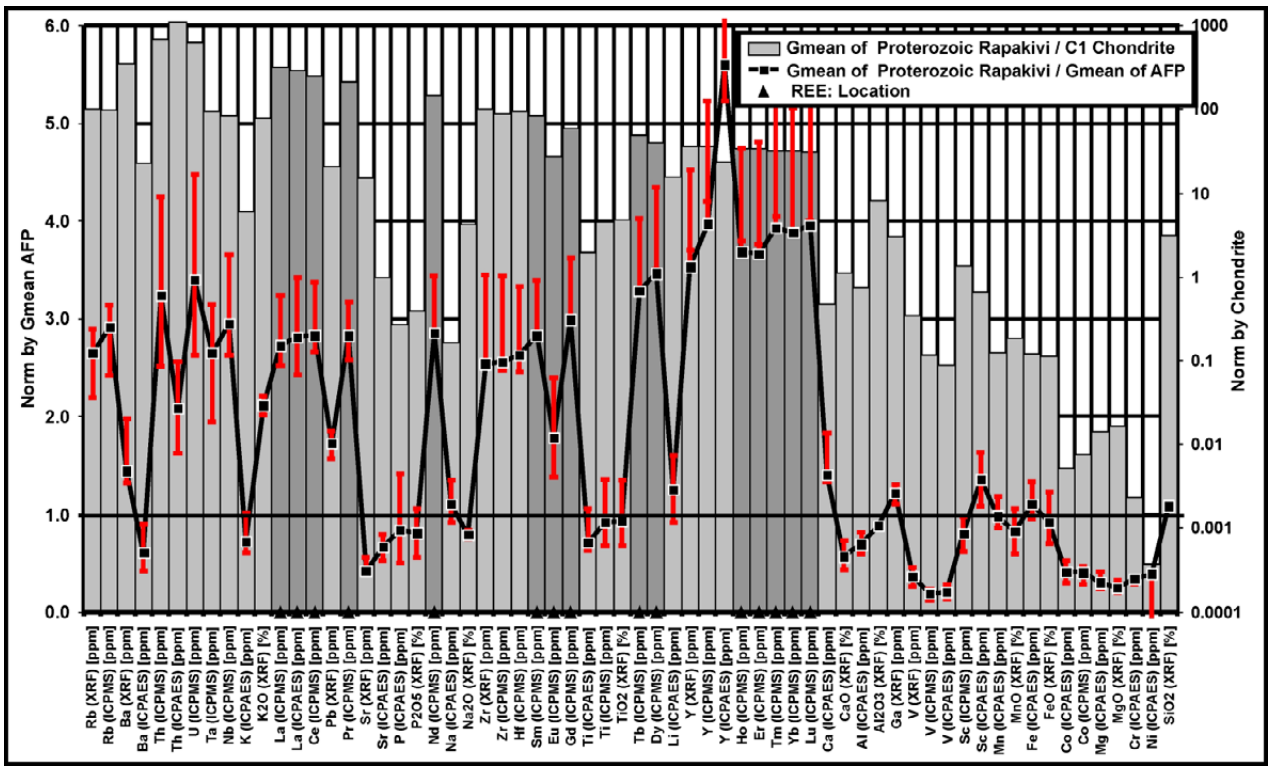

Fig. 22. Pearce–Peate diagrams of Proterozoic rapakivi granites. Note that the vertical scale is larger than that of 'normal' granites above.

It is interesting to note that there is a strong negative correlation between the AFP-normalized PP diagrams of rapakivi and adakitoid samples in both trends and the sign of the peaks, as demonstrated in Figure 23. In principle, the chemical characteristics of the rapakivis are similar to what one could expect for the complementary, deeply located source restite of adakitoids, which is not in contradiction with the primary source of rapakivis attributed to the lower crust–upper mantle border zone (Rämö & Haapala 2005). However, due to the significant age difference and multistage evolution of rapakivis (e.g. Rämö 1991 and Rämö & Haapala 2005), the connection with rapakivis and adakitoids is not straightforward and needs more profound consideration.

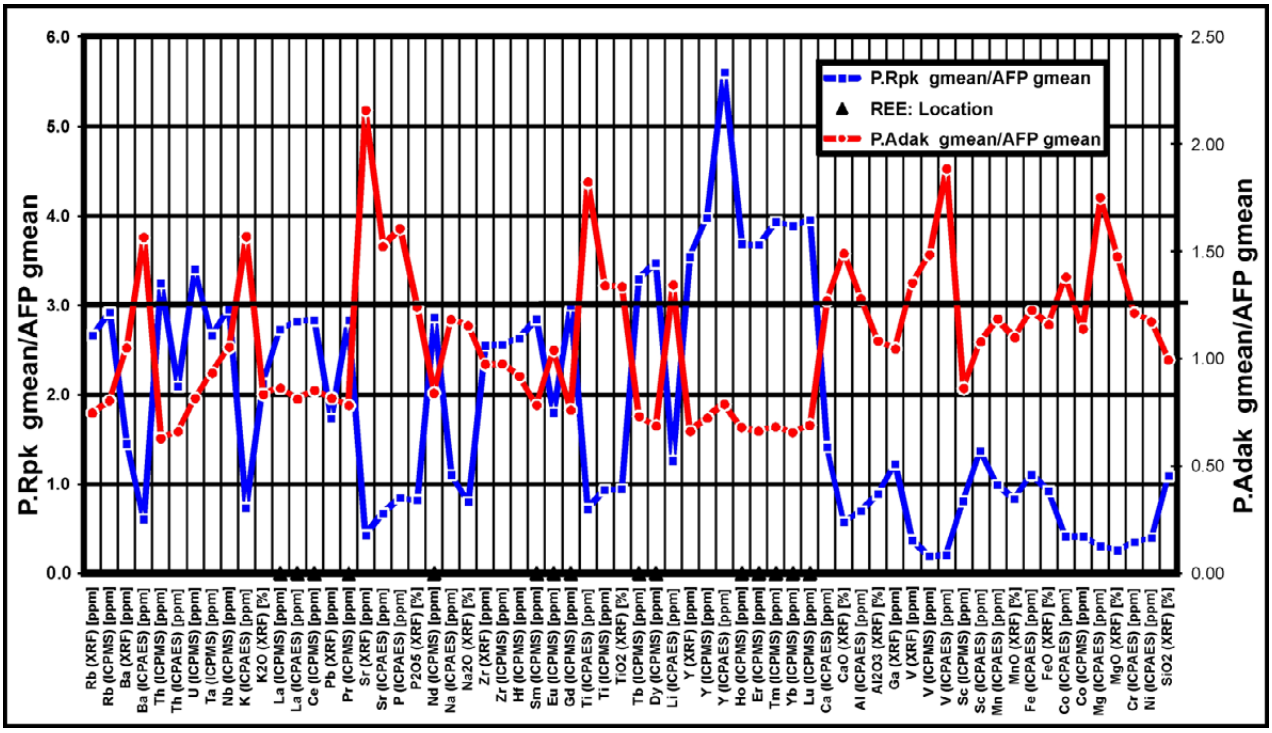

Fig. 23. Relationship between the AFP-normalized Pearce–Peate diagrams of Proterozoic adakitoids (P.Adak) and rapakivi granites (P.Rpk). The complementary characteristics of the diagrams are evident. Note the different vertical scales of the diagrams.

1.5 Determination of the restites of adakitic melts

The determination of primary source and restite material from rock samples representing melt fractions is generally difficult. One way to evaluate the restitic material is to analyse phenocrysts (Chappell et al. 1987, Thorkelson & Breitsprecher 2005), or enclaves/xenoliths representing restite fragments in outcrops (e.g. White et al. 1999, Peltonen et al. 2006). A common way to evaluate the mineralogy of restitic material is also to analyse the relative contents and ratios of certain key elements of rock samples (e.g. Defant & Drummond 1990, Castillo 2006; Table 1). The uncertainty of these methods is increased, for example, by multi-stage fractionation and magma contamination during uplift and by large variations in partition coefficients.

In this study, the major restite minerals are assumed to be those represented by Peltonen et al. (2006; Table 3). They investigated the origin of the lower crust of the Karelian craton from mafic garnet granulite xenoliths recovered from Neoproterozoic kimberlites located in Archaean central Finland. In their samples, orthopyroxene only occurs in high-plagioclase xenoliths (plg ≥ ca. 50%; Table 3), which relates to their origin at shallower depths, within the plagioclase stability field. However, the low plagioclase samples are rich in ‘restitic’ minerals (garnet

Table 3. Examples of mineral modes based on point counting of low and high plagioclase xenoliths samples from Peltonen et al. (2006). Note that mafic, low plagioclase samples are high in 'restitic' minerals (garnet clinopyroxene and amphibole), in contrast to high plagioclase (+ orthopyroxene) samples representing the felsic 'melt phase'.

Type	Rock	Minerals
Low-Plg	**Mafic garnet granulite, coarse grained**	**Grt_{26} Cpx_{21} Am_{37} Plg_{9}** Op_7 (Ap)
Low-Plg	**Mafic garnet granulite, cumulate texture**	**Grt_{19} Cpx_{25} Am_{47} Plg_{5}** Op_4 (Ap, Zr)
High-Plg	Felsic granulite (monzodiorite), recrystallised igneous texture	**Opx_4** Am_2 **Plg_{63}** Bt_6 Qtz_4 Kfs_{19} Op_2
High-Plg	Felsic granulite (tonalite), recrystallised igneous texture	**Opx_4** Am_{12} **Plg_{50}** Bt_1 Qtz_{32} (Ap, Op, Cpx, Zr)

Grt: garnet; Cpx: clinopyroxene; Opx: orthopyroxene; Am: amphibole (hornblende); Plg: plagioclase; Op: opaques; Qtz: quartz; Ap: apatite; Bt: biotite; Zr: zircon; Kfs: potassium feldspar.

clinopyroxene and amphibole), recording their higher P–T origin.

In the following, I estimate the mineralogy of adakitoid restite using partition coefficients for basaltic and basaltic andesite liquids approximating (coarsely) 'primary' source material for adakitic melts. Their partition values have been summarized by Rollinson (1993). A basaltic, garnet-bearing source for adakite TTG-like rocks has been proposed by Drummond & Defandt (1990), Smithies et al. (2003) and Väisänen et al. (2012), among others. For simplicity, I assume that clinopyroxene, orthopyroxene, garnet and amphibole represent the most probable sinks for the compatible elements in restite (Peltonen et al. 2006; Table 3, Rollinson 1993, Martin & Moyen 2002, Martin et al. 2005).

Table 4 presents the relative ratios for the coefficient pairs used here. If the ratio of normalized elements is less than one (decreases) in the table, the denominator dominates in the restitic mineral, and vice versa. For example, if orthopyroxene dominates in the restite, Zr more likely remains in the restitic mineral (orthopyroxene) phase and the ratio Nd/Zr decreases (<1) in restite. Furthermore, Nd is then relatively enriched in the mobile adakitic melt phase and the Nd/Zr ratio of adakitoid samples should become relatively enriched in Nd. It must be emphasized that the estimated values of partition coefficients can vary over a wide range and thus their relative effect on the content of elements in the melt and remaining restite fraction can only roughly be evaluated. Therefore, the inferred restite mineral distributions presented in the following must be taken as preliminary estimates. Because no 'standard' element ratios are known for adakitic samples, I compare the ratios of each sample against the averages of all adakitic samples.

By this principle, the possible enrichment of elements in the adakitic melts is evaluated using the element ratios of each adakitoid sample normalized by the geometric means of all adakitoid samples. Thus, using elements analysed by ICPMS (see Table 2), the relative enrichment/depletion of sample element ratios are as follows:

Table 4. Simplified ratios of mineral/melt partition coefficients for basaltic and basaltic andesite liquids using coefficients summarized by Rollinson (1993 and references therein). <1 means that the ratio decreases in restite minerals (increases in the adakitic melt); >1 means that ratio increases in restite minerals (decreases in adakitic melt).

Restite mineral:	**Orthopyroxene**	**Clinopyroxene**	**Hornblende**	**Garnet**
Nd/Zr	<1	>1	<1	<1
La/Ce	>1 (*)	<1	<1	<1
Er/Lu	<1	>1	>1	<1

(*) = Evaluated for andesitic liquids (only available)

Orthopyroxene: Nd/Zr >1, La/Ce <1, Er/Lu >1
Clinopyroxene: Nd/Zr <1, La/Ce >1, Er/Lu <1
Hornblende: Nd/Zr >1, La/Ce >1, Er/Lu <1
Garnet: Nd/Zr >1, La/Ce >1, Er/Lu >1

Or, in a simplified form, demonstrating the unambiguity of the combinations:
Orthopyroxene: (1,0,1)
Clinopyroxene: (0,1,0)
Hornblende: (1,1,0)
Garnet: (1,1,1)

These combinations allow evaluation of the distributions of all these restite minerals in the study area. Using three element ratio combinations for each mineral, the reliability of the method is increased. In Figure 24 and Figure 25, the locations of minerals calculated to dominate in the restites of adakitoids are given. Using the ratios above, ca. 46% of adakitoids did not fulfil all the conditions above and thus their restite mineralogy was not estimated. The method was also tested using AFP-normalized element ratios, which gave very similar results to normalization by the geometric mean of adakitoids used here. It must be emphasized that these minerals are assumed to dominate in restitic rocks deep in the lower crust/upper mantle, not in outcrops.

On the maps in Figure 24, the dominating mineral in the restites is clinopyroxene, existing in both Archaean and Proterozoic sub-areas. Orthopyroxene exists relatively evenly in southern and central Finland, referring to 'shallower' depths, where some plagioclase may also exist (see Table 3 above), but less in the north. In Figure 25, clusters of amphibole and garnet in

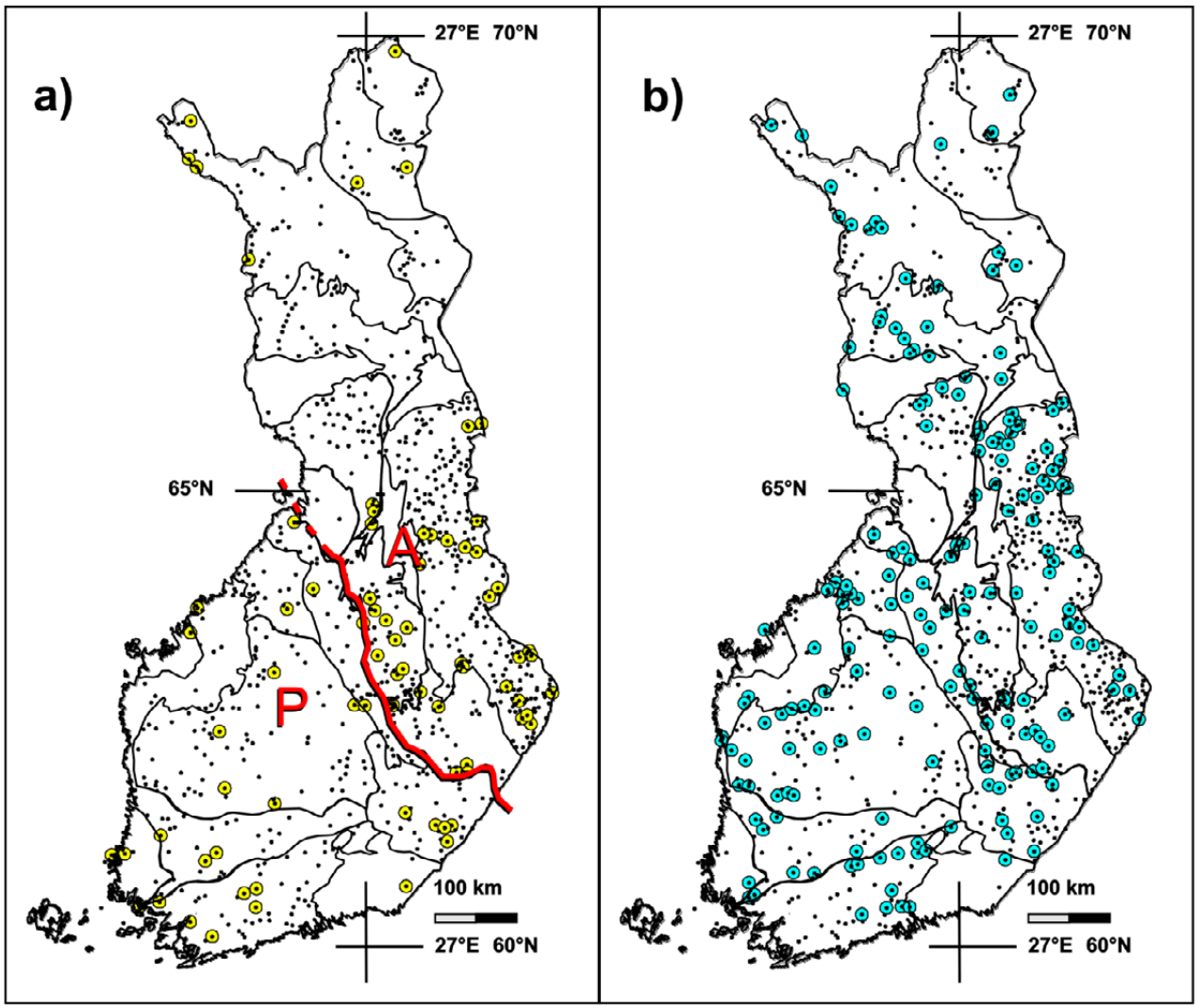

Fig. 24. Distributions of adakitoids having restite dominated by (a) orthopyroxene or (b) clinopyroxene on the basis of their trace element ratios. The borders of sub-areas have been adopted from Figure 3: A = Archaean, P = Proterozoic.

restite dominate almost solely in the Archaean sub-areas of eastern Finland, with only a few samples in Proterozoic sub-areas of southern and central Finland. The garnet-rich restites of Archaean adakitoids refer to higher P–T fractionation environments compared to Proterozoic adakitoids (e.g. Obata & Thompson 1981).

It must be emphasized that on the maps in Figure 24 and Figure 25, restites were relatively rigorously calculated using all element pair ratios for all restite minerals (the number of equations is larger than number of unknowns = 'overdetermined system'). It is, however, also possible to use only two selected element pairs for the calculation of restite minerals, which results in a larger distribution of interpreted restite minerals. However, I prefer the more reliable results presented in Figure 24 and Figure 25.

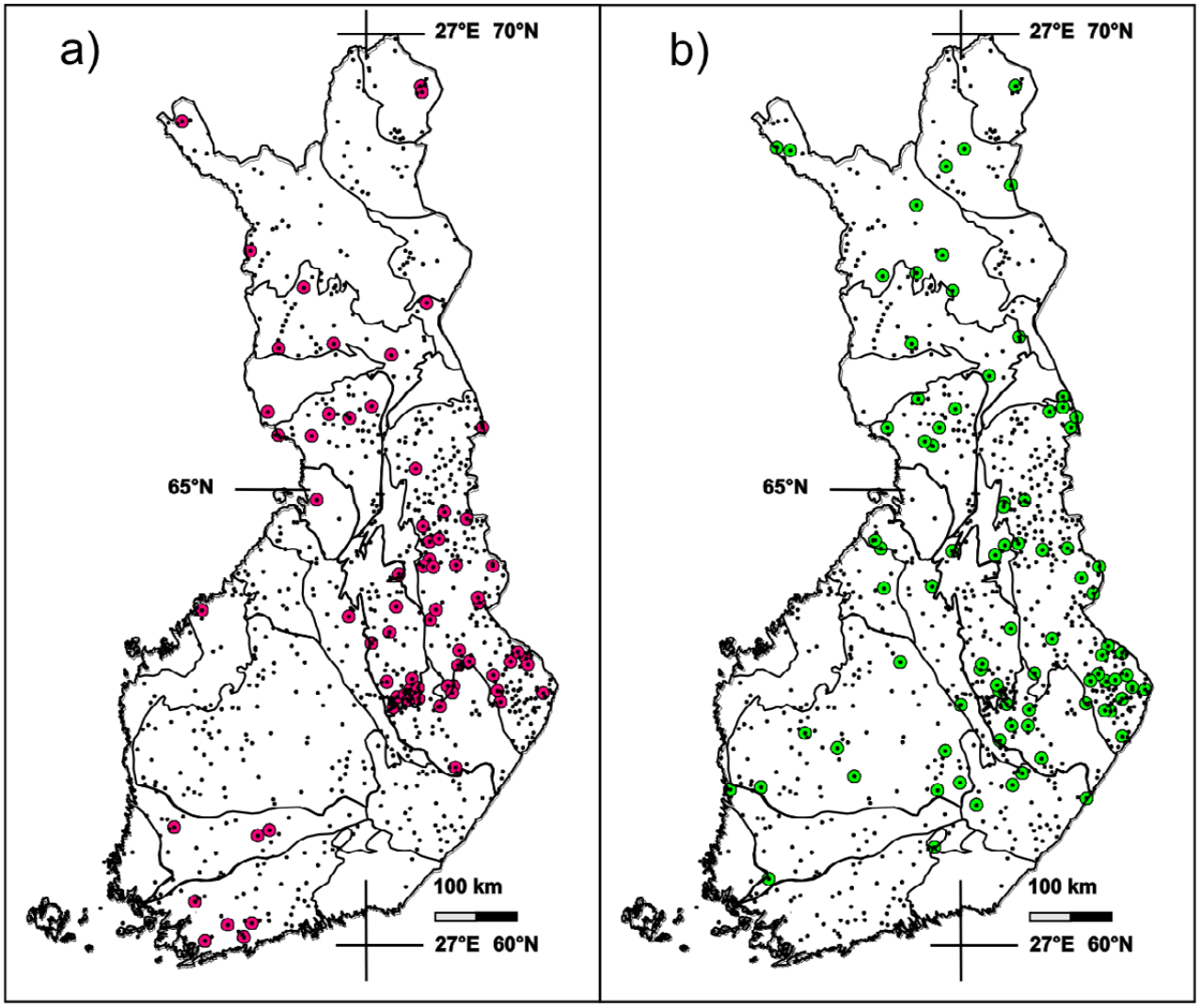

Fig. 25. Distributions of adakitoids having restite dominated by (a) garnet or (b) amphibole on the basis of their trace element ratios.

1.6 Comparison with known adakites, adakitoids, sanukitoids and TTGs

In the following, the chemical spectra of Finnish adakitoids are compared with some adakites, TTGs and sanukitoids adopted from the literature. It must be emphasized that the data from the literature are not as numerous as those from the GTK database. Moreover, the analytical methods and accuracy are not unambiguous in each case. The standards used for normalization are indicated on the y-axis of the spectra and their values are given Table 2.

In Figure 26, the C1-chondrite-normalized geometric average of all Finnish adakitoids studied above is compared with the corresponding spider diagram of Solander Island adakites (New Zealand) and Panama compiled by Reay & Parkinson (1997). From the diagram, it appears that the main trends of Finnish adakitoids correspond relatively well with much younger, 'modern' adakitoids, the deviations being of same magnitude as those between Solander and Panama data. However, the strong damping effect of the logarithmic vertical scale must be noted when comparing the spectra of various rock groups, as is demonstrated by the spectra in Figure 2 and Figure 16 to Figure 17.

In the following, the comparison is made in more detail using the AFP-normalized Pearce–Peate spectra of available elements. To minimize the effect of altered or in other ways assimilated samples in these comparisons, only those Finnish adakitoids that fulfil all eight criteria ('100% adakitoids') defined above for adakites by Defant & Drummond (1990) and Thorkelson & Breitsprecher (2005) are used in the diagrams.

Figure 27 presents the Pearce–Peate spectra of adakites from the Neoarchaean active continental margin of the Shimoga schist belt, Western Dharwar Craton, India (Naqvi & Rana Prathap 2007) and from Solander Island, New Zealand (Reay & Parkinson 1997). The adakites from the Shimoga schist belt mainly consist of quartz, plagioclase and minor amphiboles and are interlayered with the turbidites. The authors classify them as high SiO_2 and low Mg#, Ni and Cr type adakites. These adakites show compositional similarities with Meso- and Neoarchaean tonalite–trondhjemite–granodiorites (TTGs) experimentally generated by the partial melting

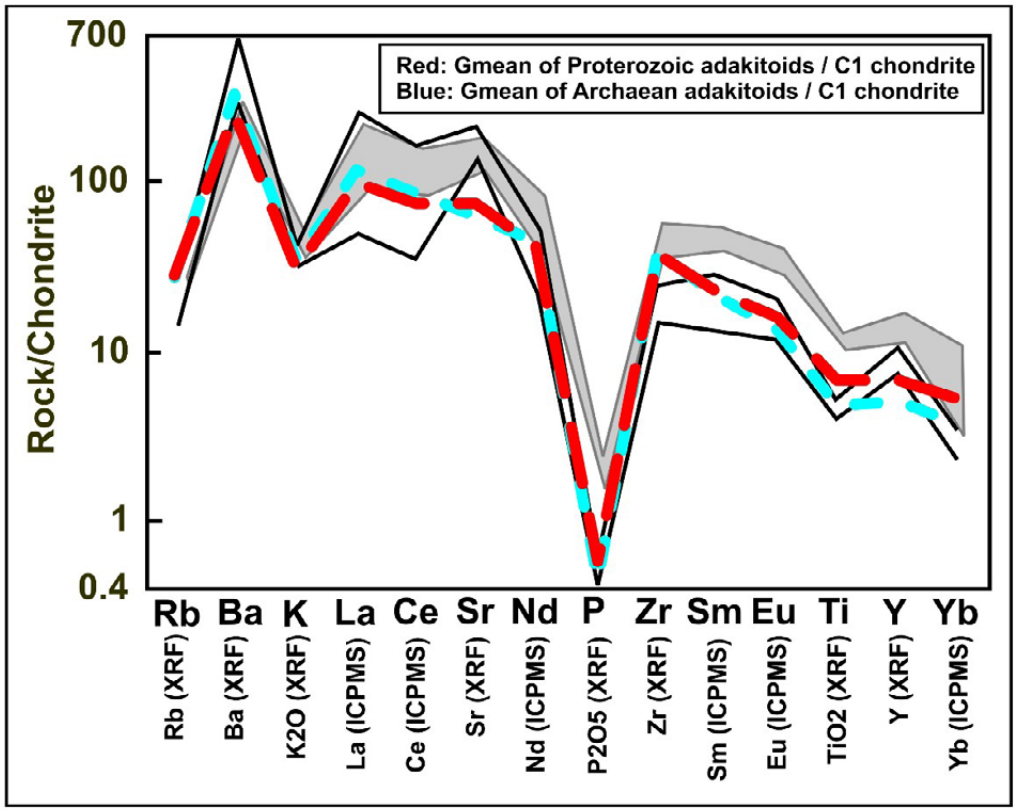

Fig. 26. Chondrite-normalized spider diagram of Solander Island adakites (New Zealand; shaded) and Panama (between solid, thin lines) adopted from Reay & Parkinson (1997). The red and blue lines represent the chondrite-normalized geometric averages of all Finnish adakitic plutonic rocks.

of hydrous basalts similar to adakitic glass veins found in peridotite xenoliths of the Kamchatka arc.

The subduction-related, island arc Pleistocene volcano of Solander Island in New Zealand is composed of adakites formed by the partial fusion of young oceanic crust under eclogitic facies conditions. Comparison with other adakite localities suggests that the presently subducting oceanic crust in the nearby trench may be <25 Ma old. See also Figure 26, in which the chondrite-normalized Finnish adakitic plutonic rocks are compared with the corresponding spider diagram of Solander Island adakites and Panama compiled by Reay & Parkinson (1997).

The spectrum of adakites from the Shimoga schist belt, India, in Figure 27a is relatively flat with a slight peak in Eu and increased compatibles. Moreover, the level of LREE is roughly the same as that of HREE, thus not correlating very well with Finnish adakitoids. However, the spectrum of Solander Island adakites in Figure 27b is very close to that of Finnish adakitoids, with LREE > HREE and high Sr, Eu and compatibles/HREE, as is also suggested by the similarity in the diagrams in Figure 26 above.

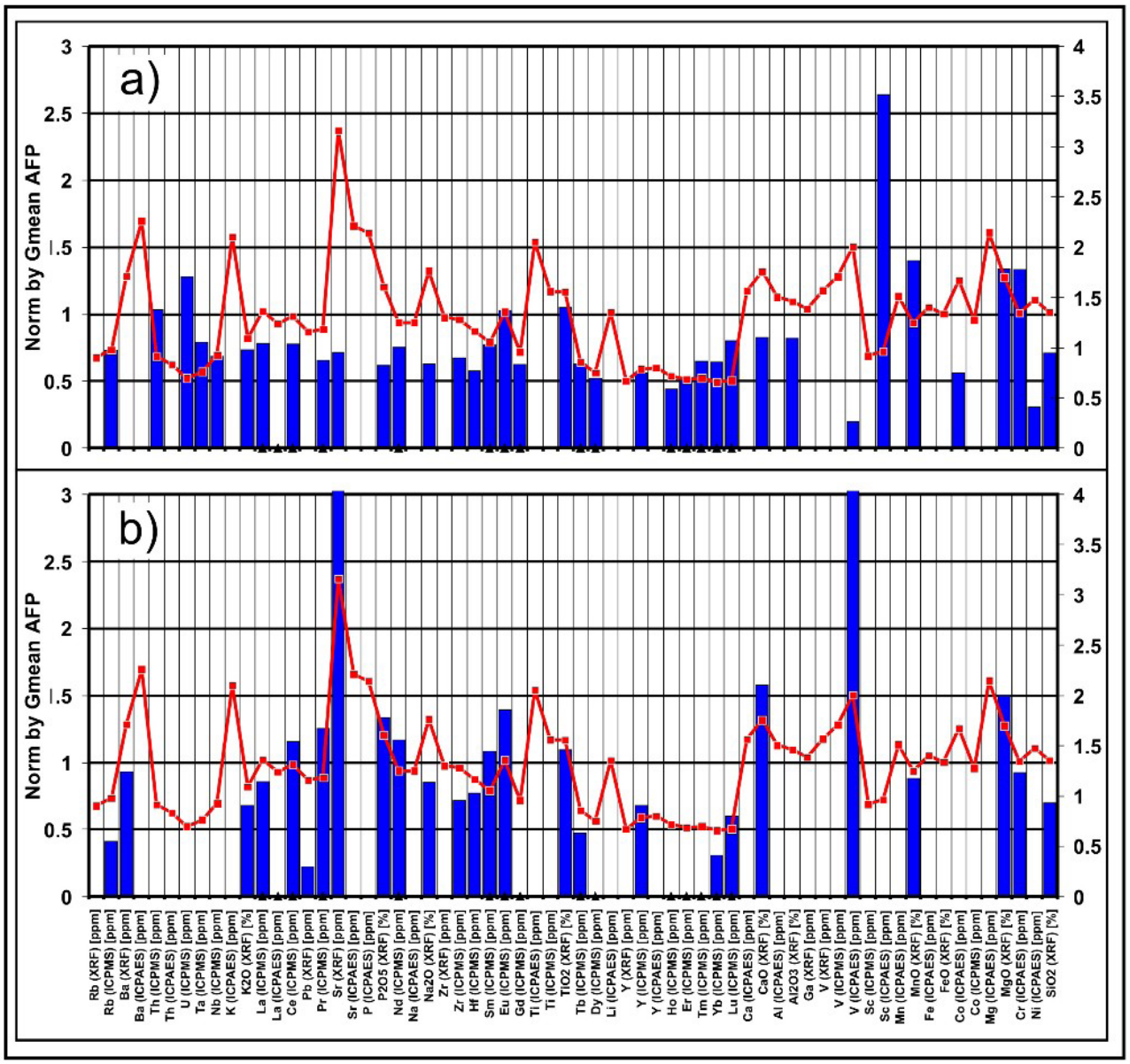

Fig. 27. AFP-normalized gmeans of adakites from (a) the Neoarchaean active continental margin of Shimoga schist belt, Western Dharwar Craton, India (Naqvi & Rana Prathap 2007; 18 samples, blue bars, right vertical axis) and from (b) Solander Island, New Zealand (Reay & Parkinson 1997; 9 samples, blue bars, right vertical axis). The red line indicates the variations in the AFP-normalized geometric means of all '100% adakitic' Finnish plutonic rock samples (left vertical axis).

Figure 28 depicts the AFP-normalized Pearce–Peate spectra of late Mesozoic adakitic granitoids from the north-western Jiaodong Peninsula, east China (Hou et al. 2007). They represent two suites of granitoids, the Early Cretaceous (130–126 Ma) Guojialing suite (Fig. 28a) and the Late Jurassic (158 ± 3 Ma) Linglong suite (Fig. 28b) in the northwestern Jiaodong Peninsula, eastern China. The Guojialing suite includes at least five plutonic bodies of both granodiorite and monzogranite. The rocks are composed of plagioclase, alkali feldspar, quartz, Mg-rich amphibole and Mg-rich biotite. The Linglong suite is a monzogranite comprising alkali feldspar, plagioclase, quartz and Fe-rich biotite. The authors conclude that the Guojialing suite was formed by the reaction of delaminated eclogitic crust-derived melt with the upwelling asthenospheric mantle, whereas the Linglong suite was derived by partial melting of Neoarchaean metamorphic lower-crustal rocks at depths greater than 50 km with eclogite residue. The petrogenesis of these two adakitic granitoids suggests intensive lower-crustal delamination during Early Cretaceous times, following a crustal thickening process from the late stage of the Early Jurassic to the early stage of the Late Jurassic, with a crustal thickness of less than 32 km to over 50 km, respectively.

Thus, these rocks are not directly connected to subduction, but to remelting and fractionation processes below thickened crust in contact zones of lower crust/upper mantle. To consider the possible similarities, in Figure 28 are plotted Pearce–Peate spectra of these Chinese suites together with Finnish Proterozoic and Archaean adakitoids. In the diagrams, both Chinese adakitic granitoids agree relatively well with Finnish adakitoids, the apparent correlation being slightly better with Archaean adakitoids.

Deep seismic soundings have demonstrated that in Finland, the Proterozoic crust is locally exceptionally thick, being close to 60 km (e.g. Luosto et al. 1984, Kukkonen & Lahtinen 2006, Fig. 82). Moreover, delamination-remelting of central Finnish lower crust with restite containing garnet-clinopyroxene has been interpreted by Kukkonen et al. (2008), among others. Thus, similar lower crust/upper mantle melting and fractionation processes also appear possible in Finnish bedrock evolution. For example, Väisänen et al. (2006) considered Svecofennian calc-alkaline and adakite-like 1.90–1.86 Ga magmatism in SW Finland. They interpreted a felsic trondhjemite sample, dated at ca. 1867 ± 4 Ma (ε_{Nd} =+2.6), characterized by inherited zircons with 2667–1965 Ma cores and 1842 ± 5 Ma metamorphic rims to be generated through crustal melting of the lower part of the previously generated thickened crust at a minimum pressure of 10 kbar (≧ ca. 35 km).

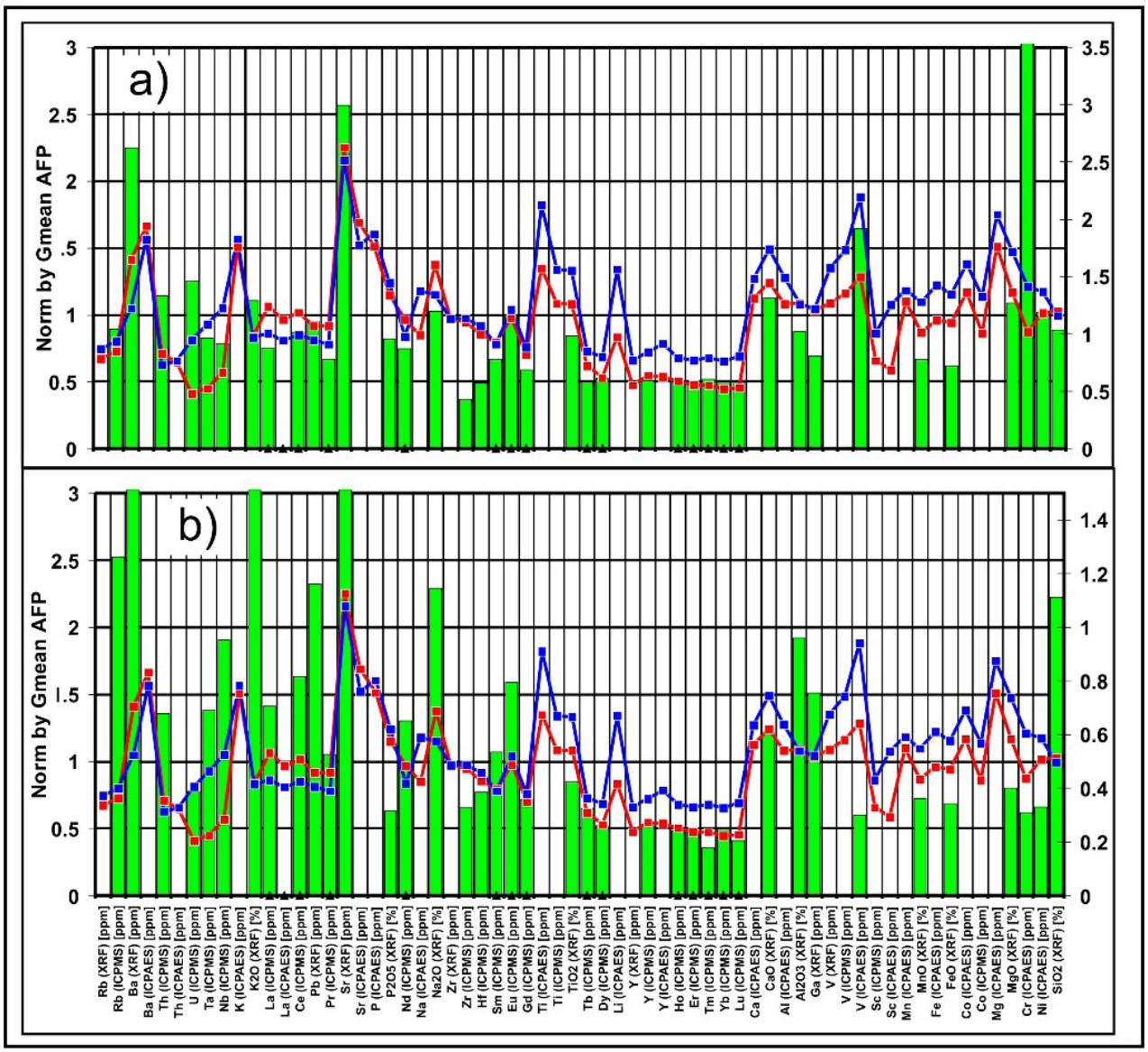

Fig. 28. AFP-normalized Pearce–Peate spectra of gmeans of adakitic (a) Early Cretaceous Guojialing suite (3 samples, green bars, right vertical axis) and (b) Late Mesozoic Linglong suite (7 samples, green bars, right vertical axis) located in the north-western Jiaodong Peninsula, eastern China (Hou et al. 2007). The red lines indicate the spectrum of Finnish Archaean AFP-normalized '100% adakitic' plutonic rocks (178 samples: left vertical axis). Correspondingly, the blue lines indicate the spectrum of Finnish Proterozoic adakitic plutonic rocks (106 samples).

Figure 29 presents the AFP-normalized Pearce–Peate spectra of TTGs and sanukitoids, adopted from Martin et al. (2005; Fig. 29a), and sanukitoids from Halla (2005; Fig. 29b), compared with Finnish AFP-normalized '100% adakitic' plutonic rocks. Martin et al. (2005) considered the chemical composition of primitive Archaean TTG magmas evolved from ca. 4.0 to 2.5 Ga. Over this period of time, Mg#, Ni, and Cr contents increased. The authors interpreted these changes in terms of changes in the degree to which the TTG magmas interacted with mantle peridotite. In the Early Archaean, it appears that these interactions were very rare or absent, leading to the conclusion that subduction was typically flat and lacked the development of a mantle wedge. In contrast, the lower heat production by ~2.5 Ga resulted in sanukitoid melts due to slab melting at greater depths, where plagioclase was no longer stable and the development of a thick mantle wedge ensured interaction between the slab melts and mantle peridotite. Thus, TTG compositions differ from the Late Archaean sanukitoids, which resulted from melting of mantle peridotite modified by reaction with slab melts.

The changes observed from Early Archaean TTG to Late Archaean sanukitoids reflect change in both the nature and efficiency of interaction between slab-melt and mantle-wedge peridotite. The changes in the degree and style of these interactions are a direct consequence of the cooling of the Earth, which modified the thermal and dynamic parameters at the subducted slab–mantle wedge interface. Therefore, in principle, in the PP spectra of Finnish Proterozoic adakitoids, the compatibles/HREE ratio should be higher due to mantle contamination than that of the Archaean adakitoids. In the spectra in Figure 19 (and, later in Fig. 96), it appears that the compatibles/HREE ratios of Proterozoic adakitoids are slightly higher, thus supporting the conclusions by Martin et al. (2005). Moreover, in the petrophysics summary in Figure 8, the density of Proterozoic adakitoids is clearly higher than that of Archaean adakitoids, which supports the more mafic component in Proterozoic adakitic rocks.

Halla (2005) examined Nilsiä and Koitere intrusion sanukitoids in eastern Finland, having similar geochemical signatures to high-Mg sanukitoid series from other parts of the Karelian domain and Archaean sanukitoid suites from Canada. They generally have low SiO_2 contents and high Mg numbers. They are enriched in K_2O, P_2O_5, Sr, Ba, Cr and LREE (Heilimo et al. 2010). Their Nd-depleted mantle model ages are 2768–3035 Ma. The geochemical and isotopic data suggest that they originated from a mantle wedge source enriched in LILE, U, Th and Pb by recycling of continental material in subduction-related slab dehydration processes shortly before melting. A considerable amount of crustal lead was contributed from subducting sediments into the overlying mantle wedge. Consequently, crustal lead isotope signatures overprinted the isotopic composition of mantle-wedge lead.

From the spectra in Figure 29, it can be seen that, in general, the TTGs and sanukitoids from Halla (2005) and Martin et al. (2005) correlate well with Finnish adakitoids: high Sr, Eu, LREE/HREE and compatibles/HREE. However, in all those spectra, the V, Cr and MgO (in TTGs) appear to be higher than in Finnish adakitoids, thus reflecting a relatively higher mantle component in the melt. From the TTG diagrams in Figure 29a, it can be seen that there is no age group distinctly closest to Finnish adakitoids.

Using correlation analysis, I found eight of 284 adakitic plutonic rock samples ('100% adakitoids') whose element chemistry correlates significantly (correlation coefficient above 0.9) with the corresponding average chemistry of sanukitoids studied by Halla (2005; Fig. 30) and 25 samples having a correlation coefficient above 0.8. In the diagrams in Figure 30, the averages of adakitoids with a sanukitoid signature and Halla's sanukitoids are almost identical, with the exception of Cr and Ni, possibly reflecting a higher mantle component in the sanukitoids.

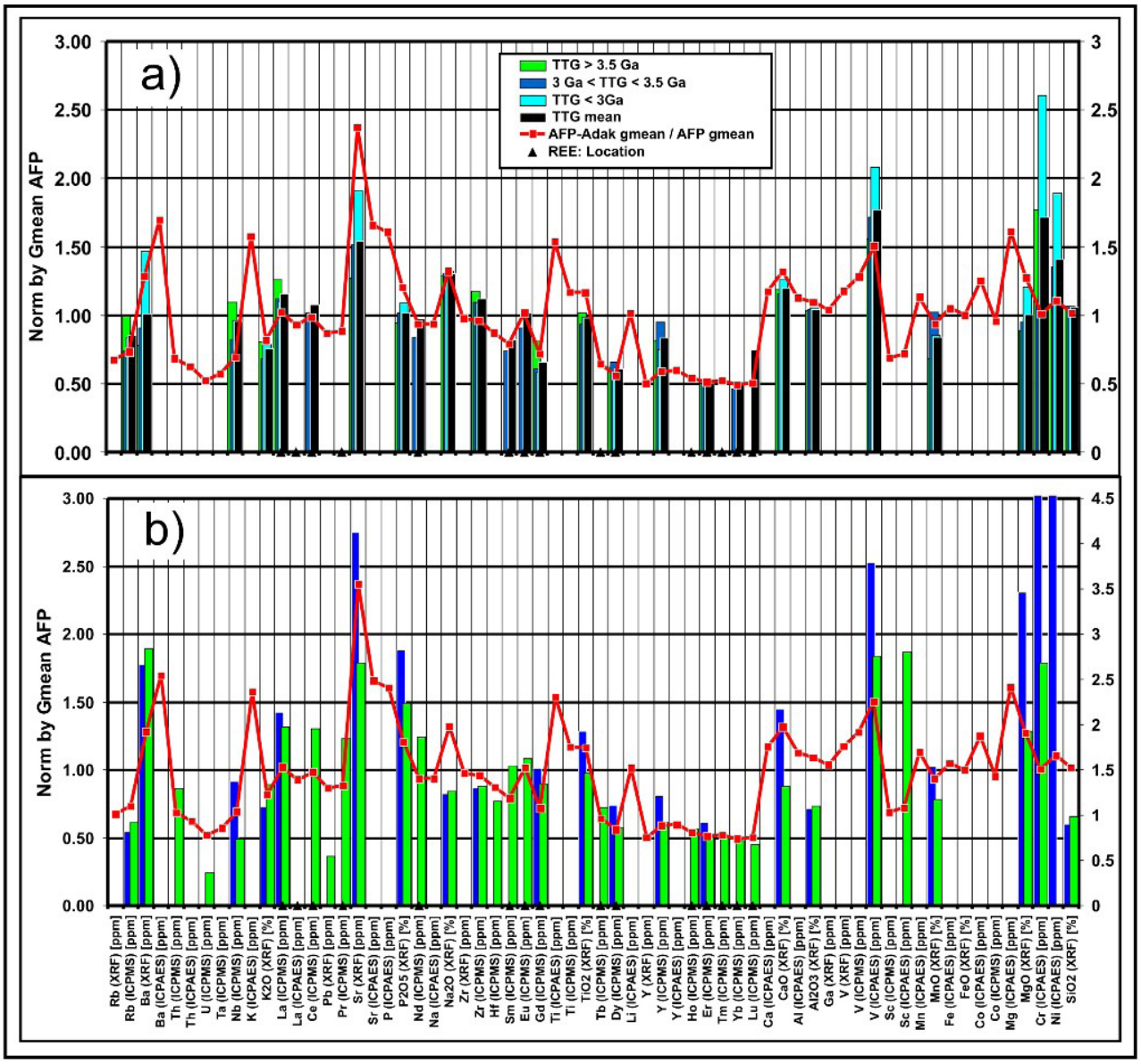

Fig. 29. (a): AFP-normalized Pearce–Peate spectra of gmeans of TTGs (right vertical axis: TTG age over 3.5 Ga, number of samples (n) = 108; TTG, age between 3.0–3.5 Ga, n = 320; TTG below 3.0 Ga, n = 666) and their average (TTG mean) adopted from Martin et al. (2005). In (b) are presented the AFP-normalized geometric means of sanukitoids adopted from Halla (2005; green bars, right vertical axis, 11 samples) and Martin et al. (2005; blue bars, right vertical axis, 31 samples). The red lines indicate the course of Finnish AFP-normalized '100% adakitic' plutonic rocks (178 samples: left vertical axis).

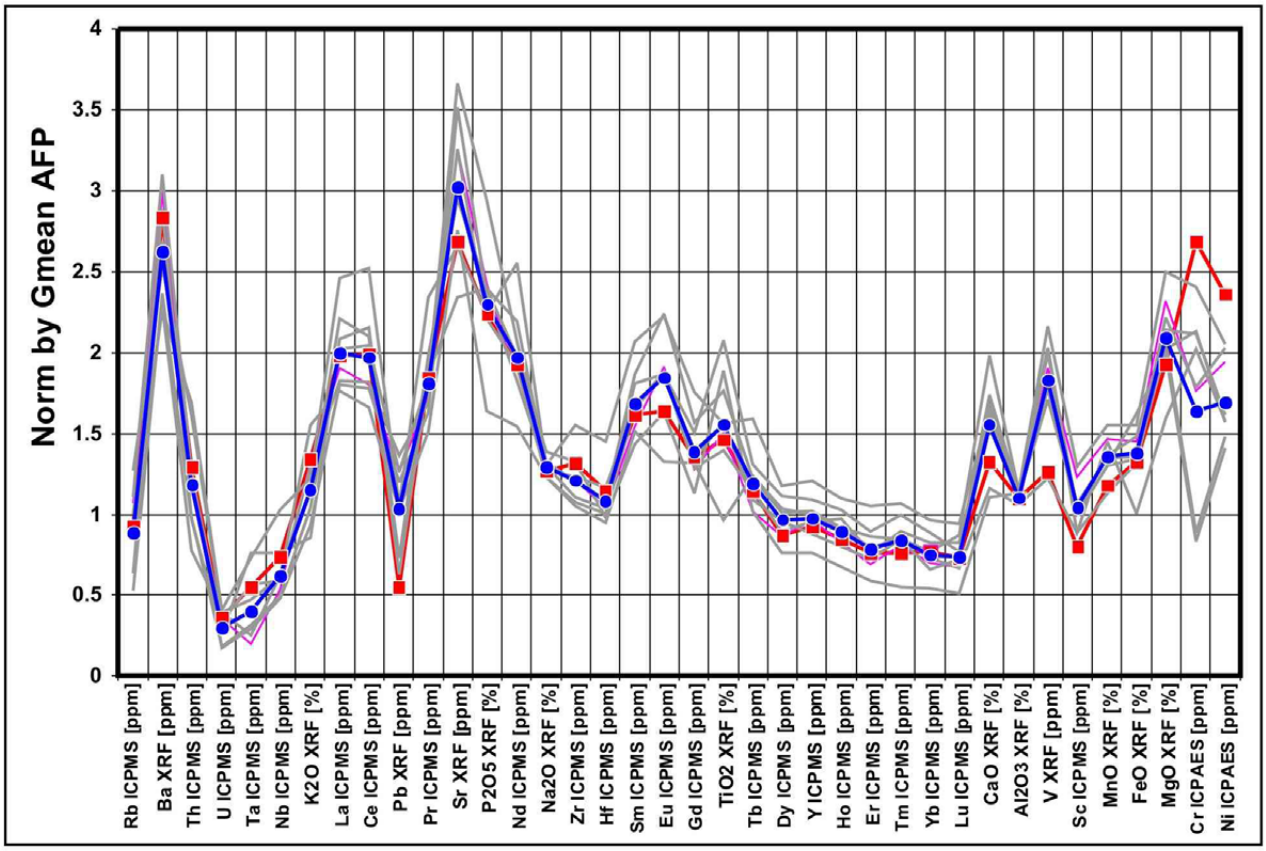

Fig. 30. Spectra of AFP-normalized adakitic plutonic rocks correlating (R > 0.9) with AFP-normalized sanukitoids adopted from Halla (2005). Red line: 'Halla sanukitoids'. Blue line: geometric mean of eight 'sanukitic' adakitoids from the GTK database (grey lines).

1.7 Relationship between adakitoids, TTGs and sanukitoids

As mentioned in the previous chapter, some adakitoids correlate with sanukitoids, although they do not fulfil all the criteria given, for example, by Halla (2005): SiO_2 = 55–60%, Mg numbers > 0.6, Ni > 100ppm, Cr > 200 ppm, K_2O > 1%, Sr and Ba > 500 ppm and Rb/Sr ratios < 0.1. However, more sanukitoids were observed from the GTK database when using the broader definition given by Heilimo et al. (2010): SiO_2 = 55–70%, Na_2O/K_2O = 0.5–3, MgO = 1.5–9%, Mg number = 45–65, K_2O = 1.5–5.0%, Ba+Sr > 1400 ppm and $(Gd/Er)_N$ = 2–6.

In the Na_2O/K_2O vs. Ba + Sr diagram in Figure 31, adopted from Halla et al. (2009), blue dots represent adakitic RGDB samples fulfilling all 8 criteria defined by Defant & Drummond (1990) and Thorkelson & Breitsprecher (2005), i.e. '100% adakitoids'. Correspondingly, the red dots represent sanukitoid samples fulfilling the criteria of Heilimo et al. (2010) given above.

In the diagram, the adakitic samples form a continuity from high Na_2O/K_2O TTGs to high Ba+Sr sanukitoids, referring to a mixed and complex origin for the adakitoids and sanukitoids. Moreover, the division of their primary source from a primitive basaltic source to enriched mantle fields in the diagram is arbitrary and difficult to define unambiguously. It can also be noted that not all sanukitoid samples overlap adakitoids; i.e. they do not all fulfil the criteria given for adakitic rocks above. Correspondingly, not all adakitic samples in the sanukitoid field fulfil the criteria by Heilimo et al. (2010). Also note the relatively high Ba+Sr values of all samples, excluding the TTGs with low Ba+Sr values.

On the map in Figure 32, rock samples with a sanukitoid and adakitic composition from RGDB are presented. It is interesting to note the large number of Proterozoic sanukitoid samples defined by the criteria of Heilimo et al. (2010),

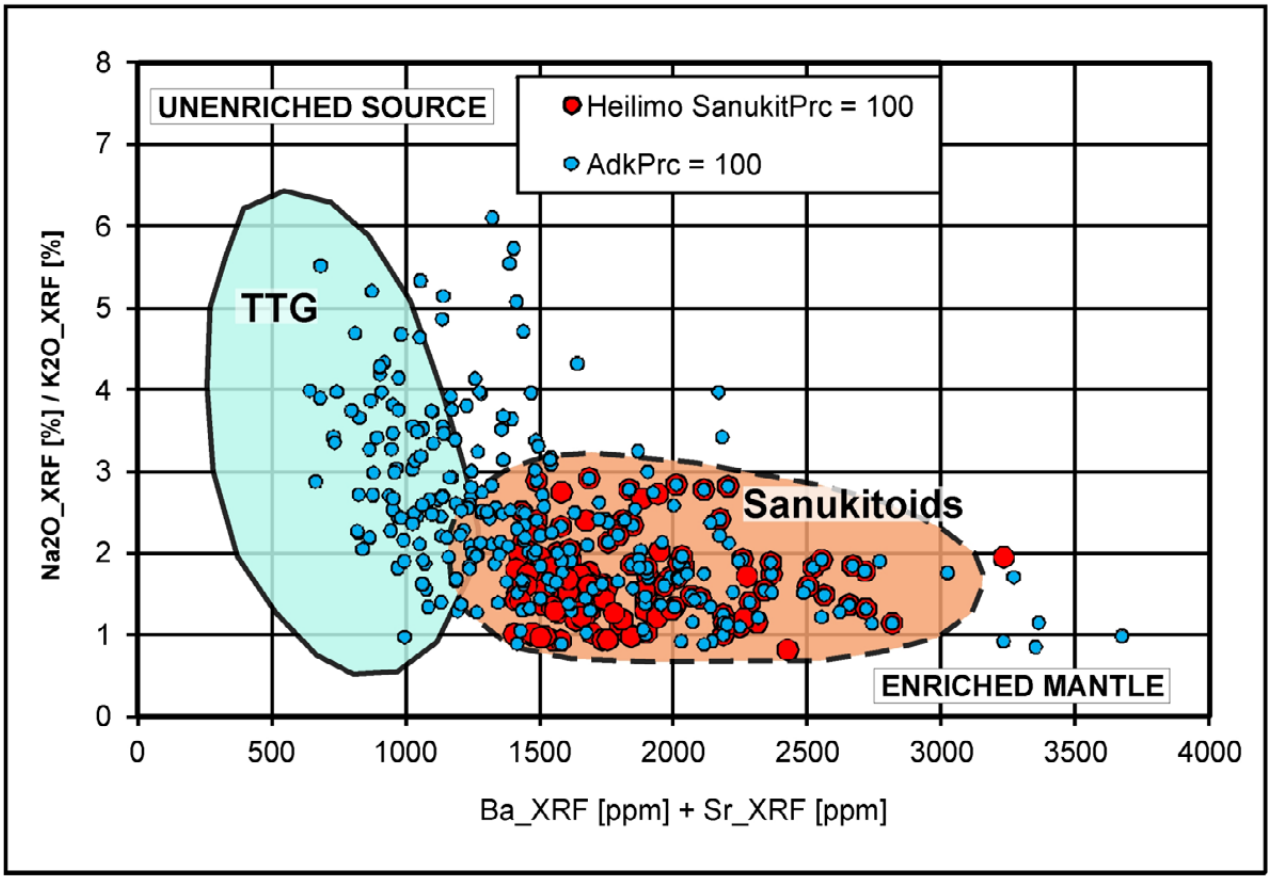

Fig. 31. Na_2O/K_2O vs. Ba+Sr plot for discriminating the high Ba+Sr sanukitoid group from the TTG groups. The hypothetical source end members are enriched mantle (high Ba+Sr, low Na_2O/K_2O) and a basaltic unenriched source (low Ba+Sr, high Na_2O/K_2O). Adopted from Halla et al. (2009).

concentrated in the Uusimaa sub-area (USM), Central Finland granitoid sub-area (CFG) and Ladoga–Bothnian Bay zone (LBZ). The USM and CFG sub-areas have been interpreted as island arcs and LBZ as primitive arc + back-arc basin (Ruotoistenmäki 1996, Nironen 1997, Lahtinen et al. 2005). In Archaean sub-areas, most sanukitoids are concentrated in the southern part of the Iisalmi sub-area (IC) and Ilomantsi sub-area (IL). Hölttä et al. (2012b) indicated sanukitoid arc type tectonic settings in the Ilomantsi area.

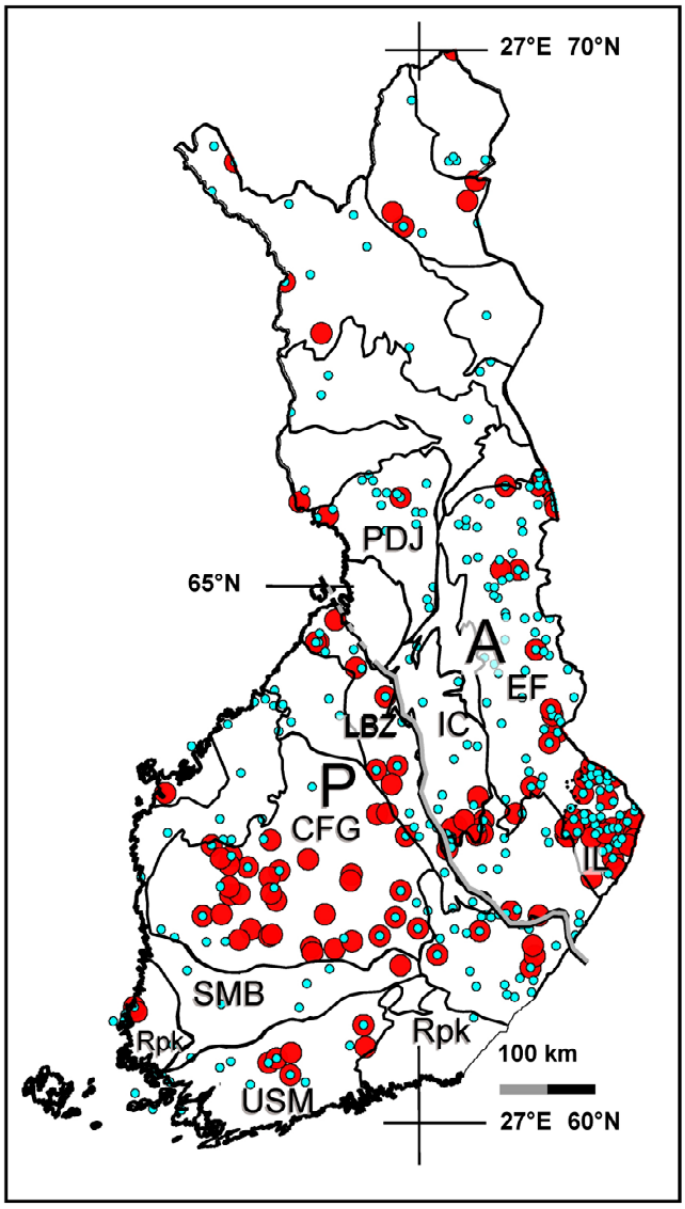

Fig. 32. Areal distribution of all Finnish '100%' compositionally sanukitoid samples (red dots) defined by the criteria of Heilimo et al. (2010) and '100%' adakitic samples (blue dots) fulfilling all 8 criteria defined by Defant & Drummond (1990) and Thorkelson & Breitsprecher (2005). Note that not all 'sanukitic' samples are also 'adakitic'. LBZ = Ladoga–Bothnian Bay zone. Rpk = rapakivi sub-areas in southern Finland. USM = Uusimaa sub-area, SMB = southern Finland migmatite sub-area, CFG = central Finland granitoid sub-area, EF = eastern Finland sub-area, IL = Ilomantsi sub-area (southernmost part of EF bordered by the dashed line), IC = Iisalmi sub-area, PDJ = Pudasjärvi sub-area.

1.8 Summary: Characteristics of Finnish adakitic plutonic rocks

Based on the references and considerations presented above, adakitic plutonic rocks, or adakitoids, can be summarized as derivatives from melts fractionated below the plagioclase stability depth, i.e. depths greater than ca. 30–60–... km (ca. 0.8 to 1.6 Gpa – ...). Chemically, they are characterized by SiO_2 > 56%, Al_2O_3 > 15%, Na_2O > 3.5%, Sr > 400 ppm, Y < 18 ppm, Sr/Y > 40, Yb < 1.9 and La/Yb > 20. When defining an adakitoid more widely, i.e. if it fulfills at least 6 of 8 criteria defined above, the number of adakitic plutonic rock samples in RGDB is 323 out of 1784 Proterozoic area samples (18%) and 540 of 1275 Archaean area samples (42%). Thus, their number and areal distribution is relatively large, especially in Archaean sub-areas. Only some supracrustal sub-areas lack adakitic plutonic rock samples. The comparison of adakitoids with Archaean and Proterozoic gabbros and granites (including rapakivis) emphasizes features only distinctive for adakitoids.

The Proterozoic adakitoids are denser than Archaean adakitoids, but their magnetic distributions are very similar to all Finnish plutonics, having both paramagnetic and ferromagnetic characteristics. Adakitoids are heavier than granites and lighter, less magnetic than gabbros. The susceptibility distributions of adakitoids are higher than Proterozoic granites, but below Archaean granite distributions.

In lithological tectonomagmatic R1-R2 diagrams, Proterozoic adakitoids range from syn- to post-collisional granodiorite–tonalite–diorite fields, while Archaean adakitoids have a wider lithological range also including a significant late- to post-collisional monzonitic–monzodioritic group. Overall, adakitoids fall between granite and gabbro fields. The Proterozoic and Archaean granites ('granitoids') range from syn- to late-orogenic granoriorites to monzo- and syenogranites. Gabbros vary from noritic to monzogabbros.

The capability to distinguish Archaean and Proterozoic rock groups in [Na_2O+K_2O vs SiO_2], [FeO/(FeO+MgO) vs SiO_2], [K_2O+Na_2O-CaO vs SiO_2] and A/CNK diagrams is relatively poor. In the [Nb/Ta vs Zr/Sm] diagram, there are systematic differences between the averages of the rock groups: Archaean and Proterozoic adakitoids are very close to each other, having the highest Nb/Ta and Zr/Sm ratios, both above Finnish plutonic rock averages. Proterozoic gabbros and granites have higher Nb/Ta and lower Zr/Sm ratios compared to corresponding Archaean rocks. Moreover, granites of both groups have a higher Zr/Sm ratio compared to gabbros.

In AFP-normalized Pearce–Peate diagrams, adakitoids are characterized by a high LREE/HREE ratio; i.e. a steep slope of lanthanides. Their Sr and Eu peaks are relatively high, reflecting increased plagioclase in the melt phase and deep lower crust/upper mantle fractionation depth. Moreover, their compatibles/HREE ratio is high, which can be associated with a high mafic component in the source material.

The AFP-normalized LREE/HREE ratio of granites is also high, but clearly less than that of adakitoids. Their compatibles/HREE ratio is opposite to that of adakitoids, i.e. the values of compatibles are strikingly low. In addition, their Sr and Eu values are at relative minima. All these features reflect upper to mid-crustal fractionation of a relatively felsic magma source, where stable plagioclase remains in restite. The spectrum of rapakivi 'granites' differs significantly from that of other granites. In particular, the slope of the AFP-normalized REE curve is positive, i.e. HREE > LREE. Moreover, the spectrum of rapakivis is almost complementary to that of adakitoids, having characteristics of the presumed complementary restite of adakitic melts.

The AFP-normalized lanthanide trends of gabbros are opposite to those of granites and adakitoids, i.e. HREE > LREE, their Sr and Eu values are high and compatibles rise strongly. All these refer to upper mantle/lower crust processes and a high component of mantle material in the source.

As a whole, it can be noted that adakitoids have characteristics of both felsic and mafic rock groups, but a clearly different evolutionary history from both of them.

Because adakitoids are evidently melts fractionated at great depths, the possible restitic minerals affecting the REE curves, in particular, were tested by selecting pairs of elements having estimations of partition coefficients for orthopyroxenes, clinopyroxenes, amphiboles and garnets. By studying the ratios of these elements, it was observed that the dominating mineral in

the restites appears to be clinopyroxene existing evenly in both Archaean and Proterozoic sub-areas. Orthopyroxene appears to exist relatively evenly in southern and central Finland, but less in the north. However, clusters of amphibole and especially garnet in restite dominate almost solely in the Archaean sub-areas of eastern Finland, referring to a higher pressure and/or temperature environment for Archaean adakitoid evolution.

The chemical spectrum of adakitoids is wide, forming a continuity from TTGs to sanukitoids, thus referring to a mixed and complex origin of their primary source from a basaltic source to enriched mantle. As a whole, all these classes can primarily be classified as 'plagioclase instability depth melts'.

2 CHARACTERISTICS OF ADAKITIC PLUTONIC ROCKS IN SELECTED PROTEROZOIC AND ARCHAEAN SUB-AREAS

In the previous section, I introduced areal, chemical and physical variations of Finnish adakitoids on a regional scale covering all Archaean and Proterozoic sub-areas of Finland. The following sections present examples of Finnish adakitoid characteristics and their evolution on a more local, up to sample scale.

2.1 Sub-areas and sample descriptions

This section considers adakitic plutonic rock samples collected from four Proterozoic and four Archaean sub-areas indicated on the map in Figure 33:

Proterozoic:
1. Uusimaa sub-area (USM)
2. Southern Finland migmatite sub-area (SMB)
3. Central Finland granitoid sub-area (CFG)
4. Ladoga–Bothnian Bay zone (LBZ)

Archaean:
1. Pudasjärvi sub-area (PDJ)
2. Iisalmi sub-area (IC)
3. Eastern Finland sub-area (EF)
4. Ilomantsi sub-area (IL)

The selected Proterozoic sub-areas represent examples of proposed plate tectonic marine and island arc sub-areas (e.g. Ruotoistenmäki 1996, Nironen 1997), while the Archaean blocks are examples of more or less 'exotic' TTG-dominated sub-areas, separated by tectonic and lithological discontinuities, whose evolution is more undefined (e.g. Ruotoistenmäki 1996, Hölttä et al. 2012a, 2012b).

In this chapter, the plutonic rock samples are also selected from the Rock Geochemical Database of Finland. The elements, standards, units and analytical methods are presented in Table 2. In this section, a sample is classified as an 'adakitoid' if it fulfills all eight criteria defined above for adakites by Defant & Drummond (1990) and Thorkelson & Breitsprecher (2005), i.e. '100%' adakitoid/adakitic plutonic rock.

In the following, I summarize and compare the data on these sub-areas using selected diagrams presented in the previous section. Lithological classifications are provided for all plutonic rock samples, including adakitoids, and separately for adakitoids alone. Thus, the 'all-plutonic' rock samples represent a rough estimate of the crustal composition in the selected sub-areas. For detailed statistics, the areal and lithological variations, classification and correlations of the RGDB chemistry of the sub-areas are given in the Lithogeochemical Atlas of Finland (Ruotoistenmäki 2016).

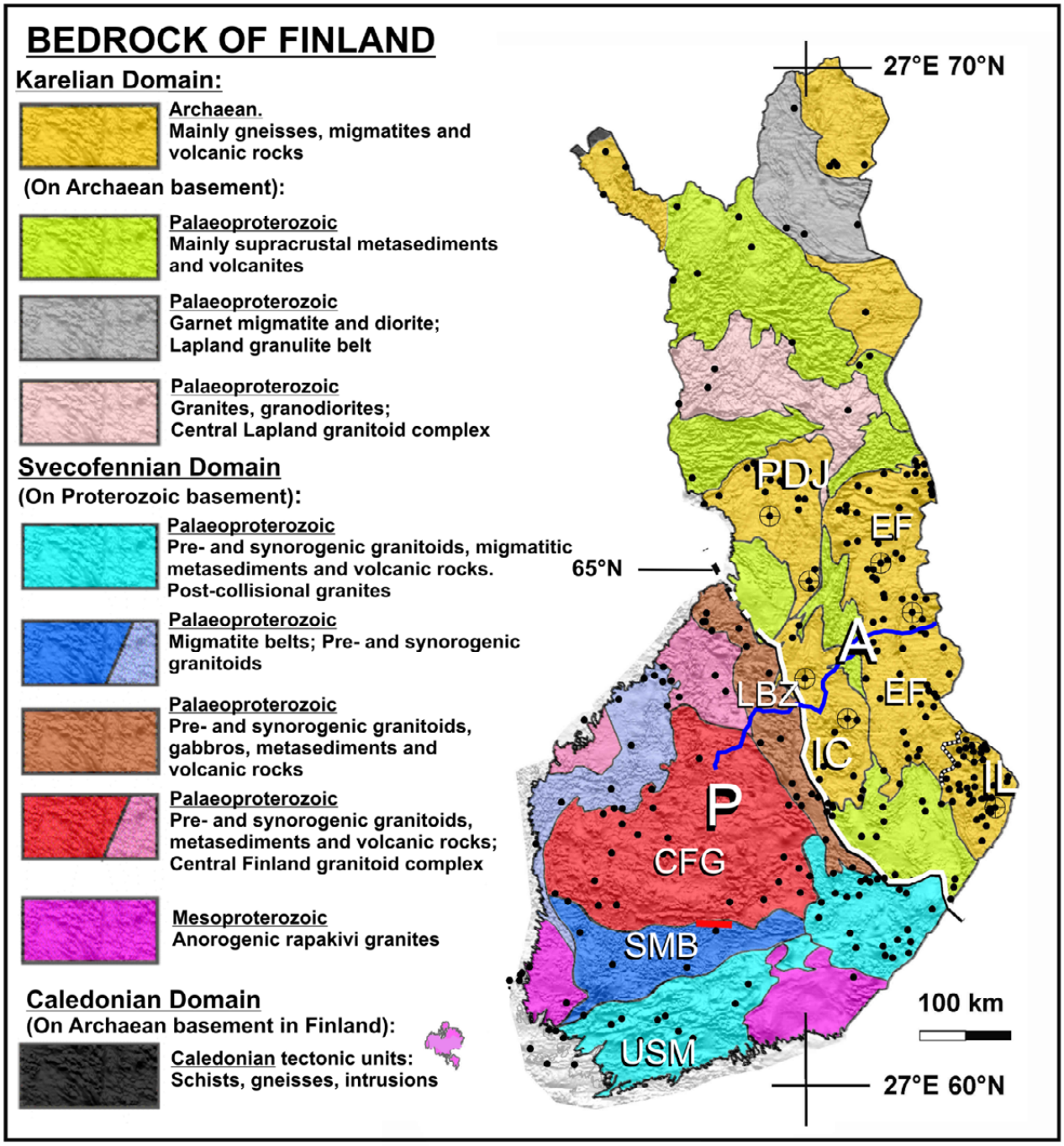

Fig. 33. Location of the sub-areas considered in this section. The black dots depict the location of "100%" adakitoids. For details, see Figure 3. The samples surrounded by a thin circle will be considered in next section (Fig. 50).

Uusimaa sub-area (USM)

This sub-area consists of two separate 'belts', named the 'Uusimaa' and 'Häme' belts by Nironen et al. (2002). They characterized the Uusimaa Belt by sedimentary-dominated rocks containing mica schists and gneisses interlayered with carbonate rocks and felsic sedimentary rocks. The volcanic rocks in area are mafic-intermediate to bimodal. The supracrustal rocks are cross-cut and migmatized by 1.88 Ga and 1.84–1.82 Ga granitoids. The Häme Belt contains volcanic rocks, granitoids and migmatized sedimentary rocks. The volcanics include older, intermediate and younger mafic-intermediate rocks. The granitoids occur as two age groups, 1.88 Ga and 1.84–1.82 Ga, that are cross-cut and migmatized by the supracrustal rocks (Nironen et al. 2002).

The total number of plutonic rock samples from the sub-area is 281, of which 14 samples (ca. 5%) are classified as "100%" adakitoids. In the diagrams in Figure 34, the plutonic rocks from this sub-area range from granodiorites–granites to gabbros, with adakitoids mainly being sub-alkaline, quartz-diorites–granodiorites. There is a distinct alkali granite group in the area, which may be connected with the 1.85–1.82–1.79 Ga leucogranites (e.g. Kurhila et al. 2005). In tectonomagmatic classification, plutonic rocks range from pre- to late-orogenic, while adakitoids are in pre- to post-collision uplift fields.

In the Pearce–Peate spectrum of this sub-area in Figure 35, a characteristic feature is a strong negative correlation between all samples and adakitoid samples. The all-sample spectrum is flat: LREE/HREE is ca. 1.0 and compatibles/HREE ≤ 1.0 (see the note "Elements used for ratios" above). However, the slope of the adakitoid REE spectrum is steep (LREE/HREE ca. 1.51) and compatibles are emphasized compared to HREE (compatibles/HREE ca. 1.9), referring to significant fractionation and a mafic signature in the adakitic samples. The opposing maxima and minima at, for example, Rb, Th, Sr and Eu, as well as the different REE slopes, indicate a middle to upper crust component for average 'all-plutonic rocks' and lower crust/upper mantle fractionation depths for adakitoids (also see the rapakivi spectra in Fig. 22 and Fig. 23). As shown on the maps in Figure 24 and Figure 25, the dominant restite minerals of adakitoids appear to be pyroxenes and five samples referring to garnet in the USM sub-area.

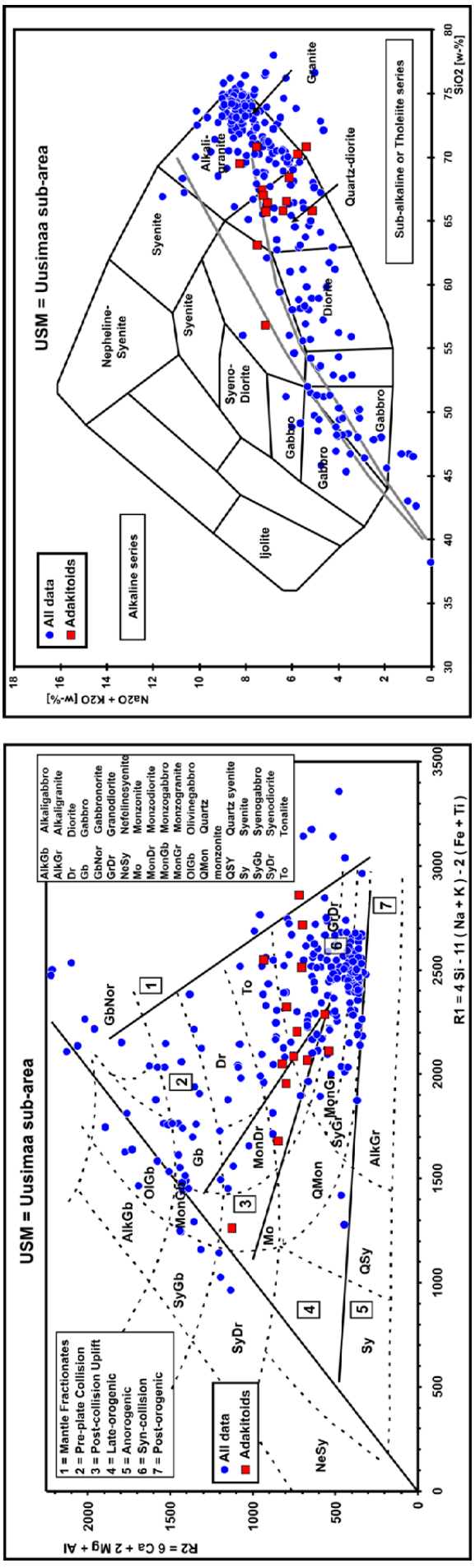

Fig. 34. Left: Lithological classification of the samples from the Proterozoic Uusimaa sub-area in the R1-R2 diagram (de La Roche et al. 1980). The red boxes in the diagrams refer to adakitic samples. The tectonomagmatic fields have been adopted from Batchelor & Bowden, (1985) and rock type boundaries have been modified according to Rollinson (1993). Right: Classification of samples in the Na_2O+K_2O vs SiO_2 diagram by Cox et al. (1979) modified for plutonic rocks by Wilson (1989). The alkaline/sub-alkaline boundary zone is adopted from Rickwood (1989).

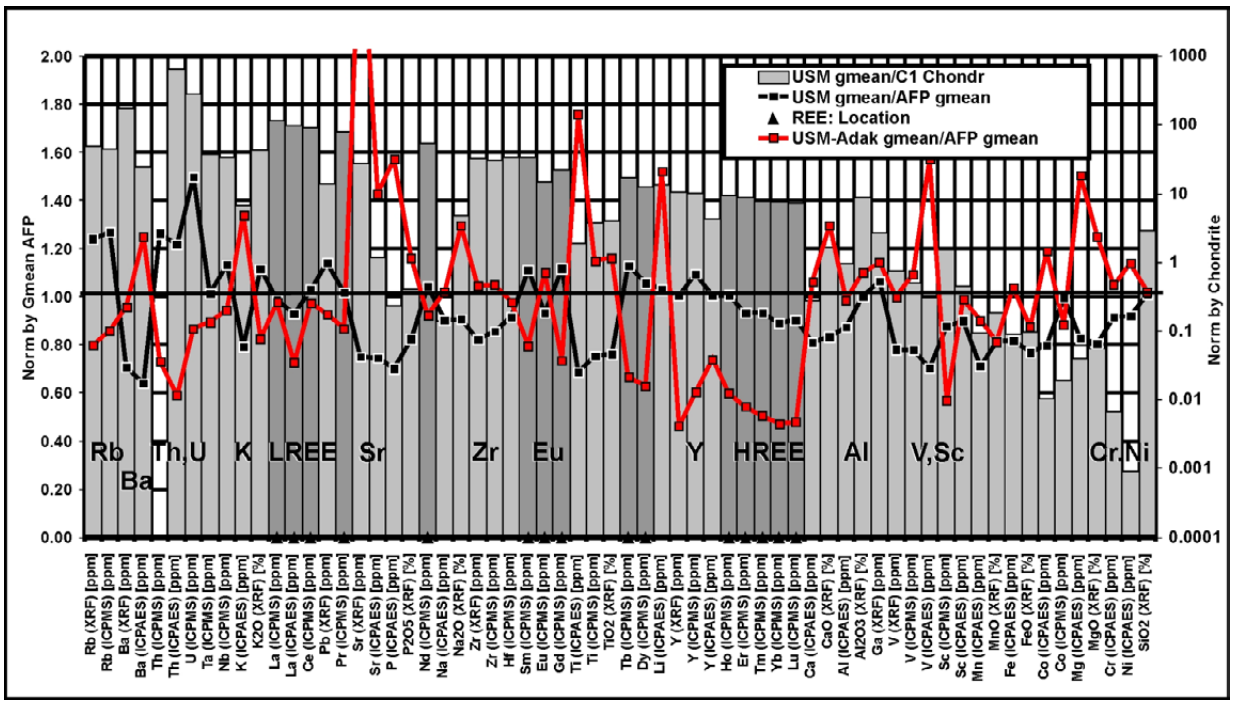

Fig. 35. Pearce–Peate spectra of samples from the Proterozoic Uusimaa sub-area. The black and red lines indicate the AFP-normalized data for all samples and for adakitic samples, respectively (left vertical axis). The grey bars show chondrite normalized values for all samples (right vertical axis). The black triangles and darker grey bars indicate the locations of REE.

Southern Finland migmatite sub-area (SMB)

This sub-area has been named the 'Pirkanmaa Belt' in Nironen et al. (2002), mainly consisting of migmatitic, turbiditic mica gneisses, with black schists and graphite-bearing schists as interlayers. They reported mafic and ultramafic plutonic rocks and 1.88 Ga granitoids cross-cutting the supracrustal rocks.

The total number of plutonic rock samples from this sub-area is 168, of which only six samples (ca. 3.5%) are classified as "100%" adakitoids. In the diagrams in Figure 36, the plutonic rocks from this sub-area range from mainly sub-alkaline granodiorites–granites to diorites and gabbros, adakitoids mainly being sub-alkaline, quartz-diorites–granodiorites–tonalites. In tectonomagmatic classification, the majority of the group of all-plutonic rocks of this sub-area, including adakitoids, are in the pre-collisional field.

A striking feature of the Pearce–Peate spectrum for this sub-area in Figure 37 is that the main peaks of 'all-plutonic rocks' are opposite to those of the Uusimaa sub-area above, reflecting their distinct differences. Moreover, although the proportion of pure adakitoids is only 3.5% in this area, their peaks coincide strikingly well with those of all-plutonic rocks, although the general trends are opposite. The LREE/HREE ratio of this sub-area is 0.72 for all-plutonic rocks and 1.27 for adakitoids, reflecting a higher degree of fractionation of the adakitoids. The corresponding compatibles/HREE ratios are 1.28 and 2.13, which both reflect a relatively high proportion of the mafic component in the samples.

Ruotoistenmäki (1996) interpreted a marine origin for SMB. This can explain the number of common peaks in the Pearce–Peate diagrams of all-plutonic rocks and adakitoids: 'All-plutonic rocks' are related to the collision and compression of rocks dominated by marine volcanic and sedimentary material and mafic sea floor of SMB between the Uusimaa sub-area and central Finland granitoid sub-area considered below. Correspondingly, adakitoids can be related to subduction/underthrusting and the high P–T fractionates of these rocks + mantle component below CFG. For more details, see also section 4., as well as Figure 82 and Figure 83.

On the maps in Figure 24 and Figure 25, the major restite minerals of adakitoids in SMB and close to its southern border appear to be pyroxenes and minor garnet.

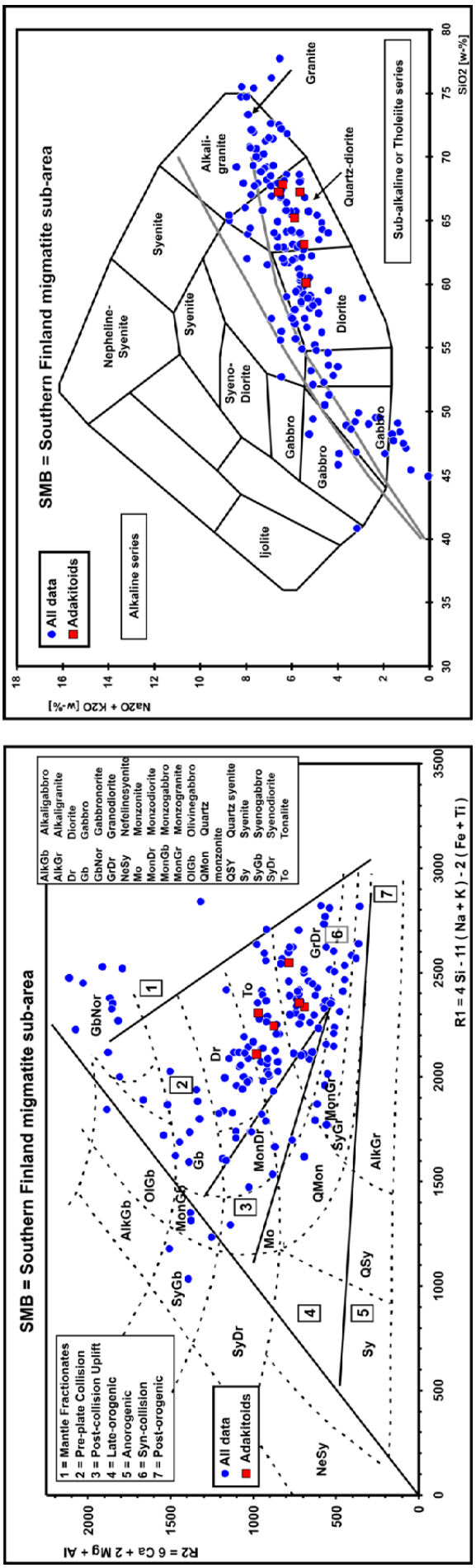

Fig. 36. Lithological classification of the samples from the Proterozoic southern Finland migmatite sub-area in the R1-R2 diagram (de La Roche et al. 1980) and the Na_2O+K_2O vs SiO_2 diagram (Cox et al. 1979). For details, see the caption of Figure 34.

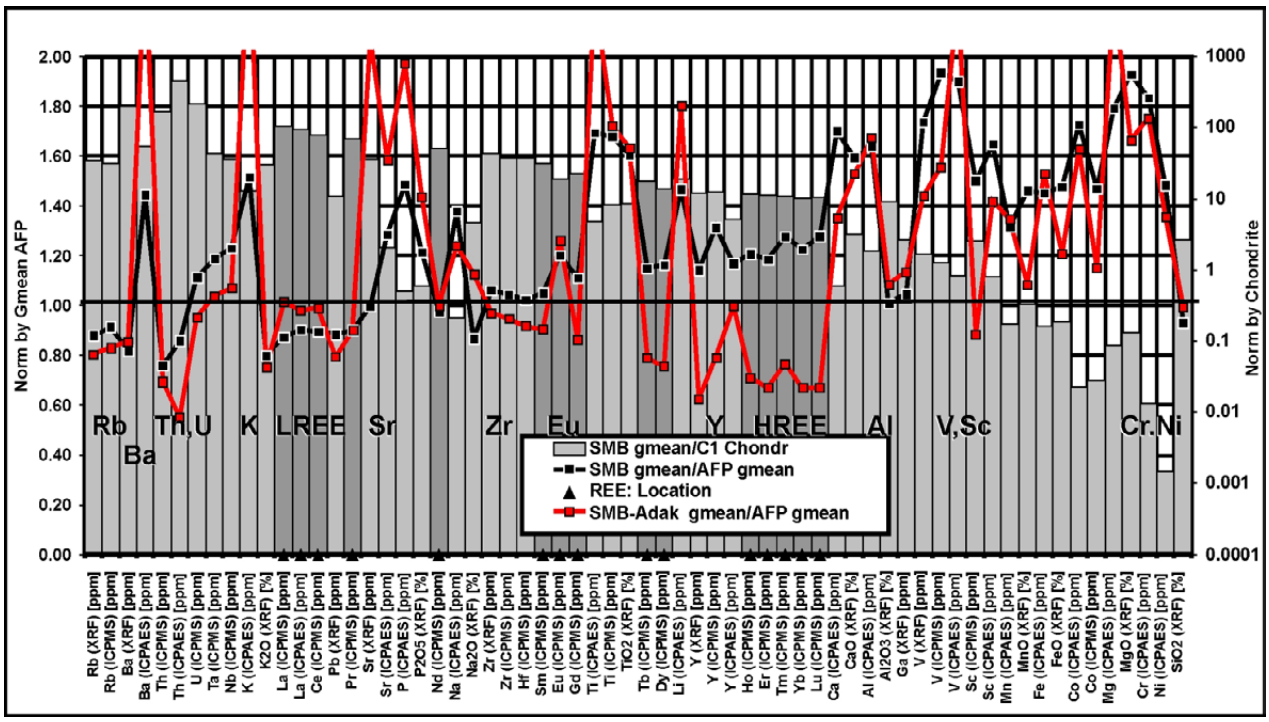

Fig. 37. Pearce–Peate spectra of samples from the Proterozoic southern Finland migmatite sub-area. The black and red lines indicate the AFP-normalized data for all samples and for adakitic samples, respectively (left vertical axis). For details, see Figure 35.

Central Finland granitoid sub-area (CFG)

This sub-area consists of 1.89–1.88 Ga synkinematic tonalites, granodiorites and granites, and 1.88–1.87 Ga post-kinematic quartz monzonites and granites. In addition, there are minor areas of subvolcanic intermediate rocks, mafic igneous rocks and remnants of supracrustal belts (Nironen et al. 2002).

The total number of plutonic rock samples from CFG is 583, of which 22 samples (ca. 3.8%) are adakitic. In the diagrams in Figure 38, the plutonic rocks from this sub-area range from granites–diorites to gabbros, adakitoids being mainly sub-alkaline granodiorites–tonalites–diorites. In tectonomagmatic classification, adakitic plutonic rocks are pre-collisional, while all-plutonic rocks range from pre- to late-orogenic fields.

The Pearce–Peate spectra of this sub-area in Figure 39 appear to be halfway between those of the USM and SMB. The main peaks of all samples appear to correlate with those of the adakitoids, as in the southern Finland migmatite sub-area. The trend of all-plutonic rocks is flat/gently increasing (LREE/HREE ca. 0.79; HREE slightly emphasized) and the relative proportion of compatibles is low (compatibles/HREE ca. 0.85), as in the USM sub-area above. The content of lanthanides is relatively high, ca. 1.2–1.4 times the Finnish average (AFP).

The peaks in the adakitoid spectrum are sharp and relatively high, the REE slope of the spectrum is steep (LREE/HREE ca. 1.6) and compatibles are enhanced (compatibles/HREE ca. 1.55). From the Pearce–Peate spectra and lithological diagrams, it can thus be concluded that the sample group of all-plutonic rocks consists of relatively mixed plutonic rocks, the majority resulting, however, from processes in the mid-/upper crust (e.g. flat REE slope, low Eu values). The steeply sloping REE, high Sr, Eu and compatibles of adakitoids reflect processes concentrated in the depths of the lower crust/upper mantle and apparently less crustal contamination. Ruotoistenmäki (1996) interpreted CFG as an island arc having ‘continental’, plutonic characteristics. In that model, the adakitoids can be connected with magmas related to SMB subduction/underthrusting below CFG (see Figure 82 and Figure 83 and comments on SMB above). This sub-area is characterized by a significant proportion of plutonic rocks having a sanukitoid composition, as demonstrated on the map in Figure 32.

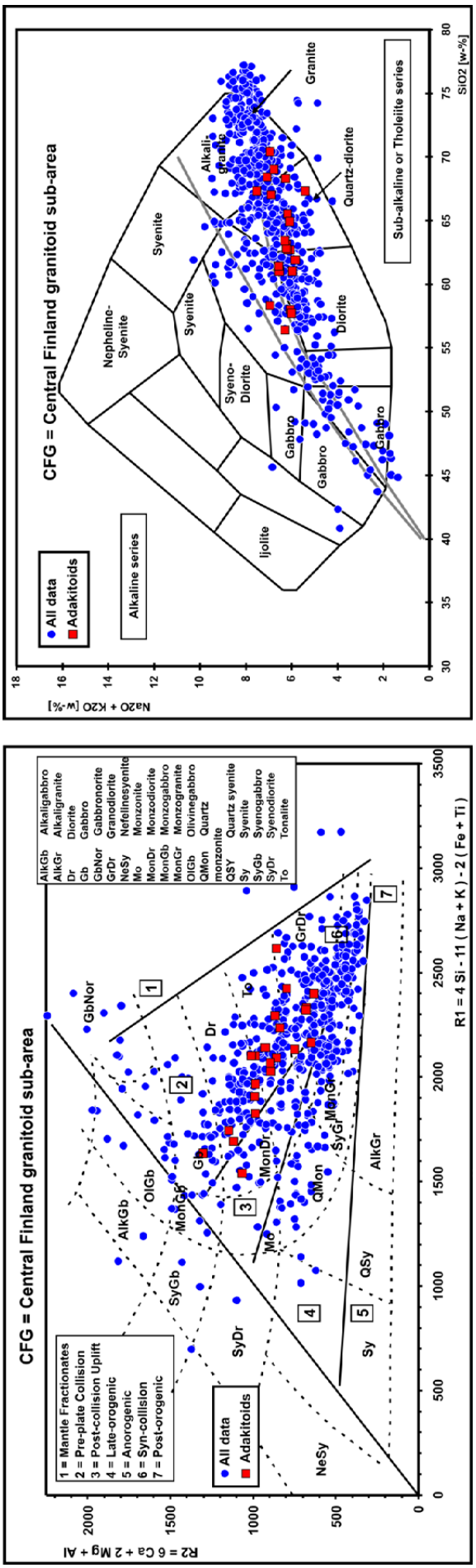

Fig. 38. Lithological classification of the samples from the Proterozoic central Finland granitoid sub-area in the R1-R2 diagram (De La Roche et al. 1980) and the Na_2O+K_2O vs SiO_2 diagram (Cox et al. 1979). For details, see the caption of Figure 34.

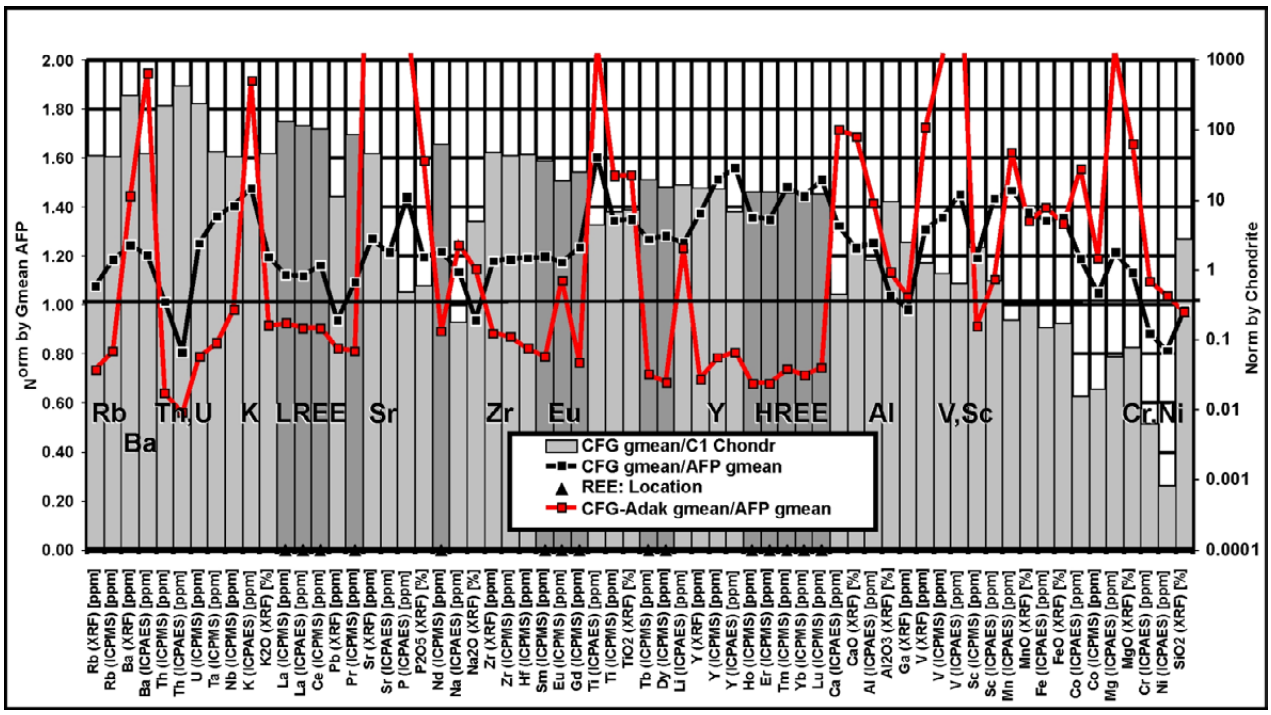

Fig. 39. Pearce–Peate spectra of samples from the central Finland granitoid sub-area. The black and red lines indicate the AFP-normalized data for all samples and for adakitic samples, respectively (left vertical axis). For details, see Figure 35.

On the maps in Figure 24 and Figure 25, the major restite minerals of adakitoids appear in this sub-area to be pyroxenes and minor amounts of amphibole, which refer to the subduction of a relatively hot and shallow, gently dipping plate (e.g. Herzberg 1995, Martin & Moyen 2002).

Ladoga–Bothnian Bay zone (LBZ)

This sub-area 'Savo Belt' is characterized in Nironen et al. (2002) by mica gneisses having volcanics, graphite schists, black schists and carbonate rocks as interlayers. The volcanic rocks consist of two groups: a 1.92 Ga bimodal group, and 1.89–1.88 Ga mafic-intermediate group. Moreover, they document 1.92 Ga gneissic tonalites and 1.89–1.88 Ga granitoids in the sub-area. The area is cut by numerous shear zones.

The total number of plutonic rock samples from LBZ is 177, of which 18 samples (ca. 10%) are adakitoids. Thus, this zone is the 'most adakitic', having the highest percentage of adakitic samples of the Proterozoic sub-areas considered here. In Figure 40, the plutonic rocks range from granodiorites–granites–monzogranites to gabbros and the adakitoids are mainly sub-alkaline granodiorites–diorites–monzodiorites. In this sub-area, monzonitic adakitoids are more common when compared, for example, to CFG above. In tectonomagmatic classification, adakitic plutonic rocks fall between pre- and post-collisional fields, the post-collisional characteristics being dominant. The all-plutonic rocks range from pre- to syn- and post-collisional classes.

A striking feature of the Pearce–Peate spectrum of this sub-area in Figure 41 is that the spectra of both all-plutonic rocks and adakitoids are very similar to those of the SMB. This is also demonstrated in Table 6 below, which presents the correlations of the AFP-normalized Pearce–Peate spectra of all sub-areas considered here. In LBZ, the peaks of the all-plutonic rock spectrum also correlate with those of the adakitoids, although the REE trends are opposite. The LREE/HREE ratio of this sub-area is 0.82 for all-plutonic rocks and 1.32 for adakitoids, reflecting the high degree of fractionation of the adakitoids. The corresponding compatibles/HREE ratios are 1.1 and 1.74, which both reflect a relatively high content of mafic components in the samples. Thus, it can be concluded that the fractionation processes of adakitic plutonic rocks in LBZ took place deep in the lower crust/upper mantle, as also in SMB. This is also supported by the high

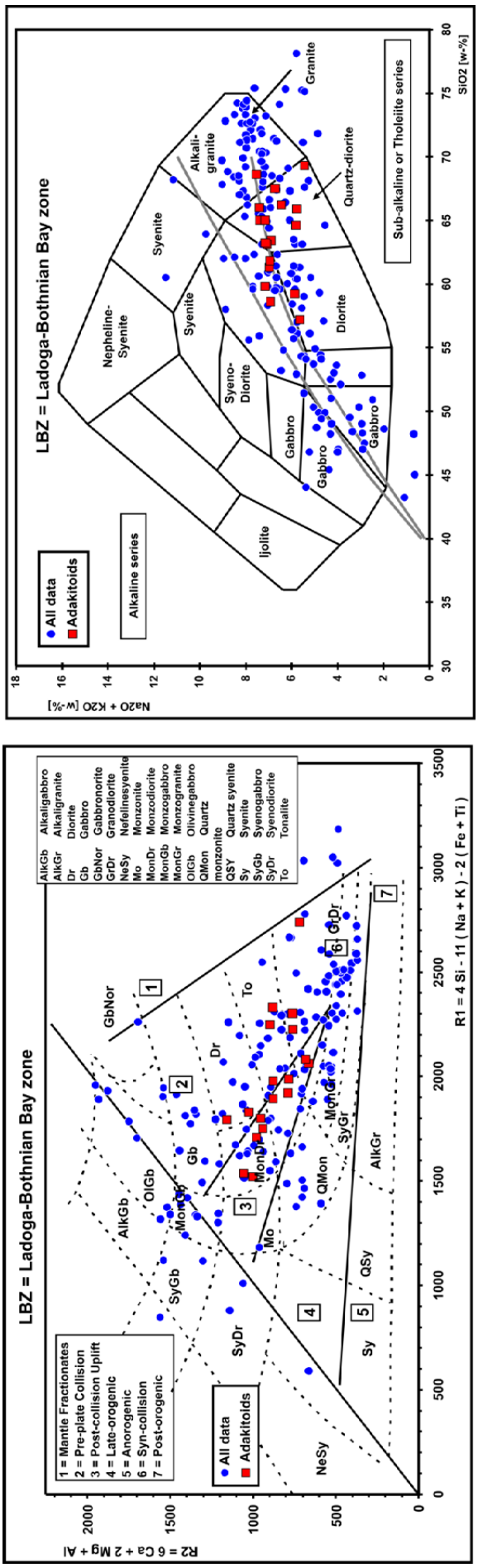

Fig. 40. Lithological classification of the samples from the Proterozoic Ladoga–Bothnian Bay zone sub-area in the R1-R2 diagram (de La Roche et al. 1980) and the Na_2O+K_2O vs SiO_2 diagram (Cox et al. 1979). For details, see the caption of Figure 34.

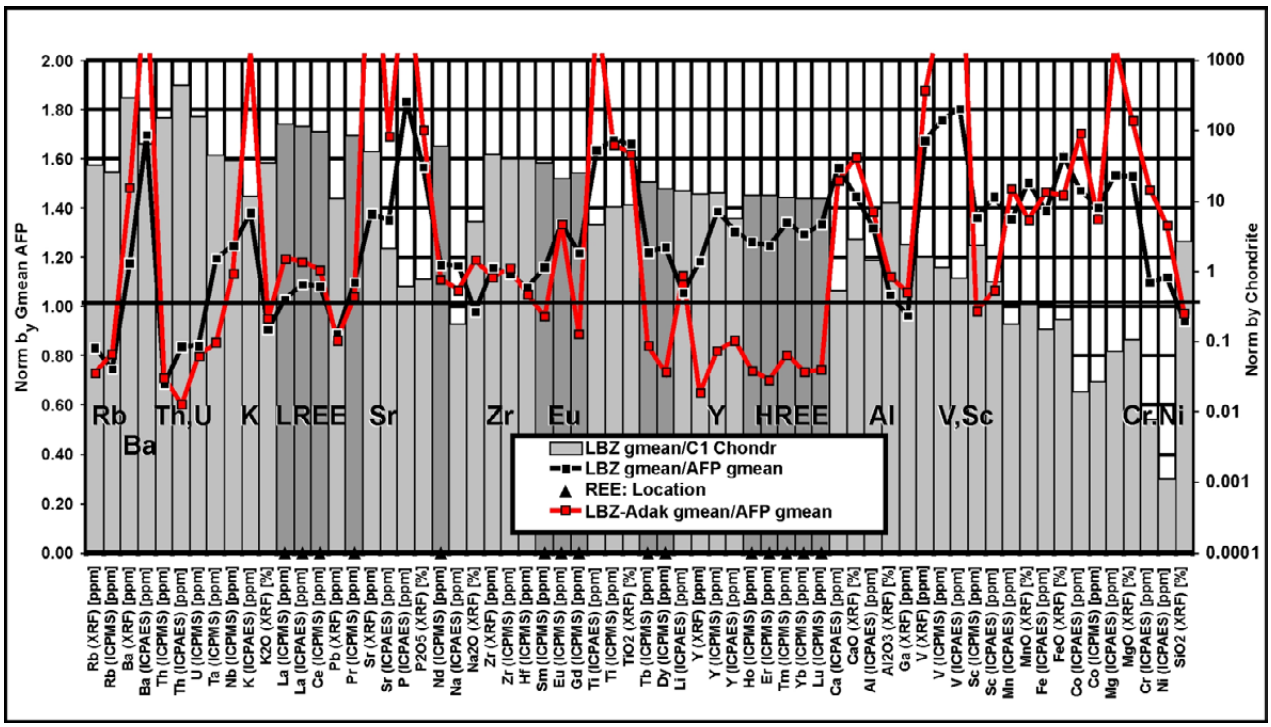

Fig. 41. Pearce–Peate spectra of samples from the Proterozoic Ladoga–Bothnian Bay zone sub-area. The black and red lines indicate the AFP-normalized data for all samples and for adakitic samples, respectively (left vertical axis). For details, see Figure 35.

quantity of mafic rocks in the sub-area. Ruotoistenmäki (1996), as well as Nironen (1997) and Lahtinen et al. (2005), interpreted LBZ, like SMB above, as a marine basin, which thus refers to a similar, common oceanic plate-dominated origin for both all-plutonic rocks and adakitoids in LBZ. The 'all-plutonic' rocks are related to seafloor and primitive island arc collision/accretion against Archaean crust. Correspondingly, adakitoids are related to subduction/underthrusting. See also section 5 and the tectonic model displayed in Figure 94 and Figure 95. The major restite minerals of adakitoids in LBZ are mainly clinopyroxene and orthopyroxene on the maps in Figure 24 and Figure 25.

Pudasjärvi sub-area (PDJ)

This sub-area has been named by Nironen et al. (2002) as the 'Pudasjärvi Complex', consisting of Archaean gneisses and granitoids, as well as amphibolites that are presumably remnants of Archaean greenstone belts. Proterozoic granites and diabase dykes have intruded the gneisses. Mänttäri (2012) reports ages from ca. 2640 Ma to 2877 Ma from adakitic samples from Pudasjärvi area (Fig. 58 to Fig. 59). Mutanen & Huhma (2003) documented ca. 3.5 Ga zircon ages from gneisses in this sub-area.

The total number of plutonic rock samples from this sub-area is 98, of which 18 samples (ca. 19%) are adakitic. Thus, there is a significant number of adakitic samples compared to any of the Proterozoic sub-areas. In the diagrams in Figure 42, the plutonic rocks are mainly felsic, granitic-granodioritic with a distinct, high SiO_2 alkali-granite group. The adakitoids range from sub-alkaline granites to diorites. In tectonomagmatic classification, all-plutonic rocks are syn- to late-orogenic, while adakitoids are pre- to syn-collisional.

The Pearce–Peate spectra of this sub-area are presented in Figure 43. Because of high number of adakitic samples, their general trends are similar, with the correlation being relatively high (0.59 in Table 6). The LREE/HREE ratios of the all-plutonic rock samples and adakitoids are high (1.55 and 2.26, as well as compatibles/HREE rations (ca. 1.53 and 2.14, respectively). In the restite maps in Figure 24 and Figure 25, clinopyroxene, garnet and amphibole all appear to be equally represented in this sub-area. In

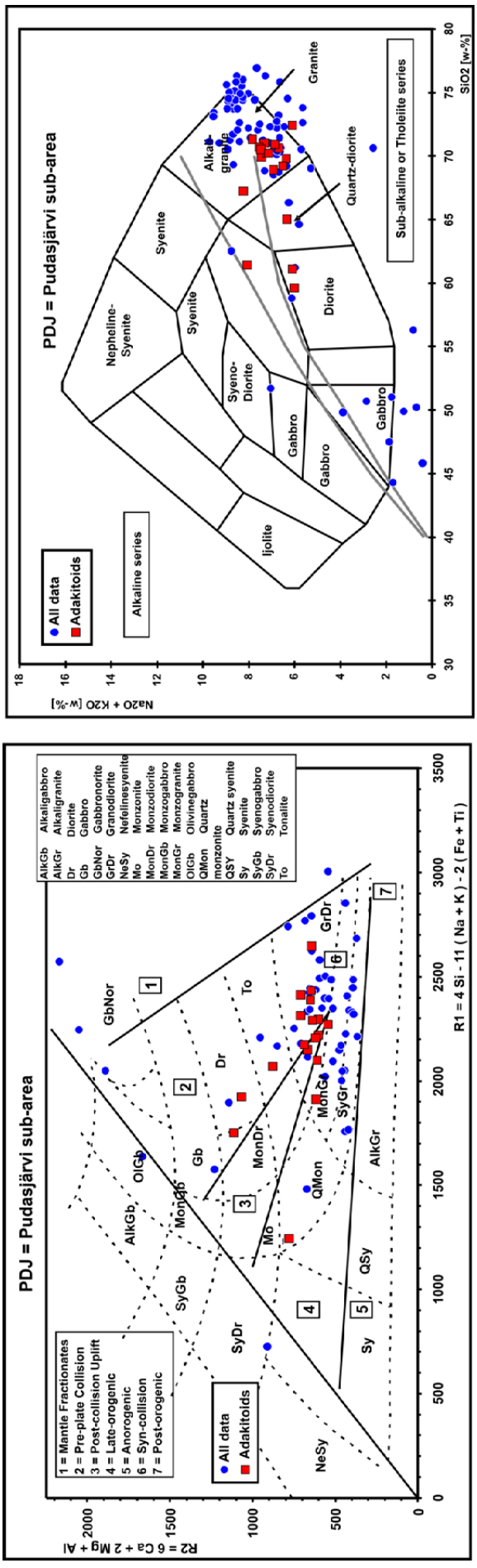

Fig. 42. Lithological classification of the samples from the Archaean Pudasjärvi sub-area in the R1–R2 diagram (de La Roche et al. 1980) and the Na_2O+K_2O vs SiO_2 diagram (Cox et al. 1979). For details, see the caption of Figure 34.

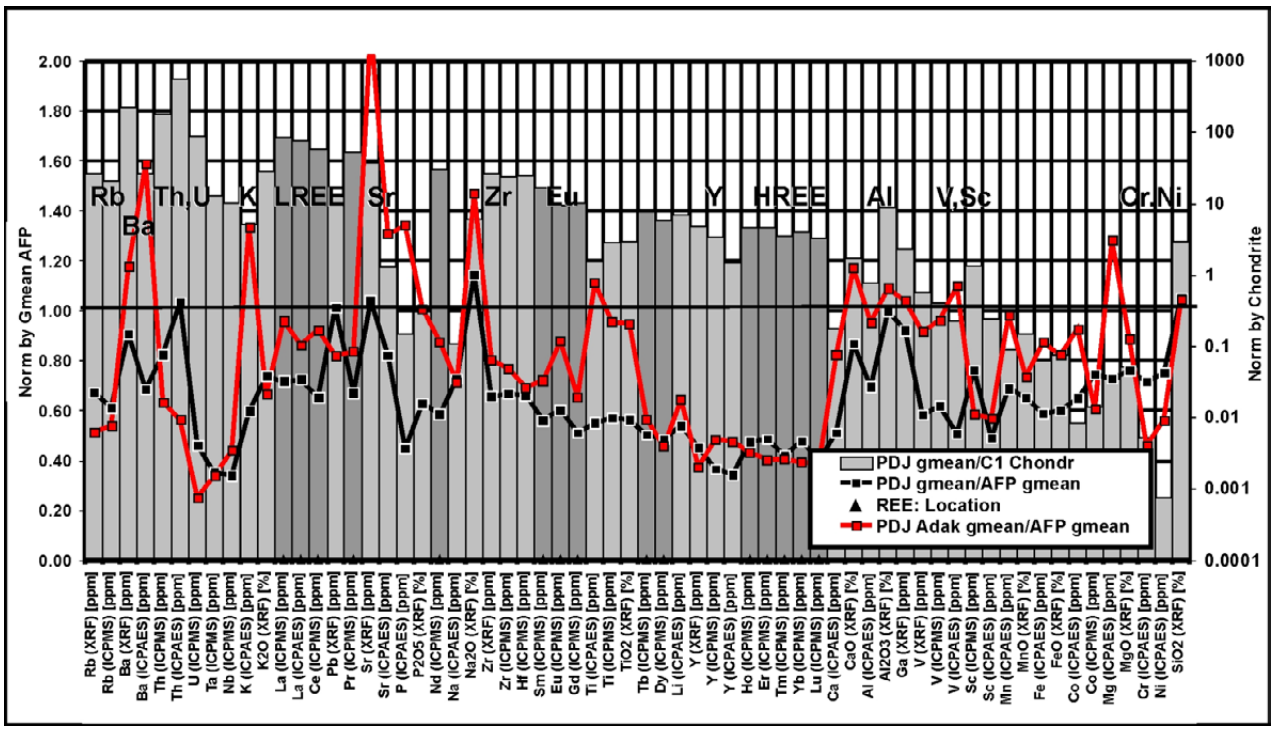

Fig. 43. Pearce–Peate spectra of samples from from the Archaean Pudasjärvi sub-area. The black and red lines indicate the AFP-normalized data for all samples and for adakitic samples, respectively (left vertical axis). For details, see Figure 35.

particular, garnet reflects higher P–T conditions in the fractionation environment compared to the Proterozoic sub-areas above. This is also supported by the steep REE curve and high amounts of compatibles in the Pearce–Peate spectrum of adakitoids.

Iisalmi sub-area (IC)

This sub-area consists of 3.2–2.6 Ga tonalitic gneisses and amphibolitic migmatites metamorphosed at granulite grade in large areas (Nironen et al. 2002; 'Iisalmi Complex'). Nironen et al. (2002) also documented paragneisses and a carbonatite complex in the area. The gneisses have been locally deformed by Proterozoic overprinting and intruded by Proterozoic granites and diabase dykes (Ruotoistenmäki et al. 2001, Nironen et al. 2002).

In section 5., I consider ca. 1880–1860 Ma syn- to late-/post-collisional Proterozoic intrusives cross-cutting this sub-area, some of which are also adakitic. However, the majority of those samples show negative ε_{Nd} values referring to primary Archaean source material. Those samples are not connected to the data used in this section.

The total number of plutonic rock samples from this sub-area is 123, of which 11 samples (ca. 9%) are classified as adakitoids. Thus, there is also a relatively high number of adakitic samples compared to those in the Proterozoic sub-areas above. From Figure 44, it can be seen that the plutonic rocks range from granites–granodiorites to gabbros, the samples mainly being sub-alkaline. The adakitoids range from slightly sub-alkaline granites to monzodiorites. In tectonomagmatic classification, the majority of plutonic rocks, including adakitoids, are syn- to post-collisional.

The peaks of the Pearce–Peate spectra of all-plutonic rocks and adakitoids of this sub-area in Figure 45 are very coincident, as can be seen from the high correlation (0.73) in Table 6, reflecting a similar evolutionary history. The LREE/HREE ratio of the all-plutonic rock spectrum is ca. 1.0, while that of adakitoids is ca. 2.3, which is very high compared to the Proterozoic adakitoids above. In addition, the relative maxima of compatibles in this sub-area are higher than in previous Proterozoic sub-areas, the compatibles/HREE ratios being ca. 1.36 and 2.16 for all-plutonic rocks and adakitic plutonic rocks, respectively. It can be concluded that the

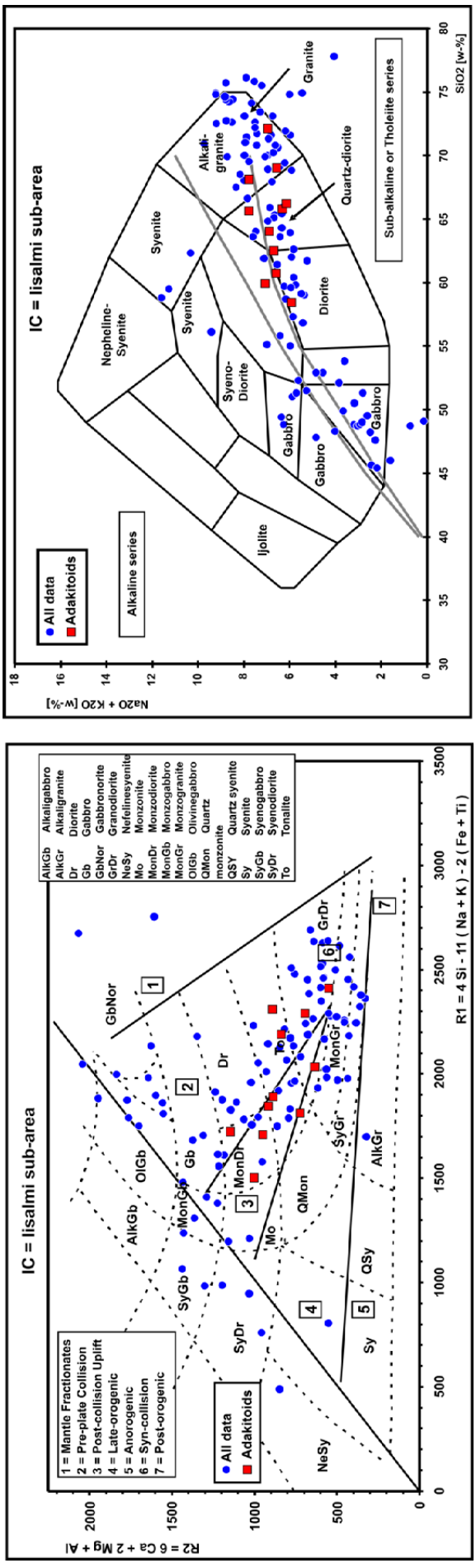

Fig. 44. Lithological classification of the samples from the Archaean Iisalmi sub-area in the R1–R2 diagram (de La Roche et al. 1980) and the Na_2O+K_2O vs SiO_2 diagram (Cox et al. 1979). For details, see the caption of Figure 34.

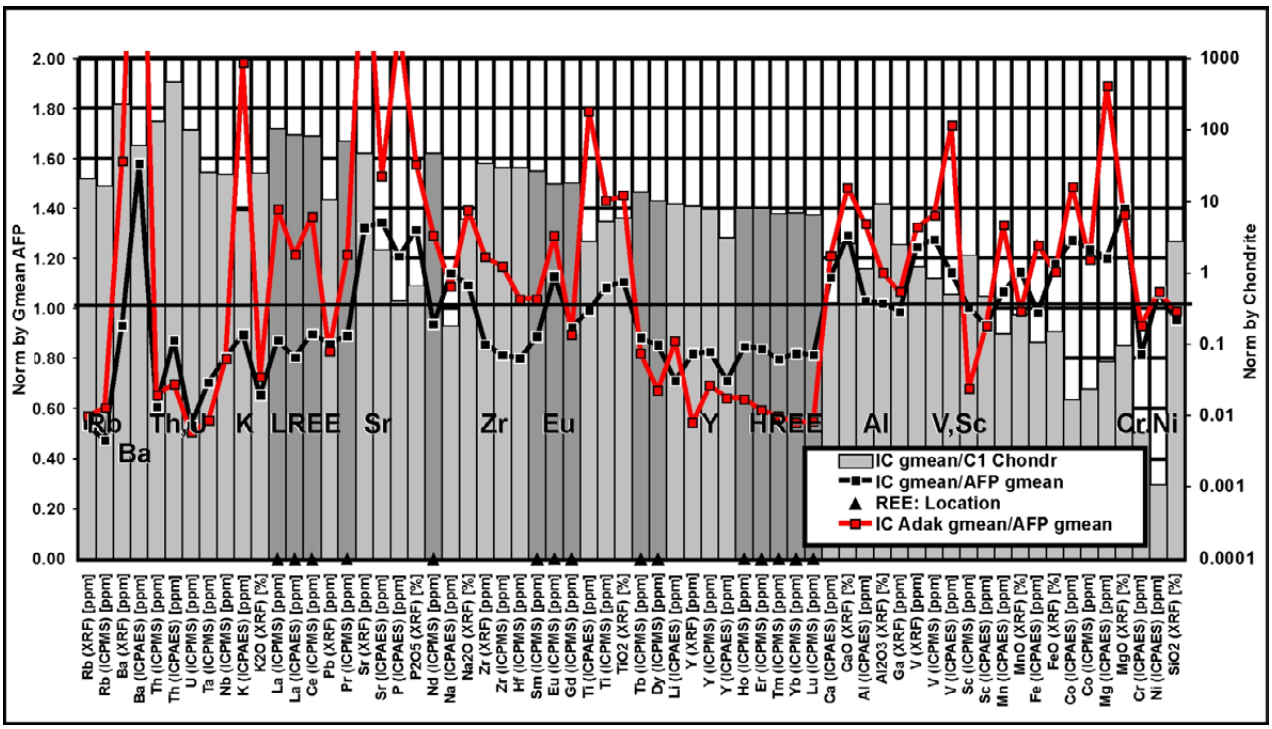

Fig. 45. Pearce–Peate spectra of samples from the Archaean Iisalmi sub-area. The black and red lines indicate the AFP-normalized data for all samples and for adakitic samples, respectively (left vertical axis). For details, see Figure 35.

adakitic (TTG) signature is dominant in this sub-area as a whole. The AFP-normalized LREE values of adakitoids (above 1.2) are exceptionally high in this area, i.e. clearly above the average for Finnish plutonic rocks.

On the maps in Figure 24 and Figure 25, the major restite minerals of adakitoids appear to be pyroxenes and, in southern part, garnet and amphibole. In particular, garnet reflects higher P–T conditions in the fractionation environment compared to the Proterozoic sub-areas above. This is also supported by the steep REE curve and high contentof compatibles in the Pearce–Peate spectrum of adakitoids.

For tectonic analysis of this sub-area, see also section 5., as well as Figure 94 and Figure 95.

Eastern Finland sub-area (EF)

This sub-area mainly consists of 2.85–2.69 Ga granitoids and migmatites (Nironen et al. 2002; ‘Eastern Finland Complex’). In addition, there are paragneiss-dominated areas intruded by Proterozoic granites and diabase dykes. Proterozoic deformation and alteration have locally caused strong overprinting, especially in the western part of the complex. In this sub-area, I also include the ‘Kuhmo greenstone belt’ (Nironen et al. 2002), consisting of 2.97 Ga mafic and intermediate volcanics and 2.79 Ga mafic volcanics with ultramafic parts. Iron formations and mica schist interlayers are found in the central parts of the greenstone belt area.

The total number of plutonic rock samples from this sub-area is 317, of which 66 samples (ca. 21%) are classified as adakitoids. Thus, this sub-area also has a significantly higher proportion of adakitic samples compared to those in Proterozoic sub-areas above. In the diagrams in Figure 46, the all-plutonic rocks from this sub-area are bimodal: mainly granitic-granodioritic, with a smaller group of gabbroic samples. The adakitoids range from sub-alkaline granites to monzodiorites. In tectonomagmatic classification, all-plutonic rocks including adakitoids are in pre-, syn- to post-collisional fields.

In this sub-area, the Pearce–Peate spectra of all-plutonic rocks and adakitoids in Figure 47 correlate very strongly (correlation 0.87 in Table 6), the trends and peaks of adakitoids being more emphasized. The LREE/HREE ratios of the all-plutonic rock samples and adakitoids

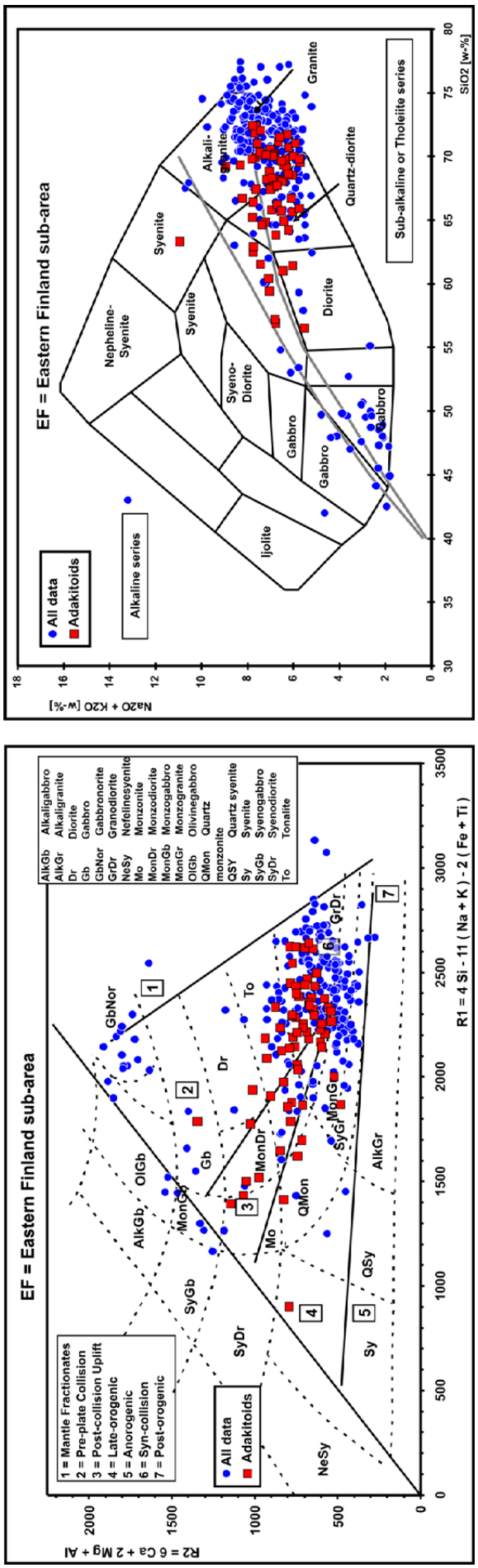

Fig. 46. Lithological classification of the samples from the Archaean Eastern Finland sub-area in the R1–R2 diagram (de La Roche et al. 1980) and the Na_2O+K_2O vs SiO_2 diagram (Cox et al. 1979). For details, see the caption of Figure 34.

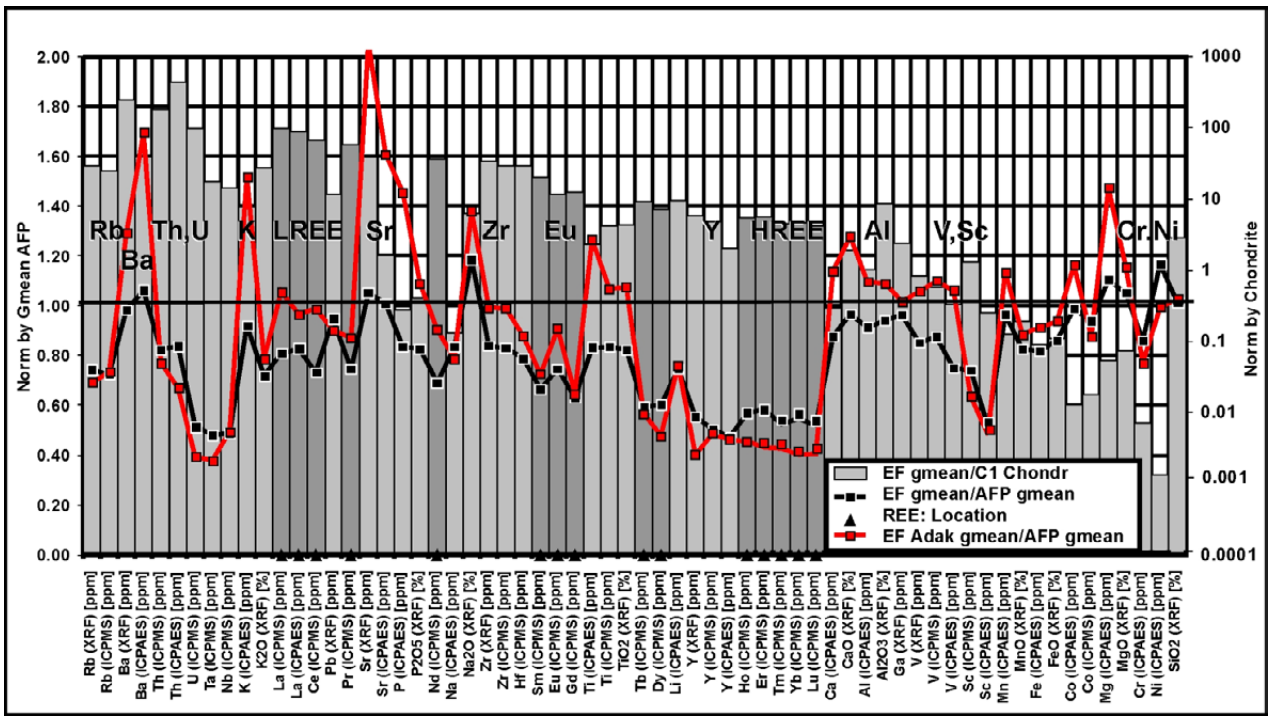

Fig. 47. Pearce–Peate spectra of samples from the Archaean Eastern Finland sub-area. The black and red lines indicate the AFP-normalized data for all samples and for adakitic samples, respectively (left vertical axis). For details, see Figure 35.

are 1.55 and 2.33 and those of compatibles/HREE 1.5 and 2.42, respectively. These values refer to a significant component of adakitic/TTG material fractionated at great depths in the lower crust/upper mantle.

The major restite minerals of adakitoids in this sub-area on the maps in Figure 24 and Figure 25 appear to be pyroxenes, garnet and amphiboles. Garnet refers to higher P–T conditions in the fractionation environment compared to Proterozoic sub-areas.

Ilomantsi sub-area (IL)

This sub-area, named in Nironen et al. (2002) as the 'Ilomantsi greenstone belt', is part of a larger belt that extends to Russia. In the area, they documented ca. 2.75–2.70 Ga sedimentary rocks, iron formations and mafic volcanics. Hölttä et al. (2012b) noted arc-type tectonic settings characterized by calc-alkaline volcanic rocks, crustal signatures in the geochemistry of ultramafic rocks and high abundances of volcaniclastic greywackes. Thus, this sub-area may be related to 'modern type' plate tectonic processes.

The total number of plutonic rock samples from this sub-area is 104, of which 41 samples (ca. 39%) are classified as adakitoids. Thus, there is a very significant number of adakitic samples in this zone compared to all other Proterozoic or Archaean sub-areas. In the diagrams in Figure 48, the plutonic rocks are strikingly felsic, mainly granitic-granodioritic, monzodioritic. The adakitoids range from alkaline granites to monzodiorites. In tectonomagmatic classification, all-plutonic rocks are in syn- to post-collisional fields, while adakitoids are mainly late to post-collisional.

In this sub-area, the Pearce–Peate spectra of all-plutonic rocks and adakitoids in Figure 49 are almost identical (correlation 0.87 in Table 6), as can be expected because of the high number of adakitic samples. The LREE/HREE ratios of the all-plutonic rock samples and adakitoids are 1.6 and 2.0 and those of compatibles/HREE 1.5 and 2.1, respectively. These values for adakitoids are lower than for the other Archaean sub-areas above, referring to a lower degree of fractionation and mantle contribution. It must also be noted that although the rocks of this sub-area are strikingly felsic, granitic–granodioritic, their PP spectra differ strongly from the spectra of granites in Figure 21. In particular, the steep slope of REE and relative amount of compatibles

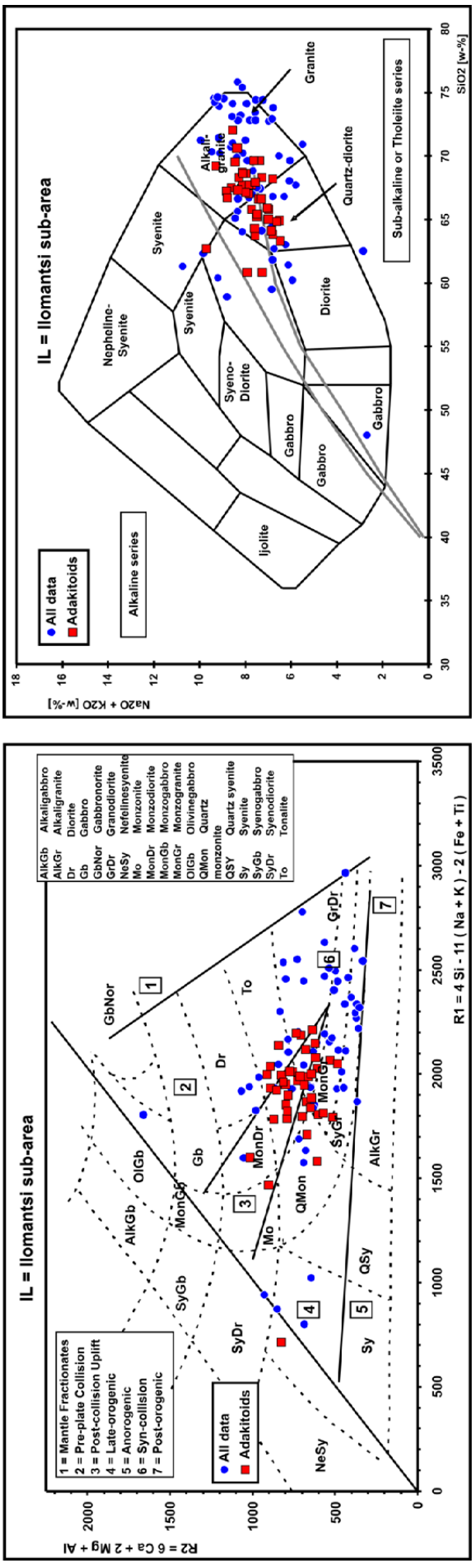

Fig. 48. Lithological classification of the samples from the Archaean Ilomantsi sub-area in the R1-R2 diagram (de La Roche et al. 1980) and the Na_2O+K_2O vs SiO_2 diagram (Cox et al. 1979). For details, see the caption of Figure 34.

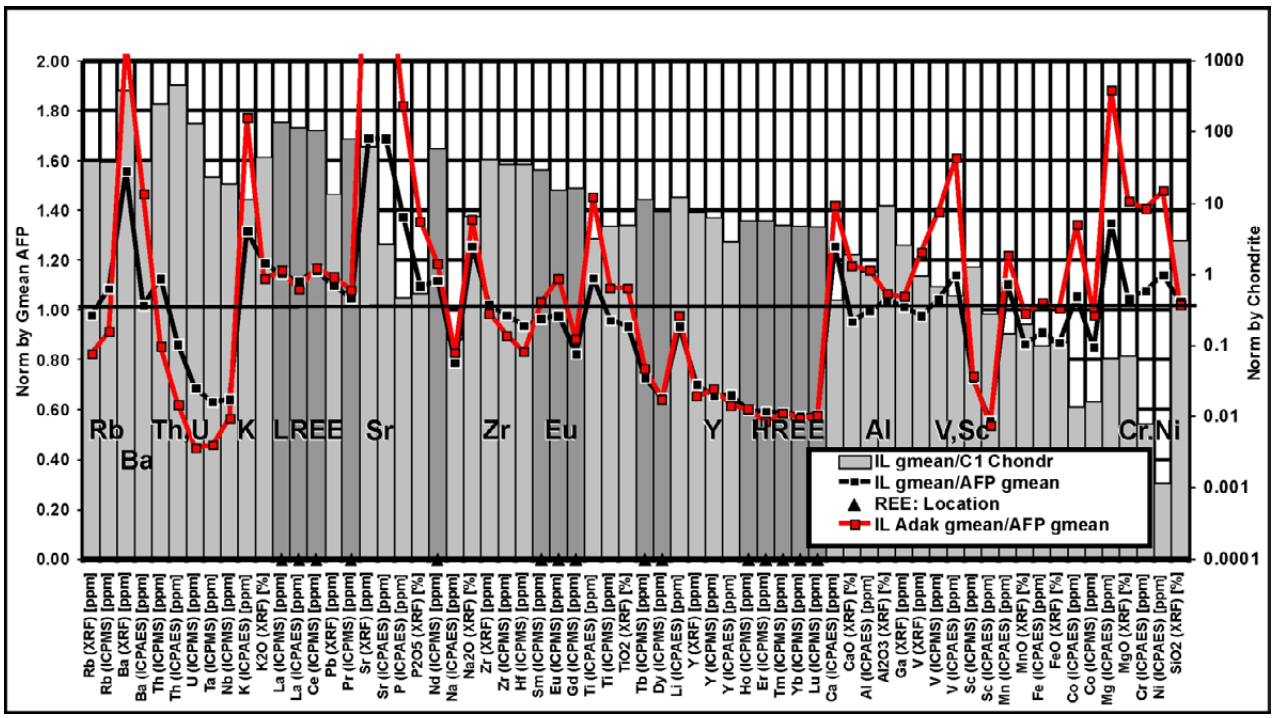

Fig. 49. Pearce–Peate spectra of samples from the Archaean Ilomantsi sub-area. The black and red lines indicate the AFP-normalized data for all samples and for adakitic samples, respectively (left vertical axis). For details, see Figure 35.

is much more significant in the Ilomantsi area. In this sub-area, the major restite minerals of adakitoids on the maps in Figure 24 and Figure 25 appear to be mainly amphiboles and to a lesser degree pyroxenes and garnet, reflecting shallower fractionation depths compared to the other Archaean sub-areas considered in this section.

2.2 LREE/HREE and compatibles/HREE ratios of the sub-areas and correlations of their Pearce–Peate spectra

Table 5 summarises the LREE/HREE and compatibles/HREE ratios of the sub-areas. From the table, it can be seen that these ratios are clearly higher in most Archaean sub-areas for adakitic samples and all-plutonic samples correspondingly. The highest LREE/HREE ratios of adakitic samples from CFG and EF refer to a deep fractionation depth (compatibles in restite). The highest compatibles/HREE ratios in adakitoids of SMB and EF refer to a high mafic component due to the mantle contribution (underplating?) of the sources (see Fig. 67). The relatively low ratios in Proterozoic sub-areas, as well as in IL, refer to a shallower fractionation depth and less significant mantle contribution (shallower/gentler ~ 'hotter'/younger subduction'?).

Table 6 presents the correlations of the AFP-normalized Pearce–Peate spectra of all sub-areas considered above. From the table, it can be seen that all adakitoid spectra of Archaean and Proterozoic sub-areas correlate strongly with each other. However, the correlation of all-plutonic rocks between these sub-areas is generally low. Moreover, majority of the Archaean sample groups correlate with each other and with adakitoids, as can be expected because of the large number of adakitic samples in these groups, i.e. Archaean sub-areas are characteristically adakitic (TTGs) as a whole. However, the correlation between adakitoids and the all-plutonic rock group for Proterozoic samples is generally low. In particular, the correlation between

Table 5. Summary of LREE/HREE and compatibles/HREE ratios of the sub-areas.

ALL Data:	USM	SMB	CFG	LBZ
LREE/HREE	1.0	0.72	0.79	**0.82**
Compatibles/HREE	1.0	**1.28**	0.85	1.1
Adakitoids:	USM Adak	SMB Adak	CFG Adak	LBZ Adak
LREE/HREE	1.5	1.27	**1.6**	1.32
Compatibles/HREE	1.9	**2.13**	1.55	1.74

ALL Data:	IC	EF	IL	PDJ
LREE/HREE	1.0	1.55	**1.57**	1.55
Compatibles/HREE	1.36	**1.74**	1.5	1.53
Adakitoids:	IC Adak	EF Adak	IL Adak	PDJ Adak
LREE/HREE	2.3	**2.33**	2.0	2.26
Compatibles/HREE	2.16	**2.42**	2.1	2.14

adakitoids and all samples of the USM is very low or even negative, referring to similarities between the Uusimaa sub-area, characterized by numerous post-tectonic leucogranites, and the anorogenic/post-tectonic rapakivi samples considered above (see Fig. 23 and Fig. 35).

It is interesting to note that the all-plutonic samples from SMB correlate strongly with Proterozoic adakitoids and with all-plutonic samples from LBZ. Characteristic of these sub-areas is a significant oceanic signature in bedrock, e.g. volcanism (pillow lavas), black schists, turbiditic mica gneisses, carbonatic rocks and graphite-bearing schists (Nironen et al. 2002, Ruotoistenmäki 1996). As commented above, the high correlation of LBZ, SMB and adakitoids may refer to a similar, although not simultaneous, marine plate-dominated origin (collision and subduction/stacking related under-/overthrusting). The significant correlation between CFG and LBZ can be explained by their island-arc characteristics: Ruotoistenmäki (1996) interpreted CFG as an island arc and LBZ as dominantly oceanic, with remnants of island arc (e.g. Nironen 1997, Lahtinen et al. 2005).

It must also be emphasized that, exceptionally, Proterozoic sub-areas LBZ and SMB also correlate significantly with the all-plutonic samples of the Archaean sub-area IC. This is possibly due to effect of Proterozoic overprinting and partial underthrusting of LBZ below IC, as noted in an evolution model by Ruotoistenmäki (1996; see section 5., as well as Fig. 94 and Fig. 95.)

Table 6. Correlation matrix of the Pearce–Peate spectra of all-plutonic and adakitoid samples of separate sub-areas. Correlations above 0.5 have been emphasized by bolding.

	EF-Adak	IL-Adak	PDJ-Adak	IC	EF	IL	PDJ	USM-Adak	SMB-Adak	CFG-Adak	LBZ-Adak	USM	SMB	CFG	LBZ
IC-Adak	0.88	0.78	0.87	0.73	0.66	0.60	0.30	0.66	0.74	0.66	0.87	-0.30	0.32	0.21	**0.56**
EF-Adak		0.89	0.94	0.66	0.87	0.79	**0.55**	0.61	0.70	0.68	0.81	-0.35	0.24	0.13	0.39
IL-Adak			0.86	0.54	0.74	0.87	0.47	0.64	0.65	0.63	0.77	-0.26	0.18	0.16	0.34
PDJ-Adak				0.63	0.78	0.75	**0.59**	0.66	0.60	0.59	0.79	-0.26	0.09	0.12	0.33
IC					**0.65**	0.43	0.34	**0.54**	**0.64**	**0.62**	**0.78**	-0.15	**0.60**	0.24	**0.77**
EF						**0.84**	**0.79**	**0.53**	**0.56**	**0.72**	**0.62**	-0.14	0.23	-0.03	0.25
IL							**0.69**	**0.55**	0.47	**0.57**	**0.56**	0.01	0.06	0.10	0.15
PDJ								0.36	0.11	0.38	0.23	0.16	-0.20	-0.30	-0.18
USM-Adak									**0.72**	**0.72**	**0.77**	0.17	0.31	0.11	0.38
SMB-Adak										**0.87**	**0.85**	-0.27	**0.72**	0.36	**0.66**
CFG-Adak											**0.72**	-0.13	**0.55**	0.04	0.41
LBZ-Adak												-0.27	**0.52**	0.36	**0.72**
USM													-0.16	0.01	-0.20
SMB														0.46	**0.83**
CFG															**0.66**

The correlations in Table 6 suggest that adakitoids/TTGs of all sub-areas are quite similar, even across the Archaean–Proterozoic border. The similarity of all-plutonic samples and adakitoids/TTGs of Archaean sub-areas indicates that they have had a relatively similar history, i.e. more profound 'adakite-type', high P–T fractionation evolution/'homogenisation'. The relative homogenization in Archaean sub-areas may be connected with the very long history of Archaean adakitoids, up to 400 Ma (Fig. 66).

However, the main phase in the evolution of Finnish Proterozoic (Svecofennian) sub-areas is much shorter (less than ca. 100 Ma), referring to rapid processes, apparently related to Proterozoic plate tectonic evolution, as modelled in Ruotoistenmäki (1996), Nironen (1997) and Lahtinen et al. (2005).

In the following, a more detail study of eight adakitic samples from the Archaean sub-areas considered in this section is presented.

3 CHEMICAL AND ISOTOPIC CHARACTERISTICS OF EIGHT ADAKITIC SAMPLES FROM FOUR ARCHAEAN SUB-AREAS AND THEIR COMPARISON WITH PROTEROZOIC ADAKITOIDS

This section considers eight adakitic (TTG/sanukitoid) plutonic rock samples selected from four major Archaean sub-areas considered above in section 2.: Pudasjärvi, East-Finland, Iisalmi and Ilomantsi sub-areas (Fig. 50). The plutonic rock samples used in this study are, as in previous sections, from the Rock Geochemical Database of Finland (RGDB; Rasilainen et al. 2007). In this study, they fulfil all adakitoid criteria ("100%" adakitoids) defined above by Defant & Drummond (1990) and Thorkelson & Breitsprecher (2005). The purpose of this section is to consider the similarity and evolution of these Archaean rocks, commonly classified simply as 'TTGs'. The location of samples is indicated on the map in Figure 50. The division and descriptions of Finnish bedrock sub-areas are given above in section 2. For detailed statistics, areal and lithological variations, classification and correlations of sub-area chemistry, see Ruotoistenmäki (2016). From each sub-area, two samples are selected (northern and southern). Rock type names are adopted from RGDB; also see the chemical rock-type classifications in Figure 51 and Figure 52:

Pudasjärvi sub-area (PDJ)
Sample 93001908 (isotope lab code = A1966): Homogeneous, 'granitic' granodiorite
Sample 94003693 (A1965): Gneissic tonalite

East-Finland sub-area (EF)
Sample 95001782 (A1962): Homogeneous granodiorite
Sample 94002667 (A1960): Banded, deformed gneissic tonalite

Iisalmi sub-area (IC)
Sample 94003640 (A1959): Tonalitic, tectonized gneiss
Sample 93003031 (A1958): Homogeneous tonalite

Ilomantsi sub-area (IL)
Sample 94002572 (A1964): Sheared, granite / granitic gneiss
Sample 90010130 (A1963): Sheared granodiorite

As noted above, the number of adakitic plutonic rock samples is 18 of 98 samples (18%) from the Pudasjärvi sub-area, 66 of 317 samples (21%) from the East Finland sub-area, 11 of 123 samples (9%) from the Iisalmi sub-area and 41 of 104 samples (39%) from the Ilomantsi sub-area. Thus, with the exception of the Iisalmi sub-area, the Archaean sub-areas are characterized by abundant adakitic rocks. The plutonic rock samples from the Ilomantsi sub-area range from granites to diorites. Granitic and granodioritic rocks also dominate in the Pudasjärvi area, while in the East Finland and Iisalmi sub-areas, the relative proportion of more mafic rocks is higher. The adakitic samples are mainly sub-alkaline with the exception of the Ilomantsi area, where the samples are more alkaline. Moreover, all adakitic rocks in the sub-areas are characterized by a steep (fractionated) REE pattern, high Eu

and Sr, and increased abundances of compatible elements.

In this study, these Archaean samples are also compared with Palaeoproterozoic sample data from Väisänen et al. (2012). They presented detailed isotopic and chemical data on intermediate to felsic plutonic rocks connected with voluminous synorogenic magmatism related to Svecofennian accretionary tectonics in southwestern Finland. They document an ion microprobe single zircon dating of a diorite sample yielding an age of 1872 ± 3 Ma (ε_{Nd} = +2.2) and a

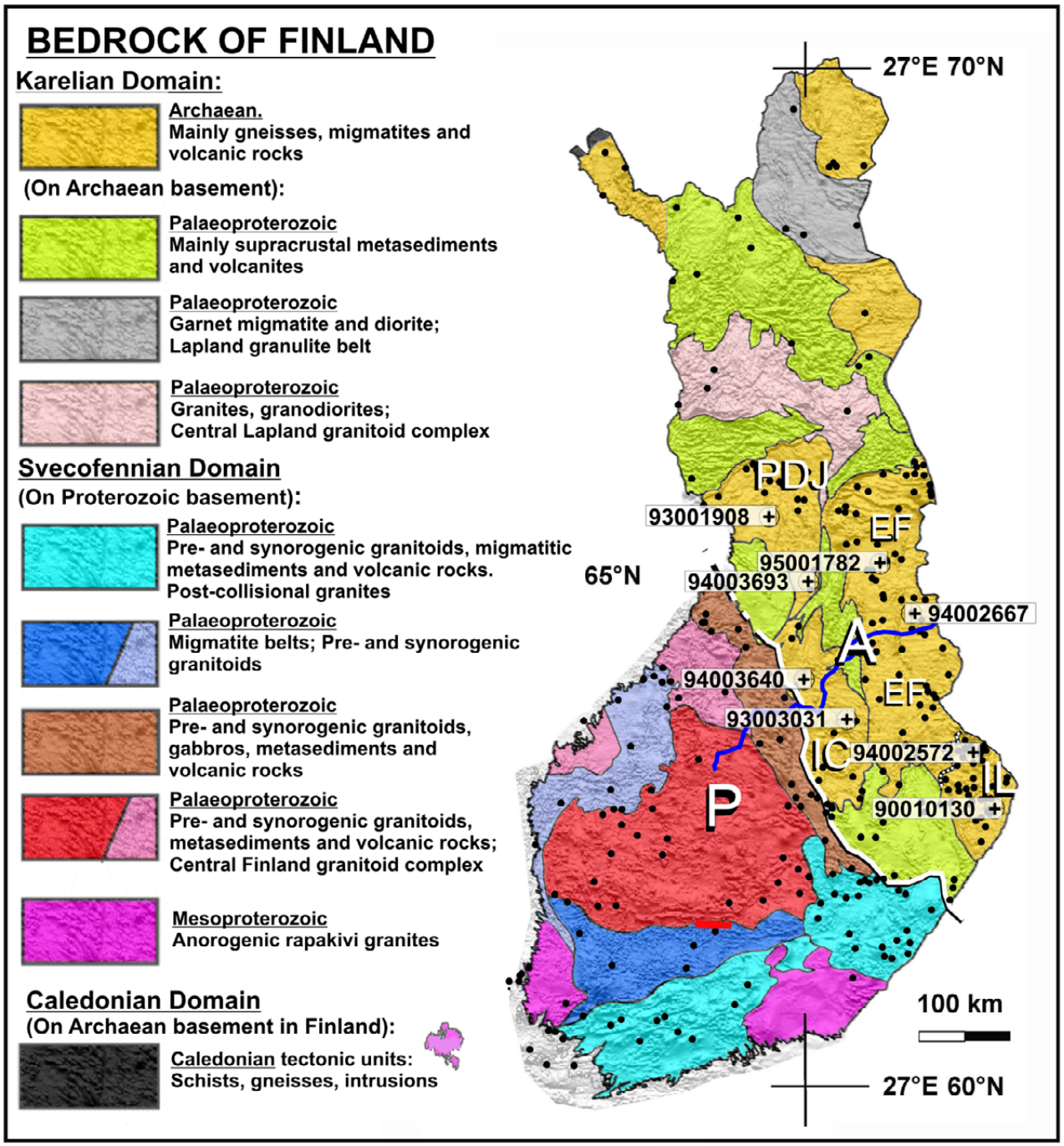

Fig. 50. Location of the samples considered in this study (+). Black dots (•) refer to all Finnish "100%" adakitic plutonic rocks selected from the Rock Geochemical Database of Finland (RGDB). A: Archaean, P: Proterozoic, PDJ: Pudasjärvi sub-area, EF: East Finland sub-area, IC: Iisalmi sub-area and IL: Ilomantsi sub-area. The white line approximates the course of the Archaean–Proterozoic border zone. The blue line depicts the FIRE1 seismic reflection profile considered later in the text. Modified from Ruotoistenmäki (2012). See also Figure 4, depicting the areal distribution of all Finnish plutonic rock samples and of 'adakitoids' fulfilling at least 6 of 8 criteria defined above by Defant & Drummond (1990) and Thorkelson & Breitsprecher (2005), i.e. '75% adakitoids'.

trondhjemite sample with an age of 1867 ± 4 Ma (ε_{Nd} = +2.6). The dioritic magmas are interpreted to be mantle-derived and slightly enriched by subduction-related processes. The felsic (trondhjemitic) magmas show elevated Sr/Y and La/Yb ratios, which are typical for adakite- and TTG-like magmas. The felsic magmatism is inferred to be generated through crustal melting of the lower part of the previously generated volcanic-arc type crust at a minimum pressure of 10 kbar (ca. 37 km), with evidence of a 15 kbar (ca. 55 km) pressure for trondhjemites with the highest Sr/Y ratio. Väisänen et al. (2012) proposed that arc accretion combined with magmatic intrusions thickened the crust so that melting of the lower crust yielded adakite- and TTG-like compositions. The mafic magmatism is considered to be the heat source.

3.1 Chemical characteristics of the samples

In the following, geochemical variation between adakitic samples is considered using various major and trace element diagrams, some of which are adopted from the literature, while others have been generated for the present study. The samples are from the Rock Geochemical Database of Finland (RGDB; Rasilainen et al. 2007). For details, see Table 2 above. Their areal distribution is given on the map in Figure 50. In each of the following diagrams, the symbols in the legends are arranged in the order: 1) Pudasjärvi sub-area (boxes), 2) East Finland sub-area (circles), 3) Iisalmi sub-area (triangles) and 4) Ilomantsi sub-area (diamonds). From each sub-area, two samples are considered, the red symbol representing the northernmost sample. The diagrams also show the corresponding geometric means of Proterozoic adakitic plutonic rock samples (P.Adk, '+'), Archaean adakitic plutonic rocks (A.Adk, '**X**') and all-plutonic rock samples (AFP, '**O**').

Chemical classification of rock types

Figure 51 and Figure 52 present the distributions of the samples on the total alkali vs. SiO_2 (TAS) diagram by Middlemost (1994) and the R1-R2 diagram by de la Roche et al. (1980). In

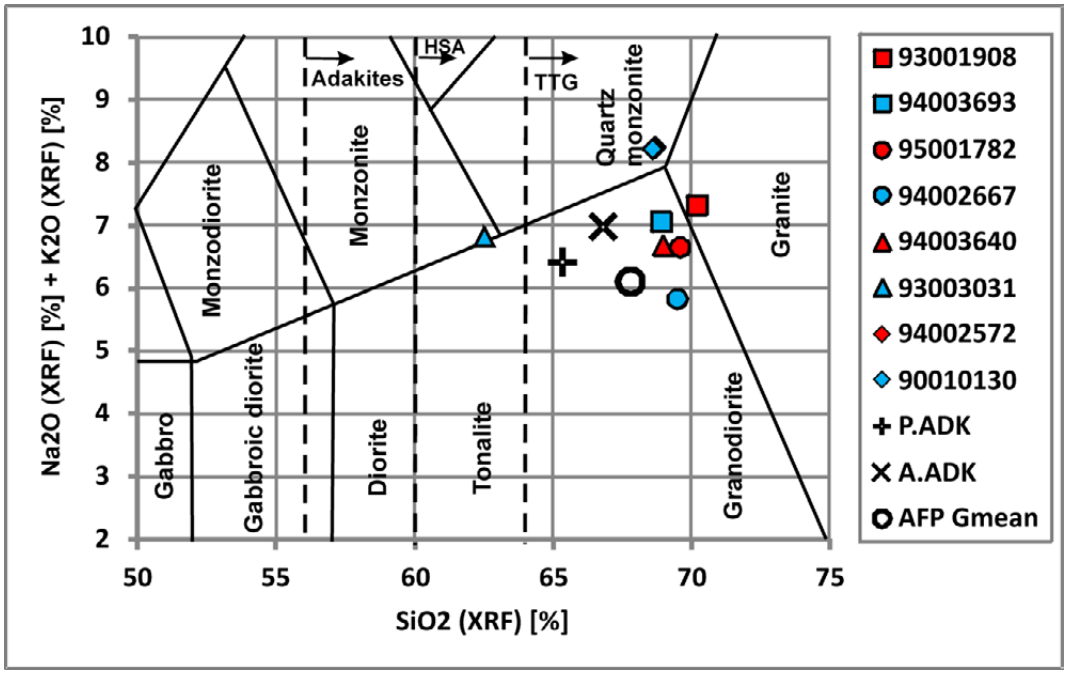

Fig. 51. Total alkali vs. SiO_2 (TAS) diagram after Middlemost (1994) with added SiO_2 division lines (dashed) for adakites, high-silica adakites (HSA) and tonalites–trondhjemites–granodiorites (TTG) adopted from Martin et al. (2005) and Väisänen et al. (2012). Boxes = Pudasjärvi sub-area, circles = East Finland sub-area, triangles = Iisalmi sub-area, diamonds = Ilomantsi sub-area (samples overlapping in this diagram). The diagram also gives the corresponding geometric means for Proterozoic adakitic plutonic rock samples (P.Adk, '+'), Archaean adakitic plutonic rocks (A.Adk, 'X') and all Finnish plutonic rock samples (AFP, 'O').

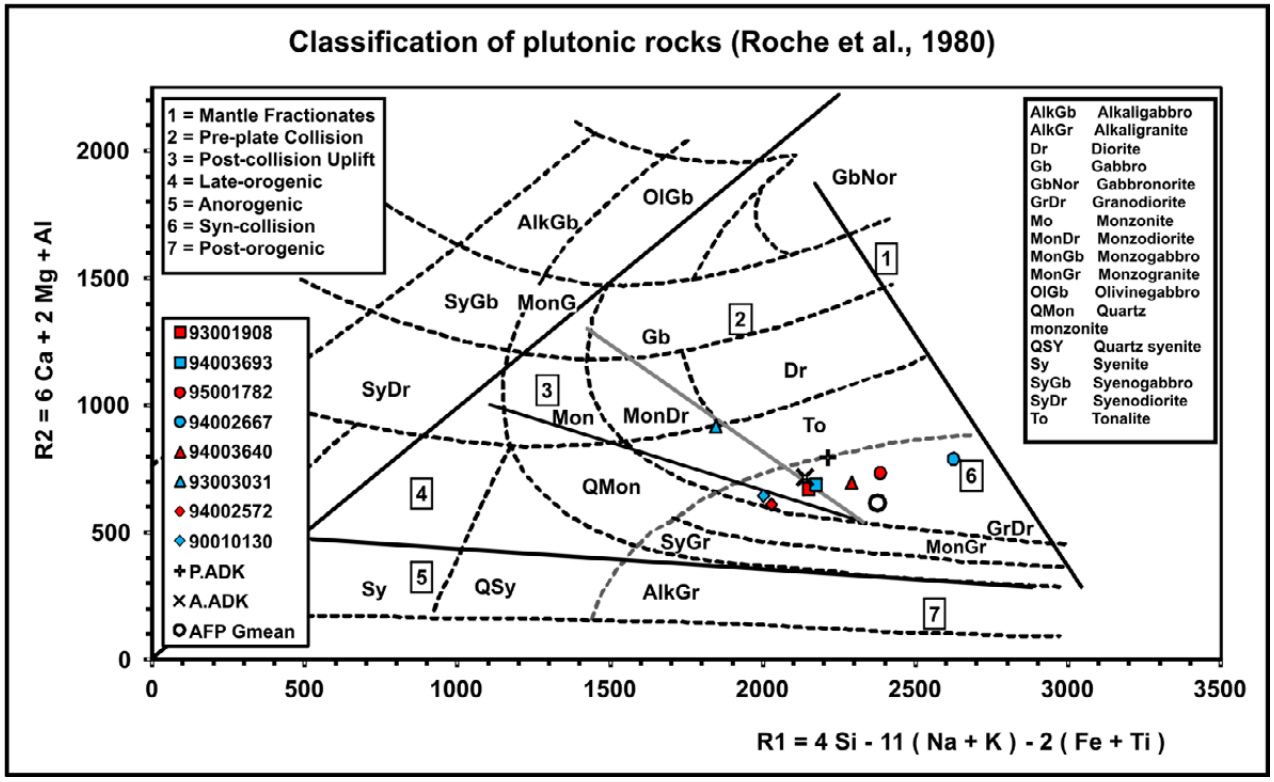

Fig. 52. Classification of samples in the R1-R2 diagram (de la Roche et al. 1980). The tectonomagmatic fields have been adopted from Batchelor & Bowden (1985) and rock-type boundaries have been modified according to Rollinson (1993).

both diagrams, the majority of samples plot in granodiorite fields. The tonalitic, southern Iisalmi sample (93003031) has the lowest SiO_2 value, below 65%, while all other samples have clearly higher SiO_2 values, above 68%, which is higher than that of A.Adk, P.Adk and AFP. In the R1-R2 diagram, the majority of samples plot in syn- to post-collision tectonomagmatic fields. The relatively random (non-systematic) scatter of data in these diagrams indicates that their resolutions are inadequate for clearly discriminating the adakitic samples from, for instance, AFP.

Major and trace elements

Figure 53 and Figure 54 illustrate the variations of selected major and trace elements and their ratios vs. SiO_2 of the samples. The diagrams also show the approximate enveloping curves of Proterozoic adakitic tonalitic and trondhjemitic samples from Väisänen et al. (2012), which they interpreted to indicate melting at pressures of 10–15 kbar (~30–50 km) in thickened Proterozoic crust in SW Finland. These diagrams are summarized in Figure 55.

Table 7. Major lithogeochemical groups of the samples.

(A) High-Na-Al, low-K group:			(B) High-K-Mg 'Ilomantsi'group:			(C) High-Fe-Mg group:		
Sample	Rock type	Area	Sample	Rock type	Area	Sample	Rock type	Area
93001908	granodiorite	Pudasjärvi	94002572	granite	Ilomantsi	93003031	tonalite	Iisalmi
94003693	gneissic tonalite	Pudasjärvi	90010130	granodiorite	Ilomantsi			
95001782	granodiorite	East Finland						
94002667	tonalite	East Finland						
94003640	gneiss	Iisalmi						

The Sr/Y and La/Yb ratios in Figure 54 and summarized in Figure 55 are used as indicators of restite mineralogy related to the fractionation depth. The high Sr is related to the melting of plagioclase or absence of plagioclase in the residue, while low Y, high Sr/Y and low Yb indicate garnet and amphibole in the residue. Moreover, high La/Yb indicates LREE enrichment relative to HREE and garnet in the residue (e.g. Castillo 2006; Table 1).

Based on their chemistry, I divided the samples in 2+1 major groups (Table 7 and Fig. 55):

The high-Na-Al, low-K group (A) is characterized by:

High Al_2O_3, Na_2O, high SiO_2; low FeO, K_2O, K_2O/Na_2O and MgO, but relatively high Mg#. The high La/Yb (steep REE) and high Sr/Y ratios refer to a high degree of fractionation and relatively high plagioclase content, indicating a lower crust/upper mantle fractionation depth. In the diagrams in Figure 53 and Figure 54, these samples are close to the Proterozoic high-SiO_2, adakitic Uki trondhjemites reported by Väisänen et al. (2012; green field in the diagrams). In the K_2O vs SiO_2 diagram, they plot on the tholeitic–calc-alkaline border. The SiO_2 content of these samples varies between ca. 68.9–70.2 wt%. In the TAS diagram in Figure 51 and R1-R2 diagram in Figure 52, these samples represent syn- to post-collisional granitic–granodioritic rocks.

The high-K-Mg 'Ilomantsi' group (B) is characterized by:

High K_2O, K_2O/Na_2O, MgO and Mg#; lower Al_2O_3, Na_2O, SiO_2 and La/Yb (~ gentler REE ≈ less fractionated) and lower Sr/Y (~ lower plagioclase ≈ shallower fractionation depth). In the diagrams in Figure 53 and Figure 54, these samples are closer to Proterozoic, more mafic 'Uki tonalites' (yellow field in the diagrams) considered by Väisänen et al. (2012). The SiO_2 content of these samples varies between ca. 68.6–68.7 wt%. In the K_2O vs SiO_2 diagram, they plot in the middle of the high-K calc-alkaline field. Wilson (1989) stated that at the present time, magmas of the calc-alkaline series are restricted in their occurrence to subduction-related tectonic settings. Consequently, she continues, the recognition of calc-alkaline characteristics in the geochemistry of ancient volcanic sequencies may be an important petrogenetic indicator. Moreover, calc-alkaline magmas are typical of mature arcs and active continental margins. These conclusions, however, are probably oversimplications, if applied to AFP gmean and Archaean and Proterozoic adakitoid averages also located in the calc-alkaline field in Figure 53. In the TAS diagram in Figure 51 and R1-R2 diagram in Figure 52, these samples are classified as late-orogenic granodioritic–monzonitic rocks.

The high-Fe-Mg group/sample (C) is characterized by:

The highest Al_2O_3, FeO and MgO contents, and lowest SiO_2 (62.5 wt%). The K_2O content (calc-alkaline), K_2O/Na_2O, Na_2O and Mg# values are 'intermediate'. The La/Yb ratio is low (~ gentler REE ≈ less fractionated) as also Sr/Y (~ lower plg ≈ shallower fractionation depth). The trace element distribution of this sample is similar to that of the High-K-Mg 'Ilomantsi´ group (B) above. It must be noted that because of the constant sum effect (e.g. Wilson 1989, Rollinson 1993), the relative abundances of other elements increases when SiO_2 is low. In the TAS diagram in Figure 51 and the R1-R2 diagram in Figure 52, this sample represents a post-collision, tonalitic rock.

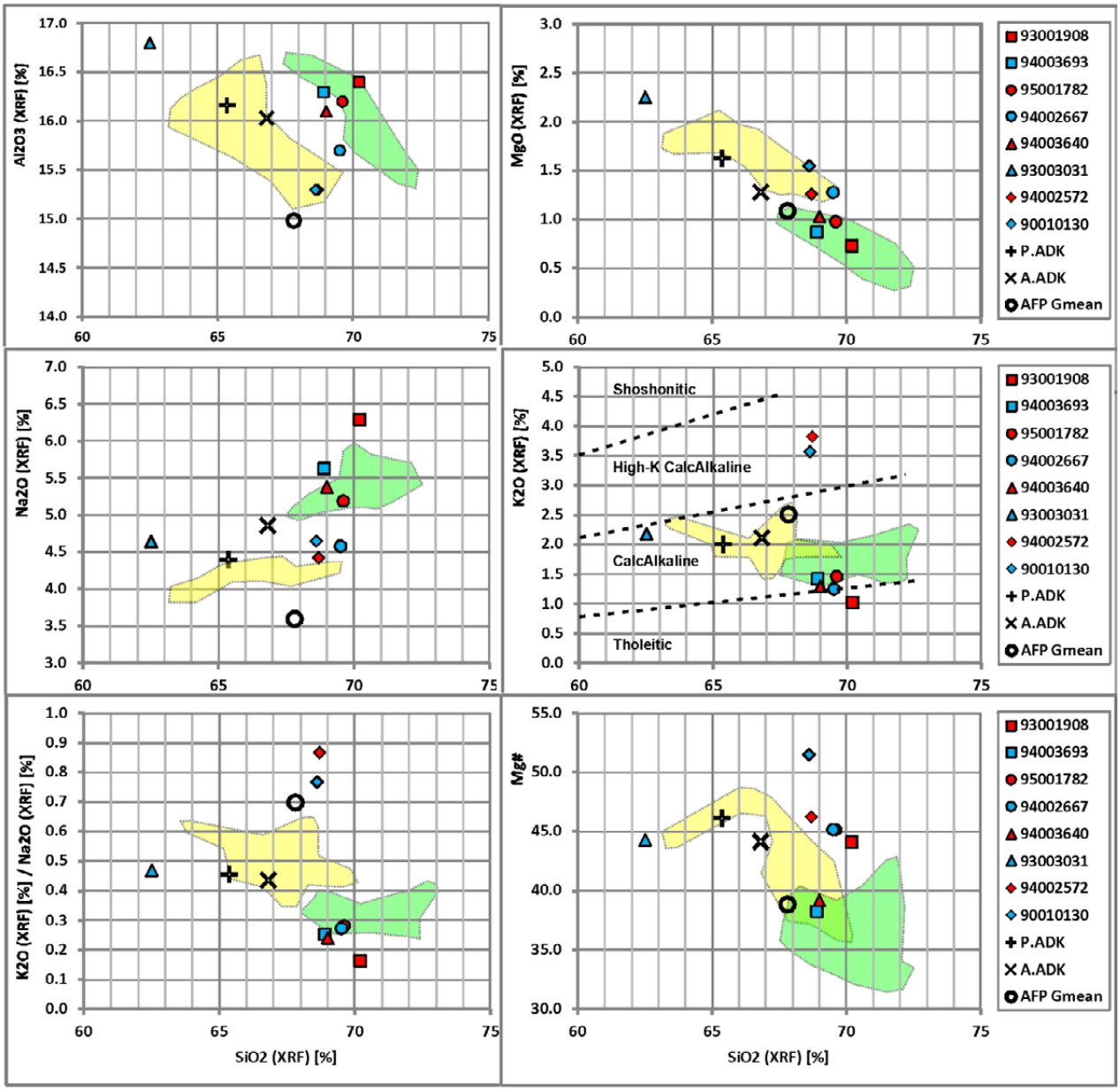

Fig. 53. Selected major elements, K_2O/Na_2O and Mg# vs. SiO_2 diagrams for the samples. The yellow and green fields approximate enveloping curves of Proterozoic tonalitic ('Uki tonalite', yellow) and trondhjemitic (green) samples considered by Väisänen et al. (2012).

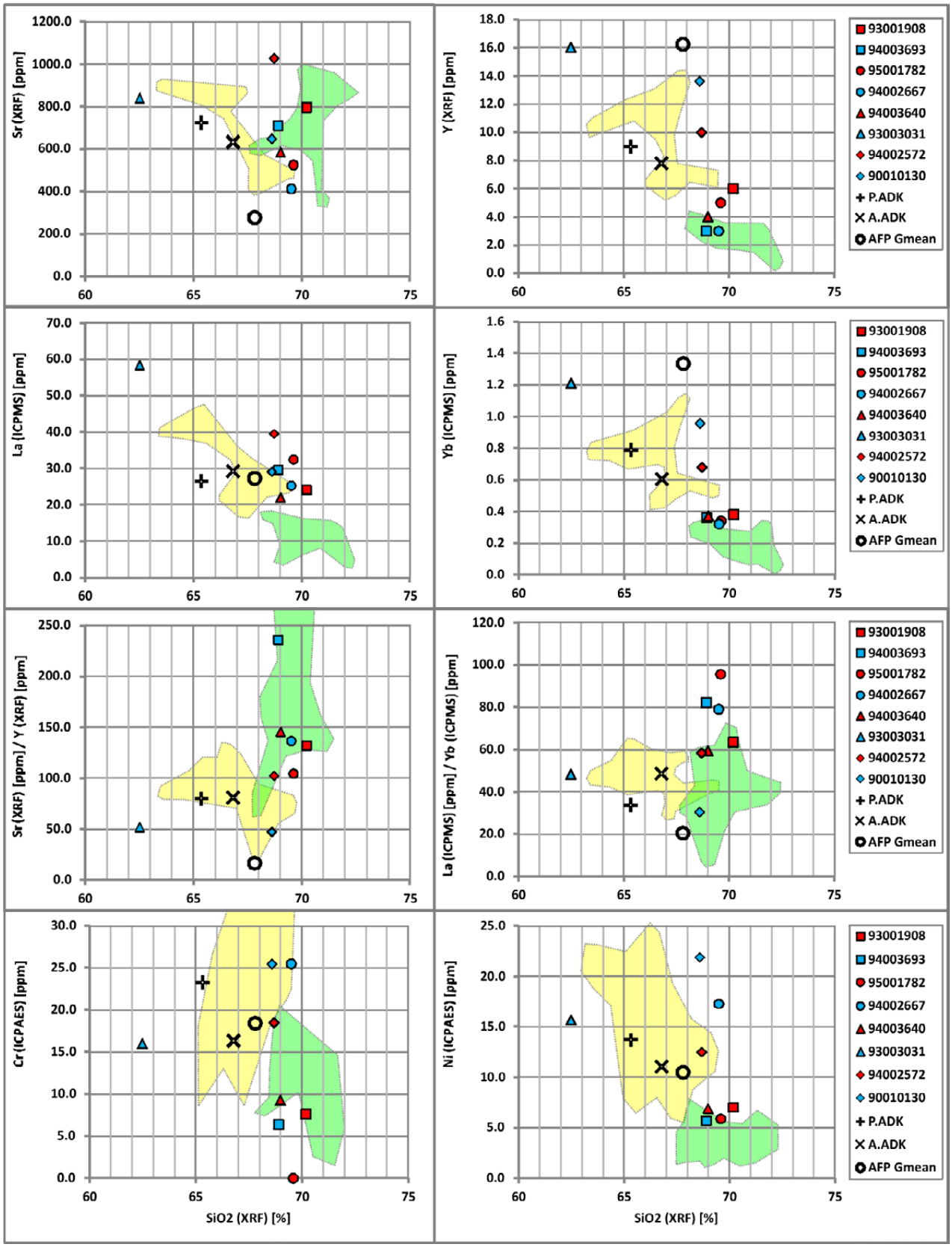

Fig. 54. Selected trace elements and trace element ratios vs. SiO_2 diagrams for the samples. The yellow and green fields approximate enveloping curves of Proterozoic tonalitic ('Uki tonalite', yellow) and trondhjemitic (green) samples considered by Väisänen et al. (2012).

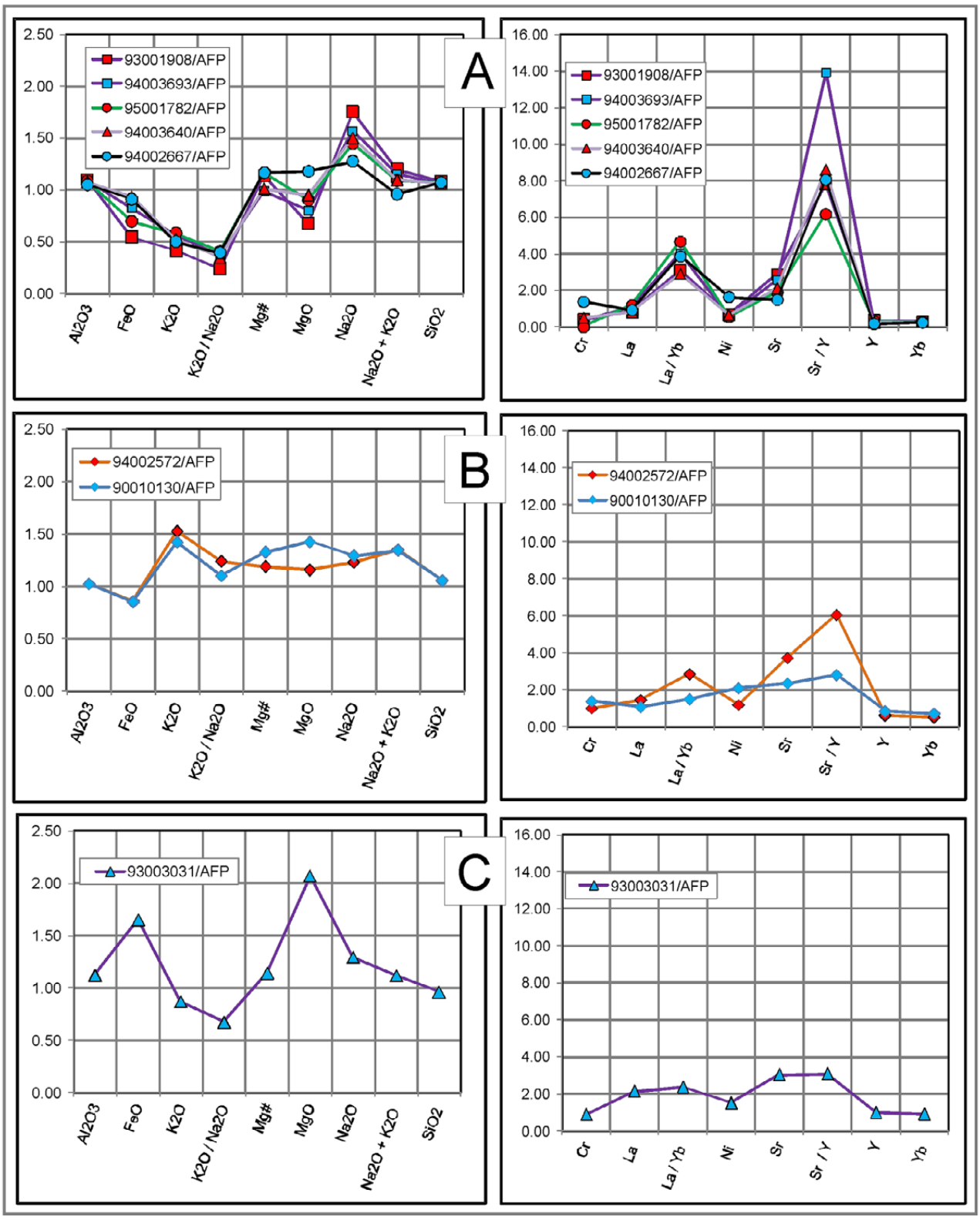

Fig. 55. Summary of the diagrams in Figure 53 and Figure 54. For comparison, the values and their derivatives have been normalized by the geometric averages of all Finnish plutonic rock samples (AFP; Ruotoistenmäki 2012; Table 2). (A) High-Na-Al group; (B) high-K-Mg group; (C) high Fe-Mg group sample. Analytical methods and units are the same as in Figure 53 and Figure 54. FeO and MgO are given separately, besides Mg#.

Na_2O/K_2O vs. Ba + Sr diagram

Halla et al. (2009) used the Na_2O/K_2O vs. Ba + Sr diagram in Figure 56 to discriminate more juvenile TTGs from sanukitoids, extracted from a more enriched mantle source. This diagram was also applied in Ruotoistenmäki (2012) to analyse the characteristics of all adakitic samples from the sub-areas considered in this study (smaller symbols in Fig. 56; see also Fig. 31 in section 1.7.). In the diagram, the majority of Ilomantsi area samples (smaller diamonds), as well as many of Iisalmi area samples (smaller triangles), are sanukitic, Pudasjärvi samples (smaller boxes) mainly plot as TTGs, and East Finland area samples (smaller circles) form a continuum from TTGs to sanukitoids.

The samples analysed in this study (larger symbols) have a relatively wide distribution in this diagram: The samples of group (A) East Finland (larger circles) plot inside the TTG field, but the Pudasjärvi samples (larger squares) and northern Iisalmi sample (larger red triangle) have both TTG and sanukitoid characteristics. The high-K-Mg 'Ilomantsi' group (B) samples (larger diamonds) and southern Iisalmi high Fe-Mg sample (group C; larger blue triangle) locate in the sanukitoid, enriched mantle field. Thus, this diagram also supports classification of the samples into two main 'adakitic' groups: (A ≈ 'TTGs') and (B+C ≈ 'Sanukitoids').

Kovalenko et al. (2005) reported high K_2O, Ba, Sr, and high ε_{Nd} sanukitoid rocks from Russian Karelia, close to the Ilomantsi area. They interpreted these rocks as products of melting of metasomatized mantle by subduction or underplating processes between ca. 2.7–2.74 Ga.

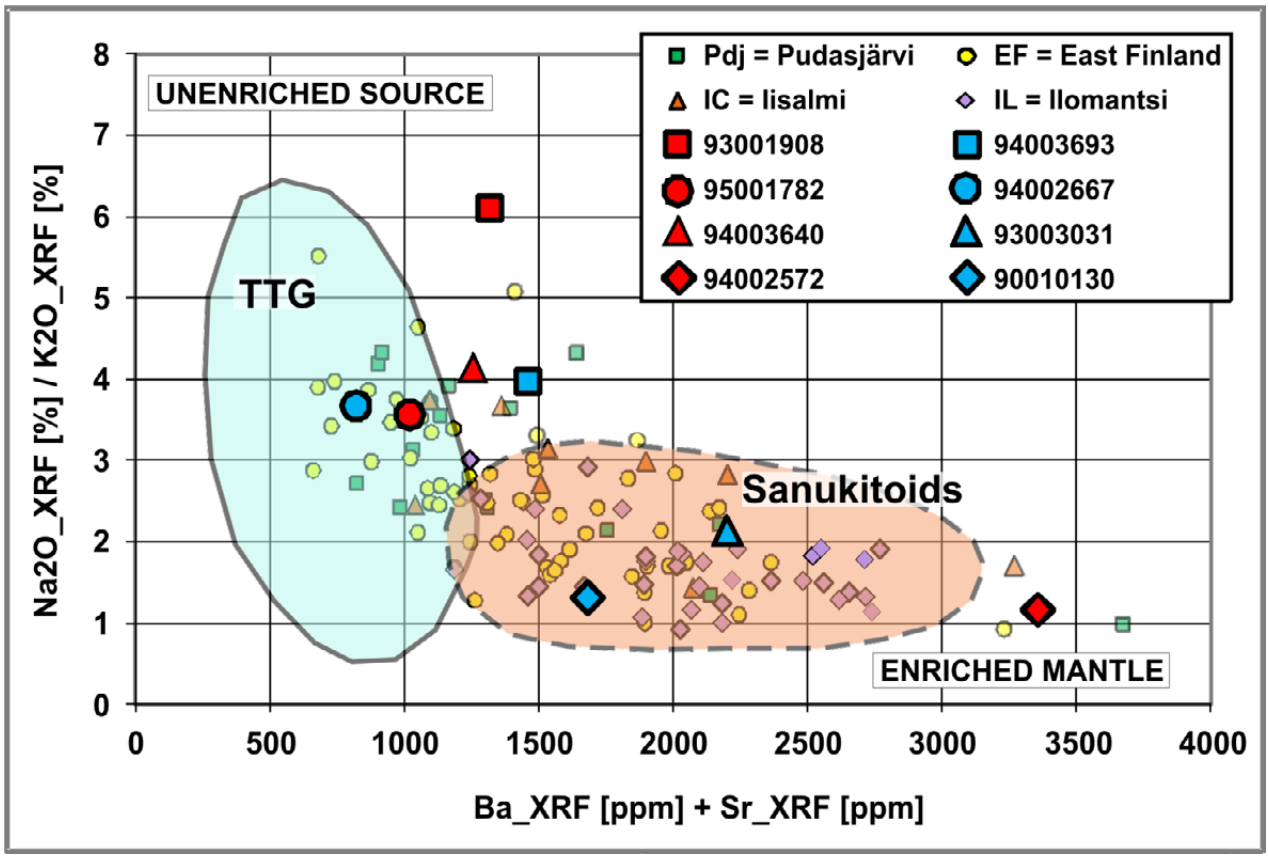

Fig. 56. Na_2O/K_2O vs. Ba + Sr plot for discriminating the high-Ba-Sr sanukitoid group from the TTG group. Adopted from Halla et al. (2009). The hypothetical source end members are enriched mantle (high Ba + Sr, low Na_2O/K_2O) and unenriched primitive basalt (low Ba + Sr, high Na_2O/K_2O). The distribution of all Pudasjärvi, East Finland, Iisalmi and Ilomantsi adakitoids have been adopted from Ruotoistenmäki (2012; smaller symbols). Boxes: Pudasjärvi samples; circles: East Finland; triangles: Iisalmi; diamonds: Ilomantsi area symbols.

REE spectra

Figure 57 is a plot of the REE patterns of the samples normalized against C1 chondrite (Table 2) and the geometric means of all Finnish plutonic rock samples (AFP; Table 2). The diagrams also show the normalized $La_{(ICPMS)}/Yb_{(ICPMS)}$ ratios (= chondrite normalized: $(La_{ICPMS}/La_{C1})/(Yb_{ICPMS}/Yb_{C1})$ and AFP-normalized $(La_{ICPMS}/La_{AFP})/(Yb_{ICPMS}/Yb_{AFP})$), reflecting the steepness of the curves and hence an approximation of the degree of REE fractionation.

In the diagrams in Figure 57, the slope of group 'A' (high-Na-Al, low-K) is markedly steeper than that of Neoarchaean late to post-tectonic sanukitoid intrusions sampled from the Karelian province, Finland, by Heilimo et al. (2010), indicated by the yellow field in the C1-normalized spectra. The averages of Archaean and Proterozoic adakitoids (A.ADK, P.ADK) are

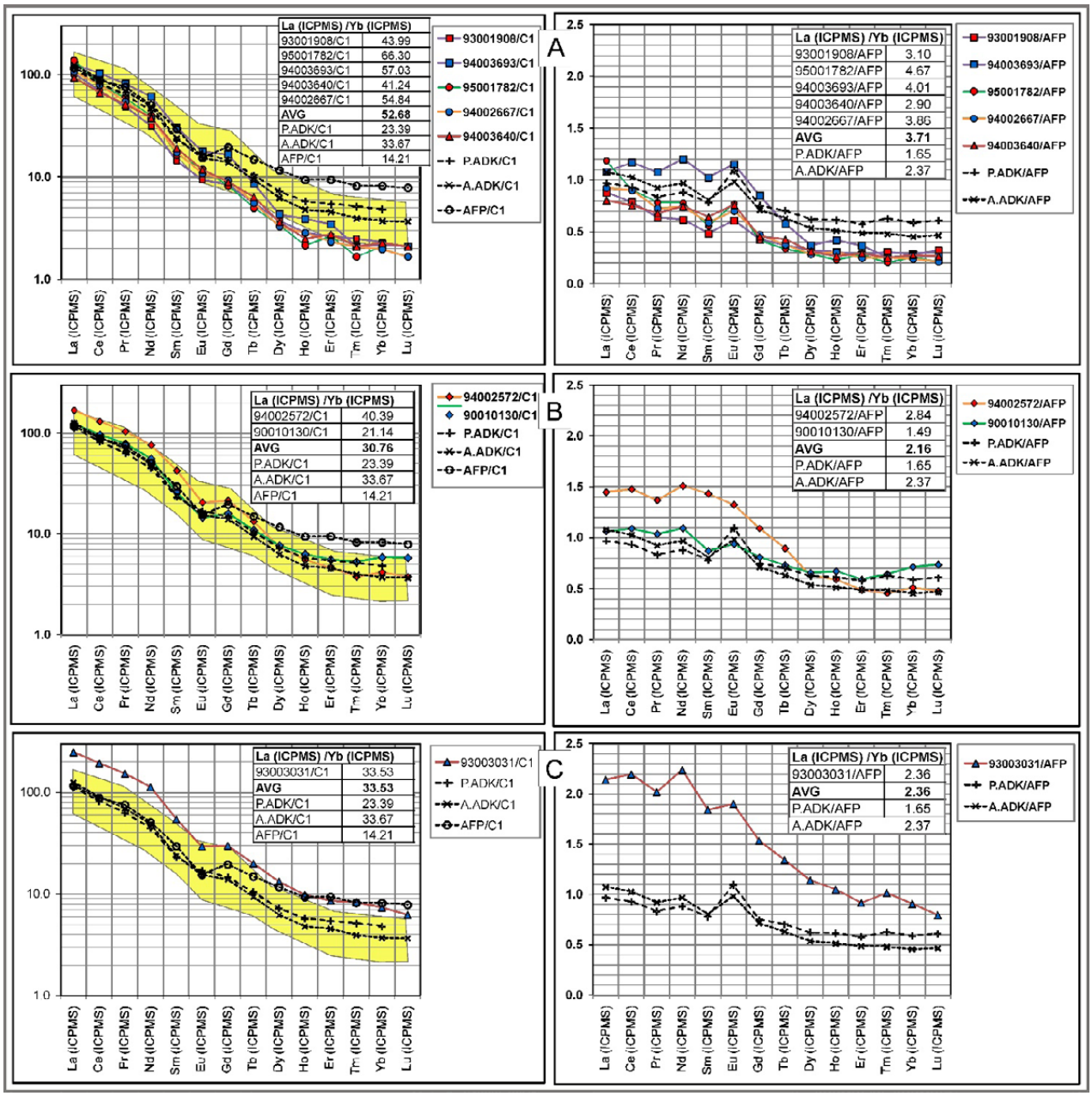

Fig. 57. Summary of REE diagrams normalized against C1 chondrite (Anders & Grevesse 1989, Kerrich & Wyman 1996) and geometric means of all Finnish plutonic rock samples (AFP; Table 2). (A): High-Na, low-K group; (B): High-K-Mg group; (C): High-Fe-Mg group. The diagrams also show the normalized $La_{(ICPMS)}/Yb_{(ICPMS)}$ ratios reflecting the steepness ~ degree of REE fractionation. AVG: ratio averages of samples. The shaded yellow area shows the compositional range of Neoarchaean late to post-tectonic sanukitoid intrusions sampled from the Karelian province, Finland by Heilimo et al. (2010).

in the sanukitoid field, while the slope of AFP is clearly gentler. The relative Eu maxima in the AFP-normalized spectra indicate an increased plagioclase content relative to AFP (e.g. Rollinson 1993).

The 'Ilomantsi' group 'B' (high-K-Mg) samples coincide closely with the sanukitoid field. This is in agreement with the comments on the Na_2O/K_2O vs. Ba + Sr plot given in Figure 56. The LREE level of the northern Ilomantsi sample 94002572 is increased.

It is interesting to note from Figure 57 that the most mafic, high Fe-Mg, low SiO_2 sample 'C' (high-Fe-Mg) is significantly enriched in REE relative to C1 and AFP. In particular, the incompatile LREEs are high, being up to twice the Finnish average (AFP). The slope of this group is close to that of the sanukitoid field. The potential of this rock (type) for economic REE mineralizations may be worth consideration.

3.2 Isotopic studies on the samples

The secondary-ion mass spectrometry (SIMS) U-Pb age analysis of the zircons from the samples considered here have been analysed and reported by Mänttäri (2012). This report gives a detailed description of analytical methods, analysed zircons, concordia plots, summary tables and error estimates of the data. Therefore, in this section, I mainly consider the age results without more profound methodological study.

In the following, I provide graphical summaries of $^{207}Pb/^{206}Pb$ isotopic age distributions for each sample, and ages ('magmatic ages' ≈ proposed magmatic crystallization ages) estimated from averages of the most common, 'stable' age groups in these diagrams. For comparison, ('magmatic') ages calculated by Mänttäri (2012) are also given. It should be noted that in the following, the term 'inherited zircons' may refer to primary source material (e.g. a juvenile mantle component mixed with older zircons in sedimentary material), or to contamination by crust during magma ascent to the present level of depth.

In the report by Mänttäri (2012), the ε_{Nd} values of samples summarized by Hannu Huhma (GTK; unpublished note; Huhma 2009, Huhma et al. 2012), indicating their magmatic source history, are also given. The model ages applied in the calculation of ε_{Nd} values are 2700 Ma.

93001908 granodiorite, Pudasjärvi sub-area

The number of analyses from this sample is 9. The $^{207}Pb/^{206}Pb$ age distribution is relatively continuous from ca. 2712 to 2731 Ma, the range being 19 Ma (Fig. 58). Three values, interpreted here as the main magmatic age, concentrate around ca. 2727 Ma. The slightly older 2731 Ma

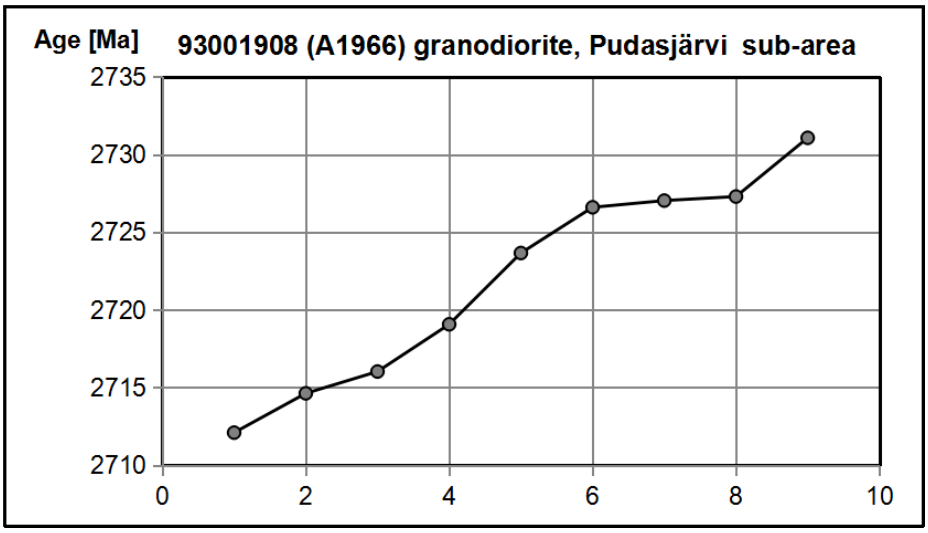

Fig. 58. Distribution of $^{207}Pb/^{206}Pb$ isotopic ages for sample 93001908 (A1966) granodiorite, from the Pudasjärvi sub-area. The ages are adopted from Mänttäri (2012). Horizontal axis: number of samples.

value probably represents the early stages of this magmatic main stage. The ca. 12 Ma age group from 2712–2724 Ma refers to the continuity of tectonomagmatic processes (pressure and/or temperature). The age estimated from the whole group of 9 analyses is ca. 2722 ± 7 Ma. The ε_{Nd} (T=2700 Ma) value is +2.1, indicating derivation from juvenile (ca. 2730 Ma?) source material with a relatively short crustal residence time.

Mänttäri (2012) reported a concordia age of 2722 ± 4 Ma for this sample (9 zircon domains), which agrees well with the age calculated from the whole data group above.

94003693 gneissic tonalite, Pudasjärvi sub-area

The number of analyses from this sample is 31. The $^{207}Pb/^{206}Pb$ ages vary between ca. 2640–2877 Ma (Fig. 59). The most homogeneous group varies between ca. 2697–2713 Ma, the magmatic age estimated from the average being ca. 2705 ±7 Ma; 13 analyses. There is also a less distinct group of inherited zircons between ca. 2776–2877 Ma. The lower age group varies between 2640–2691 Ma, representing overprinting by later processes. The ε_{Nd} (T=2700 Ma) value of +1.6 indicates derivations from juvenile source material with a relatively short crustal residence time, which is in contradiction with the observed large number of old inherited zircon ages.

Mänttäri (2012) gives a concordia age 2706 ± 4 Ma for this sample (15 accepted analyses), which agrees well with the average age given above.

95001782 granodiorite, East Finland sub-area

The number of analyses is 26. In Figure 60, there is a distinct and homogeneous age group between ca. 2961–3003 Ma, the magmatic age estimated from the average being ca. 2981 ± 11 Ma; 20 analyses. Thus, it appears, that there was a significant, ca. 40 Ma(?) continuity of heat pulses tectonizing/remelting pre-existing, ca. 3 Ga old Archaean crust. Two less distinct groups of younger overprinting ages vary from ca. 2686–2708 Ma and ca. 2900–2931 Ma. The relatively low ε_{Nd} (T = 2700 Ma) value of -4.6 refers to a recycled component of older Archaean crust (or may be due to a too small model age).

Mänttäri (2012) gives a concordia age of 2980 ± 6 Ma (19 analyses) for this sample. The oldest measured age was 3003 ± 2 Ma (Pb–Pb age). Both ages agree with ages above. Zircon cores are mostly zoned with thin metamorphic rims.

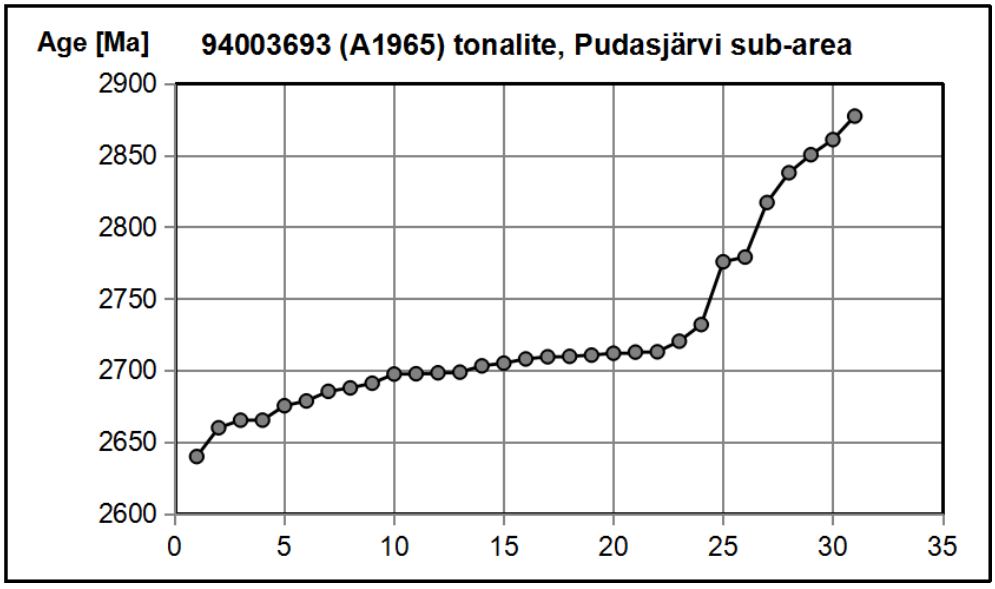

Fig. 59. Distribution of $^{207}Pb/^{206}Pb$ isotopic ages of sample 94003693 (A1965) tonalite, Pudasjärvi sub-area. Ages are adopted from Mänttäri (2012). Horizontal axis: Number of samples.

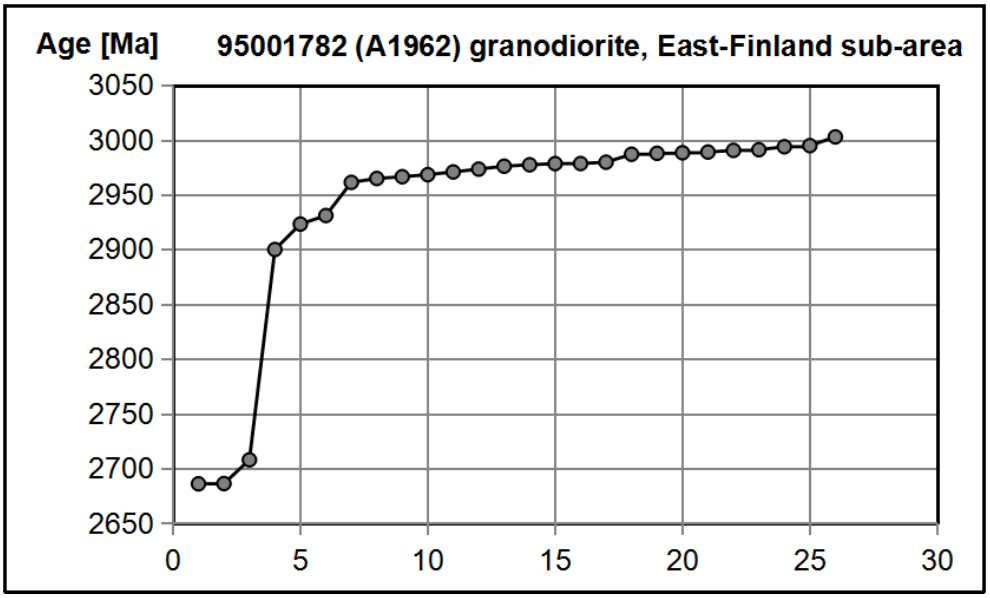

Fig. 60. Distribution of $^{207}Pb/^{206}Pb$ isotopic ages of sample 95001782 (A1962) granodiorite, East Finland sub-area. Ages are adopted from Mänttäri (2012). Horizontal axis: Number of samples.

94002667 tonalite, East Finland sub-area

The number of analyses from this sample is 28. In Figure 61, there are two homogeneous age groups representing the main magmatic periods: ca. 2774–2803 Ma (2787 ± 9 Ma; 7 analyses) and 2820–2853 Ma (2835 ± 10 Ma; 16 analyses). Four inherited ages are between ca. 2903–2954 Ma. The ε_{Nd} (T = 2700 Ma) value of -1.5 indicates derivation from a source (ca. 2853 Ma?) with a relatively short crustal residence time, which is in contrast to the inherited ages (contamination by older crustal material?). The young age of ca. 2630 Ma is uncertain.

Mänttäri (2012) gives a concordia age of 2836 ± 5 Ma for this sample (16 analyses), which agrees with the older age given above.

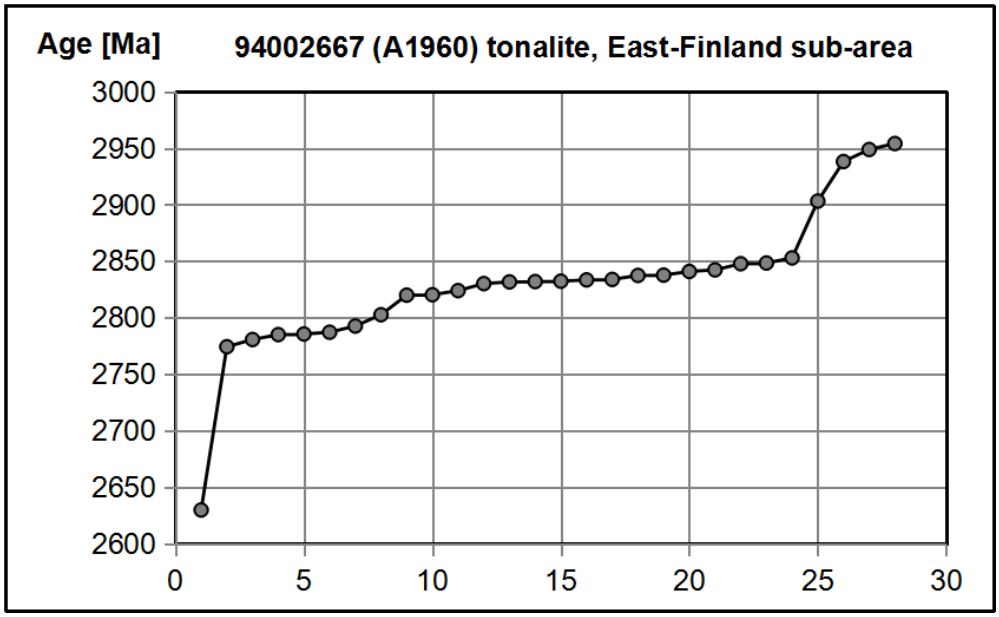

Fig. 61. Distribution of $^{207}Pb/^{206}Pb$ isotopic ages of sample 94002667 (A1960) tonalite, East Finland sub-area. Ages are adopted from Mänttäri (2012). Horizontal axis: Number of samples.

94003640 gneiss, Iisalmi sub-area

The number of analyses from this sample is 29. The complicated history of the Iisalmi sub-area is evident from the complex distribution curve of ages in Figure 62. From the diagram, two more homogeneous groups can be detected: ca. 2742–2761 Ma (2750 ± 8 Ma; 8 analyses) and 2884–2889 Ma (2889 ± 5 Ma; 6 analyses). The overprinting groups between ca. 2784–2871 Ma and 2613–2732 Ma are more scattered, reflecting continuous and complex tectonomagmatic processes in the Iisalmi sub-area. The ε_{Nd} (T = 2700 Ma) value is +0.8, which refers to derivation from juvenile source material with a relatively short crustal residence time. However, the complex age distribution refers to a mixture of varied-age Archaean source material.

Mänttäri (2012) gives a concordia age of 2742 ± 7 Ma (7 analyses) and several older cores for this sample. This age is difficult to perceive in the diagram in Figure 62.

93003031 tonalite, Iisalmi sub-area

The number of analyses from this sample is 18. The age distribution curve in Figure 63 has one relatively homogeneous group between ca. 2688–2697 Ma (2693 ± 3 Ma; 9 analyses). Using all older points between ca. 2672–2702 Ma, the magmatic age would be ca. 2691 ± 8 Ma; 14 analyses. All younger ages, including the ca. 2645–2651 Ma (2647 ± 3 Ma; 3 samples) age group, can be connected with overprinting processes. This sample, further to east from the A–P border in Figure 50, is clearly more homogeneous and younger compared to the westernmost sample 94003640 in Figure 62. The ε_{Nd} (T = 2700 Ma) value of +1.1 implicates juvenile source material (ca. 2.7 Ga) with a relatively short crustal residence time, which is in agreement with the age distribution curve in Figure 63.

Mänttäri (2012) gives a concordia age 2696 ± 4 Ma for this sample (7 analyses), which agrees well with the average age given above.

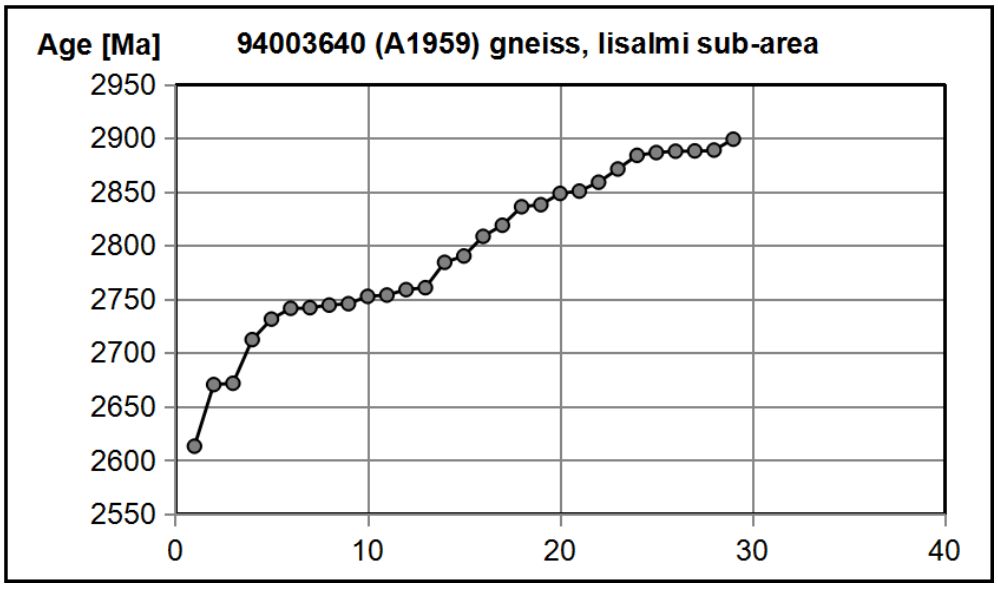

Fig. 62. Distribution of $^{207}Pb/^{206}Pb$ ages of sample 94003640 (A1959) gneiss, Iisalmi sub-area. Ages are adopted from Mänttäri (2012). Horizontal axis: Number of samples.

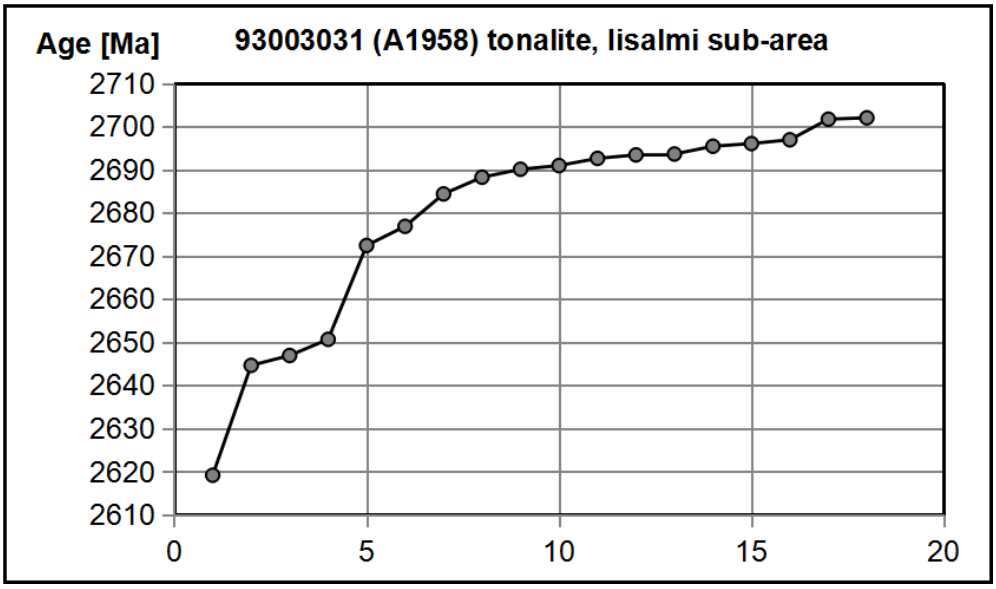

Fig. 63. Distribution of $^{207}Pb/^{206}Pb$ ages of sample 93003031 (A1958) tonalite, Iisalmi sub-area. Ages are from Mänttäri (2012). Horizontal axis: Number of samples.

94002572 granite, Ilomantsi sub-area

The number of analyses from this sample is 21. The wide, ca. 180 Ma and multistage age distribution curve in Figure 64 indicates a complex history in the Ilomantsi area. The magmatic age estimated from the oldest ages between ca. 2822–2837 Ma is ca. 2829 ± 6 Ma, 4 analyses, continuing in three successive points between 2791–2805 Ma. The younger group between ca. 2663–2752 Ma (2699 ± 30 Ma; 14 analyses) represents a ca. 90 Ma more or less continuous series of magmatic processes (varying pressure and/or temperature). The ε_{Nd} (T = 2700 Ma) value is -0.3, which indicates derivation from juvenile source material (ca. 2837 Ma?) with a relatively short crustal residence time, which is difficult to relate to the wide age distribution of the sample.

Mänttäri (2012) gives a concordia ages of ca. 2832± 10 Ma (4 analyses) and 2728 ± 12 Ma (4 analyses) for this sample, of which the older age agrees well with the older average age given above.

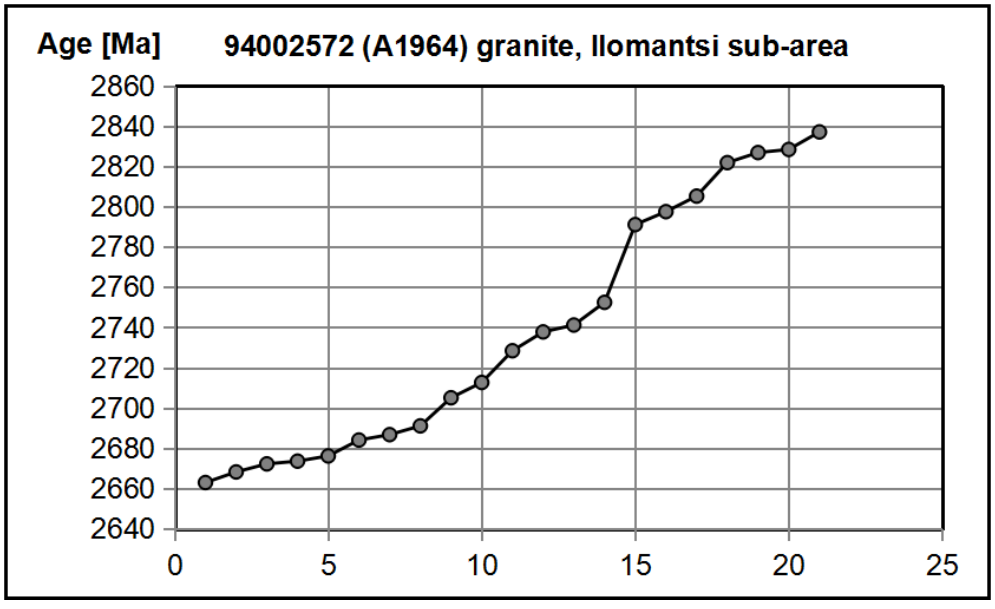

Fig. 64. Distribution of $^{207}Pb/^{206}Pb$ ages of sample 94002572 (A1964) granite, Ilomantsi sub-area. Ages are from Mänttäri (2012). Horizontal axis: Number of samples.

90010130 granodiorite, Ilomantsi sub-area

The number of analyses from this sample is 14. In the diagram in Figure 65, the ages vary continuously between ca. 2719–2740 Ma, the range being 21 Ma. Two oldest ages define an age of ca. 2740 Ma. Two younger homogeneous three-point clusters are at ca. 2727 Ma and 2732 Ma, which are close to the approximate average of all ages in this group (2730 ± 6 Ma; 14 analyses). Note the significant age differences between this sample and the granitic Ilomantsi sample 94002572 considered above (ca. 2829 ± 6 Ma and 2699 ± 30 Ma; Fig. 64). The ε_{Nd} (T = 2700 Ma) value is -0.2, referring to juvenile source material (ca. 2740 Ma?) with a relatively short crustal residence time.

Mänttäri (2012) gives a concordia age of 2730 ± 3 Ma for this sample (13 analyses), which agrees well with the average age given above.

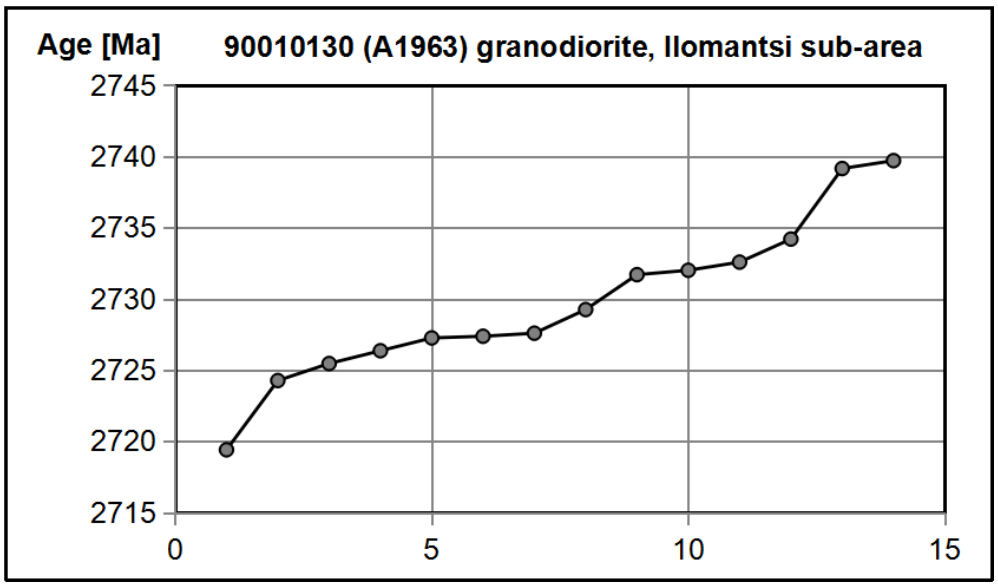

Fig. 65. Distribution of $^{207}Pb/^{206}Pb$ ages of sample 90010130 (A1963) granodiorite, Ilomantsi sub-area. Ages are from Mänttäri (2012). Horizontal axis: Number of samples.

3.3 Discussion

This study considers eight 'adakitic' TTG samples from four major Archaean sub-areas in central Finland: Pudasjärvi, East Finland, Iisalmi and Ilomantsi sub-areas, selected from 178 Archaean adakitic/TTG samples from the GTK lithogeochemical database studied by Ruotoistenmäki (2012). All samples fulfil the chemical characteristics defined for adakitoids by Defant & Drummond (1990) and Thorkelson & Breitsprecher (2005).

Chemical classification

The majority of the adakitic samples considered in this study are classified in the R1-R2 diagram in Figure 52 as syn- to post-collisional granodiorites, with the exception of the low SiO_2, southern Iisalmi tonalitic sample. In the Na2O/K2O vs. Ba + Sr plot in Figure 56, the East Finland samples are in the TTG field. The Pudasjärvi samples and northern Iisalmi sample have both TTG-like and sanukitoid characteristics. However, the Ilomantsi samples and southern Iisalmi sample are clearly in the sanukitoid field.

Based on their major and trace elements, the samples are divided here into 2+1 major groups:

1) The 'TTG-type' Pudasjärvi, East Finland and N-Iisalmi high-Na-Al, low-K group (A), is also characterized by high La/Yb and Sr/Y ratios. The slopes of chondrite- and AFP-normalized REE curves of this group (Fig. 57) are clearly steeper than those of samples in groups (B) and (C). The major and trace

chemistry of this group has chemical characteristics closer to Proterozoic adakitic Uki felsic trondhjemites reported by Väisänen et al. (2012), which they interpret to be generated through crustal melting of the lower part of thickened volcanic-arc-type crust. The southern Pudasjärvi sample (94003693 gneissic tonalite) is also characterized by inherited zircons referring to older, recycled components (Fig. 59).

2a) The sanukitoid Ilomantsi group (B) is characterized by high K, Mg, and lower La/Yb and Sr/Y ratios. The slopes of the chondrite-normalized REE curve of this group (Fig. 57) coincide closely with sanukitoids described by Heilimo et al. (2010). This is in agreement with the observations in the Na_2O/K_2O vs. Ba + Sr plot in Figure 56, in which Ilomantsi samples are located in the sanukitoid field.

2b) The sanukitoid, most mafic, southern Iisalmi, Fe- and Mg-rich sample is characterized by La/Yb and Sr/Y ratios similar to group (B). The slope of the chondrite-normalized REE curve of this sample (Fig. 57) coincides with sanukitoids described by Heilimo et al. (2010) and group (B), but the REE level is clearly higher. This sample can be classified as a mafic member of group (B). It is interesting to note that although most mafic, this sample is significantly enriched in REE relative to chondrite and AFP. The incompatile LREEs are especially emphasized.

The differences in element contents in these groups indicate variations in the primary source composition, degrees of source fractionation and contamination of the adakitic melts. The high Al_2O_3, Na_2O and highest La/Yb and Sr/Y contents of group (A) adakitoids are interpreted here as being due to the relatively higher plagioclase content in samples and fractionation at deeper levels compared to groups (B) and (C). The high K_2O values in group (B) can be explained by phlogopite-enriched source material (e.g. Heilimo et al. 2010). For example, when considering Pliocene high-potassium magmas from the Sierra Nevada Mountains, Elkins-Tanton & Grove (2003) proposed that subduction-derived fluids drive a reaction that consumes garnet + orthopyroxene to create clinopyroxene + phlogopite, and that the high-potassium Sierran magmas are created by melting of phlogopite-clinopyroxene metasomatized peridotite.

The lower La/Tb, Sr/Y and high FeO and MgO (compatibles) values in groups (B) and (C) refer to less fractionated (mafic) source material. Martin et al. (2005) connected sanukitoids and low-silica adakitoids with mantle melts metasomatized by slab melts. Halla et al. (2009) also connected high Ba-Sr sanukitoids to melting of an enriched mantle source, probably as a result of a slab breakoff following a continental collision or attempted subduction of a thick oceanic plateau or TTG protocontinent.

From Figure 53, it is evident that, with the exception of N Iisalmi and S Pudasjärvi samples, the Mg# value of all samples are high, within 44–68, thus implying interaction with mantle material (e.g. Heilimo et al. 2010). The SiO_2 content of all samples (with exception of the S Iisalmi sample) is higher than averages of Proterozoic and Archaean adakitoids (P.ADK and A.ADK) and all Finnish plutonic rock samples (AFP).

The major elements of these samples correlate only poorly with the Proterozoic 'Uki' samples from Väisänen et al. (2012). However, the averages of all Proterozoic and Archaean adakitoids (P.ADK and A.ADK) correlate more closely with the 'Uki tonalite' in Figure 53 and Figure 54 (yellow field). The data for all Finnish plutonic rock samples (AFP) do not show any systematic similarities with these groups.

Isotope ages

The age results of analysed samples are summarized in diagrams in Figure 66. In the diagrams, the ages distribute within a wide, overlapping and continuous range from ca. 2620 to 3000 Ma, reflecting long-lasting, multistage magmatic and tectonic crustal processes in the evolution of Finnish Archaean crust. The scattered oldest ages in the distribution curves indicate 'contamination' by older, inherited sedimentary and crustal material during magma generation and uplift to crustal levels. Moreover, the 'tails' of the youngest ages demonstrate the overprinting of the later chemical and tectonic processes on the samples.

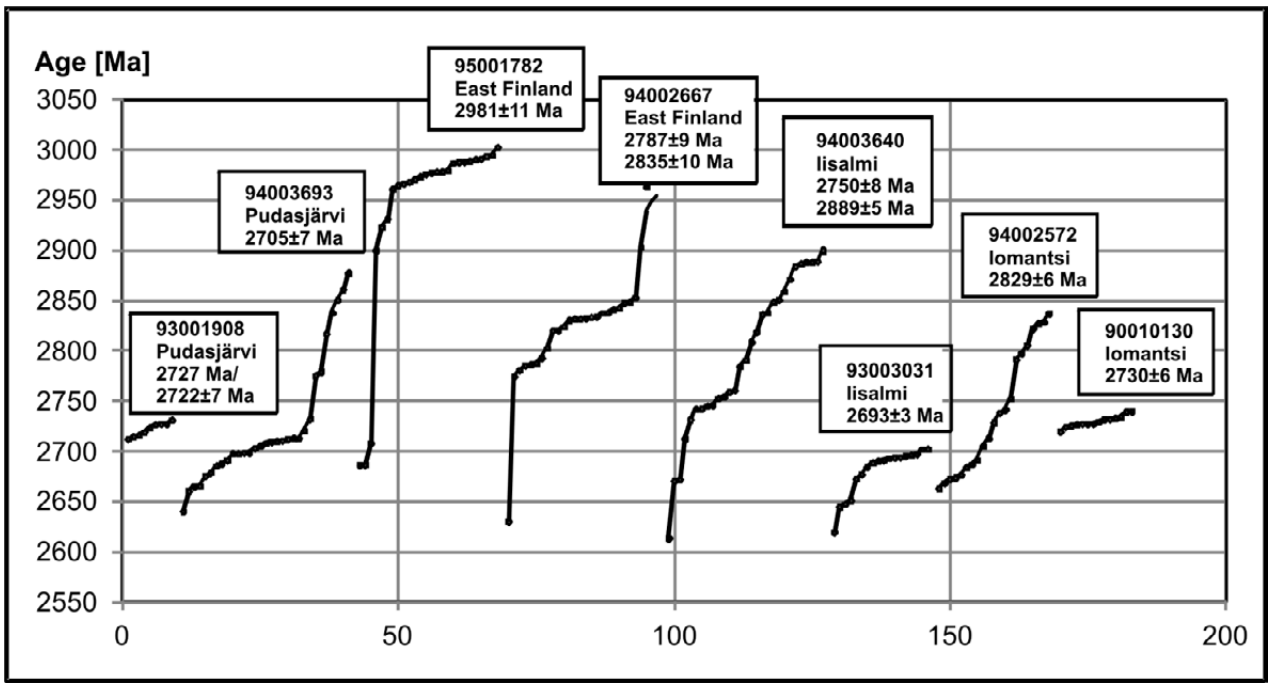

Fig. 66. Summary of the distributions of $^{207}Pb/^{206}Pb$ ages adopted from from Mänttäri (2012). The average of all U–Pb ages is ca. 2782 ± 102 Ma and the range varies between ca. 2613–3000 Ma.

The interpreted magmatic/emplacement ages of the samples vary from ca. 2.69 Ga to ca. 2.98 Ga, the majority (6 of 8) nevertheless being tightly bracketed between ca. 2.75–2.69 Ga. It is interesting to note that these ages agree with worldwide Archaean crust formation ages, noted by Condie (2005), Rino et al. (2004) and Rey et al. (2003), among others, who explain the ca. 2.75–2.65 Ga global, geodynamic event by the combination of a thermal anomaly from a mantle plume blanketed by greenstone crust cover.

The high ε_{Nd} values of most samples from ca. -0.2 to +1.6 refer to their juvenile, relatively 'uncontaminated' source material. However, in each Archaean sub-area considered here, there are also samples characterized by old ages related to inherited zircons (Fig. 66). Thus, it must be concluded that inherited, older assimilated crustal and/or recirculated sedimentary material is common in the adakitic Archaean rocks in Finland.

The ca. 40 Ma systematic age range of the oldest northern East Finland sample zircons (Fig. 60) refers to a significant and long-lasting heat input tectonizing/remelting pre-existing, ca. 3 Ga Archaean crust.

Tectonic model

Figure 67 is a greyscale image of the migrated section of the FIRE 1 seismic reflection profile across the Proterozoic–Archaean boundary in East Finland (blue line in Fig. 50). A few major reflection surfaces are also emphasized in the section. Kontinen & Paavola (2006) noted that the FIRE 1 profile area comprises a thrust stack of dominantly 2.85–2.70 Ga high-grade, granite–migmatite gneiss units, accreted in a continent–continent-type collisional orogeny. They conclude that these intense stacked tectonic characteristics along the profile are chiefly of Archaean origin, less affected by later Svecofennian orogenic overprinting.

Peltonen et al. (2006) noted that the zircon ages of East Finland kimberlite xenoliths vary over a wide range, from ca. 3.6 Ga to 1.7 Ga. The main age group indicates Svecofennian overprinting, between ca. 1.9–1.8 Ga, and only a small peak correlates with the Archaean crustal ages, around ca. 2.7 Ga. They note, however, that the oldest grains preferentially tend to recrystallize in each later event, which explains their low proportion in the Archaean protoliths. Thus,

based on lower crustal xenoliths, Kontinen & Paavola (2006) interpret the less reflective lower part of the profile, between ca. 20–40–60 km (between the dashed and dotted lines in Fig. 67) to be due to conductive heating of the lower crust during the 1.9–1.8 Ga Svecofennian thrust burial associated with metamorphic dehydration/recrystallization and related homogenization.

In the East Finland area, in spite of the profound Svecofennian overprinting in the lower crust, there is no notable adakitic Svecofennian magmatism, which should be characteristic for magmas fractionated at lower crust/upper mantle depths. On the contrary, ca. 2.85–2.65 Ga plutonic rock samples dominate in the area (Hölttä et al. (2012b). Only in the western Iisalmi sub-area, close to the Archaean–Proterozoic boundary, Ruotoistenmäki et al. (2001) documented adakitic plutons having Svecofennian/Proterozoic ages (ca. 1860–1880 Ma; see section 5. below). Therefore, it is more plausible that the very extensive and profound seismic homogenization of the lower crust is mainly due to Archaean underplating processes connected with the large-scale adakitic (/TTG/sanukitoid) magmatism. The Svecofennian overprinting has reset the U-Pb 'clocks' in kimberlite xenoliths, but caused only minor melting and magmatism as a whole. Moreover, as is evident from Figure 58 to Figure 66, the metamorphic overprinting ages distribute between ca. 2.7–2.6 Ga and no notable Proterozoic/Svecofennian ages below ca. 2.5 Ga exist in these samples.

A significant feature in the eastern part of the seismic profile between ca. 0–2500 CPM (from east to west) in Figure 67 is the abrupt thinning of upper crust from ca. 40 km to 20–25 km and the deep, highly reflective upper mantle (darker zone between the dashed and dotted lines in Fig. 67b). These features can be best explained by collision-related crustal thickening, crustal delamination allowing hot mantle upwelling and mixing of crustal and mantle material, i.e. by a stacking/thickening/mantle underplating model for the genesis of adakitic rock melts in the eastern East Finland sub-area. Rapp et al. (2003) interpreted that the evolution of Archaean TTGs took place beneath granite-greenstone complexes developing along Archaean intraoceanic island arcs by imbricate thrust-stacking and tectonic accretion.

Compared to present-day plate tectonic processes, the heat flow from the Earth's mantle and core was higher in the Archaean and early Proterozoic eons, the convective flows were faster and the plates were generally smaller and moving more rapidly (e.g. Bickle 1978, Nisbet 1987). A combination of these models can be generalized to explain high-Na, low-K TTG group 'A' (Pudasjärvi, East Finland, Iisalmi North) samples characterized by steep REE: chaotic stacking processes involving more or less exotic Archaean microplates and contamination by older crustal material. These sub-areas also lack substantial traces of 'modern type' subduction-related magmatism and sedimentary rock associations (eroded/migmatized?).

The oldest, ca. 3–2.98 Ga northern East Finland sample (Fig. 60) is also characterized by the lowest ε_{Nd} value of -4.6, as well as zoned zircons with metamorphic rims (Mänttäri 2012) and the steepest REE curves (highest La/Yb). Therefore, it can be associated with a ca. 40 Ma lasting series of complex recycling/stacking/collision processes of the type envisaged by Kröner et al. (2011), who suggested extensive recycling of even the earliest-formed granitoid crust and mixing with juvenile material to produce successive generations of TTGs and associated felsic volcanic rocks.

When considering granitoid magmatism of Neoarchaean plate tectonics in the Karelian and Kola cratons, Halla et al. (2009) related high- and low-HREE TTGs to low- and high-angle (-pressure) subduction. Moreover, they connected high Ba-Sr sanukitoids to melting of an enriched mantle source, probably as a result of 1. slab breakoff following a continental collision or 2. attempted subduction of a thick oceanic plateau or 3. TTG protocontinent. However, the 'modern' plate tectonic model is not easy to apply in explaining the evolution of Pudasjärvi, East Finland and Iisalmi areas lacking notable signatures of 'modern' plate tectonic rock associations. Thus, based on the notes above, and following the guidelines presented by Rapp et al. (2003), a generalized model for the evolution of Finnish Archaean sub-area blocks can be proposed, encapsulating boundary conditions for the majority of TTG samples considered here:

(1) Periodic, ca. 3.1–2.8–2.7 Ga increased mantle plume activity, acting as thermal and magmatic source and driving force =>
(2) Fast-moving, local-scale microplates having a ca. 3.1–2.9 Ga crustal greenstone-dominated 'kernel' (e.g. the ca. 2.79–2.97 Ga Kuhmo greenstones considered by Sorjonen-Ward & Luukkonen 2005) =>
(3) 'Pack ice tectonics', i.e. collision, under- and overthrusting (~ local scale 'subduction' and 'obduction'), stacking, folding and overturning resulting in significant crustal thickening.
(4) High P–T partial melting and fractionation =>
(5) Plagioclase-rich melts and garnet+amphibole+clinopyroxene in restites (+ orthopyroxene in lesser amounts =>
(6) Plagioclase-rich high-LREE, low-HREE adakitoids, sanukitoids and TTGs enriched by incompatible elements and contaminated by crustal and sedimentary material.

…

– Later overprinting by Post-Archaean Svecofennian re-homogenization of lower crust and upper mantle.

The 'modern' model of island arc – subducting marine plate tectonic evolution can best be applied to the sanukitic high-K-Mg Ilomantsi group and (on a more local scale) the mafic high-Fe-Mg Iisalmi samples. They are characterized by gentler REE, more likely related to fractionated mixtures of melts from gently dipping subducting/underthrusting plate, mantle wedge and sedimentary wedge during modern,

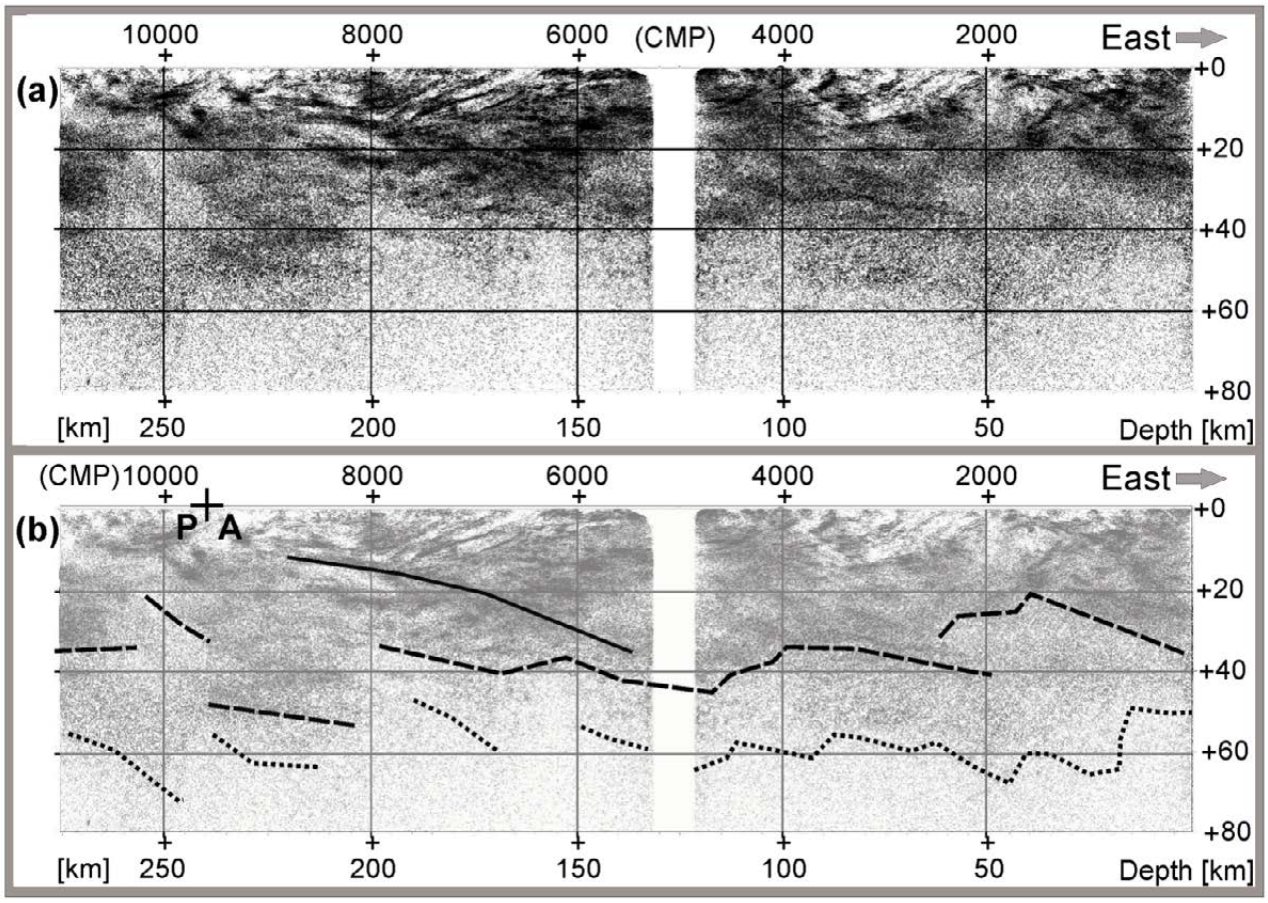

Fig. 67. (a): Greyscale image of the migrated section of the FIRE 1 reflection profile. The course of the profile is given in Figure 50. The overlay in (b) emphasizes some regional features in the profile. Solid line: example of a thrust zone through the whole upper crust. Dashed line: approximate course of the upper crust base = upper border of the altered high velocity zone. Dotted line: approximate base of the 'mixed' crust–mantle alteration zone (even below 60 km). The Proterozoic–Archaean border (P+A) outcropping at a common midpoint (CMP) of ca. 9600 has been marked with a larger cross (+). Note that at that point, the Archaean crust dips west, below the Proterozoic crust. However, at deeper levels, the Proterozoic crust appears to dip deeply below the Archaean crust. Adopted and modified from Kukkonen & Lahtinen (2006) and Kontinen & Paavola (2006).

'Andean type' subduction, as noted by Ruotoistenmäki (2012). O'Brien et al. (1993) and Hölttä et al. (2012a) also noted that calc-alkaline volcanic rocks, crustal signatures in the geochemistry of ultramafic rocks and high abundances of volcaniclastic greywackes in the Ilomantsi sub-area are consistent with arc-type tectonic settings, and hence may be more plausibly interpreted in terms of 'modern type' subduction processes.

Conclusions

- The Finnish Archaean adakitic samples considered here are classified into two main lithogeochemical groups: 1) the 'TTG-type' high Na-Al, low K, high La/Yb (LREE/HREE) and high Sr/Y group and 2) the sanukitoid group characterized by high K and Mg, and lower La/Yb and Sr/Y ratios. This group also contains the sanukitic, mafic Iisalmi sample, characterized by the highest Al_2O_3, FeO, MgO and very high REE, the lowest SiO_2 and lower La/Yb and Sr/Y ratios.
- The majority of U–Pb zircon ages of all samples distribute within a very wide range from ca. 2613–3000 Ma, reflecting long-lasting multistage magmatic and tectonic crustal processes in the evolution of Fennoscandian Archaean crust. The TTG East Finland group is the oldest (ca. 2770–3000 Ma), but otherwise, the ages of TTG and sanukitic groups are overlapping.
- The homogeneous age distributions and high ε_{Nd} values of northern Pudasjärvi, southern Iisalmi and southern Ilomantsi samples refer to their relatively juvenile 'uncontaminated' source material.
- In each sub-area considered here, there are also samples related to a wide age distribution and containing inherited zircons, which refer to older components in the sample sources in spite of their relatively high ε_{Nd} values (from ca. -0.2 to +1.6, one sample -4.6).
- The tectonic evolution of the TTG group is connected here with collision-related stacking and crustal thickening processes and high P–T lower crust/upper mantle melting, mixing and fractionation processes resulting in seismically homogeneous, high velocity, poorly reflecting zones in the lower crust. The restites are interpreted to be strongly depleted of plagioclase and enriched by garnet, amphiboles and clinopyroxene but minor orthopyroxene. These sub-areas lack notable subduction-related magmatic and supracrustal associations.
- The sanukitic Ilomantsi group, also characterized by island arc-type rock associations, is more likely due to 'modern type' gently dipping subduction-related processes. In this model, the restites of this sub-area contain more plagioclase and orthopyroxene and less garnet, amphiboles and clinopyroxene due to shallower fractionation depths. Basically, the Ilomantsi 'sanukitoids' (defined chemically in Fig. 56) appear to be 'adakites', i.e. subducting plate fractionation melts contaminated by various amounts of material from overlying sedimentary wedge, mantle wedge and crustal material.
- The sanukitic REE-enriched, but most mafic, southern Iisalmi sample probably represents poorly fractionated melts from enriched mantle, thus closely approximating the definition by Halla et al. (2009), who connected high-Ba-Sr sanukitoids to melting of an enriched mantle source.
- Later stage Archaean tectonomagmatic processes caused heating, partial re-melting and mixing (underplating) in the crust–mantle boundary, shown as a 2.6–2.7 Ga 'tail' of younger ages in age distribution curves. These processes and later, Svecofennian overprinting reheated the high-velocity zones below the crust, causing the Proterozoic zircon ages of the kimberlite xenolith samples. The minor Svecofennian magmatism in Finnish Archaean sub-areas demonstrates the relatively low degree of Proterozoic lower crust melting.
- The high-Na-Al, low-K group samples are closer to the Proterozoic adakitic Uusikaupunki (Uki) trondhjemites and the high-K-Mg 'Ilomantsi' group samples approximate Proterozoic, more mafic 'Uki tonalites' considered by Väisänen et al. (2012). As a whole, however, the correlation between all these Archaean samples and the Proterozoic adakitic samples used for comparison is relatively poor.

4 CHARACTERISTICS OF ADAKITIC PLUTONIC ROCK SERIES IN A PROTEROZOIC COLLISION ZONE, SOUTHERN FINLAND

This section considers high-Al, high-Sr, high-Eu, high magnetite and LREE-enriched mafic-intermediate plutonic rock series in a Proterozoic collision (accretion) zone in southern Finland (white-black squares in Fig. 3), having adakitic characteristics when normalized to a common value of SiO2. The samples were collected from a ca. 60 km long and 20 km wide profile cross-cutting a distinct lithological and geophysical discontinuity. The characteristics of this adakitic group are compared with a more felsic tholeitic plutonic rock series sampled on the same profile. This study is based on notes in Ruotoistenmäki (1999).

4.1 Introduction

When studying the volcanic rocks overlying sedimentary rocks in the Proterozoic Tampere schist belt, between the southern Finland gneiss-migmatite belt (SMB, Fig. 3) and the central Finland granitoid sub-area (CFG), Simonen (1953) noticed that they resemble a volcanic island arc association. However, it was not until much later that Hietanen (1975) applied the concept of plate tectonics in explaining the generation of the potassium-poor magmas of the Proterozoic Svecofennian crust in Finland.

The BABEL deep crustal seismic reflection profiles under the Bothnian Bay indicated a gently dipping reflector penetrating from lower crust into the upper mantle (Babel Working Group 1993 and references therein). This reflector has been interpreted as a remnant of an early Proterozoic subducting plate dipping N–NE below Archaean crust at ca. 65°N below the NW continuation of the Ladoga–Bothnian Bay zone (LBZ) in Figure 3. The CFG and SMB sub-areas have also been traversed by the deep seismic refraction profiles SVEKA (e.g. Luosto et al. 1984) and Fennia (Heikkinen et al. 1995), and also more recently by detailed deep seismic reflection profiles FIRE1 and FIRE2 (Kukkonen & Lahtinen 2006; Fig. 82).

The Proterozoic (ca. 1.93–1.88 Ga) evolution in this area has been modelled by two-stage collision tectonics (Ruotoistenmäki 1996):

1. NE–E-directed collision of CFG, interpreted as an island arc, and LBZ, interpreted as a marine basin + primitive arc, against the Archaean craton in East Finland and
2. N–NE-directed collision of USM, also interpreted as an island arc, and SMB, interpreted as a marine basin, against CFG.

Similar type plate tectonic models have been presented later by Nironen (1997) and Lahtinen et al. (2005), among others. These models also define the USM–SMB–CFG plate boundaries as resulting from the amalgamation of more or less exotic ‘terranes’, analogous to the evolution of the west coast of North America (e.g. Howell 1985, Gore & Sugar 1985, Howell 1995). The SMB–CFG discontinuity is evident from maps in Figure 68 to Figure 70.

4.2 General geology of the study area

The bedrock of the central CFG, SMB and USM has been considered in numerous papers. Simonen (1953) provided a comprehensive description and analysis of the Tampere schist belt area between the SMB and CFG. Kähkönen (1989, 2005) attributed the volcanic rocks in the area to plate convergence involving mature island arcs or active continental margins. In Kähkönen & Leveinen (1994), the turbiditic metagraywackes-mudstones in the area are interpreted to be more typical of a submarine basin depositional environment. The USM bordering the gneiss-migmatite sub-area in the south was interpreted to represent a partly subaerial, mature arc by Hakkarainen (1994). For details of the multistage deformation and metamorphic history of SMB, see also Rutland et al. (2004).

Nironen (1989) and Nironen et al. (2000) described synkinematic 1.9–1.87 Ga granitoids in central Finland. They noted that the tonalitic plutons possibly originated through mixing and mingling between crustal and mantle-derived

magma, or magma derived by partial melting of subducted oceanic slab. A revised lithological map of the CFG area (Nironen 2003) indicates that the predominant rocks there are felsic granites and granodiorites, while mafic rocks are relatively sparse. The age distribution of the rocks varies from ca. 1.9 Ga to 1.89–1.88 Ga for synkinematic plutons to ca. 1.88–1.87 Ga for postkinematic rocks. The proportion of postkinematic rocks, which are almost coeval with synkinematic rocks, is relatively high. Elliott (2001) interpreted the source magma of the postkinematic plutons to be a combination of Fe-enriched mantle-derived protolith, with assimilated crustal material.

The synkinematic magmatism in the CFG area is connected by Nironen et al. (2000) to partial melting of intermediate composition K-rich rocks in the lower crust, with magmatic addition from the mantle, leaving a granulite residue.

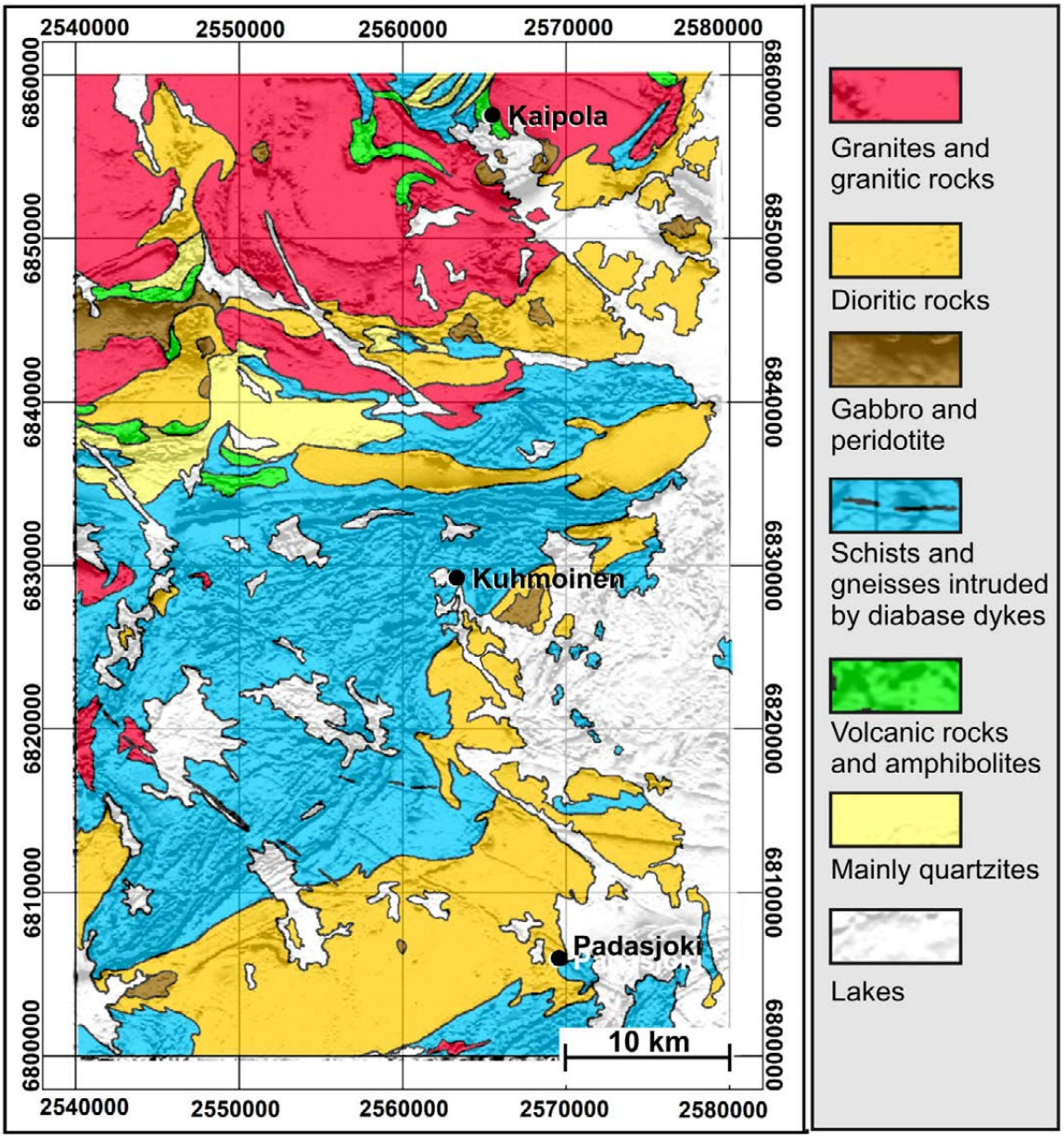

Fig. 68. Lithological map of the study area, generalized from Laitakari (1971, 1973). The map is superimposed upon an oblique-illuminated low-altitude aeromagnetic map (in greytones; the magnetic map is presented in Fig. 69). The southern half of the map consists of the Padasjoki map sheet (2143) and the northern half of the Kaipola map sheet (2144). The location of the map area is shown by white-black squares in Figure 3.

Corner point coordinates in WGS-85:
Lower left KKJ: 6800000 2540000 / WGS-84: N 61.30° E 024.74°
Upper right KKJ: 6860000 2580000 / WGS-84: N 61.83° E 025.49°

In their model, the following post-kinematic magmatism resulted from partial melting of the residue and continuing input from the mantle. Thus, their models approach the adakitoid generation model connected with crustal thickening and underplating as proposed for Archaean adakitoids above (sections 2 and 3). Also, the sanukitoid character of CFG, noted above (Fig. 32), suggests an increased mantle component.

Figure 68 presents a generalized bedrock map of the study area, linking the southern part in SMB to the northern part located in CFG. The map has been superimposed with a greyscale low-altitude aeromagnetic map to emphasize the local scale trends in the area. From the map, it can be seen that the southern part (south from ca. x = 6835000) is dominated by schists and gneisses intruded by diabase dykes, granodiorites and minor mafic and granitic intrusions. A common feature in the granodiorites is that they contain inclusions and xenoliths of gneisses, mafic rocks and amphibolites. In contrast to the southern Padasjoki map sheet area, granites, granodiorites and mafic plutonic rocks characterize the northern Kaipola sheet. The quartzites and mafic metavolcanic rocks are more abundant in the north.

4.3 Geophysical and petrophysical characteristics of the study area; Location of the samples

The local-scale magnetic anomalies of the study area and the location of samples considered here are shown on the magnetic map in Figure 69. On the map, the difference between the southern and northern areas is distinct with respect to both the anomaly level and patterning, the regional and local anomaly levels in the northern area being higher. The magnetic trends also refer to complex folding of the southern schists and regional dextral shear subparallel to the E–W contact with the CFG, due to oblique compression from NW–SE (white arrows in Fig. 69). The long linear, mainly NW–SE-trending magnetic anomalies in the southern area are due to diabase dykes, as described by Laitakari (1969), which are associated with the intrusion of the anorogenic rapakivi granites in southern Finland (Fig. 3).

In Figure 70, the aeromagnetic low-altitude map (in greytones obliquely illuminated from NE and NW) has been superimposed on the electromagnetic in-phase map (in colours). In this map, pyrrhotite- and graphite-bearing electrically conductive schists are shown by high magnetic and electromagnetic (EM) in-phase anomalies (red). Magnetite-bearing poorly conductive rocks are shown by high magnetic and low EM in-phase anomalies (blue). For the principles underlying this method, see e.g. Peltoniemi (1982 and references therein). From the map, it can be seen that the southern part of the area is dominated by folded, conductive magnetic zones due to pyrrhotite- and graphite-bearing schists, while in the northern part, the magnetic anomalies are mainly due to magnetite-bearing intrusives.

The petrophysics laboratory at GTK has measured the density, susceptibility and remanence of rock samples collected from the study area by Laitakari (1971, 1973). For detailed study, 94 of 1766 plutonic rock samples were selected and collected from GTK archives. The location of the selected samples is indicated in Figure 69. The sampling area covered a 20 km wide and 60 km long north–south trending zone crossing the contact area between southern SMB and CFG sub-areas. The selection of samples was firstly based on their petrophysical characteristics (mainly susceptibility, remanence and density), the purpose being to obtain a representative group of petrophysical types of plutonic rock samples in the area.

Figure 71 depicts the diagrams used for sample selection. In the diagrams are given the variations in density, susceptibility and Q-values for all samples in a south–north direction through the study area. The analytical procedures of the GTK petrophysics laboratory have been described in Puranen (1989, 1991) and Korhonen et al. (1993). From the diagrams, it is evident that the distributions of the selected samples effectively represent the general variations of all samples. The representativeness of samples is discussed later in the text. From the diagrams it appears that a distinct high-density, high-magnetic and low-remanence 'high-Al' group characterizes the northern part of the profile.

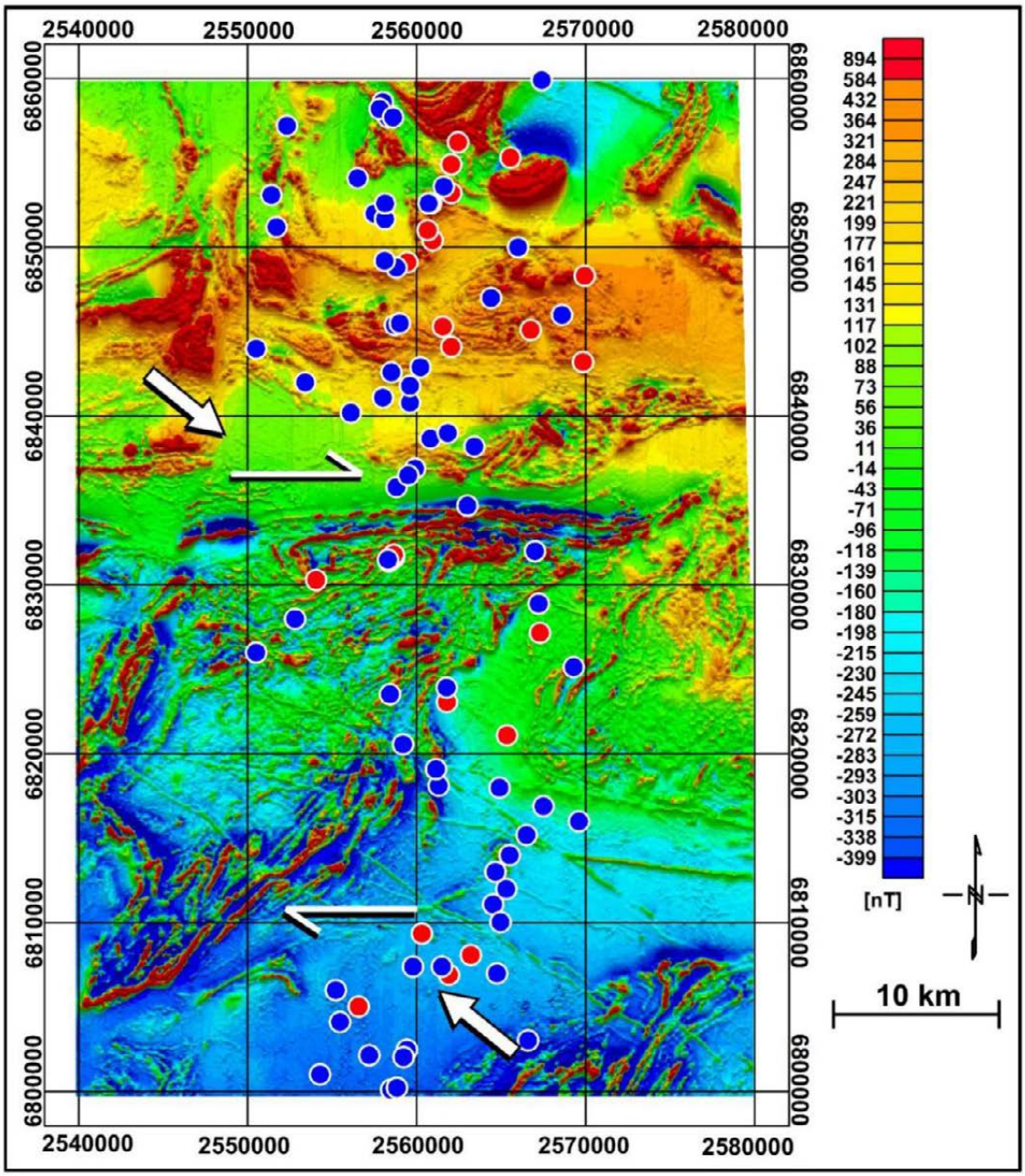

Fig. 69. Aeromagnetic low-altitude map of the study area. Data from the Geological Survey of Finland (Hautaniemi et al. 2005). The location of samples described and explained later in text is indicated with red ('high-Al' samples) and blue ('low-Al' samples) dots. The white arrows indicate inferred compression and shearing directions.

The density–susceptibility relationships of all 1766 plutonic samples in the zone are given in scatter diagrams in Figure 72. The peaks shown in the diagrams can be used for studying characteristic density–susceptibility pairs of the samples in the study area. The peaks and their values are given in Table 8. In the table, the density value of the main paramagnetic peak (1) in Padasjoki is clearly higher compared to the Kaipola area. The other paramagnetic peaks (2 and 3 in the Padasjoki area and 2, 5 and 7 in the Kaipola area) are less pronounced. In the Kaipola area, there are also distinct, ferrimagnetic, lower density, 'felsic' peaks (3 and 4) and high density–susceptibility, 'mafic' peaks (6, 8–11), which indicate a more complicated magmatism compared to that in the Padasjoki area.

Table 8 also gives estimates (weight %) of iron in silicates and the magnetite content (wFe and wM) calculated using formulas given by Puranen (1989). He concluded that paramagnetic susceptibilities are mainly due to iron in silicates,

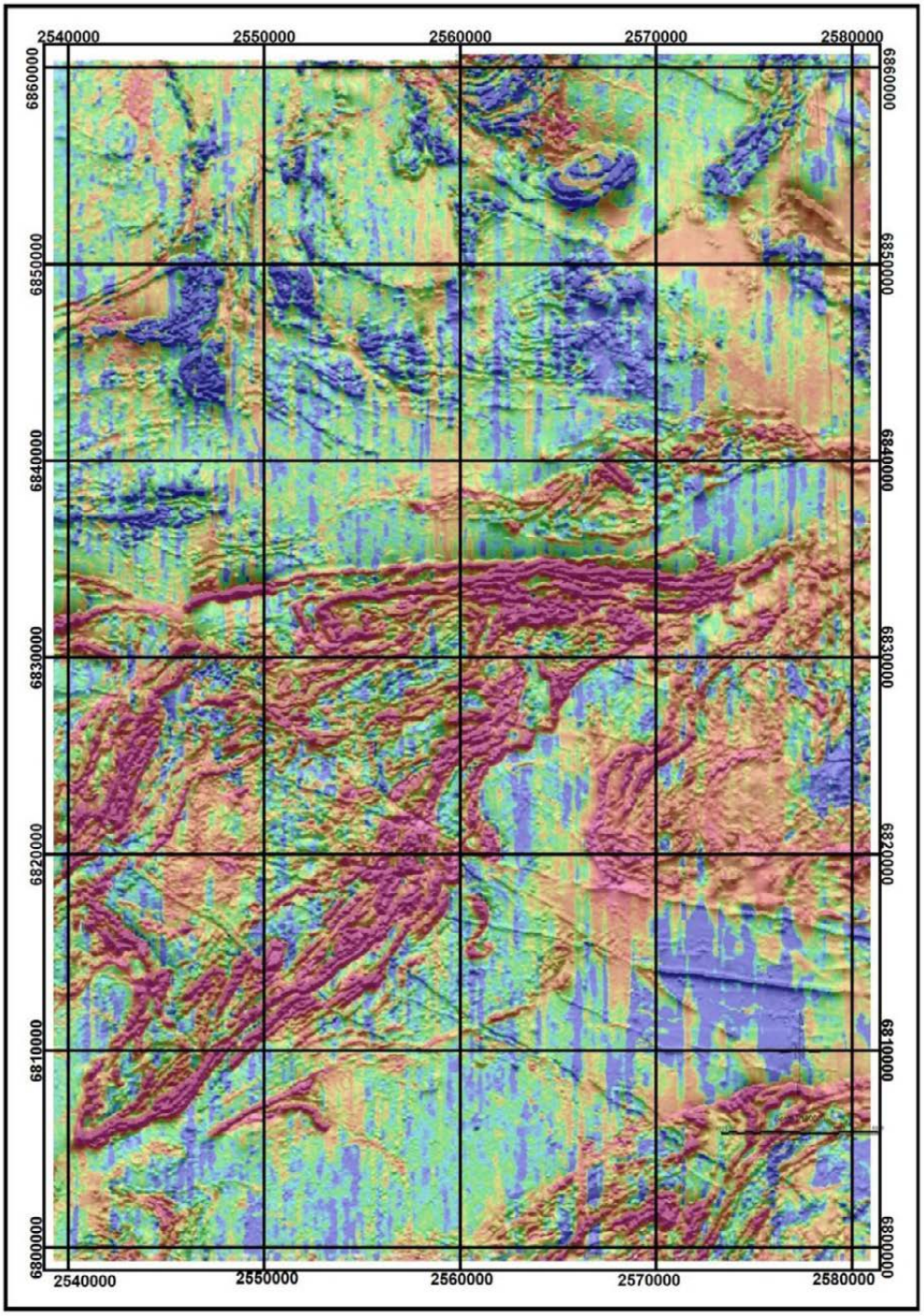

Fig. 70. Aeromagnetic low-altitude map of the study area (in greytones) combined with an electromagnetic in-phase map (in colours). Data from the Geological Survey of Finland (Hautaniemi et al. 2005). Red: conductive rocks, blue: more resistive rocks. The N–S-trending stripes are noise due to levelling variations of the electromagnetic data.

while ferrimagnetic susceptibilities are normally caused by magnetite. Thus, the contents of iron or magnetite can be evaluated using the susceptibility/density ratios (mass susceptibilities) of paramagnetic or ferrimagnetic samples, respectively. From the table, it can be seen that the iron contents obtained from the paramagnetic peaks (1–2) of the southern, Padasjoki area are clearly higher compared to those from the Kaipola area. The (seemingly) high iron content, close to 8%, obtained from some paramagnetic peaks is apparently due to the presence of some magnetite in the samples.

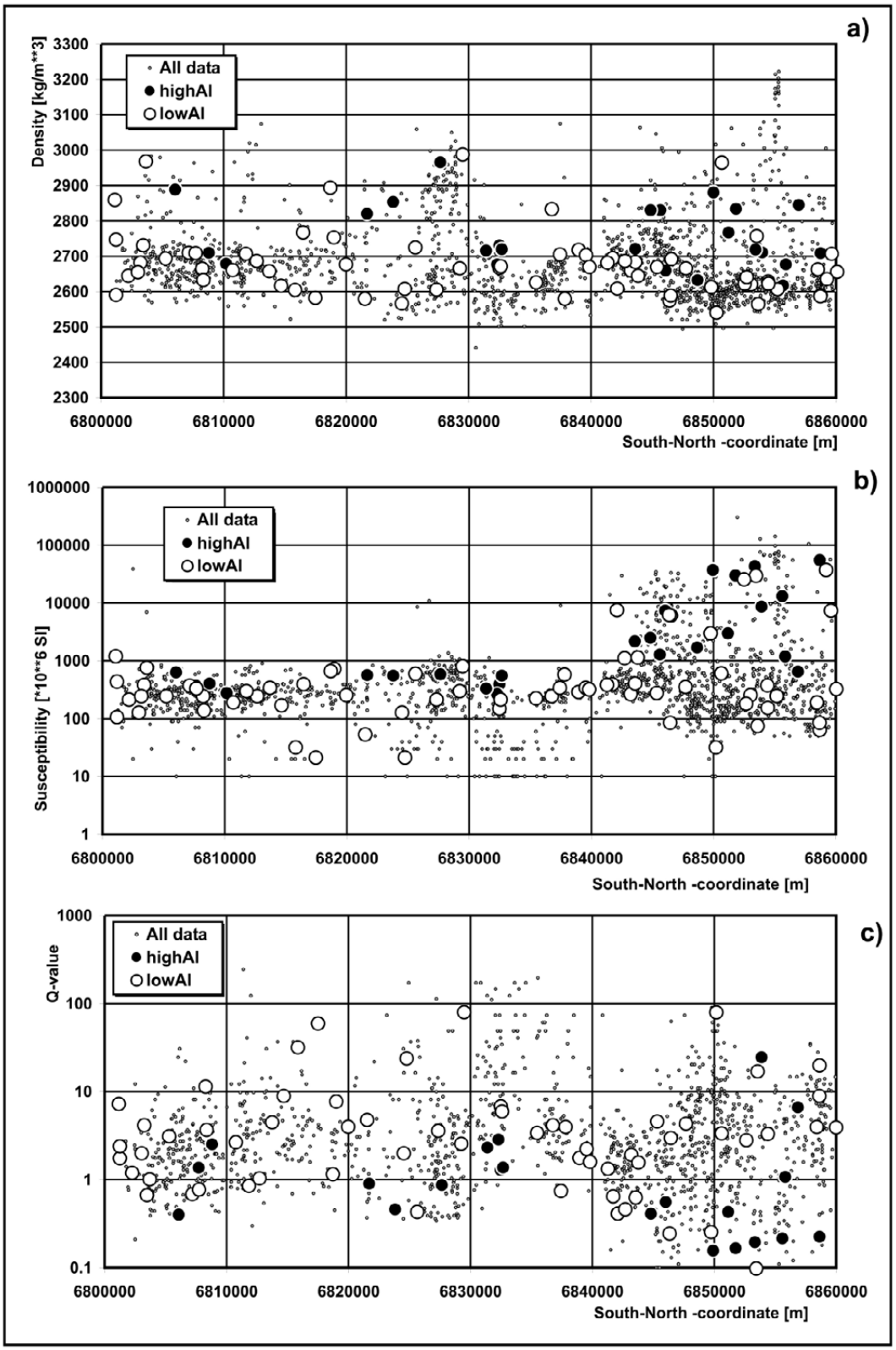

Fig. 71. Variations in density (a), susceptibility (b) and Q-values (c ≡ ratio of remanent to induced magnetization) for all-plutonic rock samples along a south–north traverse through the study area (small dots). The samples studied in more detail are indicated with larger black ('high-Al' samples) and white ('low-Al' samples) dots.

It is evident from considerations above that the petrophysical properties of plutonic rock samples from northern and southern parts of the study area differ significantly. This correlates with distinct differences in their mineralogy and chemistry and thus their evolutionary history. Ruotoistenmäki (1992) attributed the difference in magnetic characteristics to a more reducing environment in the southern part of the area compared to the northern part, resulting in preferential incorporation of iron into silicates instead of iron oxides. These conclusions have later been supported by Peltonen (1995), Lahtinen (1994) and Lahtinen & Korhonen (1996), among others.

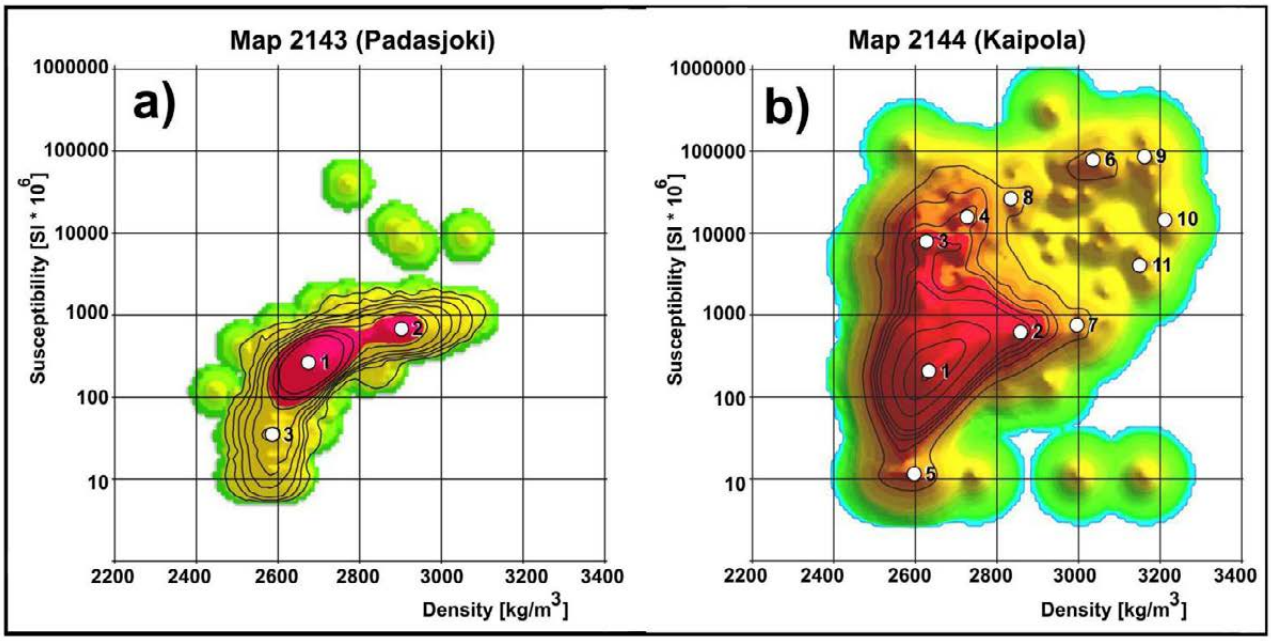

Fig. 72. Density–susceptibility diagrams for all available plutonic rock samples from the study area from the Geological Survey of Finland petrophysical database. The numbers of the peaks in the diagrams refer to susceptibility–density values given in Table 8 below.

Table 8. Characteristic density–susceptibility relationships of the samples from the study area. wFe and wM are estimates of iron and magnetite contents calculated from para- and ferrimagnetic peaks using formulas by Puranen (1989). Possible magnetite involvement in paramagnetic samples has been marked by (+Mt?).

Map 2143 (Padasjoki)			Paramagn. peaks	Ferrimagn. peaks	Map 2144 (Kaipola)			Paramagn. peaks	Ferrimagn. peaks
Peak No	Density [kg/m^3]	Susc. [SI*10^6]	wFe [wt%]	wM [wt%]	Peak No	Density [kg/m^3]	Susc. [SI*10^6]	wFe [wt%]	wM [wt%]
1	2675	267	3.49	…	1	2633	205	2.73	…
2	2900	679	8.19	…	2	2858	627	7.68 (+Mt?)	…
3	2583	35	0.48	…	3	2628	8055	…	0.46
					4	2726	16160	…	0.89
					5	2595	12	0.16	…
					6	3036	78640	…	3.89
					7	2994	774	9.05 (+Mt?)	…
					8	2835	26813	…	1.42
					9	3161	87389	…	4.15
					10	3212	14852	…	0.69
					11	3150	4015	…	0.19

4.4 Chemical classification of the samples

Alkali index vs Al_2O_3

Chemical analysis of the samples has been conducted in the laboratory of GTK. The elements, units and analytical methods, as well as the rock types of some selected samples, are given in Table 10. For detailed descriptions of the analytical methods, see e.g. Sandström (1996) and Rasilainen et al. (2007).

In the alkali-index diagram in Figure 73, a significant feature is the sharp increase in the alkali index (AI) as a function of Al_2O_3. Using this diagram, the samples have been classified as high- and low-aluminium (high-Al and low-Al). Middlemost (1975) used this diagram for differentiating basaltic rocks into tholeitic and calc-alkaline classes. He concluded that basalts from active continental margins usually contain more aluminium, sodium and potassium and less titanium dioxide than flood basalts, designating them as high-aluminium basalts. Garrison & Davidson (2003) noted that enrichment of Al_2O_3 in the melt can be attributed to the absence of plagioclase in residue: fractionation in pressure-temperature fields where plagioclase is unstable. Therefore, when studying these rock groups in detail, it can be possible to obtain indications of their fractionation depths, pressures and temperatures and furthermore, the distribution and characteristics of crustal magma sources.

It must be emphasized that, in reality, the border between high-Al and low-Al groups is not sharp, as suggested by the borderline in the diagram, but probably indefinite and the groups are overlapping. Moreover, the chemical variation of the samples can be due to variation in the primary magma sources, fractionation, contamination, mixing and metamorphic processes. Thus, when considering these groups, statistical methods are applied to define the general characteristics of the samples and differences between groups.

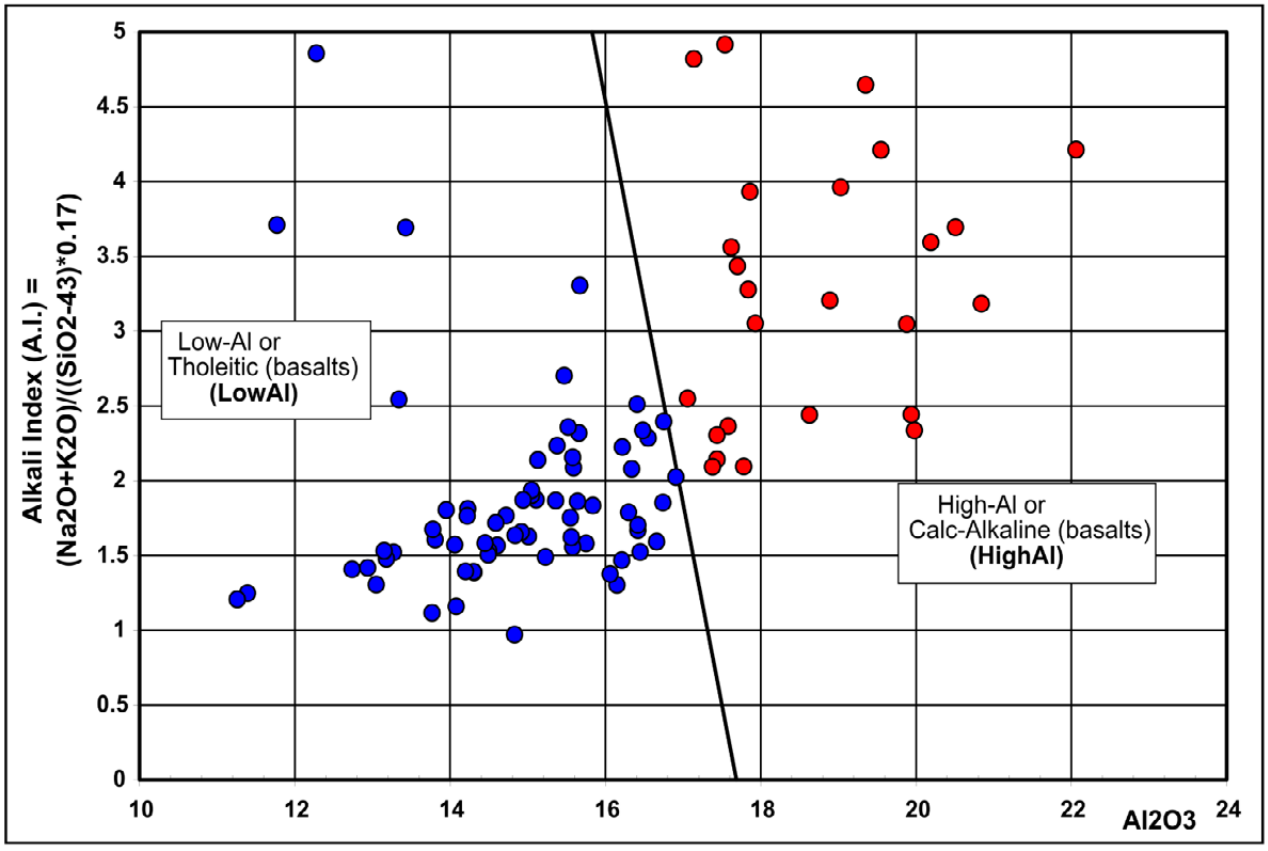

Fig. 73. Alkali index vs Al_2O_3 diagram of plutonic rock samples selected for this study. The diagram has been adopted from Middlemost (1975), who primarily used it for the classification of basaltic rocks.

Reliability of the sample size

The reliability of the sample size and classification of samples was tested and confirmed by the approximation algorithm of hypergeometric distribution by Cochran (1963). Using this method, it is calculated that the ratio (25 high-Al samples) / (69 low-Al samples) = 27% can be obtained to a 95% confidence level using 94 samples out of a total 1766 samples having this high-Al / low-Al sample number ratio. This means that the 94 samples taken are sufficient to give a satisfactory overview of the characteristics of the study area.

Table 9 lists density and susceptibility statistics for all-plutonic rock samples in the south–north profile through the study area with those samples selected for detailed study (shown in Fig. 71). The close agreement of the averages, standard deviations, medians and modes further supports the representativeness of the chosen sample population.

Table 9. Comparison of statistics for the density (D) and susceptibility (K) of all-plutonic rock samples from the south–north profile across the study area with the samples to be studied in more detail (see also Fig. 71).

	D [kg/m^3]		K [SI *10^6]	
	All	Selected	All	Selected
Number of samples	1766	94	1759	94
Minimum	2087	2540	0	20
Maximum	3222	2986	304000	51400
Range	1135	446	304050	51380
Average	**2684**	**2697**	**2470**	**3520**
Stdev	**116**	**97**	**12027**	**9326**
Median	**2658**	**2677**	**290**	**350**
Mode	2606	2676	140	230

Lithological classification of the samples

In Figure 74 and Figure 75 are given the classification of the samples according to diagrams by Cox et al. (1979) and de la Roche et al. (1980) based on the chemical content. The Cox diagram indicates that the high-Al samples are generally alkaline, more mafic and gabbroic–syenitic in composition, while the low-Al samples are subalkaline, more felsic and mainly dioritic–granitic, although with some gabbroic samples. In the Roche diagram in Figure 75, the composition of low-Al samples varies from syn- to post collisional diorites–monzogranites, the average being granodioritic, syn-collisional. The high-Al samples are mainly post-collisional monzonites–monzodiorites–gabbros, the average being post-collisional, monzodioritic.

Table 10 presents the mineralogical classification of some selected samples using the classification by Streckeisen (1976). The table also shows their rock type classifications in the Cox and Roche diagrams. The wide variation of rock-type names in the table emphasizes the uncertainty of various diagrams in defining reliable type names for plutonic rocks.

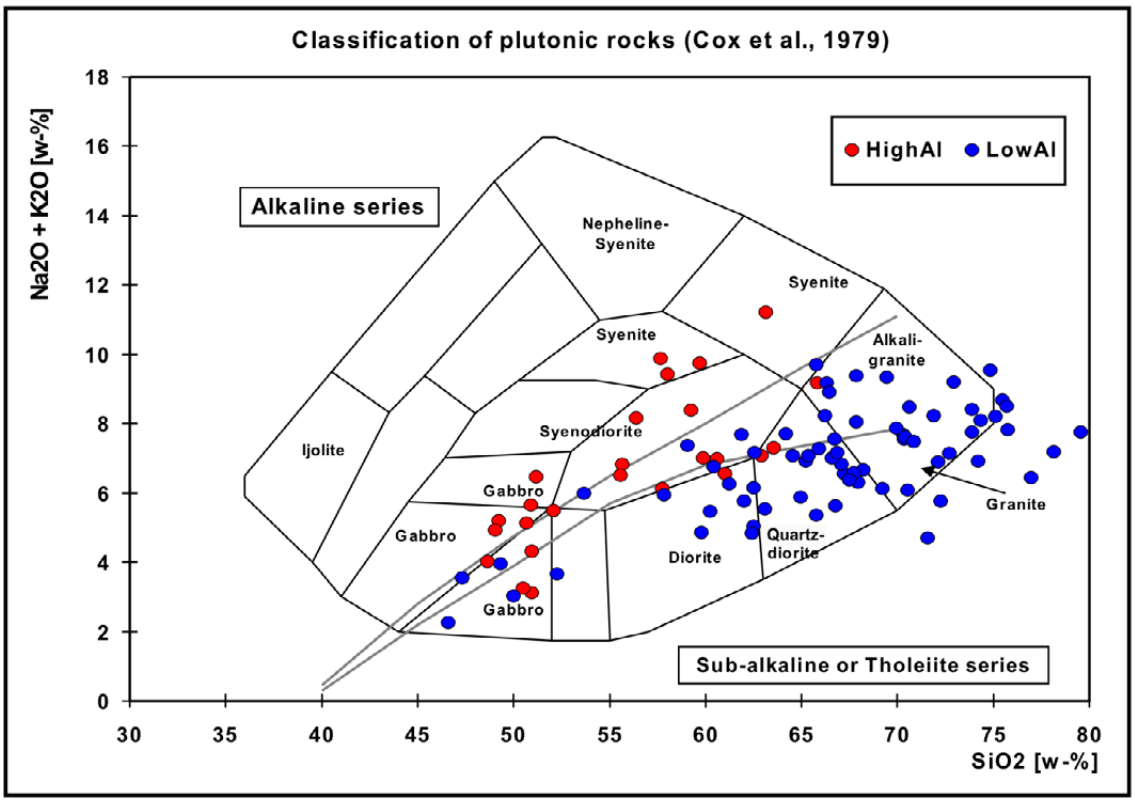

Fig. 74. Classification of samples in the Na_2O+K_2O vs SiO_2 diagram by Cox et al. (1979) modified for plutonic rocks by Wilson (1989). The alkaline/sub-alkaline boundary zone (which is not precisely located) has been adopted from Rickwood (1989).

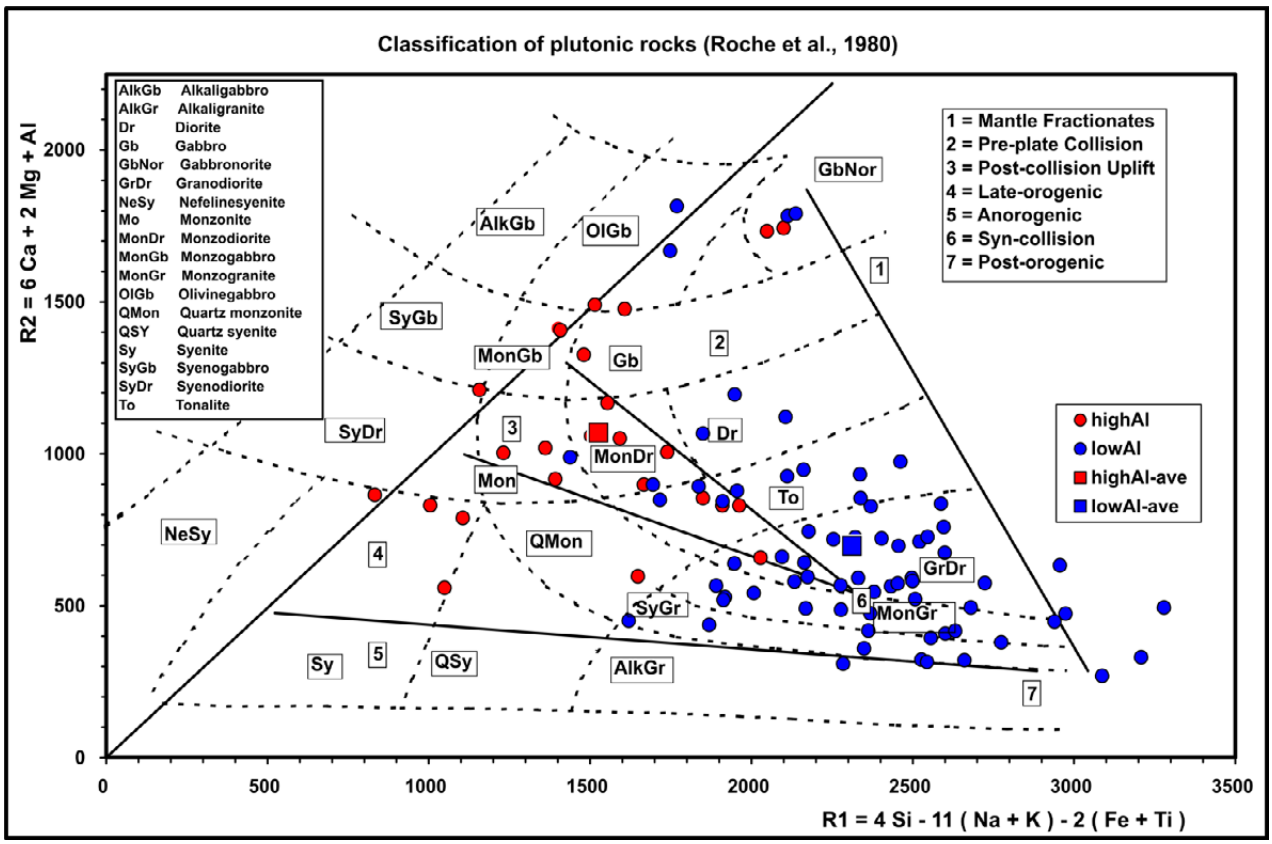

Fig. 75. Classification of Proterozoic area samples in the R1-R2 diagram (de la Roche et al. 1980). The tectono-magmatic fields have been adopted from Batchelor & Bowden (1985) and rock-type boundaries have been modified according to Rollinson (1993). Compare to diagrams in Figure 9 and Figure 10.

Table 10. Lithology, petrophysics and chemistry of some selected samples examined in this report. QAP-Rock, Roche-Rock and Cox-Rock refer to rock types obtained from diagrams by Streckeisen (1976), de la Roche et al. (1980), Figure 75 and Cox et al. (1979), Figure 74. D = density, K = magnetic susceptibility. The method of analysis is given in parentheses. QAP studies were conducted by Eeva Rintala (1994, Geological Survey of Finland; unpublished report).

Lithology and petrophysics: SampleName	**JRX66P196.D**	**GSX67P073.B**	**GSX68P541.B**	**JRX67P246**	**VSX65P280**	**LMX63P284.A**	**KKX69P588.A**	**JRX66P110.B**	**JRX67P252.A**	**GSX67P076**
high-Al vs low-Al	high-Al	high-Al	high-Al	high-Al	high-Al	low-Al	low-Al	low-Al	low-Al	low-Al
Q-A-P	26%, 9%, 65%	25%, 23%, 52%	24%, 14%, 62%	12%,10%, 78%	25%, 5%, 70%	35%, 27%, 38%	62%, 36%, 2%	39%, 47%, 14%	41%, 59%, 0%	50%, 43%, 7%
QAP-Rock	Granodiorite	Granite	Quartz-monzonite	Quartz-monzogabbro	Granodiorite	Granite	Quartz-rich granitoid	Granite	Granite	Granite
Roche-Rock	Gr	GbNor	Dr	MonGr	Gr	Gr	GrDr	To	MonGr	GbNor
Cox-Rock	Dr-SyDr	Dr-SyDr	Dr-SyDr	Gb	Gb	Dr	QDr	Gr	AlkGr	Gr
D [kg/m^3]	2730	2710	2718	2879	2852	2746	2702	2579	2612	2622
K [SI *10^6]	370	8072	40360	34690	520	410	320	50	2790	144
X-Coordinate [m]	6832465	6853886	6853342	6849910	6823798	6801210	6839521	6821503	6849734	6854400
Y-Coordinate [m]	3399597	3403988	3402762	3401202	3402342	3398491	3402235	3399784	3400693	3403712
Majors: SampleName	**JRX66P196.D**	**GSX67P073.B**	**GSX68P541.B**	**JRX67P246**	**VSX65P280**	**LMX63P284.A**	**KKX69P588.A**	**JRX66P110.B**	**JRX67P252.A**	**GSX67P076**
SiO2 [%] (XRF)	55.64	56.36	59.22	48.63	49.21	59.78	63.08	75.09	70.63	73.89
Al2O3 [%] (XRF)	20.84	20.19	19.88	19.55	17.54	16.42	15.56	14.49	13.95	13.18
CaO [%] (XRF)	4.95	4.88	4.27	8.48	7.68	4.19	1.2	0.32	1.05	1.26
Fe2O3 [%] (XRF)	6.72	5.67	4.61	10.29	9.58	7.34	7.12	0.74	2.8	2.57
K2O [%] (XRF)	2.24	4.44	4.6	0.78	2.07	2.4	3.25	3.8	6.16	4.43
MgO [%] (XRF)	1.63	1.7	1.41	3.74	4.87	3.26	2.63	0.08	0.65	0.48
MnO [%] (XRF)	0.119	0.1	0.084	0.16	0.128	0.071	0.106	0.091	0.038	0.058
Na2O [%] (XRF)	4.6	3.72	3.8	3.25	3.12	2.46	2.28	4.41	2.31	3.33
P2O5 [%] (XRF)	0.34	0.314	0.281	0.664	0.534	0.256	0.085	0.257	0.095	0.057
TiO2 [%] (XRF)	0.71	0.82	0.46	1.46	1.48	1	0.78	0.01	0.4	0.23

Table 10 continued

Traces: SampleName	JRX66P196.D	GSX67P073.B	GSX68P541.B	JRX67P246	VSX65P280	LMX63P284.A	KKX69P588.A	JRX66P110.B	JRX67P252.A	GSX67P076
Ba [ppm] (XRF)	1006	3600	3721	387	469	480	615	18	1283	348
C [ppm] (811L)	900	100	300	200	300	200	600	200	500	200
Cl [ppm] (XRF)	87	207	139	157	222	185	48	29	100	93
Cr [ppm] (XRF)	18	21	16	36	104	91	97	13	17	16
Cu [ppm] (XRF)	0	33	67	26	12	50	11	0	0	0
Ga [ppm] (XRF)	26	24	23	26	25	25	26	25	17	28
Nb [ppm] (XRF)	8	9	3	6	20	13	16	12	12	11
Ni [ppm] (XRF)	11	5	4	16	21	33	47	0	3	9
Pb [ppm] (XRF)	28	27	31	24	22	24	42	30	35	49
Rb [ppm] (XRF)	91	75	107	26	82	119	161	207	151	193
S [ppm] (XRF)	30	60	70	530	800	1530	0	0	0	0
Sr [ppm] (XRF)	1154	939	927	1370	600	366	225	8	374	93
Th [ppm] (XRF)	21	2	1	1	4	1	15	1	16	13
U [ppm] (XRF)	4	0	0	0	1	1	6	0	2	0
V [ppm] (XRF)	41	72	42	191	243	132	145	4	45	25
Zn [ppm] (XRF)	118	88	72	174	137	135	174	49	57	96
Zr [ppm] (XRF)	667	328	506	66	158	187	244	26	316	138
Sc [ppm] (ICPMS)	9	16	13	19	33	17	15	0	4	4
Y [ppm] (ICPMS)	25	15	18	16	42	7	36	12	21	35

Table 10 continued

REE: SampleName	JRX66P196.D	GSX67P073.B	GSX68P541.B	JRX67P246	VSX65P280	LMX63P284.A	KKX69P588.A	JRX66P110.B	JRX67P252.A	GSX67P076
La [ppm] (ICPMS)	142	34	22	23.2	36.6	15.6	47.6	1.56	111	29
Ce [ppm] (ICPMS)	237	60.6	38.7	50.8	98.9	30.6	102	3.03	197	59.6
Pr [ppm] (ICPMS)	22.9	6.95	4.84	7.08	14.4	4	11.8	0.43	21.6	7.73
Nd [ppm] (ICPMS)	70.4	28.2	20.5	30.9	60.2	16.5	44.4	1.26	70.8	29.9
Sm [ppm] (ICPMS)	6.52	4.5	3.97	5.68	11.4	3.36	7.86	0.23	10.2	6.73
Eu [ppm] (ICPMS)	2.35	3.17	2.96	2.39	2.09	1.42	1.06	0.03	1.04	0.47
Gd [ppm] (ICPMS)	6.19	4.26	3.41	5.48	10.9	2.56	7.32	0.52	7.3	7.2
Tb [ppm] (ICPMS)	0.78	0.57	0.52	0.74	1.46	0.36	0.99	0.17	0.86	1.21
Dy [ppm] (ICPMS)	3.44	2.51	2.29	3.16	7.77	1.09	4.98	0.94	3.32	6.3
Ho [ppm] (ICPMS)	0.65	0.45	0.54	0.67	1.58	0.16	0.96	0.21	0.59	1.31
Er [ppm] (ICPMS)	1.62	1.14	1.3	1.51	4.36	0.36	2.31	0.46	1.56	3.84
Tm [ppm] (ICPMS)	0.28	0.2	0.2	0.24	0.63	0.04	0.35	0.09	0.23	0.52
Yb [ppm] (ICPMS)	1.68	1.4	1.43	1.48	3.7	0.35	2.25	0.9	1.46	2.79
Lu [ppm] (ICPMS)	0.22	0.14	0.17	0.2	0.54	0.04	0.29	0.1	0.26	0.46

Analysis methods:
- XRF: X-ray fluorescence spectrometry using pressed powder pellets.
- ICPAES: Inductively coupled plasma atomic emission spectrometry after aqua regia digestion.
- ICPMS: Inductively coupled plasma mass spectrometry after hydrofluoric acid-perchloric acid dissolution and lithium metaborate/sodium perborate fusion. For detailed descriptions of the analysis methods, see Sandström (1996) and Rasilainen et al. (2007).

4.5 Normalization along the regression curve.

Figure 76 displays the relative variations of major elements in samples as functions of SiO2. Corresponding variations of REE are illustrated in Figure 77. In the diagrams, the elements are presented in the incompatible–compatible order by Pearce & Parkinson (1993) and Pearce & Peate (1995) (see e.g. Fig. 2). When considering the regression curves of high-Al and low-Al samples in the diagrams at a common SiO_2 value (e.g. 60%), it can be noted that the more mafic high-Al sample group has higher contents of incompatible elements and lower contents of compatible elements. Moreover, there is significant exception to the trend in Eu, which is clearly higher in most high-Al samples. In order to compare the relative variations of these groups, I normalized their element values to a common SiO_2 value using the 'normalization along the regression curve' method depicted in Figure 78.

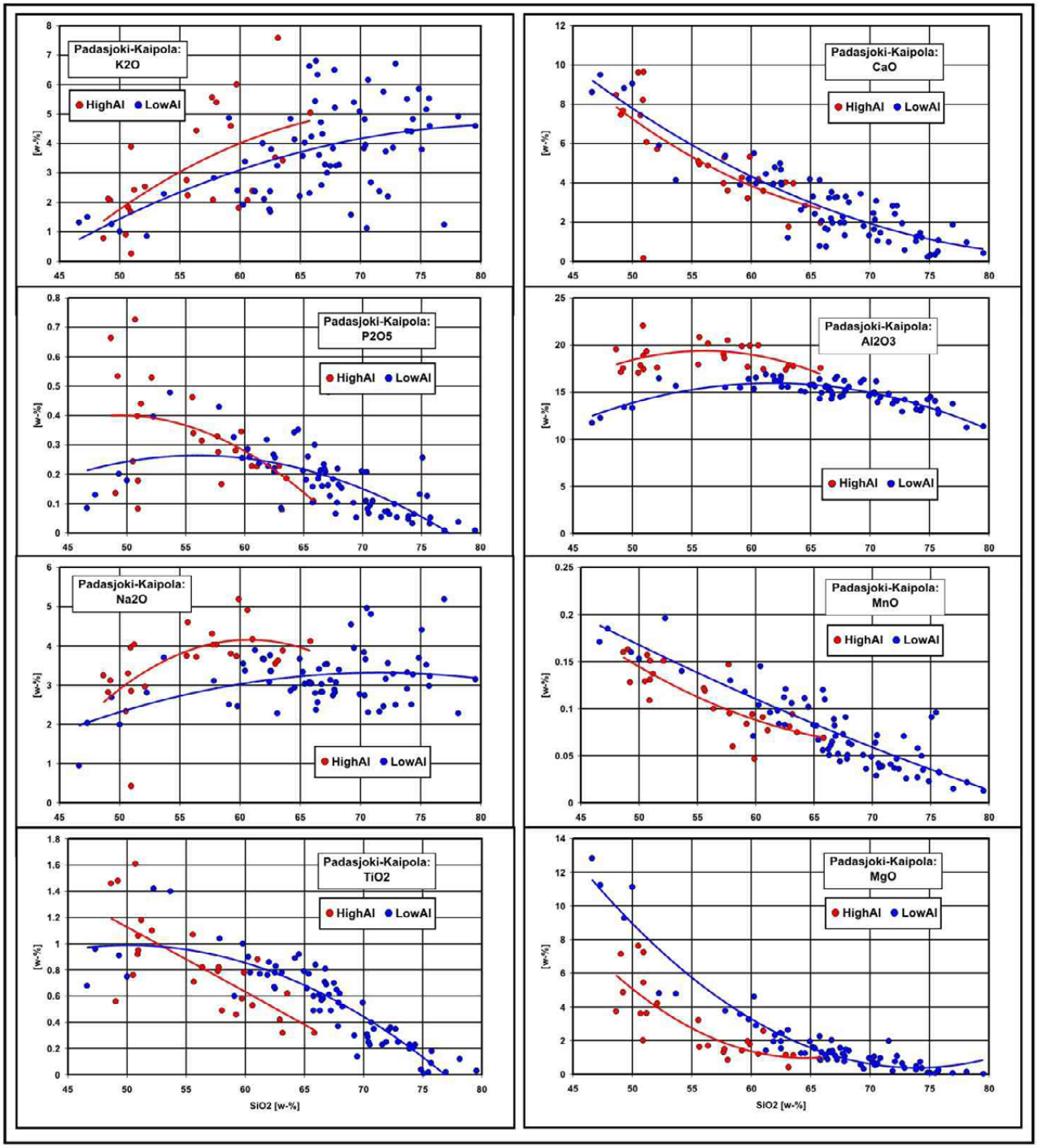

Fig. 76. Variation of major elements as functions of SiO_2. The red and blue lines are second order regression curves fitted to high-Al and low-Al samples respectively.

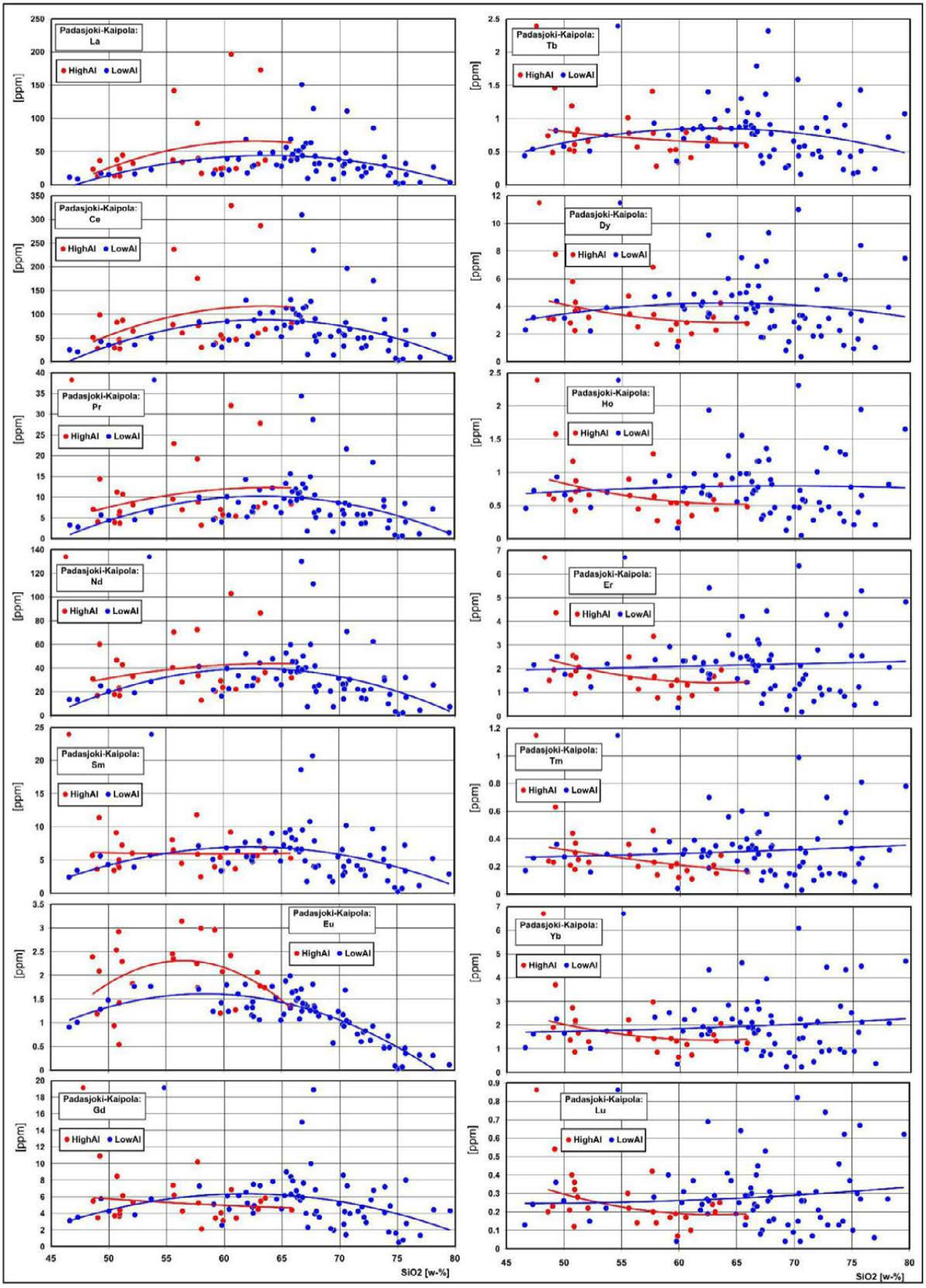

Fig. 77. Variations of REE as functions of SiO_2.

Figure 78 displays the Fe_2O_3 values of the samples as functions of SiO_2. From the diagram and diagrams above, it is apparent that the high-Al and low-Al samples define two relatively distinct series. Moreover, it can be seen that the distributions of SiO_2 contents of the sample groups are wide, overlapping, and the Fe_2O_3 content correlates strongly with the SiO_2 content. The average SiO_2 content of low-Al samples is higher and Fe_2O_3 average value lower than those of the high-Al samples. However, when considering the second order polynomial trend lines (red and blue lines in the figure), it can be seen that at a common point, say SiO_2 = 60%, the position of the trend line for the low-Al samples is clearly higher. Thus, a simple comparison of sample averages, or their normalization values using any fixed constants would be misleading. Therefore, a method defined here as 'normalization along the regression curve' is used, the principle of which is shown in the diagram:

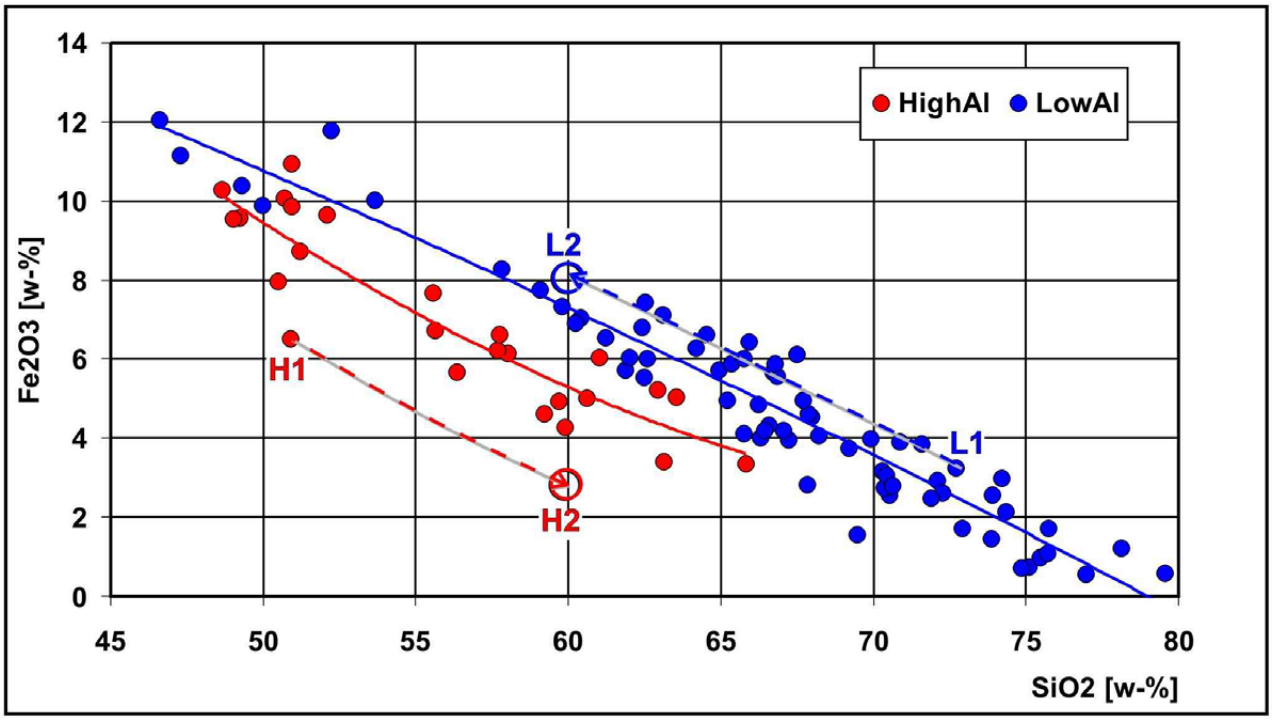

Fig. 78. Fe_2O_3 (XRF) vs SiO_2: Principle of 'normalization along the regression curve'. The solid lines are 2nd degree regression curves fitted to the data. The sample groups are the same as in the alkali index diagram, in Figure 73.

Consider two arbitrary sample points in Figure 78: H1 (high-Al samples) and L1 (low-Al samples), where the Fe_2O_3 value of H1 is higher than that of L1. In the regression curve normalization, the points are moved colinearly with the corresponding regression curves (along the dashed arrows) to a common SiO_2 value, where both groups are overlapping (60% in the figure). We thus obtain new values H2 and L2, which represent the normalized values of the original points. From the diagram it can now be seen that Fe_2O_3(L2) is clearly higher than Fe_2O_3(H2), where H2 is actually the poorest in Fe_2O_3 of all samples after normalization. Thus, although the primary average Fe_2O_3 content is lower in the original low-Al samples, it can be concluded that in reality they are more iron rich compared to high-Al samples.

The advantage of this method is that it is reliable to apply: If there is a good first- or second-degree trend between the parameters, we can expect the Fe_2O_3 values of H2 and L2 to be good estimates of the parameter values at any given (common) SiO_2 value. If the correlation between parameters is poor; i.e. the data are scattered randomly around a horizontal line, the method gives the original values, i.e. Fe_2O_3(H2) ≈ Fe_2O_3(H1) and/or Fe_2O_3(L2) ≈ Fe_2O_3(L1). Degrees of trend higher than two are generally difficult to observe and are not considered here.

When considering, for example, the plots of incompatible K_2O and of more compatible MgO

values of high- and low-Al samples against SiO_2 in Figure 76, it can be seen that the scatter of the more mobile element K_2O is greater than that for MgO, increasing at high SiO_2 values of more evolved, felsic rocks. This refers to the possibility of alteration, remobilization and contamination of these rocks during metamorphic, tectonic and magmatic processes. In Table 11, the averages of K_2O and MgO for high- and low-Al samples are compared. In addition, the table gives corresponding regression curve values at the point SiO_2 = 60%. The average values in the table would indicate that the low-aluminium samples are more enriched in incompatible elements, that is, having more mobile K_2O and depletion in MgO. However, the regression curves in Figure 76 and normalized values in Table 11 show that the ratios are actually the opposite, with the more mafic high-Al samples being enriched in potassium and depleted in magnesium compared to the low-Al samples. Thus, the trends in Figure 76 suggest a more enriched primary source composition at low SiO_2 values of the high-Al samples compared to low-Al samples.

Table 11. Comparison of averages and regression curve values at SiO_2 = 60% of K_2O and MgO for high-Al and low-Al samples.

	High-Al: K_2O	Low-Al: K_2O	High-Al: MgO	Low-Al: MgO
Calculated averages	3.1	3.72	2.89	1.94
Regression curve values at SiO_2 = 60%	4	3.15	1.6	3.3

Assuming that the high-Al adakitic samples in Figure 76 are close to 'co-magmatic', an estimate for the primary composition of their proposed basaltic source can be evaluated by studying their regression curve values at $SiO_2 \approx 50\%$. At this SiO_2 value, the major element contents are estimated to be: $K_2O \approx 1.8\%$, $P_2O_5 \approx 0.4\%$, $Na_2O \approx 3\%$, $TiO_2 \approx 1.1\%$, $CaO \approx 7.3\%$, $Al_2O_3 \approx 18\%$, $MnO \approx 0.15\%$ and $MgO \approx 5.2\%$, $Fe_2O_3 \approx 9.5\%$. It must be noted that the samples have been affected by contamination and alteration processes and the calculated values are thus only uncertain estimates. However, these values are very close (only Fe_2O_3 and K_2O emphasized) to values for the average chemical composition of basalts determined from 3594 chemical analyses of basaltic rocks given in https://www.sandatlas.org/basalt/.

Petrophysics of the samples normalized to SiO_2 = 60%

The distribution of density and susceptibility of high- and low-Al samples as functions of SiO_2 are given in Figure 79. In the diagrams, the densities are relatively tightly scattered, while susceptibilities have very wide variations due to separate groups of para- and ferrimagnetic samples, as is evident from Figure 72. From Figure 79 it can be seen that at value of SiO_2 = 60%, the regression-normalized density of low-Al samples (ca. 2735 kg/m^3) is significantly higher than that of the high-Al samples (ca. 2693 kg/m^3). However, the susceptibility of the low-Al samples is mainly paramagnetic, with a regression value at 854*10^{-6} SI units at SiO_2 = 60%, while the (more scattered) high-Al samples are generally ferrimagnetic or highly paramagnetic, the regression curve value being 1679*10^{-6} SI units at SiO_2 = 60%.

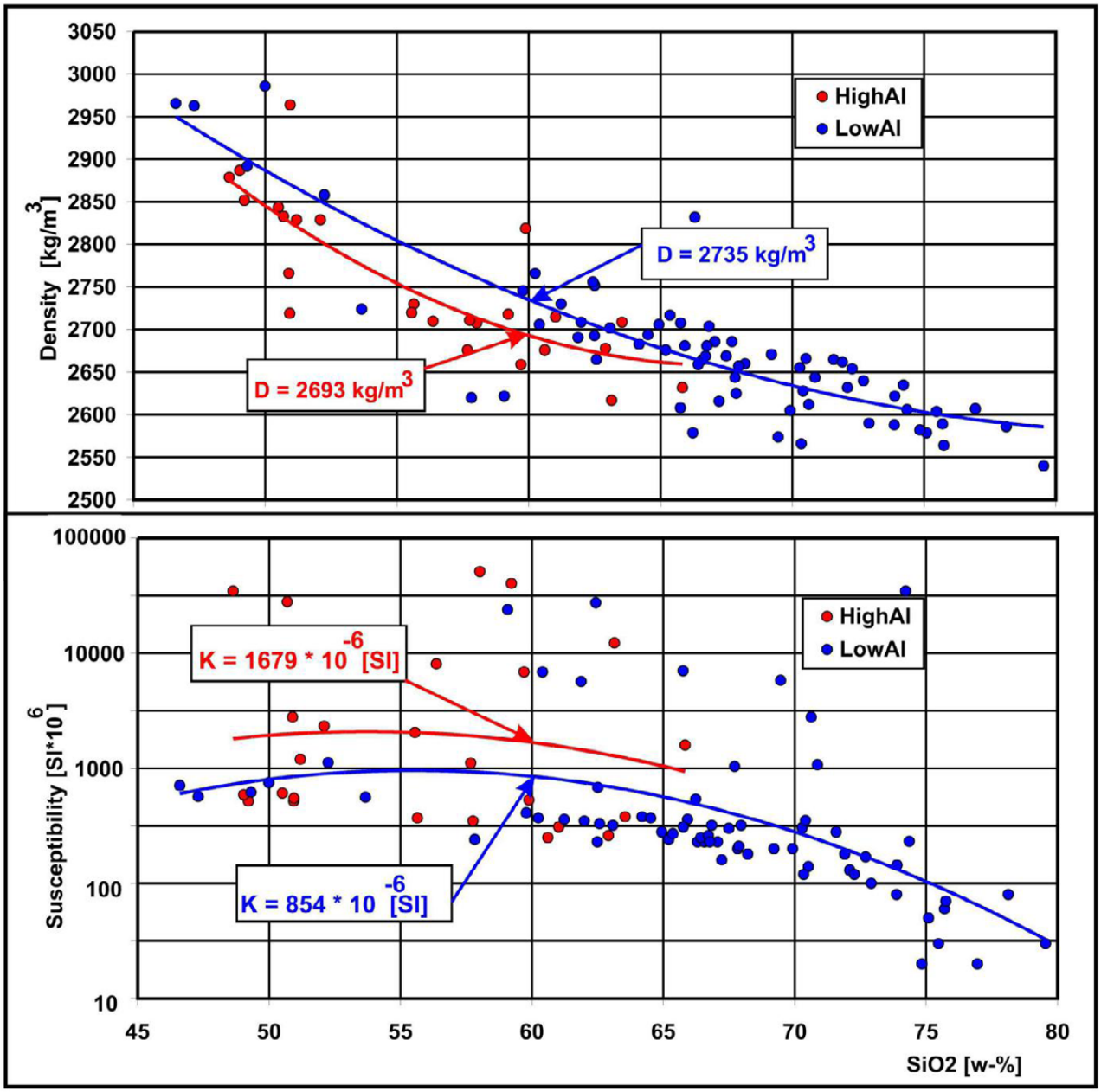

Fig. 79. The distributions of density and susceptibility of high- and low-Al samples as functions of SiO_2.

Chemical variations of the samples normalized to SiO_2 = 60%

Figure 80 presents the Pearce–Peate spectra of high- and low-Al samples using AFP-normalized (see Table 2) regression curve values at to SiO_2 = 60%. From the figure, it can be seen that the spectra of high- and low-Al data differ significantly: the low-Al spectrum is relatively flat with a LREE/HREE ratio of ca. 1.24, while that of high-Al group is clearly higher, 1.91, reflecting a higher degree of fractionation. However, the compatibles/HREE ratio of high-Al samples is lower, ca. 1.52, while that of low-Al samples is much higher, ca. 2.48, which refers to the more mafic primary material of the low-Al samples, now being a more felsic rock group, however.

The peaks of the primarily more mafic high-Al samples (average SiO_2 of original samples ca. 56%) are higher at Ba, LREE, Sr (apparently related to plagioclase), Zr, Eu (apparently related to plagioclase), Al_2O_3 and Ga (replacing Al). The low-Al samples (average SiO_2 of original samples ca. 66.6%) contain higher TiO_2, HREE, and other compatibles, except Al_2O_3 and Ga. Eu is also slightly increased in low-Al samples, possibly referring to deeper crustal fractionation depths.

The observed trends in Figure 76 to Figure 77 and in the Pearce–Peate spectrum in Figure 80 strongly indicate that the two groups cannot belong to the same fractionation series, but must have had a different evolutionary history. It is unlikely that felsic low-Al rocks could be direct derivatives of more mafic rocks when losing incompatibles in the process, nor could mafic high-Al rocks be derived from felsic rocks with an increase in incompatibles.

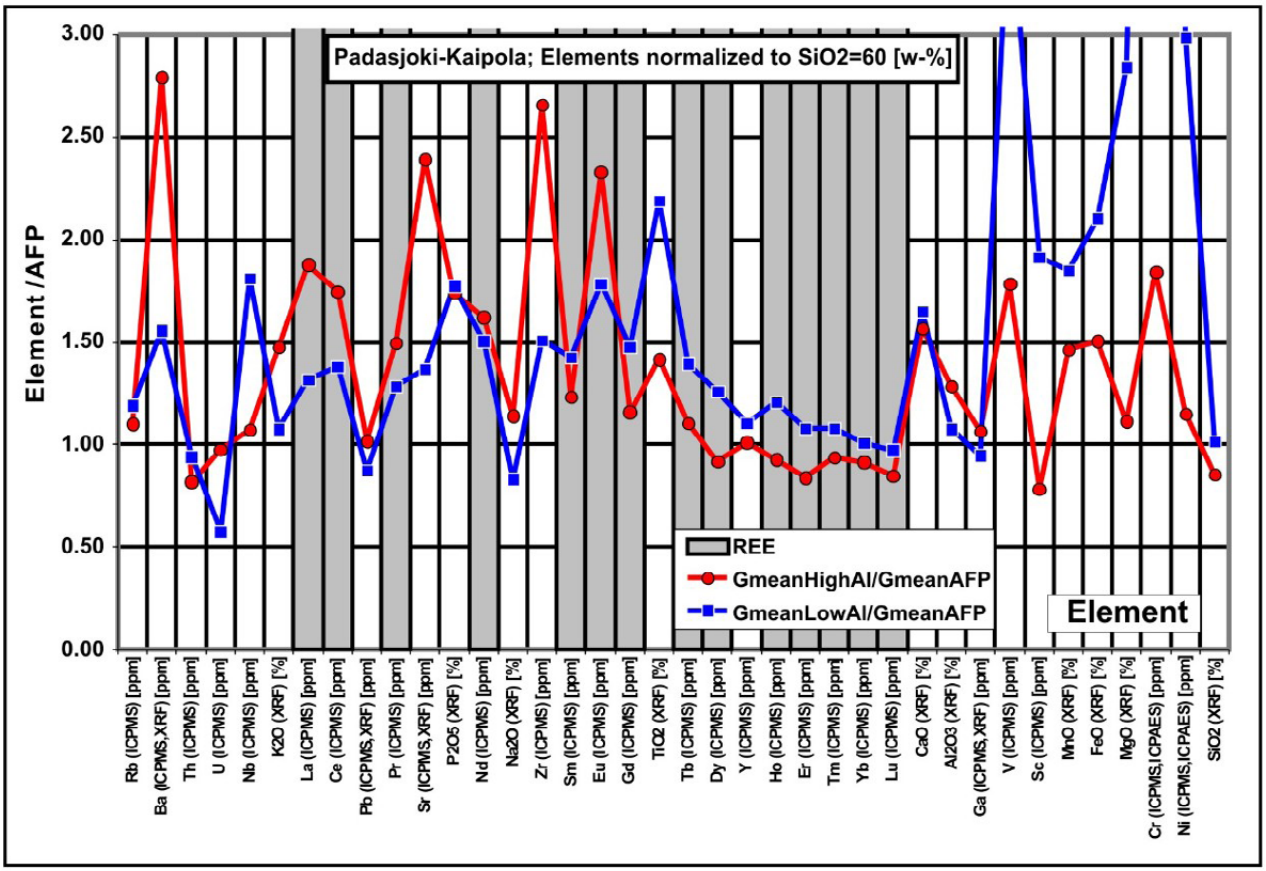

Fig. 80. AFP-normalized Pearce–Peate spectra of high-Al and low-Al samples at SiO_2 = 60%.

4.6 Sources of high- and low-Al rocks

As can be seen from Figure 68 and Figure 69, the Padasjoki–Kaipola profile studied here crosses the border of the SMB and CFG in Figure 3. When comparing the spectra of this profile in Figure 80 with those of SMB and CFG in Figure 37 and Figure 39, it can be seen that the peaks of SMB correlate with those in Figure 80. Moreover, the high-Al samples have a steep REE slope and increased compatibles, as generally for all adakitoids studied above, and can thus be considered as adakitoids, as also demonstrated in Table 12 below. However, the low-Al samples have element maxima coinciding with those of the high-Al samples and their level of compatibles is very high, but the REE spectrum is relatively flat. Thus, as with SMB 'all-plutonic rock' samples, the genesis of low-Al samples can also be connected with a collision-related marine environment with a high basaltic component, while high-Al samples are more close to 'true' adakites evolved in subduction/underthrusting-related processes.

The adakitic characteristics of high-Al and low-Al groups are evaluated in Table 12, which compares their compositions normalized to SiO_2 = 60% with adakite characteristics as defined above. It must be emphasized that many samples originally have SiO_2 well below 56%, as is evident from Figure 74. In Table 12, the parameter averages of the normalized high-Al samples are all clearly adakitic, while three of those of the low-Al samples are not (the remaining four being very close to the threshold value). The maps in Figure 24 and Figure 25 indicate that the major restitic minerals of adakitoids below this profile are pyroxenes and possibly minor garnet in SMB.

Mungall (2002) noted that the adakitic magmas may be highly oxidized and potentially fertile for Au and Cu. This is in agreement with observations in the study area, where the contact zone between the migmatite sub-area and the central Finland granitoid sub-area has been observed to be prospective for Au (e.g. Eilu et al. 2003). Moreover, from Figure 79 it can be seen that the high-Al samples are strongly ferrimagnetic, containing magnetite (iron in oxides), while low-Al samples are mainly paramagnetic, the magnetic mineral being mainly pyrrhotite (iron in sulphides or silicates).

When considering the northernmost segment of active volcanism in the Andean arc, resulting from subduction of the Nazca plate beneath South America, Garrison & Davidson (2003) concluded, that basaltic magmas derived from the mantle wedge could also produce adakitic characteristics. However, in contrast to 'high-Mg' adakites, which carry a possible mantle signature (see e.g. Scaillet & Prouteau 2001), it can be seen from Figure 76 that the relative MgO content of adakitic high-Al samples is less than that of the more felsic low-Al sample group. This suggests a relatively small mantle wedge component in the melt, i.e. a low angle of subduction. In Table 13, some sample parameters are compared with the average of 140 Cenozoic adakite samples by Drummond et al. (1996). From the table, it can be seen that the MgO and Ni abundances of the high-Al samples in particular are significantly lower than in 'modern' adakites.

Table 12. Comparison of averages of high-Al and low-Al samples 'regression curve normalized' to SiO_2 = 60%, with adakite compositions defined by Defant & Drummond (1990) and Thorkelson & Breitsprecher (2005). The (clear) 'hits' have been emphasized with bolded numbers.

	SiO_2 [%]	Al_2O_3 [%]	Na_2O [%]	Sr [ppm]	Y [ppm]	Yb [ppm]	Sr/Y	La/Yb
AveHighAl	60	**19**	**4.15**	**740**	**16.3**	**1.39**	**45.5**	**45.9**
AveLowAl	60	15.9	3.03	403	20.5	1.85	19.7	22.6
Adakite	> 56	> 15	> 3.5	> 400	< 18	< 1.9	> 40	> 20

Table 13. Comparison of averages of high-Al and low-Al samples normalized to SiO_2 = 60% with Cenozoic adakites by Drummond et al. (1996).

	SiO_2 [%]	TiO_2 [%]	Al_2O_3 [%]	FeO [%]	MnO [%]	MgO [%]	CaO [%]	Na_2O [%]	K_2O [%]	Ni [ppm]	Cr [ppm]	Sr [ppm]
Ave HighAl	60	0.63	19.0	4.75	0.09	1.56	4.12	4.15	4	21.8	72.7	740
Ave LowAl	60	0.85	15.9	6.56	0.11	3.29	4.3	3.03	3.15	36	157	403
Cenozoic Adakite	63.8	0.61	17.4	4.21	0.08	2.47	5.23	4.4	1.52	39	54	869

Table 14. Comparison of averages of high-Al and low-Al samples normalized to SiO_2 = 60% with sanukitoids by Halla (2005). Mg# is calculated from normalized values.

	Mg#	SiO_2	Ni [ppm]	Cr [ppm]	K_2O [%]	Sr [ppm]	Ba [ppm]	Rb/Sr
AveHighAl	0.37	60.00	21.8	72.7	4.0	740.	1821.	0.13
AveLowAl	0.47	60.00	36.	157.	3.15	403.	987.	0.26
Sanukitoid	> 0.6	55 - 60	> 100	> 200	> 1	> 500	> 500	< 0.1

The mantle affinity of the samples can also be evaluated by comparing their characteristics with sanukitoid plutonic rocks, which are considered to represent melting of enriched mantle wedge above the subducting slab (e.g. Stern & Hanson 1991). Table 14 compares the composition of high-Al and low-Al samples normalized to SiO_2 = 60% with sanukitoid characteristics defined above by Halla (2005). In the table, the normalized averages of high- and low-Al samples have only minor sanukitoid characteristics.

In Figure 81, the characteristics of samples in the Sr/Y vs Y diagram are compared to those in the Kitakami area of the "modern" Honsu Arc, in NE Japan, studied by Tsuchiya & Kanisawa (1994). In the diagram, the majority of high-Al

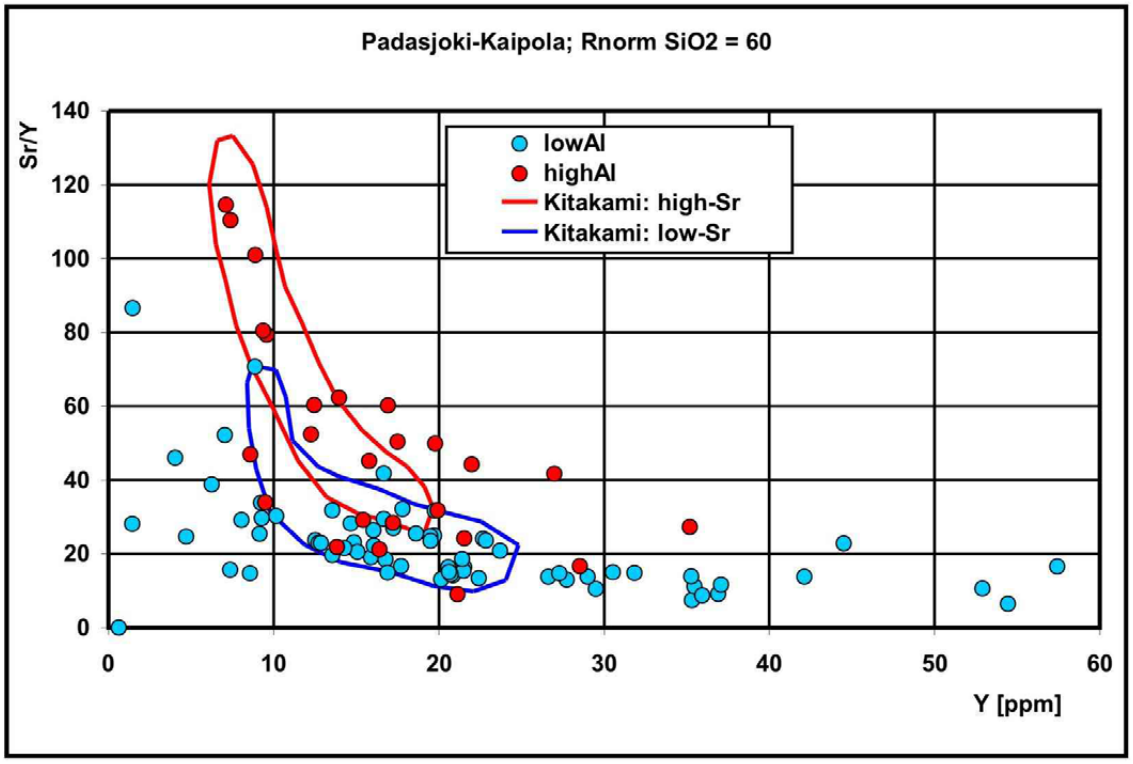

Fig. 81. Sr/Y vs Y diagram of Padasjoki-Kaipola samples compared to low-Sr and high-Sr fields in the Kitakami area, NE Japan (Tsuchiya & Kanisawa 1994).

samples plot in the Kitakami high-Sr field and the low-Al samples correlate with the Kitakami low-Sr samples.

As mentioned above, the Kitakami high-Sr rocks are characterized by higher Na, Al, Ga, P, Ba and Sr, while K, Mn, Fe, Mg and Y are lower than in low-Sr samples. Moreover, the Kitakami high-Sr rocks correlate with positive magnetic anomaly belts, as do the high-Al ('high-Sr') rocks in the study area. Thus, the regression curve normalized high-Al and low-Al samples from the present study area show many similarities with Kitakami high-Sr and low-Sr samples, except for potassium, which is higher in the high-Al samples. In their model, Tsuchiya & Kanisawa (1994) propose that the Kitakami high-Sr series magmas are derived from partial melting of subducting oceanic slab and sediments at depths of ca. 70–80 km, mixing with magma derived from overlying mantle wedge. This 'adakitic' model is also applied to the high-Al rocks of the present study area.

4.7 Evolutionary model: Subduction, collision and magma mixing

As noted above, the comparison with Kitakami area magmatism above clearly indicates that the high-Al rock samples in particular share many distinct petrophysical and geochemical characteristics with modern subduction-related adakitic magmas. Figure 82 presents a combination of the sections of the reflection seismic profiles FIRE1 and FIRE2 (Kukkonen & Lahtinen 2006), for which profile lines are shown in Figure 3. The sections show that the migmatite sub-area (SMB) dips northwards beneath the central Finland granitoid sub-area (CFG), referring to underthrusting from the SMB beneath the CFG having arc characteristics (Ruotoistenmäki 1996, Nironen 1997). Therefore, a qualitative model is given below where seafloor, marine sediments, descending slab and, to a lesser extent, mantle wedge and continental lower crust are assumed to contribute to the final magma characteristics.

The plan view in Figure 83a gives the relative location of plates at ca. 1900 Ma, when Uusimaa and central Finland granitoids (USM and CFG) were island arcs in the 'SMB' sea (a precursor for the SMB, being part of the 'Svecofennian sea' in Ruotoistenmäki 1996). In SMB, the magmatism has mainly been of the tholeitic, low-Al type (Fig. 73 and Fig. 74), generated in a marine environment and in lesser amounts in subduction zones and oceanic islands (USM and CFG). Adakitic rocks dominate oceanic islands and underthrusting subduction zones. During

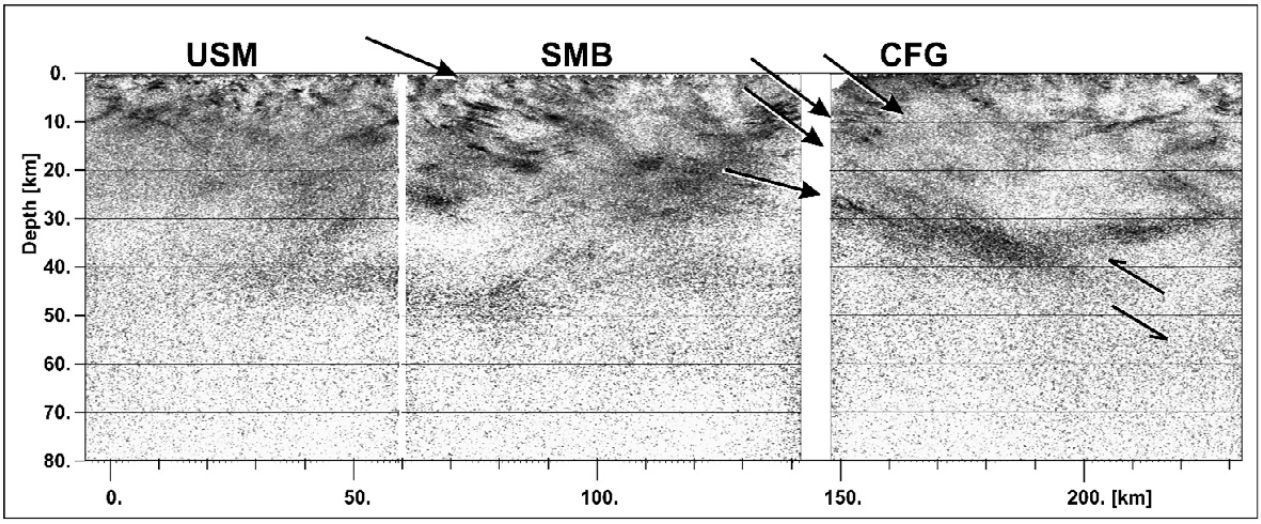

Fig. 82. Sections showing reflectors of deep seismic reflection profiles FIRE1 and FIRE2 across contact zones from USM to CFG (Kukkonen & Lahtinen 2006). The arrows indicate dipping surfaces and fault displacement sense below SMB and CFG. The location of the sections is indicated in Figure 3. The discontinuity between SMB and CFG is approximately between X = 140–150 km.

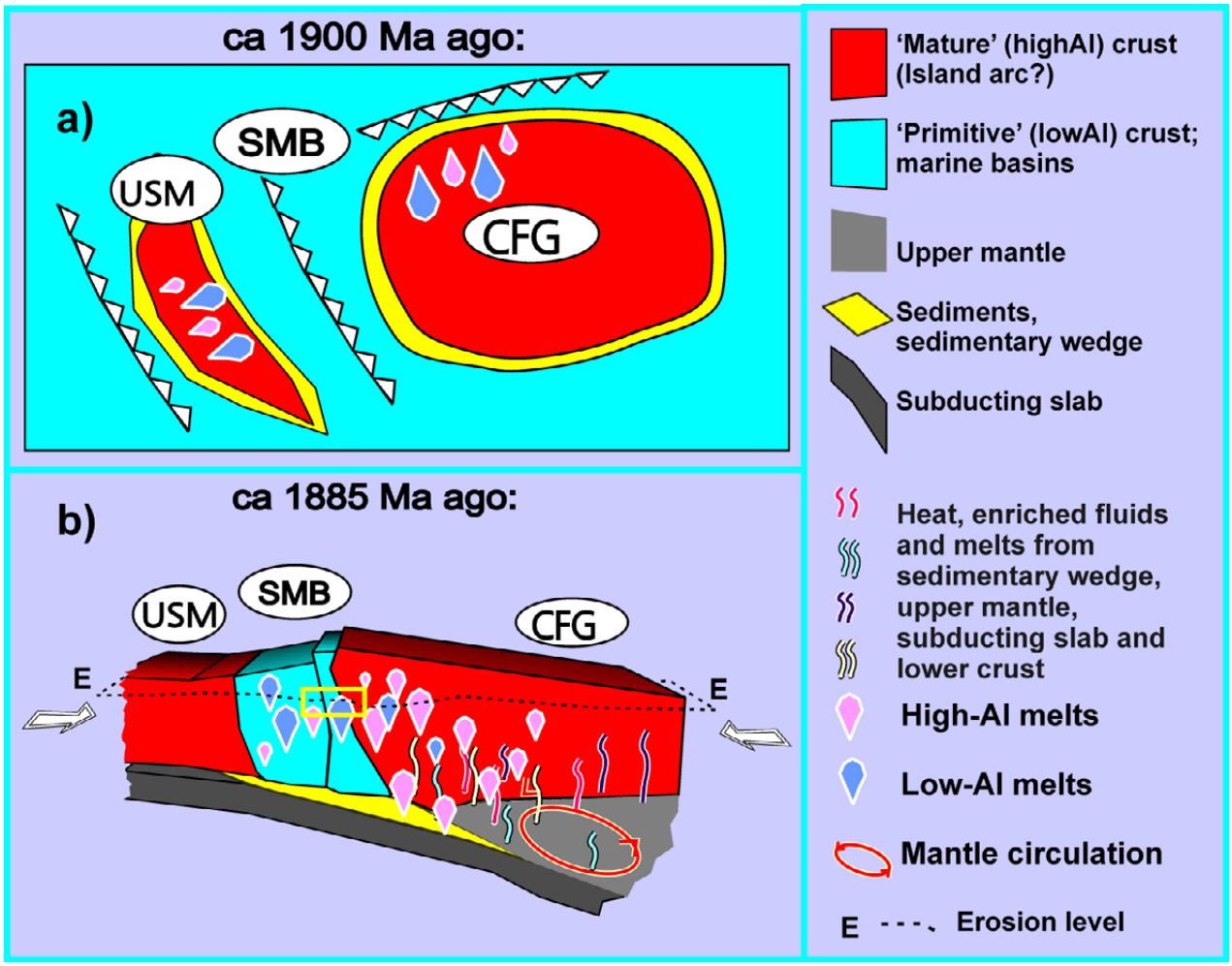

Fig. 83. Schematic evolution model of the study area modified after Ruotoistenmäki (1996): a) a marine Island arc stage and b) a cross-section during the collision stage. The yellow rectangle in (b) represents the area considered in this paper. E = present erosion level. The remains of the underthrusting/subducting plate are assumed to have been assimilated or delaminated in the mantle during later processes.

this stage, tholeitic, low-Al magmatism, characterized by relatively low Eu, Sr, high HREE, Y and Yb, is assumed to dominate over 'enriched' adakitic, high-Al magma generation (see Fig. 80).

The collision/accretion at ca. 1885 Ma in Figure 83b was relatively rapid, resulting in thickening and shortening of both the SMB and USM. The high-Al, adakitic type magmatism culminated, representing rocks fractionated from a combination of hydrous, enriched melts from the subducting slab and sedimentary wedge. They are characterized by enrichment of incompatibles and LREE, but relatively low contents of compatibles, referring to minor mantle wedge components and thus relatively gentle subduction. The characteristics of low-Al magmas refer to a combination of marine and collision-related rocks and sedimentary wedge material thrusted, stacked and folded against CFG, as is also evident from the maps in Figure 69 and Figure 70. This model has been later completed in more detail by Nironen (1997) and Lahtinen et al. (2005), among others.

After Ruotoistenmäki (1996), the opening of the 'SMB' sea in Figure 83 was modelled to have taken place at ca. 1.96 Ga, implying relatively young (less than ca. 30 Ma), hot and gently dipping subducting slab(s) during the closing stage at ca. 1.93 – 1.9 – ca. 1.88 Ga, which is in agreement with models by Drummond & Defant (1990). According to Wyllie (1984), in the case of warm, gently dipping subducting oceanic crust, dehydration of serpentine and amphibole approximates greenschist and eclogite facies boundaries between 50–100 km, correspond-

ing to the onset of slab melting at a depth of less than ca. 100 km. In this warm slab scenario, the addition of mantle and crustal melts would be minimal compared to the cooler, more steeply dipping slab situations. This appears to be the case in this study, as is indicated by the relatively low MgO, Mg# and low Ni and Cr (Fig. 80) of the high-Al samples. As concluded above, the major restite minerals of adakitoids in these areas on the maps in Figure 24 and Figure 25 are pyroxenes, but with minor garnet and amphiboles.

The low-Al rocks are here interpreted as mainly oceanic rock material intruded/fractionated at shallower depths (less than ca. 30–50 km), mainly during the primary stages of island arc and back-arc basin evolution. The low magnetite content of the low-Al magmas of the southern Finland gneiss-migmatite sub-area (SMB) can be attributed to an overall reducing environment characterized by marine turbiditic sediments including sulphides and black schists, thus favouring the crystallization of Fe-silicates instead of Fe-oxides (Ruotoistenmäki 1992, Lahtinen 1994, Peltonen 1995). The high content of Fe-silicates is reflected by the increase in high-density paramagnetic samples in the southern part of the survey area. According to Wilson (1989), magnetite suppression in reducing environments is characteristically associated with the tholeitic trend. In contrast, under oxidizing conditions, magnetite crystallizes from the outset, rapidly depleting residual liquids in iron (calc-alkaline trend). It must be noted that the existence of sulphides and black schists refers to a relatively closed basin environment with sedimentation of biogenic material, and also a lack of oxygen.

Kerrich & Wyman (1996) emphasized that high water contents suppress plagioclase fractionation, which leads to high Al contents and delays Fe and Ti enrichment. McIntyre (1980, and references therein) noted that where excess aluminium occurs in micaeous rocks, muscovite is formed in preference to biotite and iron is available to form magnetite over a broader oxygen fugacity and temperature field. In the Kitakami mountains, Tsuchiya & Kanisawa (1994) concluded that slab-derived magma shows high oxidation states due to the influence of a highly oxidized source.

For a given temperature and H_2O content, oxidized conditions favour a higher crystal/melt ratio than reduced conditions (Scaillet et al. 1997). Flood basalts showing varying degrees of iron enrichment may be related to the oxidation state of magma from which they derived (Middlemost 1975 and references therein). The fractionation of non-alkalic basaltic magma that has formed in a low oxidation state would probably result in iron enrichment (tholeitic trend). This rock group corresponds to the Fe-rich low-Al samples having both tholeitic and sub-alkaline characteristics (Fig. 73 and Fig. 74).

The compositions of the low-Al samples are in pre-, syn- and late-orogenic fields in the R1-R2 diagram in Figure 75, while high-Al samples dominate in the post-collisional field. These characteristics also support the model above: a primary oceanic stage dominated by low-Al, tholeitic magmas continuing to subduction-related high-Al magmatism generated at greater depths and thus emplacing during late- to post-collisional processes.

4.8 Summary

The Padasjoki-Kaipola area between the southern Finland migmatite sub-area and the central Finland granitoid sub-area represents a significant boundary zone between oceanic (SMB) and island arc (CFG) environments. Besides the lithological contrasts between marine, metasediments-dominated terrain in the south and a more ‘continental’, island arc-type area dominated by plutonic rocks in the north, the zone is characterized by prominent north-dipping seismic reflectors, suggesting that the sedimentary marine area was thrusted against and beneath the northern, island arc sub-area. Moreover, there is a petrophysical zonation from felsic, relatively dense, iron-rich, magnetite-poor rocks in the south to more mafic, magnetite-rich, but relatively less dense rocks in the north. A further significant contrast between the rocks is the relative enrichment (at SiO_2 = 60%) in incompatibles and light REE in the more mafic (high-Al) rocks compared to the more felsic (low-Al) rocks, which makes it improbable that

they could represent direct derivatives of one another, or be from the same source.

The adakitic characteristics of the mafic high-Al rocks and regional scale seismic interpretations suggest that the primary fractionation depth of the high-Al rocks is in subduction related environment at depths greater than ca. 30–60 km, such that mainly pyroxenes (± garnet ± hornblende?) were retained in restite. Thus, there is a significant subducting slab and minor sedimentary wedge, mantle wedge and lower crust component in the rocks. In contrast, the more felsic low-Al rocks have geochemical characteristics more consistent with plagioclase as a restitic phase and shallower, (lower) crustal fractionation depths. The above evolution model for the high-Al (-Sr) rocks shows close similarities to that presented for the Kitakami high-Sr rocks in the Honsu Arc of NE Japan by Tsuchiya & Kanisawa (1994).

Using the 'normalization along the regression curve' method, the primary source rocks of the high-Al adakitic rocks can be estimated to be iron- and potassium-rich basalts.

5 CHARACTERISTICS OF PROTEROZOIC LATE TO POST-COLLISIONAL INTRUSIVES IN THE ARCHAEAN IISALMI–LAPINLAHTI AREA, CENTRAL FINLAND

In this section, based on the study by Ruotoistenmäki et al. (2001), I consider post-collisional adakitic intrusives in the Archaean crust close to the Proterozoic–Archaean collision zone in central Finland (red square in Fig. 3). As in section **4** above, the most mafic samples of these rocks have adakitic characteristics. The geological and isotopic descriptions given here are mainly by Jorma Paavola & Irmeli Mänttäri (Geological Survey of Finland), respectively.

The generalized lithological map of the study area is presented in Figure 84. The area is predominantly composed of Archaean amphibolite-banded tonalitic-trondhjemitic-granodioritic migmatites. The zircon U–Pb ages of the migmatite components vary from 3.2 Ga of the palaeosome to 2.63 Ga of the late metamorphism (Mänttäri et al. 1998, Hölttä et al. 2000). Despite a strong Palaeoproterozoic overprint ca. 1.9–1.8 Ga ago (Kontinen et al. 1992), the study area is characterized by well-preserved Archaean granulite facies sub-areas with fresh mineral parageneses (Paavola 1984, Hölttä & Paavola 2000). The area is cut by numerous Palaeoproterozoic fractures, some of them bordering the granulite sub-areas (Fig. 85).

In addition to numerous 2.3–2.1 Ga old diabase dykes (Hölttä et al. 2000, Toivola et al. 1991), a significant amount of later Palaeoproterozoic magmatism is also characteristic of the Archaean craton margin. The magmatism consists of intrusions of varying size, chemical composition varying from basic to acid. The very variable bimodal appearance of gabbros and diorites together with younger granites and granodiorites is most characteristic of the area (Paavola 1987, 1990 2001, Lukkarinen 2000, Äikäs 2000). Microtonalite dykes (Huhma 1981, Rautiainen 2000) are also found. According to the existing zircon datings, the age of the Palaeoproterozoic magmatism is around 1.90–1.85 Ga (e.g. Paavola 1988). A comprehensive description of a geotraverse crossing the area is given in Korsman et al. (1999). The area is characterized by an exceptionally thick crust of ca. 55–60 km (Grad & Luosto 1987, Kukkonen & Lahtinen 2006; Fig. 67, Fig. 95).

The location of the samples considered in this study is indicated in the lithological map in Figure 84 and the low-altitude magnetic map in Figure 85. The area is characterized by roundish magnetic anomalies, sometimes cut by numerous younger fractures, such as the fault anomaly between samples 1 and 11 (Fig. 85).

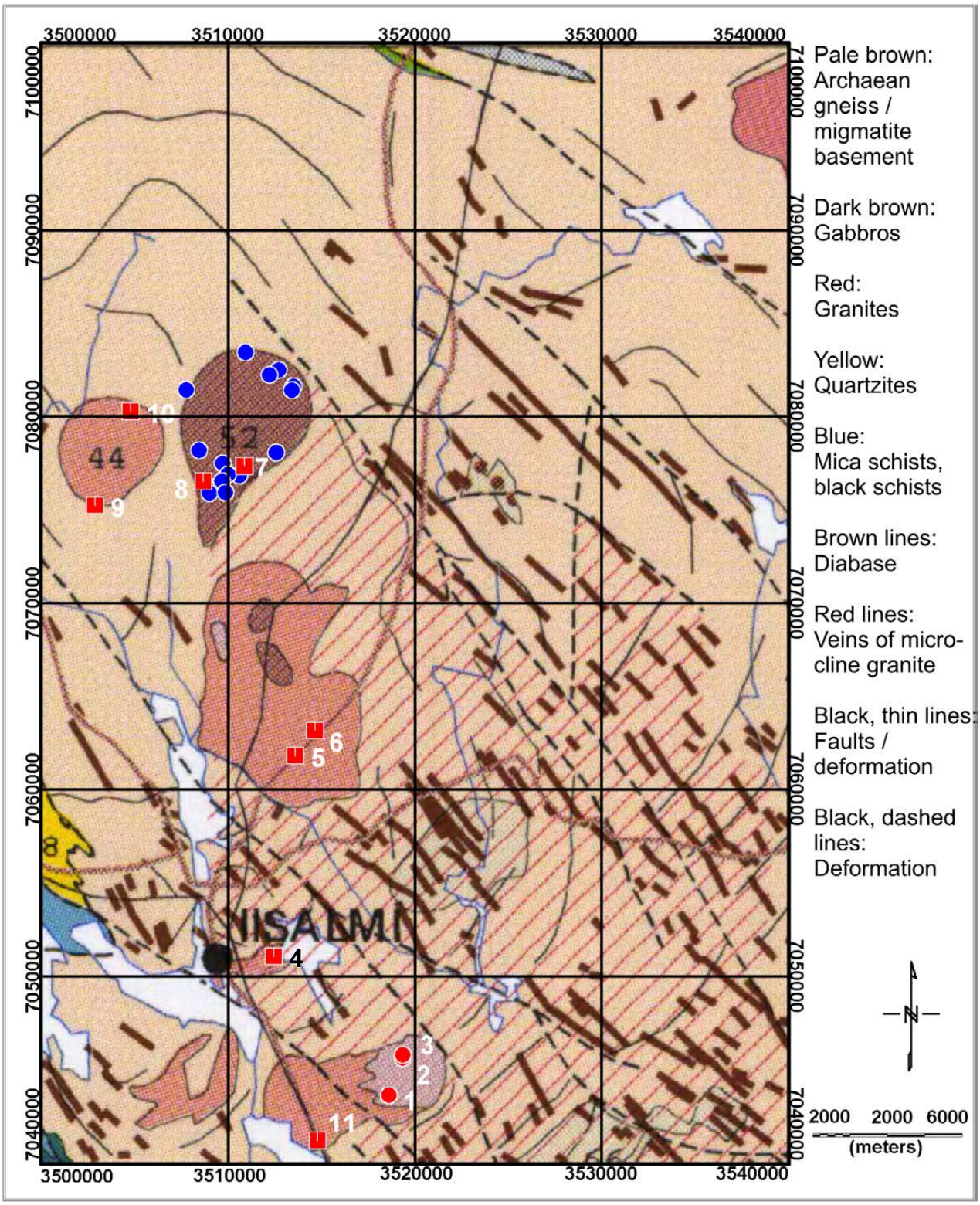

Fig. 84. A generalized lithological map of the Iisalmi–Lapinlahti area and location of the samples described below. The red dots and squares indicate the location of the samples Sa 1–11. The blue dots refer to samples Sb 1–16 (numbers not shown on the map), collected from the Kaarakkala intrusion in a separate study. The location of the map area is shown on the map in Figure 3 (red square). Adopted (cut) from Korsman et al. (1997).

Corner point coordinates in WGS-85:
Lower left KKJ: 7040000 3500000 / WGS-84: N 63.46° E 027.00°
Upper right KKJ:7100000 3540000 / WGS-84: N 64.00° E 027.81°

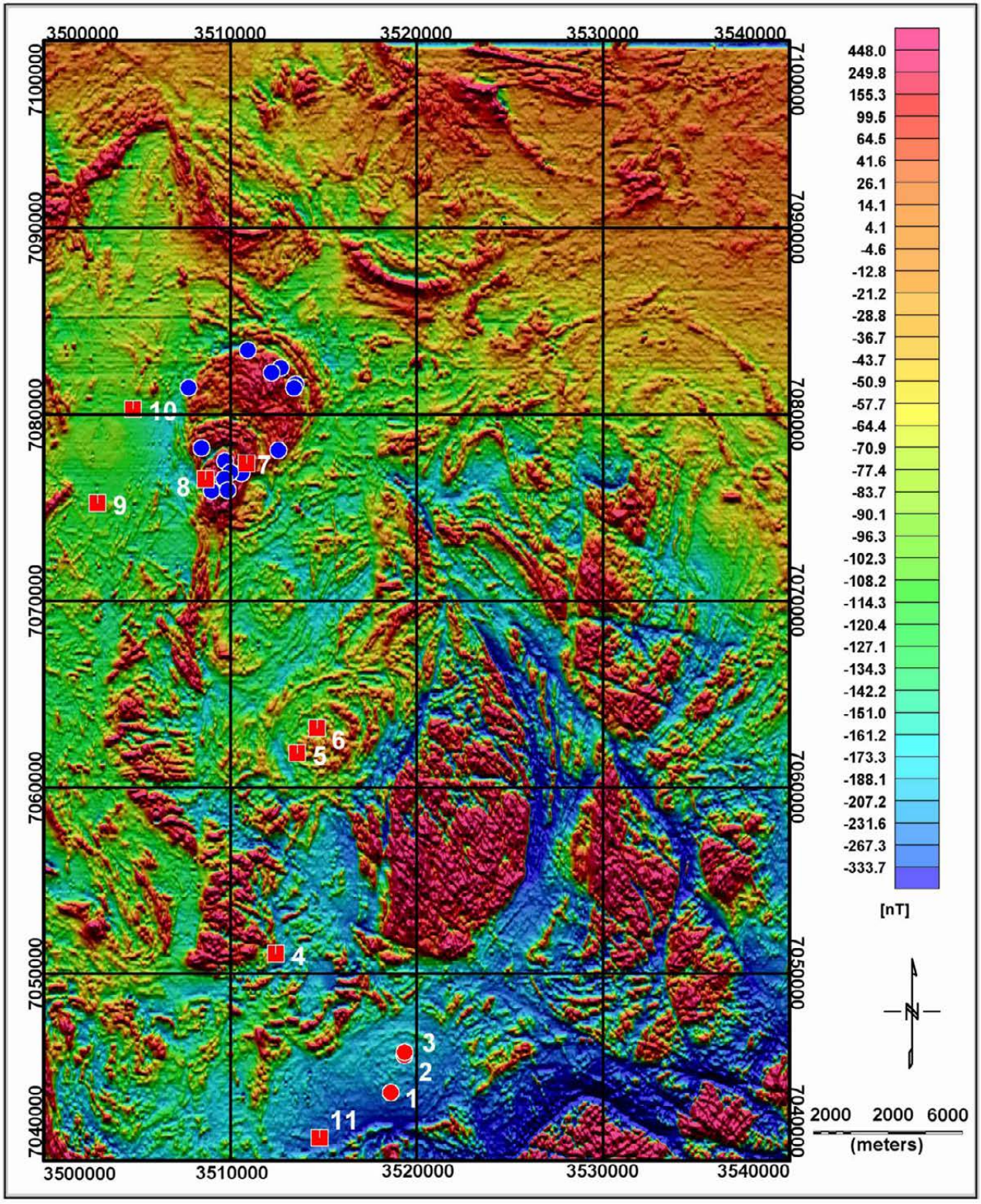

Fig. 85. A detailed low-altitude magnetic map of the Iisalmi–Lapinlahti area and location of the samples described below. The red dots and squares indicate the location of the samples Sa 1–11. The blue dots refer to samples Sb 1–16 (numbers not shown on the map), collected from the Kaarakkala intrusion in a separate study. The map is compiled from low-altitude magnetic data of the Geological Survey of Finland (Hautaniemi et al. 2005). The location of the map area is shown on the map in Figure 3 (red square). Adopted from Ruotoistenmäki et al. (2001).

5.1 Sampling (by Jorma Paavola, in Ruotoistenmäki et al. 2001)

The Palomäki quartz diorite (samples Sa 1–3) is a homogeneous and massive intrusion covering a large area commonly containing fine-grained dark fragments. The main minerals are plagioclase, quartz, biotite and hornblende. Epidote, titanite, apatite and opaques are conspicuously abundant. The Ohenmäki granite (sample Sa 11) cuts the Palomäki quartz diorite.

Sample Sa 4 is from homogeneous, grey and massive Palosvuori granite–granodiorite. The mineral composition is quartz, plagioclase, potassium feldspar and biotite. Epidote, titanite, carbonate, chlorite and opaques are the main accessory minerals.

The Ryhälänmäki granite (samples Sa 5–6) is reddish, massive and generally homogeneous, but includes dioritic and quartz dioritic xenoliths in certain areas. The granite is reddish or reddish grey and mainly medium grained. It is massive or very weakly foliated. The main minerals are quartz, plagioclase, potassium feldspar and biotite. Hornblende is rare. Varying amounts of epidote, muscovite, chlorite, titanite, apatite and opaque occur.

The Kaarakkala (leuco-) gabbroic ring intrusion (samples Sb 1–16; blue dots on the map, not numbered) causes a strong zonal magnetic anomaly (Fig. 85). Excluding the contact zones, it is undeformed and fresh. The rock is quite homogeneous but compositional banding is common. The main minerals are plagioclase, hornblende and biotite. Quartz is occasionally present. Titanite, apatite and magnetite are relatively abundant. The most basic inner part of the intrusion is nearly hornblenditic. Red medium-grained homogeneous leucogranite cross-cuts the intrusion. It follows conformly the ring structure being an essential part of the appearance of the Kaarakkala intrusion. The Nieminen sample (Sa 7) represents the granite. The Ahvenlampi sample (Sa 8) is from a typical, homogeneous leucogabbroic zone of the main Kaarakkala intrusion.

Palosenmäki granite–granodiorite is a roundish intrusion causing a negative smooth anomaly on the magnetic map (Fig. 85). The rock is relatively coarse grained, reddish white and homogeneous, consisting of plagioclase, quartz, potassium feldspar and biotite. Plagioclase is distinguished in the texture as larger, subhedral and zoned crystals. The Pirttimäki sample (Sa 9) is from the southern border zone of the intrusion, representing an anomalous, porphyric contact type, while the Hallamäki sample (Sa 10) is the most typical representative of the intrusion.

The Kiikkerinvuori granite (sample Sa 11) is reddish, massive and homogeneous. It is a part of the Ohenmäki multistage granitic intrusion.

5.2 Petrophysical characteristics of the Sa samples

During this study, several sub-samples were collected from each sampling site for petrophysical studies. Figure 86 provides a summary of the density–susceptibility variations of the sample groups Sa 1–3 and Sa 4–11 (the Kaarakkala samples Sb 1–16 are not included). In the diagram, the Palomäki samples 1–3 have a distinctly higher, 'mafic' density compared to all other groups, which have densities characteristic of felsic intrusives. The susceptibility varies from ferri- to paramagnetic (above and below of ca. 1000 $Si*10^6$) in both groups. From the diagram, it can be seen that the sub-samples of each sampling site are very homogeneous. However, the variations between sample groups are large and distinct.

5.3 Geochemical characteristics of the samples

Figure 87 presents the classification of all samples in the diagram of Cox et al. (1979). The Palomäki (Sa 1–3) and Sb samples (1–16) from Kaarakkala are close to each other in the low-SiO_2 alkaline gabbroic fields. The other Sa samples (Sa 4–11) plot in the sub-alkaline granite field.

In the diagram by de La Roche et al. (1980) and Batchelor & Bowden (1985) in Figure 88, samples Sa 1–3 and Sb 1–16 are monzonites and

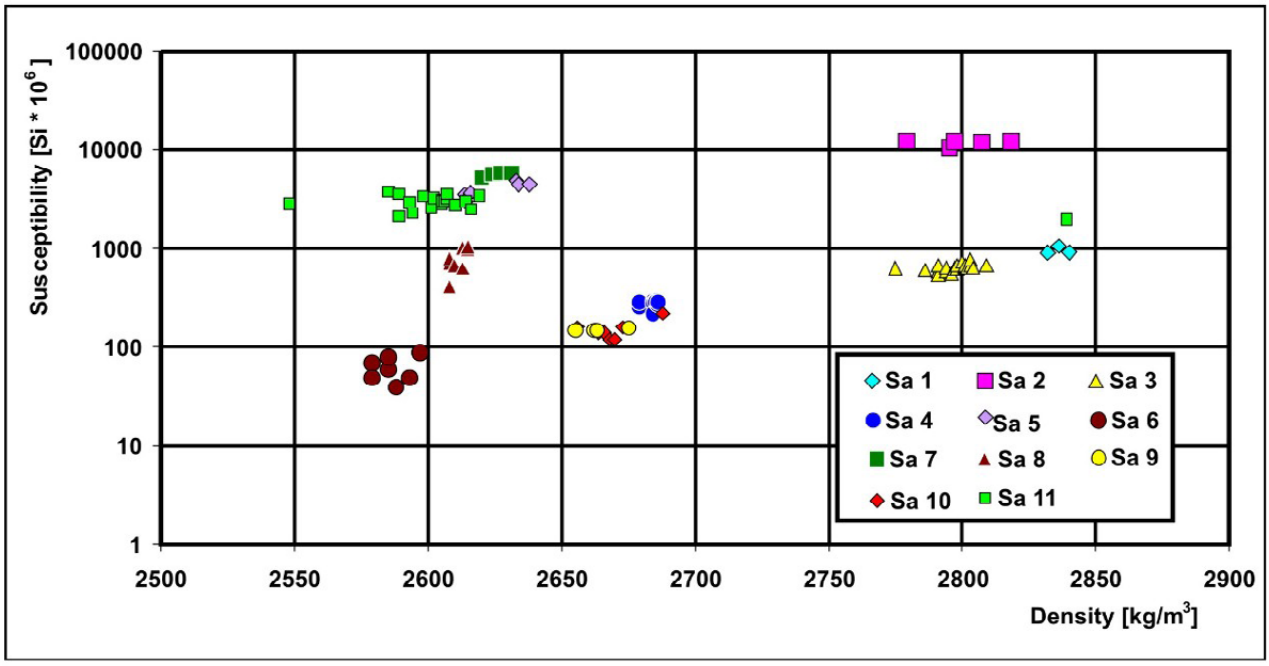

Fig. 86. Density–susceptibility variations of the samples Sa 1–11. Measured in the petrophysical laboratory of GTK. Adopted from Ruotoistenmäki et al. (2001).

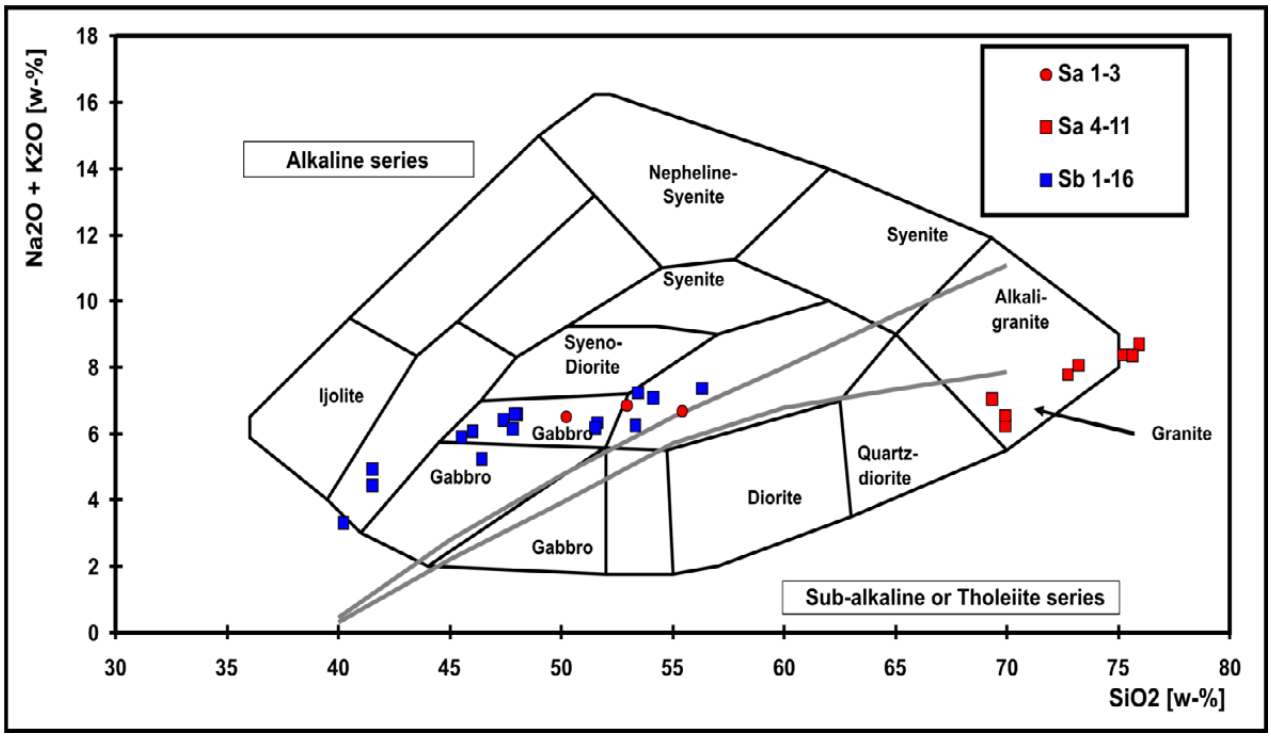

Fig. 87. Classification of the rocks in the diagram of Cox et al. (1979). See Figure 11 for details. The samples were analysed in the geochemical laboratory of GTK. See Table 2 for details. Adopted from Ruotoistenmäki et al. (2001).

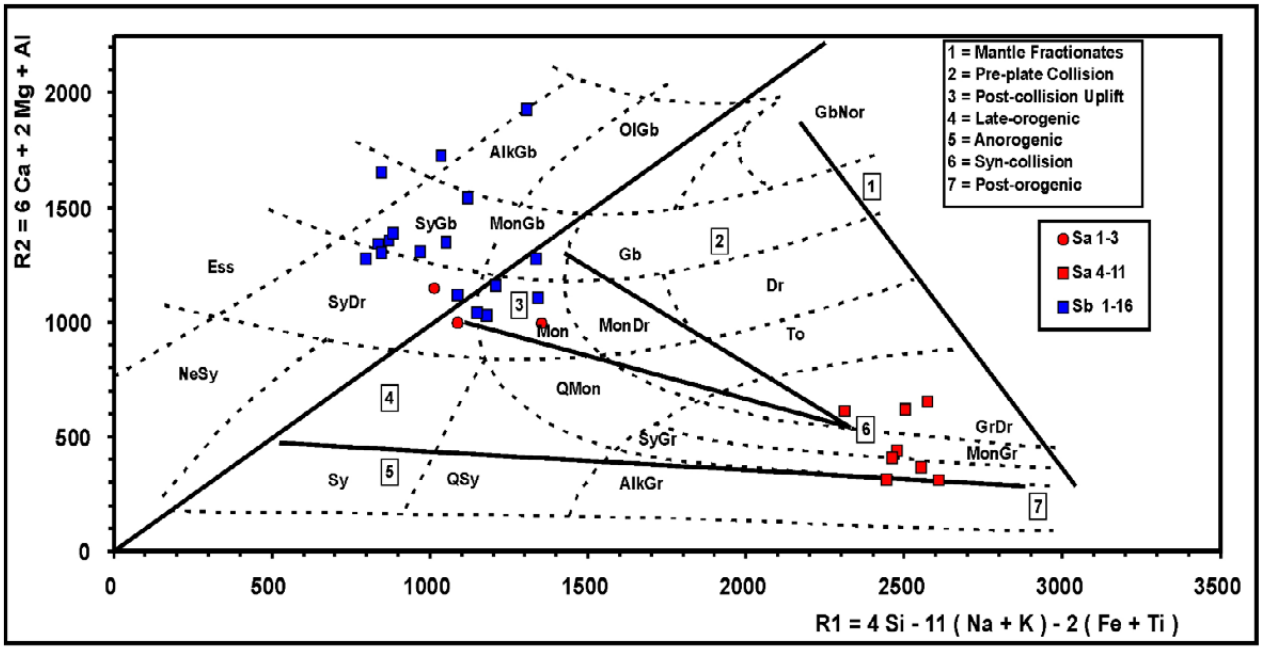

Fig. 88. Classification of the rocks in the R1-R2 diagram (de la Roche et al. 1980). See Figure 9 for details. Adopted from Ruotoistenmäki et al. (2001).

syeno-gabbros, some being in the 'post-collison uplift' field. Samples Sa 4–11 mainly cluster in the syn-collisional granodiorites and monzo- to syeno-granites. However, it is evident from tectonic and isotopic consideration above that Sa samples 4–11 also are late to post-collisional. Their geochemical characteristics were possibly contaminated during their ascent through the Archaean crust, which is evident from their isotopic and chemical compositions.

5.4 Pearce–Peate spectra of the samples

In Figure 89, the Pearce–Peate spectra of the Iisalmi–Lapinlahti area samples are compared with Finnish AFP-normalized '100% adakitic' plutonic rocks. From the diagrams, it is evident that the mafic samples from Palomäki (Sa 1–3) and Kaarakkala (Sb 1–16) correlate significantly with the Finnish adakitic plutonic rocks. Their Sr, Eu, LREE/HREE ratio and compatible levels are as high as those of the adakitoids. In particular, the Kaarakkala samples are distinctly 'adakitic', or even 'sanukitoid' due to the high values of compatibles. However, the spectrum of granitic–quartz-dioritic samples Sa 4–11 is flat and does not show any adakitic characteristics.

The above conclusions are also verified in Table 15, in which the chemistry of Iisalmi–Lapinlahti area samples is compared with adakite parameters defined by Defant & Drummond (1990) and Thorkelson & Breitsprecher (2005). From the table, it can be seen that except for the SiO_2 content, samples Sa 1–3 and Sb 1–16 fulfil the adakitic criteria. Their low SiO_2 content indicates that they are similar to the adakitic high-Al (high-Sr) samples in the Padasjoki–Kaipola area described above in section **4**. Note in particular the very high Sr content compared to the Padasjoki–Kaipola samples in Table 12.

Table 15. Comparison of the chemistry of Iisalmi–Lapinlahti area samples with adakite parameters defined by Defant & Drummond (1990) and Thorkelson & Breitsprecher (2005).

	SiO_2 [%]	Al_2O_3 [%]	Na_2O [%]	Sr [ppm]	Y [ppm]	Yb [ppm]	Sr/Y	La/Yb
Sa 1–3 (Palomäki)	52.83	**18.10**	**4.57**	**1703.67**	**16.83**	**1.28**	**101.21**	**61.43**
Sb 1–16 (Kaarakkala)	48.28	**18.94**	**4.03**	**2195.81**	**14.58**	**1.09**	**150.56**	**46.33**
Sa 4–11 (Granites)	**72.71**	14.10	**4.14**	295.88	**11.85**	**0.95**	24.96	**28.48**
Adakite	>56	>15	>3.5	>400	<18	<1.9	>40	>20

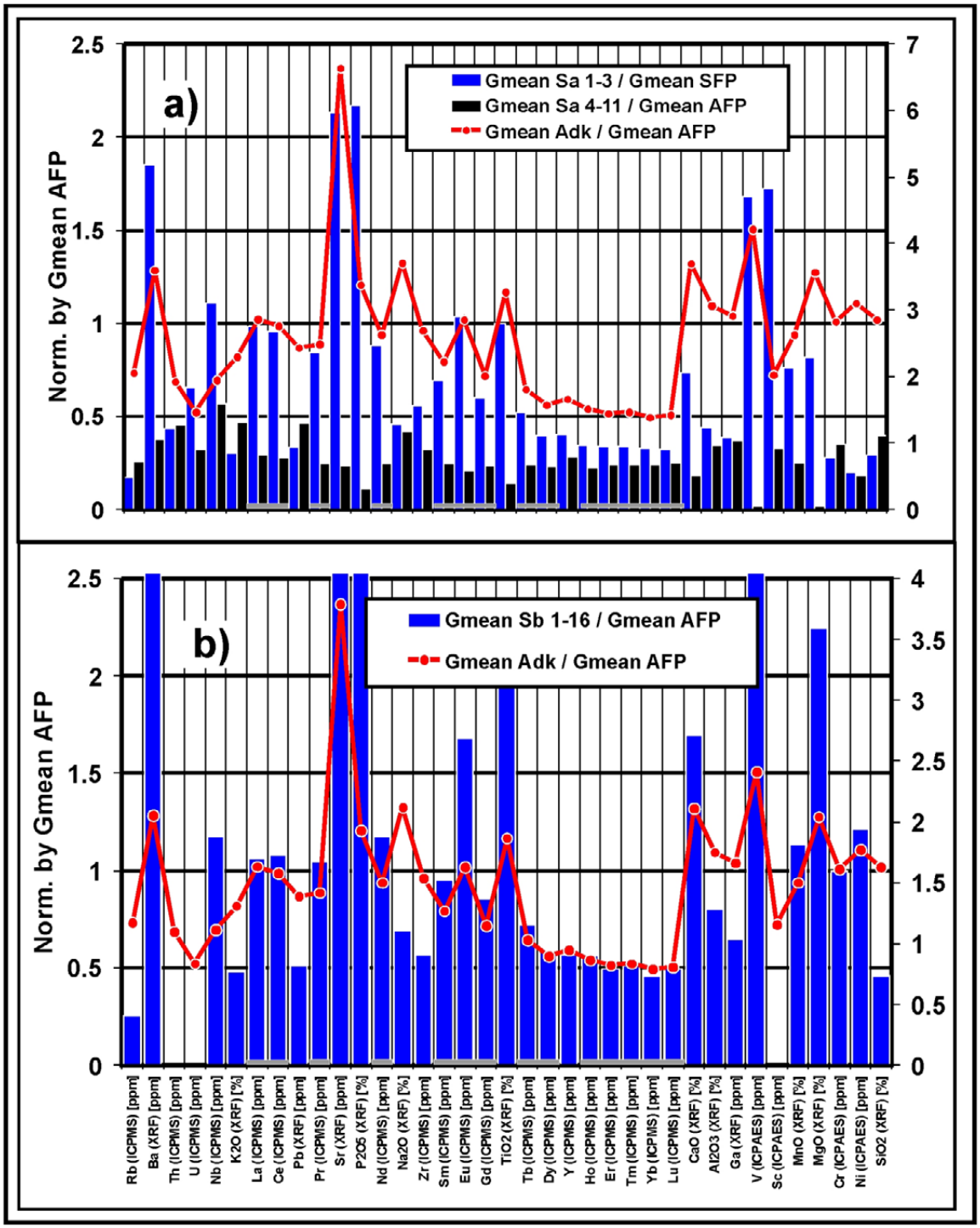

Fig. 89. Pearce–Peate spectra of samples from the Iisalmi–Lapinlahti area. The red lines indicate the course of Finnish AFP-normalized '100% adakitic' plutonic rocks (178 samples: left vertical axis). (a) Sample groups Sa 1–3 (Palomäki) and Sa 4–11 (granitic samples; bars, right vertical axis). (b) Sample group Sb 1–16 (Kaarakkala) bars, right vertical axis). Locations of REE are emphasized by horizontal grey bars above the x-axis.

5.5 Isotopic studies on the samples (by Irmeli Mänttäri, in Ruotoistenmäki et al. 2001)

The U-Pb isotopic analysis of samples, sampling of zircons and extraction of U and Pb for conventional isotopic age determination mainly followed the procedure by Krogh (1973). Zircon fractions were ≤0.65 mg in weight and the total procedural blank was ≤50 pg. ^{235}U-^{208}Pb-spiked and non-spiked isotopic ratios were measured using a VG Sector 54 thermal ionization multicollector mass spectrometer. The measured lead and uranium isotopic ratios were normalized according to accepted ratios of SRM 981 and U500 standards. The U–Pb age calculations were performed using the PbDat program (Ludwig 1991) and the fitting of the discordia lines using the Isoplot/Ex program (Ludwig 1998). For detailed isotopic data, see also Ruotoistenmäki et al. (2001).

Sb group: Sample from Ahvenlampi, Kaarakkala intrusion

The zircons from these samples are mainly long prismatic, brownish and dull. They contain inclusions of an unknown dark mineral. Brown and more rounded zircons most probably represent inherited material. Six analysed zircon fractions plot on a discordia line with intercept ages of 1864 ± 8 Ma and 76 ± 330 Ma (MSWD = 5.3; n = 6) (Fig. 90). The slightly high MSWD value indicates minor heterogeneity in zircon material and is mainly caused by zircon fractions F and B, which plot slightly on the older side of the other four data points. However, the $^{207}Pb/^{206}Pb$ ages of 1863 ± 1 and 1864 ± 1 Ma from the two nearly concordant fractions E and A independently determine the emplacement age of the Ahvenlampi diorite.

Sa sample 3, Palomäki quartz diorite

Zircons from the Palomäki quartz diorite show extreme homogeneity. These morphologically typical magmatic zircons have long prisms and are translucent to transparent and light brown in colour. Four analysed zircon fractions plot well on the same discordia line (Fig. 91). The upper intercept age of 1861 ± 1 Ma determines the age for the Palomäki quartz diorite.

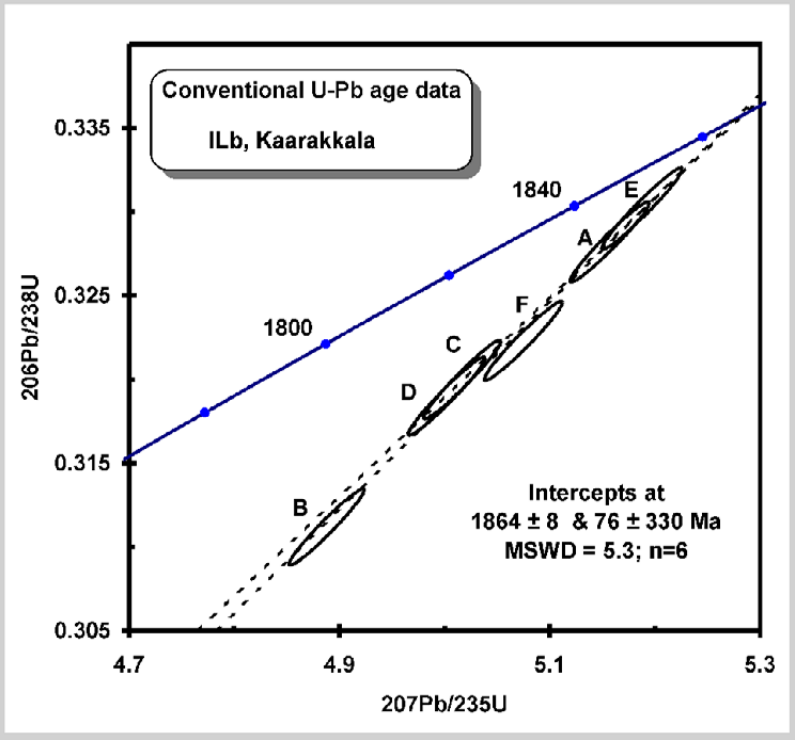

Fig. 90. U–Pb age data for Sb group samples from Ahvenlampi, Kaarakkala intrusion (diagram by Irmeli Mänttäri in Ruotoistenmäki et al. 2001).

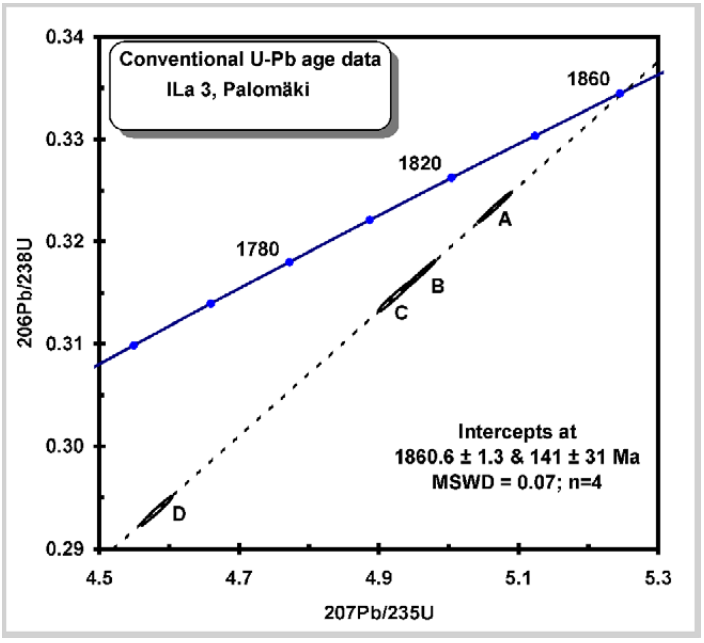

Fig. 91. U–Pb age data for Sa sample 3, Palomäki quartz diorite (diagram by Irmeli Mänttäri in Ruotoistenmäki et al. 2001).

Sa sample 4 Palosvuori, granite–granodiorite

In the Palosvuori sample, the amount of the zircon was quite small and the zircon grains were quite heterogeneous. However, some zircons contain dark mineral inclusions. Among the clearly magmatic type, there are brown and dull zircon grains and fragments with varying morphologies.

Four of the five analysed zircon fractions plot on the same line. The most discordant analysis point D plots on the older side of this discordia (Fig. 92). These highly discordant data points are normally not very reliable and can be rejected from the calculations. Although the slightly high MSWD value of 5.1 indicates some heterogeneity in the sample material, the upper intercept age of 1879 ± 11 Ma gives a good age estimate for the Palosvuori granite–granodiorite intrusion. This age, with the $^{207}Pb/^{206}Pb$ ages of 1874 and 1875 Ma for the most concordant data points (A and E), indicates that the Palosvuori granite–grano-

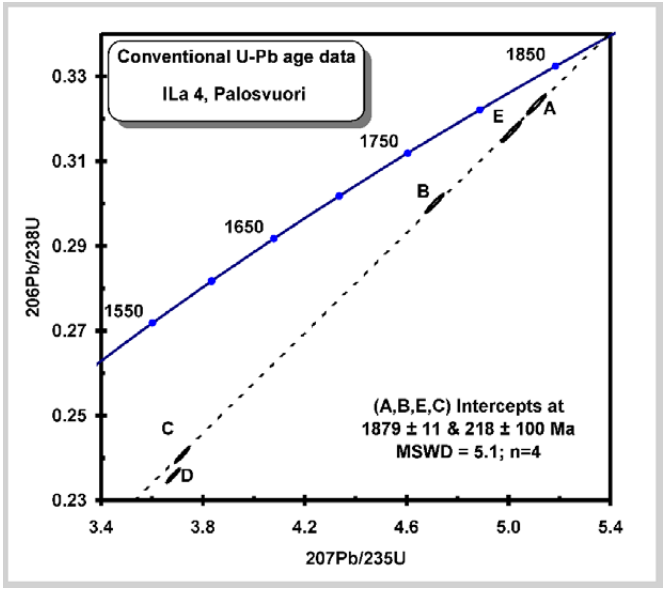

Fig. 92. U–Pb age data for Sa sample 4, Palosvuori quartz diorite (diagram by Irmeli Mänttäri in Ruotoistenmäki et al. 2001).

diorite belongs into the 1.88 Ga age group and not into the 1.86 Ga group represented by the Palomäki quartz diorite and Kaarakkala intrusion.

Sample Sa 11, Kiikkerinvuori granite

This sample yielded a very small amount of prismatic, brownish, dull zircon. Among these, there are also some irregularly shaped zircon grains. The five analysed zircon fractions were quite heterogeneous, as the MSWD value for the five-point discordia line would be as high as 28 (Fig. 93). A rough age approximation can be obtained using the discordia line from four data points. However, to reject data point C, an assumption that it contains clearly older zircon material is needed. Then, the discordia line plotted through data points A, B, D, and E gives an upper intercept age of 1851 ± 20 Ma with the MSWD value of 8.2. The high age error and MSWD value suggest that additional analysis should be conducted to ascertain whether Kiikkerinvuori granite belongs to either the syn-collisional ca. 1.88 Ga age group or the younger, ca. 1.86 Ga group.

Nd isotopes

Hannu Huhma (Geological Survey of Finland, unpublished report) has analysed the Nd isotope compositions of samples Sa 3 (Palomäki), Sa 4 (Palosvuori) and Sa 11 (Kiikkerinvuori) and calculated their ε_{Nd} values and model ages. The analytical procedures are described in Huhma (1986). The initial ε_{Nd}(T = 1900 Ma) values of the samples suggest that the Archaean crustal component is highest in Kiikkerinvuori (ε_{Nd} -6.5), decreasing to Palosvuori (ε_{Nd} -3.4) and Palomäki, (ε_{Nd} -2.2). For Kaarakkala, Huhma (2000, oral communication) reports an ε_{Nd} value of -4.5, indicative of an Archaean component in the samples.

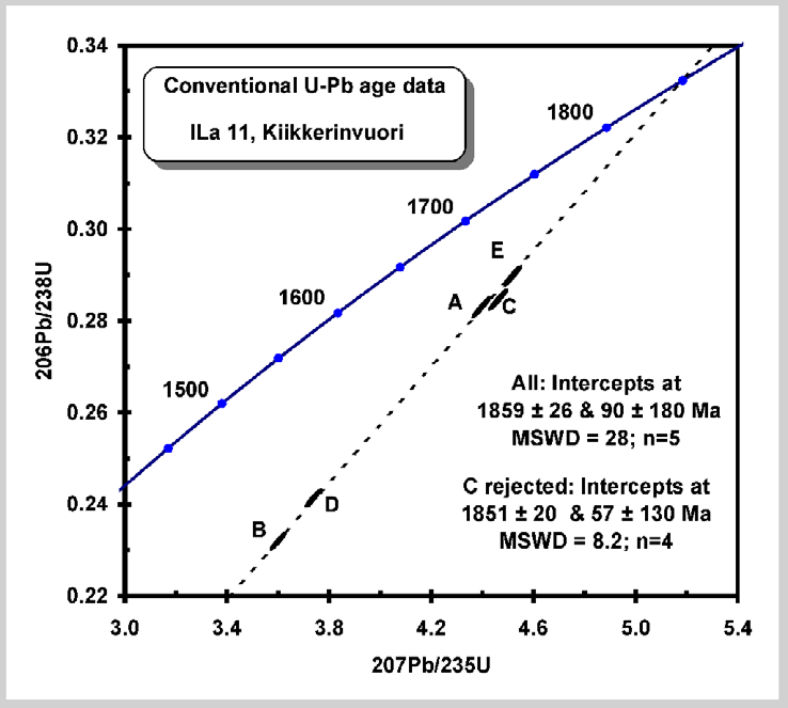

Fig. 93. U–Pb age data for Sa sample 11, Kiikkerinvuori granite (diagram by Irmeli Mänttäri in Ruotoistenmäki et al. 2001).

5.6 Discussion and implications of tectonic evolution

In the Iisalmi–Lapinlahti area, the sample ages of Proterozoic intrusives cross-cutting Archaean bedrock vary from syn- to late-/post-collisional, around ca. 1880–1860 Ma. Their elemental and Nd isotopic compositions indicate that they have varied sources of origin.

The Pearce–Peate spectra (Fig. 89) of granitic samples from Palosvuori (Sa 4; 1879 ± 11 Ma) and

Kiikkerinvuori (Sa 11; 1851 ± 20 Ma?) are flat and they are less enriched in incompatibles, LREE, Eu and Sr. Their zircons are heterogeneous and their ε_{Nd} values are strongly negative, referring to strong Archaean crustal contamination. Therefore, it is interpreted that the majority of Sa 4–11 rocks are derivatives from (re-) melting of the Archaean middle/upper crust with possibly a minor juvenile Proterozoic component.

In contrast, the younger Palomäki (Sa 1–3; 1861 ± 1 Ma) and Kaarakkala (Sb 1–16; 1864 ± 8 Ma) mafic samples have adakitic/sanukitic characteristics, being enriched in Sr, Eu, LREE and incompatible elements. The zircons from the Palomäki quartz diorite are homogeneous and the ε_{Nd} value measured from the Palomäki is highest (ε_{Nd} -2.2), referring to the smallest component of Archaean crustal contamination. From this, it can be concluded that they have a significant juvenile component, possibly from upper mantle below the Archaean crust. The zircons from Kaarakkala are more heterogeneous, probably containing inherited material. Moreover, their ε_{Nd}(T = 1900 Ma) value (-4.5) refers to a higher Archaean component in the samples.

It is interesting to note that the Palomäki and Kaarakkala samples have similarities with the ca. 800 ma older, most mafic, sanukitic ca. 2693 ± 3 Ma (ε_{Nd} (T = 2700 Ma) ≈ +1.1) tonalite sample 93003031 from the same Iisalmi sub-area considered in section **3** above. I noted: "…The sanukitic REE-enriched, but most mafic, southern Iisalmi sample probably represents poorly fractionated melts from enriched mantle, thus closely approximating the definition by Halla et al. (2009), who connected high-Ba-Sr sanukitoids to melting of an enriched mantle source, attributed to slab breakoff following a continental collision or attempted subduction of a thick oceanic plateau or TTG protocontinent…"

The observed features of rocks from the Iisalmi–Lapinlahti area can be explained by a schematic model shown in Figure 94 adopted from Ruotoistenmäki (1996), which depicts the collision of Proterozoic Svecofennian crust against the Archaean craton. In the collision process, at ca. 1.9 Ga, the Proterozoic Ladoga–Bothnian Bay zone (LBZ), having oceanic island arc characteristics, was thrusted against and below the Archaean (Iisalmi, IC) sub-area. It must be noted that because of the lack of large-scale collision-related volcanism and plutonism, the process was more like local-scale 'underthrusting' than regional-scale 'subduction' (see also Fig. 67 and Lahtinen et al. 2005).

The felsic samples Sa 4–11, containing a high Archaean crustal component, are attributed here to middle/lower crustal-related melts having a plagioclase component in restites, as suggested by the low Sr and Eu and high incompatible element values. The ca. 1879 Ma Palosvuori (Sa 4) felsic magmatism, as well as the more heterogeneous Kiikkerinvuori granite (Sa 11), can be related to syn-/late-collisional mid-crustal magmatism.

The late to post-collisional adakitic mafic Palomäki samples Sa 1–3 (1860 Ma) represent the most 'pure' slab (± mantle)-related melts with minor components from sedimentary wedge and minor, if any, Archaean crustal components.

The ca. 1863 Ma mafic Kaarakkala samples Sb 1–11 also represent late to post-collisional adakitoids/sanukitoids, but if they are slab melts they contain more 'impurities' from lower crust and mantle (± sedimentary?) wedges.

This division of magmatism into pre- and syn-orogenic stages (ca. 1880 Ma and 1860 Ma) is similar to that considered by Väisänen et al. (2012), who discussed whether the so-called early Svecofennian plutonism should be subdivided into at least two different magma generations: 1) an older pre-orogenic (i.e. syn-volcanic) stage (ca. 1880–1890–… Ma) shown today as syn-volcanic magma chambers (plutonic rocks) and 2) a younger synorogenic one (ca. 1875–1860). Their suggestion of two magma generations is supported by the ages given here.

It should be noted that the Proterozoic samples considered here are not included in the mainly Archaean Iisalmi sub-area samples considered above in Section 2.

In the collision and following extension/uplift processes, the Archaean Iisalmi–Lapinlahti crust was broken into blocks, some of which still contain well-preserved granulite facies mineral assemblages. The block margins are evident as fracture zones in the magnetic map in Figure 85 above. The collision tectonics at the Archaean–Proterozoic boundary have also been considered by Pietikäinen & Vaasjoki (1999), Nironen (1997) and Lahtinen et al. (2005), among others. The

thrust model is also supported by reflectors in the reflection seismic FIRE profile presented in Figure 95 (Kukkonen & Lahtinen 2006); see also Fig. 67.

The area is characterized by local-scale granulitic blocks indicating ca. 15–20–38 km uplift due to erosion and extensional tectonics following the Svecofennian collision (e.g. Kontinen et al. 1992, Hölttä & Paavola 2000, Korsman et al. 1999). These processes and the relatively local-scale underthrusting may explain the lack/removal of island arc (adakitic) supracrustal volcanic rocks in the area. When considering the magnetic map in Figure 85 in more detail, it can be noted that there are even more roundish, relatively 'flat' low-amplitude anomalies that can be related to the intrusives considered above. This also indicates that Proterozoic magmatism has been active in this Archaean sub-area.

The increased mafic magma content in lower crust (underplating) raised the average density of the LBZ–IC zone in the area, making it possible to sustain the isostatic balance and a very thick crust, close to 60 km, as noted in section 3 and demonstrated in the seismic sections in Figure 95 and Figure 67.

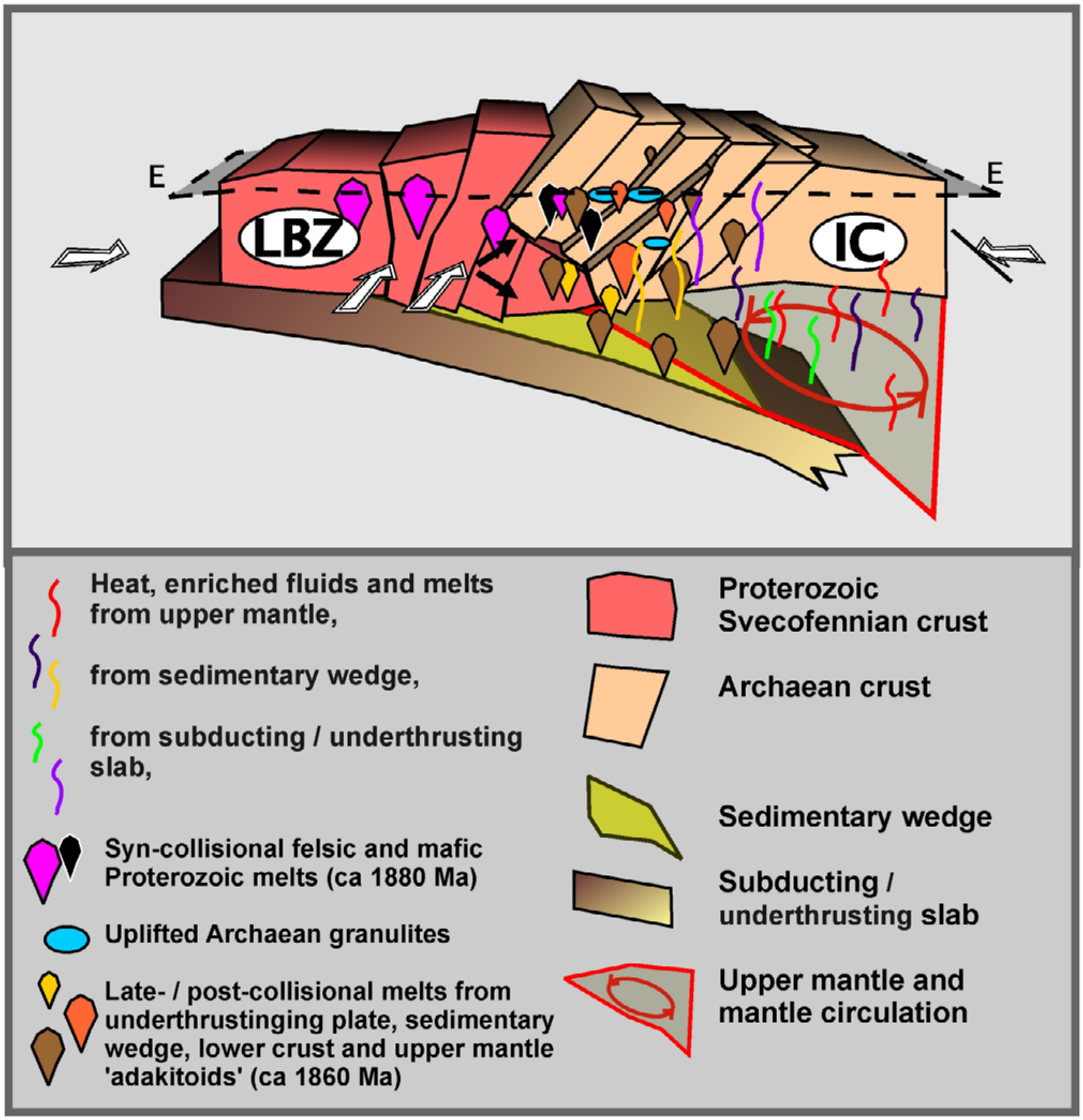

Fig. 94. A schematic model of the collision of Svecofennian crust against and under the Archaean craton and of the interconnected magmatic processes. Adopted and modified from Ruotoistenmäki (1996). LBZ = Proterozoic Ladoga–Bothnian Bay zone (~ marine + island arc association), IC = Archaean Iisalmi sub-area containing the Iisalmi–Lapinlahti area, E = present-day erosion level.

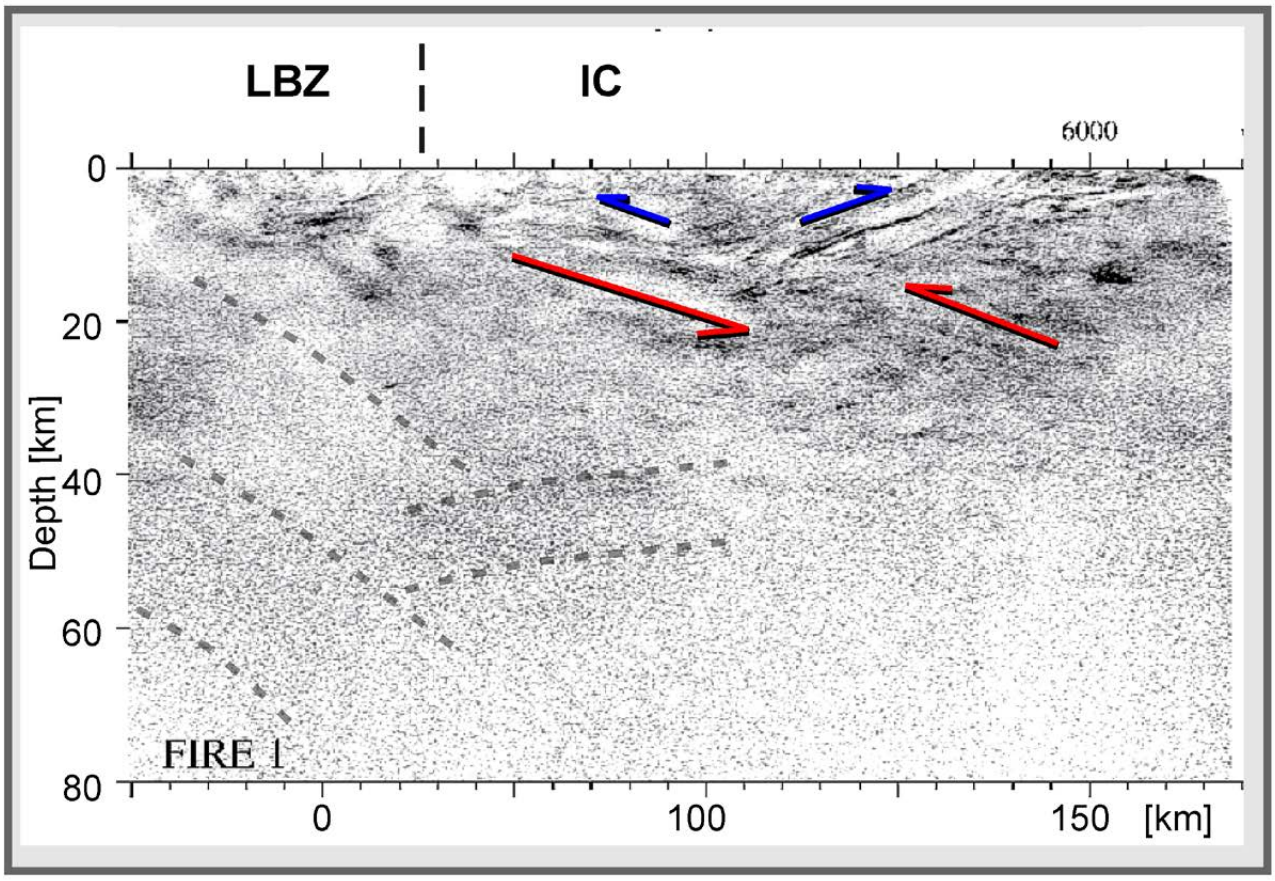

Fig. 95. Reflection seismic profile FIRE (Kukkonen & Lahtinen 2006) across the Proterozoic–Archaean border. The red arrows depict a strong reflector dipping NE below the Iisalmi–Lapinlahti area, interpreted here as a thrust fault. The blue arrows depict the borders of an uplifted block in the Iisalmi–Lapinlahti area. The dashed lines refer to some inferred reflection surfaces. The vertical dashed line shows the location of the Proterozoic–Archaean border (between LBZ and IC); see also the longer section of the profile in Figure 67 and its location in Figure 50.

6 SUMMARY: CHARACTERISTICS, SOURCES AND EVOLUTION OF FINNISH ADAKITOIDS

In this study, I have considered the chemistry, petrophysics, geophysics and isotopic data of Finnish adakitic plutonic rocks from a regional scale, covering the whole of Finland, to more local lithological and tectonic sub-areas and down to the sample scale. The samples cover both Archaean and Proterozoic domains in Finland with variable sampling density. Plutonic rocks are assumed to correspond more closely to (present) upper crustal compositions compared to supracrustal volcanic rocks, which may have been more susceptible to alteration processes and erosion. The most striking features of the adakitic plutonic rocks in Finland are their great number and wide areal distribution. Only some supracrustal sub-areas lack adakitic plutonic rock samples. The relative number of Archaean area adakitic samples is more than twice that of Proterozoic areas.

6.1 Petrophysical characteristics of Finnish adakitoids

When allowing wider SiO_2 variation ('75%' adakitoids), the rock types of adakitoids vary from granodiorites to gabbros (Fig. 9 and Fig. 10). The distributions of magnetic susceptibilities of both Archaean and Proterozoic adakitoids are alike (Fig. 8), close to that of the average of

all Finnish plutonic rocks. However, the density of Proterozoic adakitoids is clearly higher than that of Archaean adakitoids. The slightly higher paramagnetic susceptibilities and higher densities of Proterozoic adakitoids refer to a more mafic average composition and higher content of Fe-rich mafic minerals, and thus evolution in a more oxygen poor or more reducing environment favouring iron-rich silicates before magnetite, as noted by Ruotoistenmäki (1992).

6.2 Chemical characteristics of Finnish Adakitoids

Pearce–Peate spectra

The incompatible–compatible diagram of Pearce & Peate (1995) normalized by the geometric means of all Finnish plutonic rocks (AFP; Fig. 19 to Fig. 22) has been an effective and informative tool in studying the chemical characteristics and variations of the samples. A significant fact in the spectra of adakitoids in Figure 19 (summarized in Fig. 96) is that their average chemistry is very similar for both Proterozoic and Archaean suites, though their age difference can be up to 1 Ga. In AFP-normalized spectra, they both have high LREE/HREE and compatibles/HREE ratios, with relative maxima at Ba, K, Sr, Na_2O, Eu, Ti, Li, CaO, Al_2O_3, V, Mn, Fe, Co and Mg. In particular, the relatively high values of Eu and Sr in both adakitoids and gabbros indicate deeper, lower crustal or upper mantle sources for the primary melts of these rocks, i.e. depths greater than ca. 30–60 km, below the plagioclase stability depths.

It is interesting to note in the spectra in Figure 96 that although the LREE/HREE ratio is steeper for Archaean adakitoids (see also Fig. 18), the relative amplitudes of Eu and Sr, and also the compatibles/HREE ratio are clearly higher for Proterozoic adakitoids. These characteristics refer to a more mafic, plagioclase-rich source for Proterozoic adakitoids: they are less fractionated (gentler REE curve), but their Eu and Sr peaks are higher. Moreover, the map in Figure 32 indicates a high concentration of sanukitoids/sanukitic rocks in Proterozoic sub-areas. The relative minima of Rb, Th and U in the AFP-normalized adakitoid spectra in Figure 96 have been connected in section 1.4. with at least two-stage fractionation of adakitoids: 1) the removal of the fluid phase (with Rb, U and Th) and 2) magmatic fractionation.

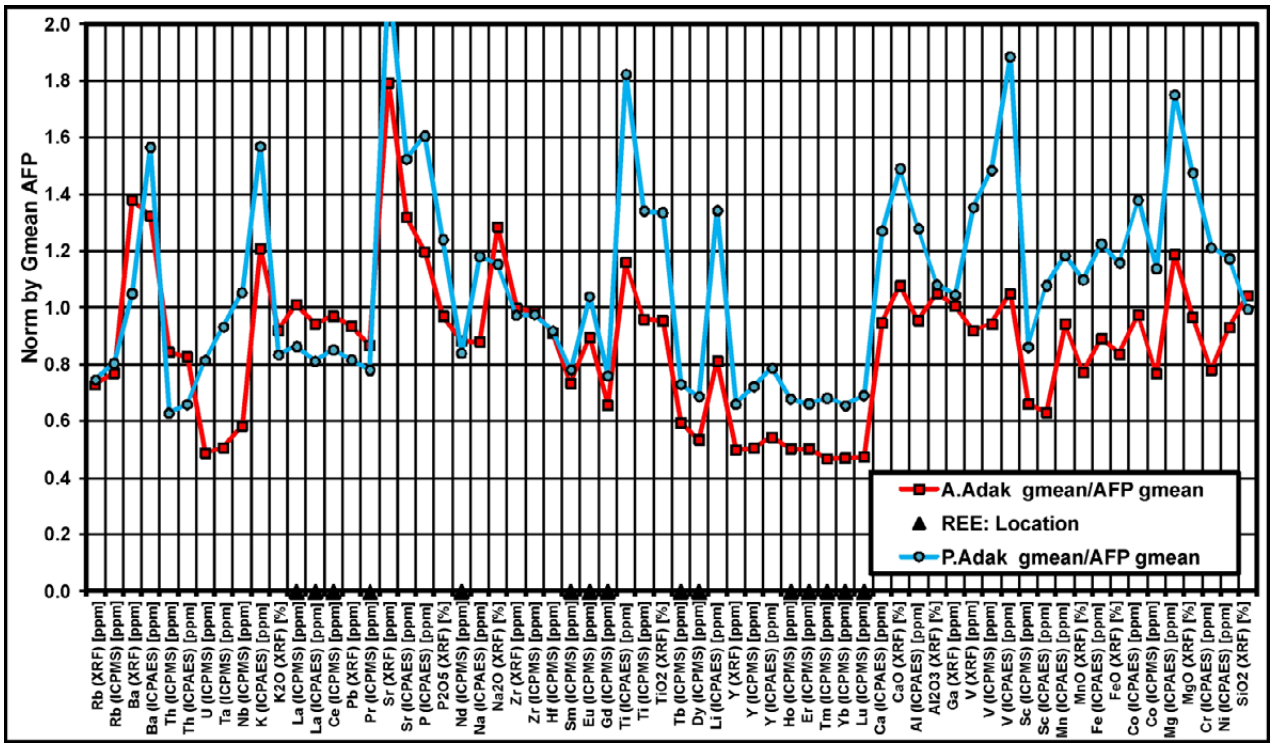

Fig. 96. Comparison of the Pearce–Peate spectra of Proterozoic and Archaean adakitoids.

The normalized Pearce–Peate diagram of Proterozoic granites (Fig. 21) is characterized by flat REE, while Archaean granites have a steeper REE curve, reflecting stronger fractionation. Both granite groups also have relative Eu minima and higher Rb, Th and U, indicating shallower, mid- to upper crustal evolution/fractionation processes at plagioclase stability depths. Compared to granites, the relatively high Eu and Sr peaks of adakitoids imply that they did not experience multistage uplift connected with notable 'granite-like' mid-crustal fractionation.

The exceptional HREE enrichment relative to LREE of rapakivi granite samples in the Pearce–Peate diagram in Figure 22 refers to an evolutionary history different from 'normal' granites and a deeper crustal primary source, possibly uplift and (partial) mid-crustal re-fractionation of primarily deep crustal restitic material. The distinct negative correlation between adakitoids and rapakivi samples refers to the opposite type of primary upper mantle/lower crust processes, suggesting the need for further studies on the relationships between adakitic melts and primary rapakivi source material (restitic to adakitoids?). In addition, the LREE/HREE ratios of gabbros in Figure 20 are also opposite to those for adakitoids, showing HREE enrichment relative to LREE and referring to a depleted, incompatible-poor mafic source for these rocks (enriched restite would be difficult to generate).

An estimate for the primary contents of the basaltic source of (Proterozoic) adakitoids can be obtained by studying the content of the adakitic, most primitive, low-SiO_2 high-Sr, high-Al magma series from the Proterozoic collision/accretion zone in the Padasjoki–Kaipola area, central Finland (Fig. 76 to Fig. 77). At $SiO_2 \approx 50\%$, the regression curve values for major elements are ca: $K_2O \approx 1.8\%$, $P_2O_5 \approx 0.4\%$, $Na_2O \approx 3\%$, $TiO_2 \approx 1.1\%$, $CaO \approx 7.3\%$, $Al_2O_3 \approx 18\%$, $MnO \approx 0.15\%$ and $MgO \approx 5.2\%$. In the Proterozoic collision zone in central Finland, the more mafic, high-Al adakitic samples are relatively enriched in incompatibles compared to more felsic, low-Al, tholeitic samples. This demonstrates that they cannot be derivatives of each other or due to the same fractionation processes. The tholeitic 'low-Al' samples are inferred to represent pre- to syn-collisional 'marine associated' samples, while adakitic 'high-Al' samples are related to deeper, late- to post-collisional subduction-derived magma fractionates.

6.3 Restites of adakitoids

The high LREE/HREE ratios of AFP-normalized adakitoids in Figure 19 and Figure 96 suggest fractionation and extraction of adakitic melt phase with ± garnet ± clinopyroxene ± orthopyroxene ± hornblende in the restite. The possible major mineralogy combinations of the restites left behind by adakitoid melts are estimated using ratios of trace elements whose partition coefficients are specific to pyroxenes, garnets or hornblende (section 1.5). These tests indicate that the main restitic minerals in the whole of Finland for adakitoids are clinopyroxene and, in southern–central Finland, also orthopyroxene (Fig. 24 and Fig. 25). In particular, in the Proterozoic sub-areas, pyroxene-rich restites appear to dominate. However, amphibole and especially garnet-rich restites dominantly cluster in Archaean sub-areas, thus referring to higher pressures and temperatures in their environment of fractionation.

In the P–T diagram in Figure 97, the garnet–hornblende stability field, interpreted to exist in Archaean sub-areas, is characterized by pressures from ca. 10 to 20 kbar (depths of ca. 40–80 km) and temperatures from ca. 900–1000 °C. In the Proterozoic areas of southern Finland, where pyroxenes dominate, the restites, and amphiboles and garnet, are relatively absent and fractionation pressures appear to have been from ca. 5 kbar to ca. 10 kbar (ca. 30–50 km), with temperatures being ca. 800–950 °C. Thus, it seems that Proterozoic adakitoids have been fractionated at shallower depths and temperatures, where more plagioclase can exist together with pyroxenes in the restite, as also demonstrated by Herzberg (1995 and references therein).

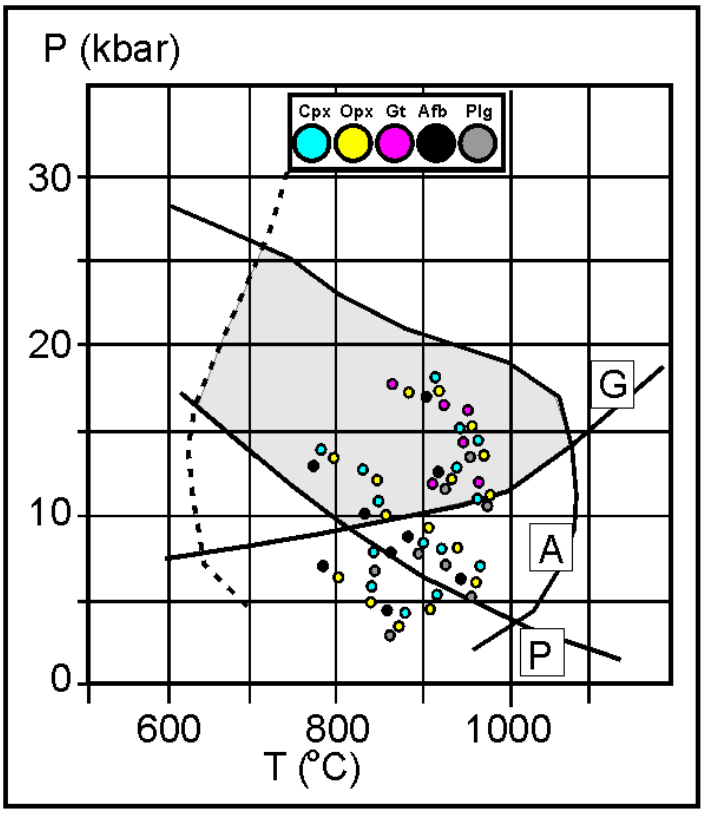

Fig. 97. A pressure–temperature (P–T) diagram simplified from Martin & Moyen (2002). Dashed line: solidus of tholeite with 5% water. The border lines A, G and P outline stability fields of amphiboles, garnet and plagioclase, respectively. The pale grey field is the P–T domain where slab melts can coexist with hornblende- and garnet-bearing residue. The dots, indicating the stability locations of clinopyroxene (Cpx), orthopyroxene (Opx), garnet (Gt), amphibole (Afp) and plagioclase (Plg), have been adopted from diagrams by Obata & Thompson (1981).

6.4 Origin and evolution of Finnish adakitoids

When considering the evolution of Proterozoic adakitoids, it is interesting to note from the Pearce–Peate spectra of the southern Finland migmatite sub-area (SMB; Fig. 37) and Ladoga–Bothnian Bay zone (LBZ; Fig. 41) that their main peaks for all-plutonic samples and adakitoids coincide strikingly well. This is also confirmed by their high mutual correlations in the correlation matrix in Table 6. Characteristic of the SMB and LBZ sub-areas is a significant oceanic signature in bedrock, for example, black schists, marine volcanic rocks and mafic plutonic rocks. It is apparent that the high correlation of LBZ, SMB and adakitoids indicates a similar, although not simultaneous, marine plate-dominated origin. Thus, it appears that when subducting marine-type plates (SMB, LBZ), the main peaks of the element contents remain, but the relative content of incompatibles increases.

In section 3, I consider eight Archaean adakitic plutonic rock samples selected from four major Archaean sub-areas, the Pudasjärvi, East Finland, Iisalmi and Ilomantsi sub-areas, and compare their chemistry with Proterozoic adakitoids. The Archaean sample ages in this section distribute within a wide, overlapping and continuous range from ca. 2620 to 3000 Ma (Fig. 66), reflecting multistage magmatic and tectonic crustal processes in the evolution of Finnish Archaean crust. The magmatic/emplacement ages of the samples vary from ca. 2.69 Ga to ca. 2.98 Ga, the majority (6 of 8) being tightly bracketed between ca. 2.75–2.69 Ga. The East Finland group is the oldest, ca. 2770–3000 Ma. The northern Pudasjärvi sample, southern Iisalmi sample and southern Ilomantsi sample are characterized by the most homogeneous (~ reliable) age distributions, with ages varying between ca.

2690–2740 Ma. The average of all U-Pb ages is ca. 2782 ± 102 Ma, approximating the East Finland, Iisalmi and Ilomantsi sample ages.

The high ε_{Nd} values of the samples from these sub-areas, varying from ca. -4.6 (one sample) to -1.5 and +2.1, refer to their juvenile, relatively 'uncontaminated' source material. However, in each sub-area there are also samples characterized by old ages given by inherited zircons (Fig. 66). Thus, it must be concluded that inherited, older assimilated crustal and/or recirculated sedimentary material is common in the source material of these adakitic Archaean rocks in Finland. The overall chemistry of these Archaean sub-areas and Proterozoic adakitoids reported by Väisänen et al. (2012) differ significantly (Fig. 53 and Fig. 54).

The youngest Proterozoic, ca. 1.86 Ga intrusives cross-cutting the Archaean Iisalmi–Lapinlahti sub-area, described in section 5, are connected with late- to post-collisional processes following the collision and thrusting of Proterozoic sub-areas against and under the Archaean crust, thus being close to 'modern' plate tectonic models. Most evident/probable adakitic samples related to Archaean plate-tectonic subduction are described from the Ilomantsi sub-area (section 3), having island arc characteristics. However, in the Pudasjärvi, East Finland and Iisalmi sub-areas, the relationship with modern plate tectonics is more uncertain. The adakitic rocks in these sub-areas lack notable island arc/marine characteristics and their age span is much wider (up to 400 Ma) compared to Proterozoic Svecofennian rocks between ca. 1.8–1.9 Ga. Thus, their evolution is related here to more complex collision, stacking, underplating and re-melting of inferred, more or less 'exotic', fast moving (3.1–2.9–... Ga) 'microplates'.

From the considerations in section 1.6, it becomes evident that adakitoids, TTGs and sanukitoids form a continuity of magmas fractionated at depths where plagioclase is more or less unstable. Their sources have inherited various amounts of material from subducting sea-floor, upper mantle (wedge), sedimentary wedge and lower crust. The chemical distinction between these rocks is more or less arbitrary (e.g. Fig. 30, Fig. 31 and Fig. 56).

6.5 Summary

In brief, the results of this study can be summarized as follows:

1. The areal distribution of Finnish adakitic/TTG/sanukitic plutonic rocks, which represent melts fractionated at lower crust/upper mantle depths, is very large, and their number is relatively high. Only some supracrustal sub-areas lack known adakitic plutonic rock samples.
2. A very effective tool for studying adakitoid chemistry is the incompatible–compatible diagram by Pearce & Peate (1995), combined with normalization by the geometric means of all Finnish plutonic rocks (AFP).
3. The characteristics of adakitoids are defined by comparing their Pearce–Peate spectra with those of (felsic) granite and (mafic) gabbro samples from the same database. The most distinctive features of adakitoids are their high Sr, Eu, and LREE/HREE and compatible element/HREE ratios. Their rock types vary from granodiorites to tonalites and gabbroic rocks.
4. The Proterozoic adakitoids are denser than Archaean adakitoids, reflecting their more mafic composition. However, their magnetic properties are alike.
5. In Proterozoic sub-areas, the characteristics of average crustal plutonic rocks and adakitoids clearly differ with the exception of two 'marine' sub-areas, whose spectral peaks coincide with those of adakitoids, although their trends (REE slopes) differ.
6. In Archaean sub-areas, the average crustal plutonic rocks and adakitoids correlate significantly, which refers to similar evolutionary environments for both adakitoids and the crust as a whole.
7. Proterozoic adakitoids are here connected with 'modern type' plate tectonic subduction-related processes, while Archaean crust and adakitoids (TTGs) are probably mainly connected with more complex collision and stacking processes of ancient local-scale 'microplates'. However, the Ilomantsi adakitoids

can be related to more 'modern' plate tectonic-type processes.

8. Proterozoic sub-areas and the Archaean Ilomantsi area are characterised by an increased sanukitic composition.
9. The major restite minerals of adakitic melts are clinopyroxene and orthopyroxene for both Proterozoic and Archaean adakitoids, while garnet and amphiboles also characterize the restites of Archaean adakitoids, reflecting their higher P–T fractionation environment.
10. The rapakivi granites correlate strongly and negatively with adakitoids, thus giving indications of the characteristics of the complementary restitic material of the adakitoids. However, due to their complex uplift history, they cannot directly be considered as adakitoid restites.
11. Relatively mafic Proterozoic adakitoid magma series studied in a collision zone in central Finland are characterized by a distinctly fractionated spectrum with a high content of incompatibles and relatively low values for compatibles compared with non-adakitic, more felsic tholeitic magma series. Thus, their magmatic evolutionary histories cannot be related.
12. Examples of low-SiO_2 Proterozoic adakitoids also include the ca. 1.86 Ga post-/late-collisional mafic intrusives cross-cutting the Archaean crust close to the Archaean–Proterozoic border. Their homogeneous zircons and relatively high ε_{Nd} values imply low crustal contamination and underthrusting/subduction-related genesis
13. The isotopic ages from the Archaean adakitoid zircons considered here range from ca. 2620 to 3000 Ma, with the magmatic ages bracketing more tightly between ca. 2690–2740 Ma. The high content of older inherited and younger, overprinted zircons reflects their complex and multistage history.
14. The potential of adakitoids for economic mineralizations, e.g. Au, Cu, REE, needs to be considered.
15. The adakitoids can all be classified as representing plagioclase instability depth melts. They form a continuity from 'true' subduction-related adakites to TTGs and sanukitoids, their chemical and mineralogical differences being obscure. As such, they provide a very valuable and informative window into magmatic processes existing at upper mantle/lower crustal depths. Moreover, the characteristics of crust between their present-day location and source depth can be studied by analysing their contamination on their way up to the present surface. Thus, their profound and comprehensive study will yield a large amount of valuable information on the evolution of our present-day crust.

ACKNOWLEDGEMENTS

Pofessor Tapani Rämö guided me through this process. He, and Professor Paterno Castillo, docents Esa Heilimo and Pentti Hölttä helped me to finish and clarify the manuscript. The cooperation in data and sample studies with Pentti Hölttä, Jorma Paavola, Irmeli Mänttäri, Eeva Rintala, Satu Vuoriainen and Heikki Säävuori from GTK has been essential for effective analysis of the data. The language has been checked by Roy Siddall and the text has been edited by Päivi Kuikka-Niemi. I want to thank them all for getting this work to the current state.

Special thanks my wife Marjatta for everyday logistic and mental support during these years, and the years to come.

REFERENCES

Äikäs, O. 2000. Juankoski. Geological map of Finland 1:100 000, Pre-Quaternary Rocks, Sheet 3333. Geological Survey of Finland.

Anders, E. & Grevesse, N. 1989. Abundances of the elements: Meteoritic and solar. Geochimica et Cosmochimica Acta 53, 197–214.

Babel Working Group 1993. Integrated seismic studies of the Baltic shield using data in the Gulf of Bothnia region. Geophys. J. Int. 112, 305–324.

Batchelor, R. A. & Bowden, P. 1985. Petrogenetic interpretation of granitoid rock series using multicationic parameters. Chemical Geology, 48, 43–55.

Bickle, M. J. 1978. Heat loss from the Earth: A constraint on Archaean tectonics from the relation between geothermal gradients and the rate of plate production. Earth Planet. Sci. Letters. 40, 301–315.

Castillo, P. R. 2006. An overview of adakite petrogenesis. Chinese Science Bulletin 51(3), 257–268.

Chappell, B. J. & White, A. J. R. 1974. Two contrasting granite types. Pacific Geology 8, 73–174.

Chappell, B. W., White, A. J. R. & Wyborn, D. 1987. The importance of residual source material (restite) in granite petrogenesis. Journal of Petrology 28, 1111–1138.

Cochran, W. G. 1963. Sampling techniques. London: Wiley.

Condie, K. C. 2005. TTGs and adakites: are they both slab melts? Lithos 80, 33–44.

Cox, K. G., Bell, J. D. & Pankhurst, R. J. 1979. The Interpretation of igneous rocks. London: Allen & Unwin. 450 p.

Defant, M. J. & Drummond, M. S. 1990. Derivation of some modern arc magmas by melting of young subducted lithosphere. Nature 347, 662–665.

Drummond, M. S. & Defant, M. J. 1990. A model for trondhjemite–tonalite–dacite genesis and crustal growth via slab melting; Archaean to modern comparisons. Journal of Geophysical Research 95, 21503–21521.

Drummond, M. S., Defant, M. J. & Kepezhinkas, P. K. 1996. The petrogenesis of slab derived trondhjemite-tonalite-dacite/adakite magmas. Transact. R. Soc. Edinb. Earth Sc. 87, 205–216.

Eilu, P., Sorjonen-Ward, P., Nurmi, P. & Niiranen, T. 2003. A review of gold mineralization styles in Finland. In: Sundblad, K. & Cook, N. J. (eds) A group of papers devoted to the metallogeny of gold in the Fennoscandian shield. Economic Geology 98 (7), 1329–1353.

Elkins-Tanton, L. T. & Grove, T. L. 2003. Evidence for deep melting of hydrous, metasomatized mantle: Pliocene high-potassium magmas from the Sierra Nevadas. Journal of Geophysical Research 108, 2350. doi:10.1029/2002JB002168.

Elliott, B. A. 2001. The Petrogenesis of the 1.88–1.87 Ga post-kinematic granitoids of the central Finland granitoid complex. Academic dissertation, University of Helsinki, Finland. 36 p.

Foley, S., Tiepolo, M. & Vannucci, R. 2002. Growth of early continental crust controlled by melting of amphibolite in subduction zones. Nature, 417, 20 June Issue, 837–840.

Frost, B. R., Barnes, C. G., Collins, W. J., Arculus, R. J., Ellis, D. J. & Frost, C. D. 2001. A geochemical classification for granitic rocks [Review]. Journal of Petrology 42 (11), 2033–2048.

Garrison, J. M. & Davidson, J. P. 2003. Dubious case for slab melting in the Northern volcanic zone of the Andes. Geology 31, 565–568

Gore R. & Sugar, J. A. 1985. Our restless planet Earth. National Geographic 168, 2, 142–181.

Grad, M. & Luosto, U. 1987. Seismic models of the crust of the Baltic shield along the Sveka profile in Finland. Annales Geophysicae 187, 5B, (6), 639–650.

Hakkarainen, G. 1994. Geology and Geochemistry of the Hämeenlinna-Somero volcanic belt, southwestern Finland: A paleoproterozoic island arc. In: Nironen, M. & Kähkönen, Y. (eds) Geochemistry of Proterozoic supracrustal rocks in Finland. Geological Survey of Finland, Special Paper 19, 85–100. Available at: http://tupa.gtk.fi/julkaisu/specialpaper/sp_019_pages_085_100.pdf

Halla, J. 2005. Late Archaean high-Mg granitoids (sanukitoids) in the southern Karelian domain, eastern Finland; Pb and Nd isotopic constraints on crust-mantle interactions. Lithos 79, 161–178

Halla, J., van Hunen, J., Heilimo, E. & Hölttä, P. 2009. Geochemical and numerical constraints on Neoarcahean plate tectonics. Precambrian Research 174, 155–162.

Hautaniemi, H., Kurimo, M., Multala, J., Leväniemi, H. & Vironmäki, J. 2005. The "Three In One" aerogeophysical concept of GTK in 2004. In: Airo, M.-L. (ed.) Aerogeophysics in Finland 1972–2004: Methods, System Characteristics and Applications. Geological Survey of Finland, Special Paper 39, 21–74. Available at: http://tupa.gtk.fi/julkaisu/specialpaper/sp_039_pages_021_074.pdf

Heikkinen, P., Luosto, U., Guterch, A., Janik, T., Denton, P., Maguire, P., Lund, C.-E., Tryggvason, A., Thybo, H. & Yliniemi, J. 1995. Refraction profile FENNIA in southern Finland. In: Solid Earth geophysics & natural hazards. Annales Geophysicae Supplement 1 to vol. 13, C 41.

Heilimo, E., Halla, J. & Hölttä, P. 2010. Discrimination and origin of the sanukitoid series: Geochemical constraints from the Neoarcahean western Karelian Province (Finland). Lithos 115, 27–39.

Herzberg, C. 1995. Phase equilibria of common rocks in the crust and mantle. In: Ahrens, T. J. (ed.) Rock Physics and Phase Relations. A Handbook of Physical Constants. American Geophysical Union Reference Shelf 3, 166–177.

Hietanen, A. 1975. Generation of potassium-poor magmas in the northern Sierra Nevada and the Svecofennian in Finland. Jour. Research U. S. Geol. Surv. 3, 631–645.

Hölttä, P. & Paavola, J. 2000. P-T development of Archaean granulites in Varpaisjärvi, central Finland. Effects of multiple metamorphism of the reaction history of mafic rocks. Lithos (50)1 3, 97–120.

Hölttä, P., Heilimo, E., Huhma. H., Juopperi, H., Kontinen, A., Konnunaho, H., Lauri, L., Mikkola, P., Paavola, J. & Sorjonen-Ward, P. 2012a. Archaean complexes of the Karelia Province in Finland. In: Hölttä, P. (ed.) The Archaean of the Karelia Province in Finland. Geological Survey of Finland, Special Paper 54, 9-20. Available at: http://tupa.gtk.fi/julkaisu/specialpaper/sp_054_pages_009_020.pdf

Hölttä, P., Heilimo, E., Huhma, H., Kontinen, A., Mertanen, S., Mikkola, P., Paavola, J., Peltonen, P., Semprich, J., Slabunov, A. & Sorjonen-Ward, P. 2012b. The Archaean of the Karelia Province in Finland. In: Hölttä, P. (ed.) The Archaean of the Karelia Province in Finland. Geological Survey of Finland, Special Paper 54, 21-73. Available at: http://tupa.gtk.fi/julkaisu/specialpaper/sp_054_pages_021_073.pdf

Hölttä, P., Huhma, H., Mänttäri, I. & Paavola, J. 2000. P T t development of Archaean granulites in Varpaisjärvi, central Finland: II. Dating of high-grade metamorphism with the U-Pb and Sm-Nd methods. Lithos (50)1 3, 121–136.

Hou, M.-L., Jiang, Y.-H., Jiang, S.-Y., Ling, H.-F. & Zhao, K.-D. 2007. Contrasting origins of late Mesozoic adakitic granitoids from the northwestern Jiaodong Peninsula, east China: implications for crustal thickening to delamination. Geological Magazine. 144 (4), 619–631.

Howell, D. G. 1985. Terranes. Scientific American 253, 5, 116–125.

Howell, D. G. 1995. Principle of terrane analysis. New applications for global tectonics. London: Chapman & Hall. 245 p.

Hu, Y., Liu, J., Ling, M., Ding, W., Liu, Y., Zartman, R. E., Ma, X., Liu, D., Zhang, C., Sun, S., Zhang, L., Wu, K. & Sun, W. 2015. The formation of Qulong adakites and their relationship with porphyry copper deposit: Geochemical constraints. Lithos 220, 60–80.

Hua, H., Polat, A. & Fryer, B. J. 2013. Origin of Archaean tonalite–trondhjemite–granodiorite (TTG) suites and granites in the Fiskenæsset region, southern West Greenland: Implications for continental growth. Gondwana Research 23(2), 452–470.

Huhma, A. 1981. Youngest Precambrian dyke rocks in North Karelia, East Finland. Bulletin of the Geological Society of Finland 53, 67–82.

Huhma, H. 1986. Sm-Nd, U-Pb and Pb-Pb isotopic evidence for the origin of the Early Proterozoic Svecokarelian crust in Finland. Geological Survey of Finland, Bulletin 337. 48 p. Available at: http://tupa.gtk.fi/julkaisu/bulletin/bt_337.pdf

Huhma, H. 2009. Arkeisten ”adakiittisten” granitoidien Sm-Nd tuloksia. Geological Survey of Finland, archive report CK41.23/2009/9.

Huhma, H., Kontinen, A., Mikkola, P., Halkoaho, T., Hokkanen, T., Hölttä, P., Juopperi, H., Konnunaho, J., Luukkonen, E., Mutanen, T., Peltonen, P., Pietikäinen, K. & Pulkkinen, A. 2012. Nd isotopic evidence for Archaean crustal growth in Finland. In: Hölttä, P. (ed.) The Archaean of the Karelia Province in Finland. Geological Survey of Finland, Special Paper 54, 176-213. Available at: http://tupa.gtk.fi/julkaisu/specialpaper/sp_054_pages_176_213.pdf

Kähkönen, Y. 1989. Geochemistry and petrology of the metavolcanic rocks of the early Proterozoic Tampere schist belt, southern Finland. Geological Survey of Finland, Bulletin 345. 104 p. Available at: http://tupa.gtk.fi/julkaisu/bulletin/bt_345.pdf

Kähkönen, Y. 2005. Svecofennian supracrustal rocks. In: Lehtinen, M., Nurmi, P. A. & Rämö, O. T. (eds) Precambrian Geology of Finland – Key to the Evolution of the Fennoscandian Shield. Developments in Precambrian Geology 14. Amsterdam: Elsevier, 343–406.

Kähkönen, Y. & Leveinen, J. 1994. Geochemistry of metasedimentary rocks of the Paleoproterozoic Tampere Schist Belt, southern Finland. In: Nironen, M. & Kähkönen, Y. (eds) Geochemistry of Proterozoic supracrustal rocks in Finland. Geological Survey of Finland, Special Paper 19, 117–136. Available at: http://tupa.gtk.fi/julkaisu/specialpaper/sp_019_pages_117_139.pdf

Käpyaho, A., Mänttäri, I. & Huhma, H. 2006. Growth of Archaean crust in the Kuhmo district, eastern Finland: U-Pb and Sm-Nd isotope constraints on plutonic rocks. Precambrian Research 146, 95–119.

Kay, R. W. 1978. Aleutian magnesian andesites: Melts from subducted Pacific ocean crust. Journal of Volcanology and Geothermal Research, Volume 4, Issues 1-2, 117–132.

Kerrich, R. & Wyman, D. A. 1996. The trace element systematics of igneous rocks in mineral exploration, an overview. In: Wyman, D. A. (ed.) Trace element geochemistry of volcanic rocks; Applications for massive sulphide exploration. Geological Association of Canada, Short Course Notes 12, 1–50.

Kontinen, A. & Paavola, J. 2006. A preliminary model of the crustal structure of the eastern Finland Archaean complex between Vartius and Vieremä, based on constraints from surface geology and FIRE 1 seismic survey. In: Kukkonen, I. T. & Lahtinen, R. (eds) Finnish Reflection Experiment FIRE 2001–2005. Geological Survey of Finland, Special Paper 43, 223–240. Available at: http://tupa.gtk.fi/julkaisu/specialpaper/sp_043_pages_223_240.pdf

Kontinen, A., Paavola, J. & Lukkarinen, H. 1992. K-Ar ages of hornblende and biotite from Late Archaean rocks of eastern Finland - interpretation and discussion of tectonic implications. Geological Survey of Finland, Bulletin 365. 31 p. Available at: http://tupa.gtk.fi/julkaisu/bulletin/bt_365.pdf

Korhonen, J. V. 2005. Airborne magnetic method: special features and review on applications. In: Airo, M.-L. (ed.) Aerogeophysics in Finland 1972–2004: Methods, System Characteristics and Applications. Geological Survey of Finland, Special Paper 39, 77–102. Available at: http://tupa.gtk.fi/julkaisu/specialpaper/sp_039_pages_077_102.pdf

Korhonen, J. V., Säävuori, H., Wennerström, M., Kivekäs, L., Hongisto, H. & Lähde, S. 1993. One hundred seventy eight thousand petrophysical parameter determinations from the regional petrophysical programme. In: Autio, S. (ed.) **Geological Survey of Finland, Current Research 1991–1992.** Geological Survey of Finland, Special Paper 18, 137–141. Available at: http://tupa.gtk.fi/julkaisu/specialpaper/sp_018_pages_137_141.pdf

Korsman, K., Koistinen, T., Kohonen, J., Wennerström, M., Ekdahl, E., Honkamo, M., Idman, H. & Pekkala, Y. (eds) 1997. Bedrock map of Finland 1:1 000 000. Espoo: Geological Survey of Finland.

Korsman, K., Korja, T., Pajunen, M., Virransalo, P. & GGT working group 1999. The GGT/SVEKA transect: structure and evolution of the continental crust in the Paleoproterozoic Svecofennian orogen in Finland. International Geology Review 41 (4), 287–333.

Kovalenko, A. V., Clemens, J. D. & Savatenkov, V. M. 2005. Petrogenetic constraints for the genesis of Archaean sanukitoid suites: geochemistry and isotopic evidence from Karelia, Baltic Shield. Lithos 79, 147–160.

Krogh, T. E. 1973. A low-contamination method for hydrothermal decomposition of U and Pb for isotopic age determinations. Geochimica et Cosmochimica Acta 37, 485–494.

Kröner, A., Wan, Y., Xie, H., Wu, F., Münker, C., Hegner, E. & Schoene, B. 2011. Origin of Early Archaean Tonalitic Gneisses and Greenstone Felsic Volcanic Rocks on the basis of Zircon Ages and Hf-Nd Isotopic Systematics. Abstract in: Abstracts volume. 23rd Colloquium of African Geology (CAG23), University of Johannesburg, Republic of South Africa 8th–14th January 2011.

Kukkonen, I. T. & Lahtinen, R. (eds) 2006. Finnish reflection experiment FIRE 2001–2005. Geological Survey of Finland, Special Paper 43. 247 p. Available at: http://tupa.gtk.fi/julkaisu/specialpaper/sp_043.pdf

Kukkonen, I. T., Kuusisto, M., Lehtonen, M. & Peltonen, P. 2008. Delamination of eclogitized lower crust: Control on the crust-mantle boundary in the central Fenoscandian shield. Tectonophysics 457 (3–4), 111–127.

Kurhila, M., Vaasjoki, M., Mänttäri, I., Rämö, T. & Nironen, M. 2005. U-Pb ages and Nd isotope characteristics of the late-orogenic, migmatizing microcline granites in southwestern Finland. Bulletin of the Geological Society of Finland 77 (2), 105–128.

Lahtinen, R. 1994. Crustal evolution of the Svecofennian and Karelian domains during 2.1-1.79 Ga, with special emphasis on the geochemistry and origin of 1.93-1.91 Ga gneissic tonalites and associated supracrustal rocks in the Rautalampi area, central Finland. Geological Survey of Finland, Bulletin 378. 128 p. Available at: http://tupa.gtk.fi/julkaisu/bulletin/bt_378.pdf

Lahtinen, R. & Korhonen, J. V. 1996. Comparison of petrophysical and geochemical data in the Tampere-Hämeenlinna area, southern Finland. Geological Survey of Finland, Bulletin 392. 45 p. Available at: http://tupa.gtk.fi/julkaisu/bulletin/bt_392.pdf

Lahtinen, R., Korja, A. & Nironen, M. 2005. Paleoproterozoic tectonic evolution. In: Lehtinen, M., Nurmi, P. A. & Rämö, O. T (eds) Precambrian Geology of Finland – Key to the Evolution of the Fennoscandian Shield. Amsterdam: Elsevier B.V., 481–532.

Laitakari, I. 1969. On the set of olivine diabase dikes in Häme, Finland. Geological Survey of Finland, Bulletin 241. 65 p. Available at: http://tupa.gtk.fi/julkaisu/bulletin/bt_241.pdf

Laitakari, I. 1971. Padasjoki. Geological Map of Finland 1:100 000, Pre-Quaternary Rocks, Sheet 2143. Geological Survey of Finland.

Laitakari, I. 1973. Kaipola. Geological Map of Finland 1:100 000, Pre-Quaternary Rocks, Sheet 2144. Geological Survey of Finland.

Lehtinen, M., Nurmi, P. A. & Rämö, O. T. (eds) 2005. Precambrian geology of Finland: key to the evolution of the Fennoscandian Shield. Developments in Precambrian Geology 14. Amsterdam: Elsevier. 736 p.

Ludvig, K. R. 1991. PbDat 1.21 for MS-dos: A computer program for IBM-PC Compatibles for processing raw Pb-U-Th isotope data: revision. U.S. Geological Survey, Open-File Report 88-542. 35 p.

Ludvig, K. R. 1998. Using Isoplot/Ex Version 1.00. Berkeley Geochronological Center, Special Publication 1. 43 p.

Lukkarinen, H. 2000. Siilinjärvi. Geological Map of Finland 1:100 000, Pre-Quaternary Rocks, Sheet 3331. Geological Survey of Finland.

Luosto, U., Lanne, E., Korhonen, H., Guterch, A., Grad, M., Materzok, R. & Perchuc, E. 1984. Deep structure of the Earth's crust on the SVEKA profile in central Finland. Annales Geophysicae 2 (5), 559–570.

Mänttäri, I. 2012 (released 2017). Zircon SIMS U-Pb ages for adakitoids from Iisalmi, Kianta, and Ranua terrains. Report to Tapio Ruotoistenmäki and Pentti Hölttä. Geological Survey of Finland, archive report 106/2012. 36 p. Available at: http://tupa.gtk.fi/raportti/arkisto/106_2012.pdf

Mänttäri, I., Sergeev, S., Paavola, J., Pakkanen, L. & Vestin, J. 1998. From conventional to ionprobe U-Pb dating of inhomogeneous zircon population: 3.2 Ga basement gneiss, Lapinlahti, central Finland. 23. Nordiske Vintermøde. Abstract volume, Århus, 1998, p. 197.

Martin, H. & Moyen, J.-F. 2002. Secular changes in tonalite-trondhjemite-granodiorite composition as markers of the progressive cooling of Earth. Geology 30, 319–322.

Martin, H., Smithies, R. H., Rapp, R., Moyen, J.-F. & Champion, D. 2005. An overview of adakite, tonalite–trondhjemite–granodiorite (TTG), and sanukitoid: relationships and some implications for crustal evolution. Lithos, 79-1/2, 1–24.

Mattila, J. 2004. Geochemical and Sm-Nd isotopic constraints on the crustal evolution of the Kitee-Lahdenpohja area, southeastern Finland and northwestern Russia. Master of Science Thesis, University of Turku, Finland. 102 p.

McIntyre, J. I. 1980. Geological significance of magnetic patterns related to magnetite in sediments and metasediments: A review, Bull. Aust. Soc. Expl. Geophy. 11, 19–33.

Middlemost, E. A. 1975. The basalt clan. Earth Sci. Rev. 11, 337–364.

Middlemost, E. A. K. 1994. Naming materials in the magma/igneous rock system. Earth-Science Reviews, 37, 215–224.

Moyen, J.-F. 2009. High Sr/Y and La/Yb ratios: The meaning of the "adakitic signature". Lithos, v 112, Issues 3-4, 556–574.

Moyen, J.-F. 2011. The composite Archaean grey gneisses: Petrological significance, and evidence for a non-unique tectonic setting for Archaean crustal growth. Lithos 123, 21–36.

Mungall, J. E. 2002. Roasting the mantle: Slab melting and the genesis of major Au and Au-rich Cu deposits. Geology 30, 915–918.

Mutanen, T. & Huhma, H. 2003. The 3.5 Ga Siurua trondhjemite gneiss in the Archaean Pudasjärvi Granulite Belt, northern Finland. Bulletin of the Geological Society of Finland, Vol. 75 (1–2), 51–68.

Naqvi, S. M. & Rana Prathap, J. G. 2007. Geochemistry of adakites from Neoarchaean active continental margin of Shimoga schist belt, Western Dharwar Craton, India: Implications for the genesis of TTG. Precambrian Research, 156 (1-2), 32–54.

Nironen, M. 1989. Emplacement and structural setting of granitoids in the early Proterozoic Tampere and Savo schist belts – implications for contrasting crustal evolution. Geological Survey of Finland, Bulletin 346. 83 p. Available at: http://tupa.gtk.fi/julkaisu/bulletin/bt_346.pdf

Nironen, M. 1997. The Svecofennian Orogen: a tectonic model. Precambrian Research 86, 21–44.

Nironen, M. 2003. Keski-Suomen granitoidikompleksi - karttaselitys. Summary: central Finland granitoid complex - explanation to a map. Geological Survey of Finland, Report of Investigation 157. 45 p. + 1 app. map. Available at: http://tupa.gtk.fi/julkaisu/tutkimusraportti/tr_157.pdf

Nironen, M., Elliott, B. A. & Rämö, O. T. 2000. 1.88-1.87 Ga post-kinematic intrusions of the Central Finland Granitoid Complex: a shift from C-type to A-type magmatism during lithospheric convergence. Lithos 53 (1), 37–58.

Nironen, M., Lahtinen, R. & Koistinen, T. 2002. Suomen geologiset aluenimet - yhtenäisempään nimikäytäntöön!. Summary: Subdivision of Finnish bedrock - an attempt to harmonize terminology. Geologi 54 (1), 8–14.

Nisbet, E. G. 1987. The young Earth. An introduction to Archaean geology. Allen & Unmin, Inc. 401 p.

Obata, M. & Thompson, A. B. 1981. Amphibole and chlorite in mafic and ultramafic rocks in the lower crust and upper mantle. Contributions to Mineralogy and Petrology 77, 74–81.

O'Brien, H., Huhma, H. & Sorjonen-Ward, P. 1993. Petrogenesis of the late Archaean Hattu schist belt, Ilomantsi, eastern Finland: Geochemistry and Sr, Nd isotopic composition. In: Nurmi, P. A. & Sorjonen-Ward, P. (eds) Geological development, gold mineralization and exploration methods in the late Archaean Hattu schist belt, Ilomantsi, eastern Finland. Geological Survey of Finland, Special Paper 17, 147–184. Available at: http://tupa.gtk.fi/julkaisu/specialpaper/sp_017_pages_147_184.pdf

Paavola, J. 1984. On the Archaean high-grade metamorphic rocks in the Varpaisjärvi area, central Finland. Geological Survey of Finland, Bulletin 327. 33 p. Available at: http://tupa.gtk.fi/julkaisu/bulletin/bt_327.pdf

Paavola, J. 1987. Lapinlahti. Geological map of Finland 1:100 000, Pre-Quaternary Rocks, Sheet 3332. Geological Survey of Finland.

Paavola, J. 1988. Lapinlahden kartta-alueen kallioperä. Summary: Pre-Quaternary Rocks of the Lapinlahti Map-Sheet area. Geological Map of Finland 1:100 000. Explanation to the Maps of Pre-Quaternary Rocks, Sheet 3332. Geological Survey of Finland. 60 p. Available at: http://tupa.gtk.fi/kartta/kallioperakartta100/kps_3332.pdf

Paavola, J. 1990. Iisalmi. Geological map of Finland 1:100 000, Pre-Quaternary Rocks, Sheet 3341. Geological Surevy of Finland.

Paavola, J. 2001. Vieremä. Geological map of Finland 1:100 000, Pre-Quaternary Rocks, Sheet 3342. Geological Survey of Finland.

Pearce, J. A. & Parkinson, I. J. 1993. Trace element models of mantle melting: application to volcanic arc petrogenesis. In: Prichard, H. M., Alabaster, T., Harris, N. B. W & Neary, C. R. (eds) Magmatic Processes and Plate Tectonics. Geological Society Special Publication 76, 373–403.

Pearce, J. A. & Peate, D. W. 1995. Tectonic implications of the composition of volcanic arc magmas. Annual Review of Earth and Planetary Sciences. 23, 251–285.

Peltonen, P. 1995. Petrology, geochemistry and mineralogy of ultramafic rocks and associated Ni-Cu deposits in the Vammala Ni-Belt, southwestern Finland. Espoo: Geological Survey of Finland. 100 p.

Peltonen, P., Mänttäri, I., Huhma, H. & Whitehouse, M. 2006. Multi-stage origin of the lower crust of the Karelian craton from 3.5 to 1.7 Ga based on isotopic ages of kimberlite-derived mafic granulite xenoliths. Precambrian Research 147, 107–123.

Peltoniemi, M. 1982. Characteristics and results of an airborne electromagnetic method of geophysical surveying. Geological Survey of Finland, Bulletin 321. 229 p. Available at: http://tupa.gtk.fi/julkaisu/bulletin/bt_321.pdf

Pietikäinen, K. & Vaasjoki, M. 1999. Structural observations and U-Pb mineral ages from igneous rocks at the Archaean - Palaeoproterozoic boundary in the Salahmi Schist Belt, central Finland: constraints on tectonic evolution. Bulletin of the Geological Society of Finland 71, Part 1, 133–142.

Puranen, R. 1989. Susceptibilities, iron and magnetite content of Precambrian rocks in Finland. Geological Survey of Finland, Report of investigation 90. 45 p. Available at: http://tupa.gtk.fi/julkaisu/tutkimusraportti/tr_090.pdf

Puranen, R. 1991. Specifications of petrophysical sampling and measurements. In: Autio, S. (ed.) Geological Survey of Finland, Current Research 1989-1990. Geological Survey of Finland, Special Paper 12, 217–218. Available at: http://tupa.gtk.fi/julkaisu/specialpaper/sp_012_pages_217_218.pdf

Rämö, O. T. 1991. Petrogenesis of the Proterozoic rapakivi granites and related basic rocks of southeastern Fennoscandia: Nd and Pb isotopic and general geochemical constraints. Geological Survey of Finland, Bulletin 355. 161 p. Available at: http://tupa.gtk.fi/julkaisu/bulletin/bt_355.pdf

Rämö, O. T. & Haapala, I. 2005. Rapakivi granites. In: Lehtinen, M., Nurmi, P. A. & Rämö, O. T. (eds) Precambrian geology of Finland: Key to the evolution of the Fennoscandian Shield. Developments in Precambrian geology 14, 533–562.

Rapp, R. P., Shimizu, N. & Norman, M. D. 2003. Growth of early continental crust by partial melting of eclogite. Nature, v. 425, 605–609.

Rasilainen, K., Lahtinen, R. & Bornhorst, T. J. 2007. The Rock Geochemical Database of Finland Manual. Geological Survey of Finland, Report of Investigation 164. 38 p. (Electronic publication). Available at: http://tupa.gtk.fi/julkaisu/tutkimusraportti/tr_164.pdf

Rautiainen, J. 2000. Arkeeisen kratonin reunalla esiintyvät intermediääriset juonet Iisalmen, Juankosken ja Siilinjärven alueilla. Unpublished M. Sc. thesis, University of Helsinki. 60 p. (in Finnish)

Reay, A. & Parkinson, D. 1997. Adakites from Solander Island, New Zealand. New Zealand Journal of Geology and Geophysics 40, 121–126.

Rey, P., Philippot, P. & Thébaud, N. 2003. Contribution of mantle plumes, crustal thickening and greenstone blanketing to the 2.75–2.65 Ga global crisis. Precambrian Research 127, 43–60.

Richards, J. P. & Kerrich, R. 2007. Special Paper: Adakite-like rocks: Their diverse origins and questionable role in metallogenesis. Economic Geology 102(4), 537–576.

Rickwood, P. C. 1989. Boundary lines within petrologic diagrams, which use oxides of major and minor elements. Lithos 22, 247–263.

Rino, S., Komiya, T., Windley, B., Katayama, I., Motoki, A. & Hirata, T. 2004. Major episodic increases of continental crustal growth determined from zircon ages of river sands; implications for mantle overturns in the Early Precambrian. Physics of the Earth and Planetary Interiors, Volume 146, Issue 1–2, 369–394.

de la Roche, H., Leterrier, J., Grandclaude, P. & Marchal, M. 1980. A classification of volcanic and plutonic rocks using R1-R2 diagram and major-element analyses – its relationship with current nomenclature. Chemical Geology, 29, 183–210.

Rollinson, H. R. 1993. Using geochemical data: Evaluation, presentation, interpretation. Longman Group UK Limited. 352 p.

Ruotoistenmäki, T. 1992. Tampereen liuskevyöhykkeen pohjoisreunan ja Keski-Suomen graniitin eteläreunan petrofysiikasta. On petrophysics of the northern edge of Tampere schist zone and the southern edge of central Finland granite. In: Global Geoscience Transects. Report on meeting 14.–15.4.1992. University of Turku, Finland, Institute of geology and mineralogy. Publication no 31, 52–54. (in Finnish)

Ruotoistenmäki, T. 1996. A schematic model of the plate tectonic evolution of Finnish bedrock. Geological Survey of Finland, Report of Investigation 133. 23 p. Available at: http://tupa.gtk.fi/julkaisu/tutkimusraportti/tr_133.pdf

Ruotoistenmäki, T. 1999. Characteristics of a Proterozoic collision zone in Padasjoki-Kaipola, southern Finland. In: European Geophysical Society 24th General assembly: society symposium, solid earth geophysics & geodesy. Geophysical Research, Abstracts 1 (1), p. 66.

Ruotoistenmäki, T. 2012. Geochemical and petrophysical characteristics of plutonic rocks from the Archaean Karelia Province in Finland. In: Hölttä, P. (ed.) The Archaean of the Karelia Province in Finland. Geological Survey of Finland, Special Paper 54. 226–243. Available at: http://tupa.gtk.fi/julkaisu/specialpaper/sp_054_pages_226_243.pdf

Ruotoistenmäki, T. 2016. Lithogeochemical Maps (Atlas) of Finland. Geological Survey of Finland, Guide 62. 123 p. Available at: http://tupa.gtk.fi/julkaisu/opas/op_062.pdf

Ruotoistenmäki, T., Mänttäri, I. & Paavola, J. 2001. Characteristics of Proterozoic late-/ post-collisional intrusives in Archaean crust in Iisalmi-Lapinlahti area, central Finland. In: Autio, S. (ed.) Geological Survey of Finland, Current Research 1999-2000. Geological Survey of Finland, Special Paper 31, 105–115. Available

at: http://tupa.gtk.fi/julkaisu/specialpaper/sp_031_pages_105_115.pdf

Rutland, R. W. R., Williams, I. S. & Korsman, K. 2004. Pre- 1.91 Ga deformation and metamorphism in the Palaeoproterozoic Vammala migmatite belt, southern Finland, and implications for Svecofennian tectonics. Bulletin of the Geological Society of Finland 76 (1–2), 93–140.

Sandström, H. 1996. The analytical methods and the precision of the element determinations used in the regional bedrock geochemistry in the Tampere-Hämeenlinna area, southern Finland. Geological Survey of Finland, Bulletin 393. 25 p. Available at: http://tupa.gtk.fi/julkaisu/bulletin/bt_393.pdf

Scaillet, B. & Prouteau, G. 2001. Oceanic slab melting and mantle metasomatism. Science Progress 84, 335–354.

Scaillet, B., Holts, F. & Pichavant, M. 1997. Rheological properties of granitic magmas in their crystallization range. In: Bouchez, J. L. (ed.) Granite: From segregation of melt to emplacement fabrics. Kluwer Academic Publishers, 11–29.

Simonen, A. 1953. Stratigraphy and sedimentation of the Svecofennidic, early Archaean supracrustal rocks in southwestern Finland. Bull. Comm. Géol. Finlande 160. 64 p.

Smithies, R. H. 2000. The Archaean tonalite-trondhjemite-granodiorite (TTG) series is not an analogue of Cenozoic adakite: Earth and Planetary Science Letters 182, 115–125.

Smithies, R. H., Champion, D. C. & Cassidy, K. F. 2003. Formation of Earth's early Archaean continental crust: Precambrian Research 127, 89–101.

Sorjonen-Ward, P. & Luukkonen, E. J. 2005. Archaean rocks. In: Lehtinen, M., Nurmi, P. A. & Rämö, O. T. (eds) Precambrian geology of Finland: Key to the evolution of the Fennoscandian Shield. Developments in Precambrian geology 14, 19–99.

Stern, R. A. & Hanson, G. N. 1991. Archaean high-Mg granodiorite: A derivative of light rare earth element-enriched monzodiorite of mantle origin. Journal of Petrology 32, 201–238.

Streckeisen, A. 1976. To each plutonic rock its proper name. Earth Science Reviews 12, 1–33.

Svetov, S. A., Huhma, H., Svetova, A. I. & Nazarova, T. N. 2004. The oldest adakites of the Fennoscandian Shield. Doklady Earth Sciences 397A (6), 878–882.

Tarvainen, T., Aatos, S. & Räisänen, M.-L. 1996. A method for determining the normative mineralogy of tills. In: Environmental geochemistry: selected papers from the 3rd International Symposium, Kraków, Poland, 12–16 September 1994. Applied Geochemistry 11 (1–2), 117–120.

Thorkelson, D. J. & Breitsprecher, K. 2005. Partial melting of slab window margins: Genesis of adakitic and non-adakitic magmas. Lithos 79, 25–41.

Toivola, V., Huhma, H. & Paavola, J. 1991. The diabase dykes in the Sonkajärvi-Varpaisjärvi area, central Finland. In: Autio, S. (ed.) Geological Survey of Finland, Current Research 1989–1990. Geological Survey of Finland, Special Paper 12, 59–61. Available at: http://tupa.gtk.fi/julkaisu/specialpaper/sp_012_pages_059_061.pdf

Tsuchiya N. & Kanisawa, S. 1994. Early Cretaceous Sr-rich silicic magmatism by slab melting in the Kitakami Mountains, northeast Japan. Journal of Geophysical Research, vol. 99, No B11, 22205–22220.

Vaasjoki, M., Korsman, K. & Koistinen, T. 2005. Overview. In: Lehtinen, M., Nurmi, P. & Rämö, O. T. (eds) Precambrian Geology of Finland – Key to the Evolution of the Fennoscandia Shield. Amsterdam: Elsevier.

Väisänen, M., Eklund, O. & Skyttä, P. 2006. Svecofennian calc-alkaline vs. adakite-like 1.90-1.86 Ga magmatism in SW Finland. The 27th Nordic Geological Winter Meeting, January 9–12.2006. Oulu, Finland. Bulletin of the Geological Society of Finland, Special Issue 1, p. 170.

Väisänen, M., Johansson, A., Andersson, U. B., Eklund, O. & Hölttä, P. 2012. Palaeoproterozoic adakite- and TTG-like magmatism in the Svecofennian orogen, SW Finland. Geologica Acta, Vol. 10(4).

Wang, P. & Glover, L. III. 1992. A tectonics test of the most commonly used geochemical discriminant diagrams and patterns. Earth Sci. Rev. 33, 111–131.

Weaver, B. L. & Tarney, J. 1981. Lewisian Gneiss Geochemistry and Archaean Crustal Development Models. Earth and Planetary Science Letters 55 (1), 171–180.

White, A. J. R., Chappell, B. W. & Wyborn, D. 1999. Application of the restite model to the Deddick granodiorite and its enclaves — a reinterpretation of the observations and data of Maas et al. 1997. Journal of Petrology 40 (3), 413–421.

Wilson, M. 1989. Igneous Petrogenesis a Global Tectonic Approach. London: Chapman & Hall. 466 p.

Wyllie, P. J. 1984. Constraints imposed by experimental petrology on possible and impossible magma sources and products. Phil. Trans. Roy. Soc. London, A310, 439–456.

Xiong, X.-L. 2006. Trace element evidence for growth of early continental crust by melting of rutile-bearing hydrous eclogite. Geology 34, 945–948.

ABBREVIATIONS

A.Adk	Archaean adakitic plutonic rock samples
AFP	All Finnish plutonic rocks (see Table 2)
CFG	Central Finland granitoid sub-area
EF	Eastern Finland sub-area
GTK	Geological Survey of Finland
HREE	Heavy rare earth elements
HSA	High-silica adakites
IAB	Island-arc basalts
IC	Iisalmi sub-area
IL	Ilomantsi sub-area
LBZ	Ladoga-Bothnian bay zone
LREE	Light rare earth elements
MORB	Mid-ocean ridge basalts
OIB	Ocean island basalts
P.Adk	Proterozoic adakitic plutonic rock samples
PDJ	Pudasjärvi sub-area
RGDB	Rock Geochemical Database of Finland
Rpk	rapakivi sub-areas in southern Finland
SMB	Southern Finland migmatite sub-area
TTG	Tonalite–trondhjemite–granodiorite rock group
USM	Uusimaa sub-area

All GTK's publications online at hakku.gtk.fi

This study considers the adakitic plutonic rocks, or 'adakitoids', representing melts fractionated below plagioclase stability depths in the lower crust/upper mantle (greater or equal to ca. 50–80 km). They cover a substantial fraction of the Finnish Precambrian bedrock. Only some supracrustal sub-areas lack adakitic plutonic rock outcrops. The study provides a summary of Finnish adakitoids: their areal, chemical, isotopic (age) and physical variations and their tectonic and magmatic evolution. It is shown that adakitoids constitute a distinct chemically defined rock group that overlaps groups defined by 'traditional' mineralogical and chemical methods. The adakitic plutonic rocks vary from granodiorites to tonalites and gabbros. The Proterozoic adakitoids are generally connected with 'modern type' plate tectonic processes, while the majority of Archaean crust and adakitoids (TTGs) are primarily connected with collision, stacking and over-/underthrusting of inferred pre-existing microplates. The adakitoids form a continuity from 'true', subduction-related adakites to TTGs and sanukitoids, their chemical and mineralogical differences being obscure. As such, they give a very valuable and informative window into magmatic processes existing at upper mantle/lower crustal depths.

gtk.fi

ISBN 978-952-217-400-0 (pdf)
ISBN 978-952-217-399-7 (paperback)